




Universitetet
i Stavanger

FACULTY OF SCIENCE AND TECHNOLOGY

MASTER'S THESIS

Study programme/specialisation: Petroleum Geoscience Engineering	Spring semester, 2020 Open
Author: Irene Nerhus	 (signature of author)
Programme coordinator: Supervisors: Dr. Udo Zimmermann Dr. Mona W. Minde Dr. Bahareh Zareeipolgardani	
Title of master's thesis: Systematic atomic force microscopy and constraints for the determination of wettability and EOR research	
Credits: 30	
Keywords: Atomic Force Microscope (AFM) Chalk Flooding Improved Oil Recovery (IOR) Enhanced Oil Recovery (EOR) Force spectroscopy Wettability	Number of pages: 125 + supplemental material/other: 66 Stavanger, 25.07.20 date/year

Title page for Master's Thesis
Faculty of Science and Technology

Systematic Atomic Force Microscopy and Constraints for the Determination of Wettability and EOR Research

**By
Irene Nerhus**

Master thesis

Petroleum Geosciences Engineering

Faculty of Science and Technology

The University of Stavanger

The University of Stavanger

June 2020

Acknowledgements

Firstly, I would like to thank my supervisor Dr. Udo Zimmermann for his guidance and for giving me the opportunity to work with this inspiring topic; IOR. It has truly been a fun challenge to try out a new direction within IOR.

Dr. Zimmermann arranged contact with co-supervisor Dr. Bahareh Zareeipolgardani at the University in Grenoble. Thanks to Dr. Zareeipolgardani for welcoming me and really introducing me to the atomic force microscope. Without this, the study would not have been completed. Thank you for assisting me and for letting me use the AFM at the university, and thanks for all help and discussions afterwards.

Another big thanks to co-supervisor Dr. Mona W. Minde for practical input and discussions during the laboratory time at the University in Stavanger.

Staff engineer Caroline Ruud also deserves a thank you for helping me preparing all the samples for the AFM at UiS. Your help and precision are really appreciated in the laboratory. Also, in need of acknowledgement is Tine V. Bredal - thank you for letting me use your samples and providing me with information about them.

I would also like to thank the National IOR centre for funding for making this thesis possible and hopefully this thesis will help the research in the center.

A big thanks to my fellow students for keeping the spirit during this tough semester and a special thanks to those sharing the lab with me and to my family. Thanks for the discussions, the long days would not have been manageable without you!

Table of Contents

Acknowledgements	iii
List of Figures	v
List of Tables.....	xii
Commonly Used Abbreviations	xiv
Abstract	xv
1. Introduction	1
1.1 Objectives and research strategy	2
1.2 The Tool: Atomic Force Microscope	3
1.3 The Object: Carbonate and Silicate Minerals.....	4
1.4 The Rationale: The Relation Between Mineralogical Composition and Rock Mechanical Properties	5
2. Samples and Methodology	7
2.1 Overview of Samples.....	7
2.2 Chalk.....	8
2.2.1 Liège: Gulpen Formation	8
2.2.2 Mons: Saint Vaast Formation	8
2.2.3 Stevns Klint: Stevns Klint Formation	8
2.3 Flooding Experiment	8
2.4 Atomic Force Microscope (AFM).....	10
2.4.1 The Application	11
2.4.2 Sample Preparation	20
3. Results	24
3.1 Topography.....	25
3.1.1 Standards.....	25
3.1.2 LTT1	34
3.1.3 MLTT.....	39
3.1.4 ULTT	43
3.1.5 OBSV4_1 – MFP-3D Origin	46
3.1.6 OBSV12_6 – MFP-3D Origin	51
3.1.7 OBSV12 – MFP-3D Origin	54
3.1.8 OBSV18 – MFP-3D Origin	55
3.1.9 Chalk SK – MFP-3D Origin	58
3.1.10 Unflooded Liège	62

3.1.11 Kaolinite – MFP-3D Origin	63
3.2 Force Spectroscopy.....	66
3.2.1 Standards.....	66
3.2.2 MLTT.....	80
3.2.3 ULTT	86
3.2.4 OBSV4_1 – MFP-3D Origin	89
3.2.5 OBSV12 – MFP-3D Origin	91
3.2.6 Unflooded Liège	93
3.3 Compilation of the results.....	96
4. Discussion	99
4.1 Topography.....	99
4.2 Force Spectroscopy.....	101
4.3 Reliability of Data	103
5. Conclusion.....	104
6. References	106
7. Appendix	110
Appendix 1 Topography	110
Appendix 2 Force spectroscopy	131

List of Figures

Figure 1 Schematic overview of fluid relations within a porous rock, where water-wet would indicate that water is in contact with the mineral grain while oil-wet rocks are those where oil is in contact with the rock. Left: Water-wet, middle: Mixed-wet, right: Oil-wet. In water-wet reservoirs the water would rather adhere to the grains while oil flow through, which gives higher oil recovery than oil-wet reservoirs. (from Abdallah et al., 2007).....	2
Figure 2 Coccolithophore in chalk flooded with synthetic sea water. (Kindly provided by Tine V. Bredal).....	6
Figure 3 Atomic Force Microscope set-up in Grenoble placed on a special movement resistant table.....	11
Figure 4 Schematic representation of the functioning principles of an AFM. (from “Nanotechnology - Wikibooks, open books for an open world,” 2018).....	12
Figure 5 Comparing deflection image (A) and amplitude image (B) of the same area taken from the unpolished sample Chalk SK.	14
Figure 6 A standard force curve demonstrating the different steps of the cantilever approaching (point A-C) and retracting the sample. (from Javadpour et al., 2012).	15

Figure 7 Demonstrating two different force curves from MFP-3D Origin (to the left) and from NaioAFM (to the right).	16
Figure 8 Correctly placed tip (red circle) before placed on the head of the MFP-3D Origin AFM.	16
Figure 9 Illustrating an example of a poor quality height image (A) versus a good quality height image (B) using the NaioAFM at UiS.....	17
Figure 10 Sample placed on the sample holder (red circle) while adjusting the height of the legs of the head.	18
Figure 11 Set-up of the AFM at UiS. AFM to the left and software to the right.	19
Figure 12 Accutom saw (A) and Struers Rotopol-35 (B) are necessary to cut and polish the samples and mounts.	21
Figure 13 Scanning head of the AFM in unloaded position with the visible short legs.	21
Figure 14 Displaying a mount with some of the mineral standards mounted.....	22
Figure 15 Set-up of the Gatan Model 601 Tuned piezo Cutting Tool. Hot plate in the front (with the specimen table on top), disc cutter back to the left and microscope back to the right.	23
Figure 16 Sample placed on the glass plate, fixed with double sided tape.	24
Figure 17 Demonstrating a standard anorthite with an area of 5 μm^2 . A) height image, B) deflection image. Noise to the left in the deflection image is due to the measurement environment.....	26
Figure 18 Illustrating a standard anorthite with an area of 5 μm^2 . A) height image, B) deflection image.	26
Figure 19 Standard calcite with an area of 10 μm^2 . A) height image, B) deflection image. Red circle indicating a flatter surface than the surroundings.	27
Figure 20 Displaying a standard calcite with an area of 5 μm^2 . A) height image, B) deflection image.	28
Figure 21 A standard dolomite grain with an area of 10 μm^2 . A) height image, B) deflection image.	28
Figure 22 Imaging a standard dolomite with an area of 5 μm^2 . A) height image, B) deflection image.	29
Figure 23 Standard fluorapatite with an area of 25 μm^2 . A) height image, B) deflection image. Red circle demonstrating a feature with a triangular shape.	29
Figure 24 Illustrating an ilmenite standard with an area of 25 μm^2 . A) height image, B) deflection image. Red circle indicating a triangular shaped feature.	30
Figure 25 A magnesite standard with an area of 25 μm^2 with a polished surface. A) height image, B) deflection image. Green circle illustrating some small, rounded features.....	31
Figure 26 Displaying a magnetite standard with an area of 10 μm^2 . A) height image, B) deflection image. The red circle indicates a flatter area.	31
Figure 27 A plagioclase standard with an area of 5 μm^2 . A) height image, B) deflection image.	32

Figure 28 Demonstrating a quartz standard with an area of 10 μm^2 . A) height image, B) deflection image.	33
Figure 29 A zircon standard with an area of 10 μm^2 . A) height image, B) deflection image..	33
Figure 30 Displaying the first measured area of LTT1, scale bar is 1 μm . A), height image, B) deflection image with red arrows indicating possible clay laths.....	34
Figure 31 Demonstrating a height profile (A) over a selected line (red line in B) in the measured area. Scale bar is 1 μm	35
Figure 32 Calculating the roughness of the masked area (gray square in the left image) with the result in the table to the right.....	36
Figure 33 Displaying the second measured area from LTT1. A) height image, B) deflection image. Scale bar is 500 nm.....	36
Figure 34 Illustrating a height profile (A) over a selected line (red line in B) in the measured area. Note the smaller scale bar with 500 nm compared to the former figures.....	37
Figure 35 The first measured area in LTT1, UiS, area of 10 μm^2 . A) height image, B) deflection image.	38
Figure 36 The second measured area in LTT1, UiS, area of 10 μm^2 . A) height image, B) deflection image.	38
Figure 37 The third measured area in LTT1, UiS, area of 2.5 μm^2 . A), height image, B) deflection image.	39
Figure 38 Displaying the calcite-rich area of MLTT with a size of 10 μm^2 . A) height image, B) deflection image. Green box marks roughly area of Figure 38.....	40
Figure 39 Zoomed-in area of MLTT, calcite part, of 5 μm^2 (green box in Figure 37). A) height image, B) deflection image.	40
Figure 40 The first measured area of MLTT, clay part, of 25 μm^2 . A) height image, B) deflection image, red circle indicating stacked features.....	41
Figure 41 The second measured area of MLTT, clay part, of 5 μm^2 . A) height image, B) deflection image.	42
Figure 42 The first measured area in MLTT, magnesite part, of 5 μm^2 . A) height image, B) deflection image.	42
Figure 43 Illustrating the second measured area in MLTT, magnesite part, of 10 μm^2 . A) height image, B) deflection image with stacking features in the red circles.....	43
Figure 44 Demonstrating the first measured area in ULTT of 10 μm^2 . A) height image, B) deflection image.	44
Figure 45 The second measured area in ULTT, 10 μm^2 . A), height image with the yellow circle indicating a stacking pattern, B) deflection image red circles displaying features with a little "depression".....	44
Figure 46 Imaging a third measured area from ULTT of 10 μm^2 . A) height image, B) deflection image.	45

Figure 47 3D image of the height from Figure 45 in ULTT, size of 10 x 10 μm in x- and y-direction.....	46
Figure 48 First measured area of OBSV4_1 with a possible coccolith. A) height image, B) deflection image. Scale bar is 500 nm.....	47
Figure 49 SEM image of part of a coccolithophore (red circle) in an unflooded chalk sample with a scale bar of 1 μm . (Kindly provided by Tine Bredal.)	47
Figure 50 Illustrating a height profile (A) over a selected line (red line in B) in the measured area. Scale bar is 500 nm.....	48
Figure 51 Displaying a second measured area from OBSV4_1. A) height image, B) deflection image with an assumed clay particle in the yellow circle. Scale bar is 600 nm.....	49
Figure 52 Illustrating a height profile (A) over a selected line (red line in B) in the measured area. Scale bar is 600 nm.....	49
Figure 53 3D image of the height from Figure 50. The assumed clay particle can be seen in the yellow circle and the assumed coccolith in the red circle. Size is 3*3 μm in x- and y-direction.	50
Figure 54 Calculating the roughness of the masked area (gray square in the left image) with the result in the table to the right.....	51
Figure 55 One measured area from sample OBSV12_6 demonstrating amplitude image (A, red circle indicating possible clay particle), height image (B) and phase image (C). Scale bar is 300 nm.....	52
Figure 56 A second measured area in OBSV12_6. A) height image, B) deflection image (red circle includes a very small phase, possibly a clay mineral; blue circle indicating a relatively flat feature). Scale bar is 400 nm.....	52
Figure 57 Illustrating a height profile (A) over a selected line (red line in B) in the measured area from Figure 55. Scale bar is 400 nm.	53
Figure 58 A second measured area from sample OBSV12_6 displaying amplitude image (A), height image (B) and phase image (C). All images indicate signs of an unknown feature in the middle of the image. Scale bar is 1 μm	54
Figure 59 Displaying a measured area from sample OBSV12. A) height image, B) deflection image. The red circles indicate a deep area. Scale bar is 3 μm	54
Figure 60 Illustrating a height profile (A) over the area from Figure 59 (red line in B). Scale bar is 3 μm	55
Figure 61 Displays a measured area from OBSV18. A) height image, B) deflection image, blue circle indicating an unknown feature. Scale bar is 1 μm	56
Figure 62 3D image of the height from Figure 61 indicating a coccolithophore in the middle. Area measures 5 x 5 μm in x- and y-direction.	56
Figure 63 Demonstrating another measured area from OBSV18. A) height image, B) deflection image, red circle indicating an unknown particle. Scale bar is 600 nm.	57
Figure 64 A third measured area from OBSV18. A) height image, B) deflection image. Scale bar is 600 nm.	58

Figure 65 Calculating the roughness of the masked area (gray square in the left image) with the result in the table to the right.....	58
Figure 66 Illustrating one of the measured areas from the unpolished sample Chalk SK. A) height image, B) deflection image. Scale bar is 1 μm	59
Figure 67 A second measured area from the unpolished sample of Chalk SK, demonstrating amplitude image (A), height image (B) and phase image (C). Scale bar is 1 μm	60
Figure 68 A measured area from the polished sample of Chalk SK, demonstrating signs of polishing dust and stripes. A) height image, B) deflection image. Scale bar is 2 μm	60
Figure 69 Calculating the roughness of the masked area (gray square in the left image) with the result in the table to the right.....	61
Figure 70 Demonstrating the difference between unpolished (A and B) and polished (C and D) sample of Chalk SK. Scale bar is 2 μm	62
Figure 71 Displaying a measured area from the Unflooded Liège sample with height image (A) and deflection image (B). Area of 10 μm^2	63
Figure 72 Another measured area from the Unflooded Liège sample with height image(A) and deflection image (B). Area of 5 μm^2	63
Figure 73 A measured area from the kaolinite sample displaying crystal structure, red circles indicating typical structure of phyllosilicates. A) height image, B) deflection image. Scale bar is 200 nm.	64
Figure 74 Demonstrating another measured area in the kaolinite sample. A) height image, B) deflection image, red circle indicating a similar shape as the crystal in Figure 73. Scale bar is 2 μm	65
Figure 75 Illustrating a height profile (A) over the area from Figure 59 (red line in B). Scale bar is 2 μm	65
Figure 76 Calculating the roughness of the masked area (gray square in the left image) with the result in the table to the right pointing to high roughness, indicating that the surface is not smooth.	66
Figure 77 Illustrating a measured area of the anorthite with the respective force curve from the red point on the marked line in B. A) height image, B) deflection image indicating where the selected force curve is marked as a red point, C) the selected force curve indicating attractive force.....	67
Figure 78 Displaying another measured area of the anorthite with the respective force curve from the red point in B. A) height image, B) deflection image indicating where the selected force curve is marked as a red point, C) the selected force curve indicating attractive force..	68
Figure 79 Demonstrating a measured area of the calcite with the respective force curves from the red, yellow, and green circles in B. A) height image, B) deflection image displaying where the selected force curves are marked with red, yellow and green circles, C) the selected force curve indicating attractive force from red circle, D) selected force curve indicating attractive force from yellow circle, E) selected force curve indicating attractive force from green circle.	69

Figure 80 Illustrating another measured area of the calcite with the respective force curves from the red, yellow, and green circles in B. A) height image, B) deflection image displaying where the selected force curves are marked with red, yellow and green circles, C) the selected force curve indicating attractive force from red circle, D) selected force curve indicating attractive force from yellow circle, E) selected force curve indicating attractive force from green circle. 70

Figure 81 Displaying a measured area of the calcite with the respective force curve from the red point in B. A) height image, B) deflection image displaying where the selected force curve is marked as a red point, C) the selected force curve indicating attractive force. 71

Figure 82 Illustrating a measured area of the fluorapatite with the respective force curve from the red point in B. A) height image, B) deflection image displaying where the selected force curve is marked as a red point, C) the selected force curve indicating repulsive force. 72

Figure 83 Demonstrating a measured area of the ilmenite with the respective force curve from the red point in B. A) height image, B) deflection image displaying where the selected force curve is marked as a red point on the red line, C) the selected force curve indicating repulsive force. 73

Figure 84 Displaying another measured area of the ilmenite with the respective force curve from the red circle in B. A) height image, B) deflection image illustrating where the selected force curve is marked as a red circle on the red line, C) the selected force curve indicating attractive force. 74

Figure 85 Displaying a measured area of the magnesite with the respective force curve from the red circle in B. A) height image, B) deflection image illustrating where the selected force curve is marked as a red circle, C) the selected force curve indicating attractive force. 75

Figure 86 Illustrating another measured area of the magnesite with the respective force curve from the red circle in B. A) height image, B) deflection image illustrating where the selected force curve is marked as a red circle, C) the selected force curve indicating repulsive force. 76

Figure 87 Demonstrating a measured area of the magnetite with the respective force curve from the red point in B. A) height image, B) deflection image illustrating where the selected force curve is marked as a red point on the red line, C) the selected force curve indicating attractive force. 77

Figure 88 Displaying another measured area of the magnetite with the respective force curve from the red point in B. A) height image, B) deflection image displaying where the selected force curve is marked as a red point on the red line, C) the selected force curve indicating repulsive force. 78

Figure 89 Illustrating a measured area of the plagioclase with the respective force curve from the red point in B. A) height image, B) deflection image displaying where the selected force curve is marked as a red point on the red line, C) the selected force curve indicating repulsive force. 79

Figure 90 Displaying a measured area of the quartz with the respective force curves from the red and yellow circles in B. A) height image, B) deflection image illustrating where the selected force curves are marked with red, and yellow circles on the red line, C) the selected force curve indicating repulsive force from the red circle, D) the selected force curve indicating attractive force from the yellow circle. 80

Figure 91 Demonstrating a measured area of MLTT calcite part with the respective force curves from the red and yellow circles in B. A) height image, B) deflection image displaying where the selected force curves are marked with red, and yellow circles on the red line, C) the selected force curve indicating attractive force from the red circle, D) the selected force curve indicating attractive force from the yellow circle. 81

Figure 92 Illustrating another measured area of MLTT calcite part with the respective force curves from the red and yellow points in B. A) height image, B) deflection image illustrating where the selected force curves are marked with red, yellow, and green points on the red line, C) the selected force curve indicating attractive force from the red point, D) the selected force curve indicating attractive force from the yellow point, E) the selected force curve indicating attractive force from the green point. 82

Figure 93 Displaying a third measured area of MLTT calcite part with the respective force curves from the red and yellow circles in B. A) height image, B) deflection image displaying where the selected force curves are marked with red, and yellow circles on the red line, C) the selected force curve indicating attractive force from the red circle, D) the selected force curve indicating attractive force from the yellow circle. 83

Figure 94 Demonstrating a fourth measured area of MLTT calcite part with the respective force curves from the red and yellow circles in B. A) height image, B) deflection image illustrating where the selected force curves are marked with red, yellow, and green circles on the red line, C) the selected force curve indicating repulsive force from the red circle, D) the selected force curve indicating repulsive force from the yellow circle, E) the selected force curve indicating repulsive force from the green circle..... 84

Figure 95 Illustrating a measured area of MLTT magnesite part with the respective force curves from the red, yellow, and green points in B. A) height image, B) deflection image displaying where the selected force curves are marked with red, yellow, and green points on the red line, C) the selected force curve indicating attractive force from the red point, D) the selected force curve indicating attractive force from the yellow point, E) the selected force curve indicating attractive force from the green point. 85

Figure 96 Displaying another measured area of MLTT magnesite part with the respective force curve from the red circle in B. A) height image, B) deflection image demonstrating where the selected force curve is marked as a red circle on the red line, C) the selected force curve indicating attractive force..... 86

Figure 97 Demonstrating a measured area of ULTT with the respective force curves from the red and yellow circles in B. A) height image, B) deflection image demonstrating where the selected force curves are marked with red, and yellow circles on the red lines, C) the selected force curve indicating attractive force from the red circle, D) the selected force curve indicating attractive force from the yellow circle. 87

Figure 98 Displaying another measured area of ULTT with the respective force curves from the red circle in B. A) height image, B) deflection image demonstrating where the selected force curves are marked with red circle on the red line, C) the selected force curve indicating repulsive force from the red circle. 88

Figure 99 Illustrating a third measured area of ULTT with the respective force curves from the red and yellow circles in B. A) height image, B) deflection image displaying where the selected

force curves are marked with red, and yellow circles on the red lines, C) the selected force curve indicating repulsive force from the red circle, D) the selected force curve indicating repulsive force from the yellow circle. 89

Figure 100 Displaying the measured area in OBSV4_1. A) height image, B) force map from the height image, C) deflection image, D) adhesion map. Numbers in B and D indicating which curve number it is. Scale bar is 200 nm. 90

Figure 101 Displaying measured force curves from sample OBSV4_1 in the area in Figure 100. A) force curve number 1 with no adhesion, B) force curve number 3 displaying mismatch of trace and retrace curves, C) force curve number 6 with a little adhesion. See Figure 100 B and D for location of the curves and Chapter Force Spectroscopy Measurements for explanation of the lines. 91

Figure 102 Demonstrating a measured area in OBSV12 with one representative force curve. A) height image, B) force map of the height, C) deflection image, D) adhesion map, E) a representative force curve displaying adhesion. Scale bar is 400 nm. 92

Figure 103 Illustrating another measured area in OBSV12 with one representative force curve. A) height image, B) force map of the height, C) deflection image, D) adhesion map, E) a representative force curve illustrating adhesion. Scale bar is 300 nm. 93

Figure 104 Demonstrating a measured area of Unflooded Liège with the respective force curves from the red, yellow, and green points in B. A) height image, B) deflection image displaying where the selected force curves are marked with red, yellow, and green points on the red lines, C) the selected force curve indicating repulsive force from the red point, D) the selected force curve indicating repulsive force from the yellow point, E) the selected force curve indicating repulsive force from the green point. 94

Figure 105 Illustrating another measured area of Unflooded Liège with the respective force curves from the red, yellow, and green points in B. A) height image, B) deflection image demonstrating where the selected force curves are marked with red, yellow, and green points on the red lines, C) the selected force curve indicating attractive force from the red point, D) the selected force curve indicating attractive force from the yellow point, E) the selected force curve indicating attractive force from the green point 95

Figure 106 Displaying a measured area of Unflooded Liège with the respective force curves from the red and yellow circles in B. A) height image, B) deflection image illustrating where the selected force curves are marked with red, and yellow circles on the red line, C) the selected force curve indicating attractive force from the red circle, D) the selected force curve indicating repulsive force from the yellow circle. 96

List of Tables

Table 1 Displaying an overview of the selected samples for this study. 7

Table 2 Compiling the topography results. Samples with “-“ in mineral growth and dissolution are not flooded and there will therefore not be precipitation nor dissolution here. Samples

marked “Grenoble” have been measured on MFP-3D Origin, whereas the rest on NaioAFM at
UiS..... 96

Table 3 Demonstrating the force spectroscopy results compiled in a table. 98

Commonly Used Abbreviations

AC = Alternating Current

AFM = Atomic Force Microscope

EOR = Enhanced Oil Recovery

HC = Hydrocarbon

IOR = Improved Oil Recovery

N = Newton

Pa = Pascal

PV = Pore Volume

SSW = Synthesized Sea Water

UiS = University of Stavanger

V = Volt

Abstract

A highly attractive strategy within the hydrocarbon industry is improving the percentage of recovery from the reservoirs, called Improved Oil Recovery/Enhanced Oil Recovery (IOR/EOR). The Atomic Force Microscope (AFM) is a tool that can help understanding the surface and forces on the surface of a mineral or a specific material. The presented application of an AFM to hydrocarbon-related research is a rather novel study approach with restricted knowledge on beforehand. Hence, a major part of this study has been focused on general and introductory work in developing a methodology to determine certain characteristics of the grains. Rock-fluid interactions are a central part of EOR techniques using flooding of rock formations. Thus, this project was defined to test the applicability of an AFM for EOR research.

The studied samples are mostly chalk from Denmark and Belgium of Cretaceous age, both flooded and unflooded by specific fluids related to EOR research. Chosen mineral standards were kindly provided from the Department of Mineral Sciences, Smithsonian Institution for the sake of comparisons.

Topographic measurements indicate similar surface topography and morphology of most of the samples. However, some minerals in certain samples displayed differences. Magnesite in samples LTT1 and ULTT, chalk flooded with $MgCl_2$, reveal a more step-like structure than other minerals which had mainly rounded shapes with smooth edges. Other samples, LTT1, OBSV4_1, OBSV12_6 and OBSV18 disclose lath-shaped and rounded phases appearing on flatter surfaces of calcite and magnesite, interpreted to be clay. The interpreted new grown phases after flooding have a height of approximately 40 nm and grow mainly on top of the existing mineral grains, more towards the edges of the flooded core than the mineral. This may be an important feature in differentiating some carbonate minerals, but further studies are necessary.

Force spectroscopy results indicate both repulsive and attractive forces on the surface of the minerals. Ilmenite, magnesite, magnetite, and quartz indicate both attractive and repulsive forces in the area (5 x 5 micron) of the same mineral. However, anorthite, calcite, dolomite, and magnesite, in some samples, exhibit only attractive force, while fluorapatite and plagioclase display only repulsive force. This feature may be used to identify specific minerals as new grown phases. However, it has to be studied in advance, which minerals that are expected to grow, and have similar characteristics.

These results together shed lights on the need for more knowledge regarding this tool, as well as the importance of studies for further use. Nonetheless, the results are very promising as they can demonstrate different characteristics measured by the AFM as a consequence of the chemical composition of the phase. Changes of chemical compositions and forces at the surface are definitely parameters that affect wettability, which in turn, are of highest interest for the hydrocarbon industry. Sample preparation is essential, and within a longer research study, different approaches can be tested. Further studies should therefore include different preparations, as well as a variety of samples to gain more insights in the relationship of adhesion related to wettability and as well tests performed in liquids.

1. Introduction

As the energy consumption in the world is still increasing, the HC (hydrocarbon) industry will still be needed for decades as the replacing methods are not as sophisticated and well distributed to replace effectively the former (Philibert, 2017; Skovbjerg et al., 2012). However, the discussion about further exploration and production is intense, especially in regard of climate issues (Burkett, 2011). Improving the percentage of recovery from the reservoirs is therefore a highly attractive tool and is denoted as Enhanced Oil Recovery/Improved Oil Recovery (EOR/IOR). EOR is also called tertiary recovery, comprising mobility-control, chemical, miscible, thermal and other processes (Green and Willhite, 1997).

Reservoirs worldwide are relatively poorly depleted for HC commodities and a large potential lies in this methodological approach with even large amounts still deposited in reservoirs of chalks in the North Sea (Skovbjerg et al., 2012). A variety of EOR methods are implemented and others are still developed with usually waterflooding as the most effective IOR method besides injection of polymers (Hermansen et al., 2000). Around 50 % of the world's hydrocarbon reservoirs are trapped in carbonates (Strand et al., 2006) and especially for Norway is the research on carbonate and chalk still a major branch of the HC industry. The oil recovery from carbonate reservoirs are usually very low, less than 30 % worldwide (Strand et al., 2006) due to fracturing, low permeability and low water-wetness.

The Norwegian Government invests large sums in EOR and co-financed a center focused on this approach, called The National IOR Centre of Norway (Stavanger, Norway). Here, a variety of research groups work on different aspects of EOR and as well those concentrating on the rock-injection interaction (Borromeo, 2018; Minde, 2018; Wang, 2018). Within this research, mineralogical changes induced by injection are the main topics and a variety of methods have been developed (Zimmermann et al., 2017). One major aspect of releasing larger amounts of hydrocarbons during or after flooding a rock in most of the cases, here chalk, is to understand the surface conditions of the minerals. This effects the wettability significantly.

“Wettability describes the preference of a solid to be in contact with one fluid rather than another” (Abdallah et al., 2007). As previously mentioned, the carbonates are usually oil-wet or mixed-wet (Figure 1), however, preferentially they should be water-wet.

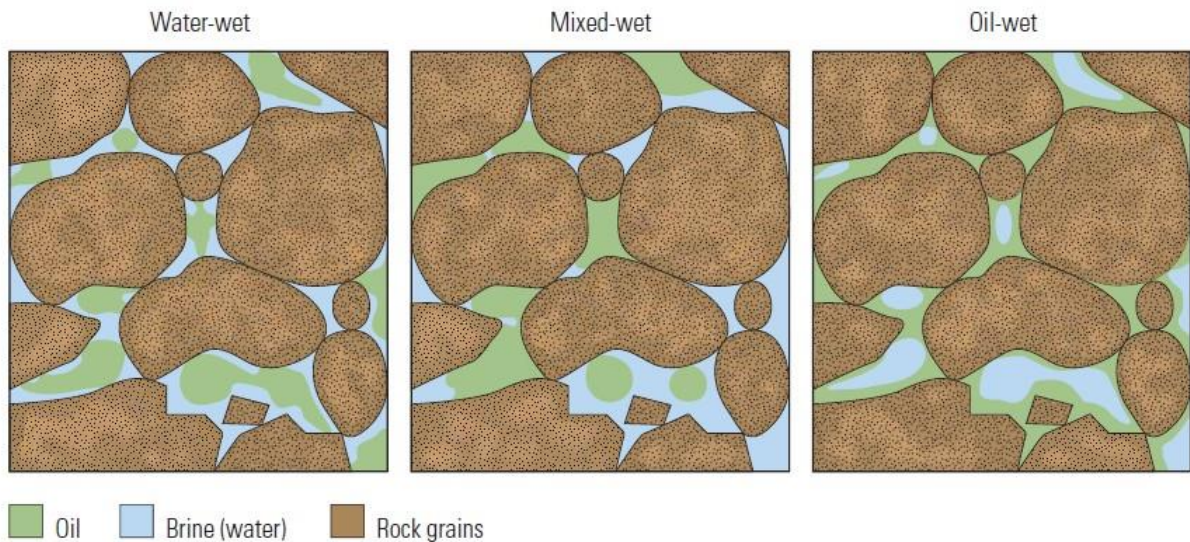


Figure 1 Schematic overview of fluid relations within a porous rock, where water-wet would indicate that water is in contact with the mineral grain while oil-wet rocks are those where oil is in contact with the rock. Left: Water-wet, middle: Mixed-wet, right: Oil-wet. In water-wet reservoirs the water would rather adhere to the grains while oil flow through, which gives higher oil recovery than oil-wet reservoirs. (from Abdallah et al., 2007).

Wettability is related to adhesion, thus it is a parameter induced on mineralogical grounds where crystallography and spatial arrangement of element govern the surface conditions in general and the charges and the surface charge of the mineral specifically. The minerals, and hence the rocks, have different adhesion characteristics to provoke or induce specific wettability conditions for specific fluids. The adhesion parameter(s) can be determined using an AFM (Atomic Force Microscope) as an expression of the surface charge.

1.1 Objectives and research strategy

The objective of the present study is to explore the surface charge/adhesion in different minerals, especially minerals to EOR and those of importance for the experiments executed at the National IOR centre at UiS (University of Stavanger) which is a relatively rarely taken approach and partly even a novel research. Thus, this study concentrates on chalk samples (Table 1) before and after so-called flooding, which is an experimental process to manipulate rock-fluid relations in changing fluids and induce mineral alteration (the detailed flooding test is described in Wang et al. (2016)). The samples will be analyzed with an AFM to observe morphology and measure different forces (repulsive and attractive) of primary and secondary minerals. From this, information regarding adhesion and possibly surface charge can be

derived. This is a rather novel study rarely used but has a high potential in the field of EOR (Borromeo et al., 2018; Skovbjerg et al., 2012). To complement and be able to relate the revealed data set, comparison data need to be collected from other rocks than chalk and different minerals than those dominating carbonates. Thus, a significant first data base of mineral characteristics collected by an AFM will be presented. This study will also result in an evaluation of the feasibility of AFM within the oil industry, especially in the field of EOR. In addition, as the method is novel, a manual for the analytical process at UiS with its available machinery will be provided.

To comply with these objectives, the sample collection for the applied material (EOR related samples) will be provided by experienced EOR researchers within the National IOR Centre of Norway (NIOR) at Stavanger. A variety of international mineral standards are used for comparison.

Nevertheless, the research would have been much more sophisticated and complete without the Corona crisis. The project included several visits at laboratories of Université Claude Bernard Lyon 1 and Université Grenoble-Alpes to apply state-of-the-art AFM techniques under perfect conditions. This was not possible, and the analytical approach had to be changed slightly with the use of the AFM (specifications see below in Chapter 2.4 Atomic Force Spectroscopy (AFM)) at UiS. This, together with the restricted access to the analytical equipment hampered the effectivity of the use. However, the rationale of the project is sufficiently attractive for academic and industry that the thesis was realized as it is. After the deadline of submission, these original aims will be fulfilled.

1.2 The Tool: Atomic Force Microscope

The AFM was developed by Binnig and Quate in 1986 with the aim of studying material surfaces (Chatterjee et al., 2010). It was later modified to be used for biological studies as well and has since been modified further for the use of other studies. The modification allowed in the most recent past to apply the microscope technology to samples related to EOR purposes (Skovbjerg et al., 2012). The detailed description of the functionality of the method will be explained in Chapter 2.4 Atomic Force Microscope (AFM). One of the usages of AFM in mineralogy is to detect the adhesion force and surface charges related to the elemental composition and bonding type of the elements. Hence, these characteristics enables to

differentiate between materials on a small scale. This property has been used for differentiating phases and hence is useful for the study of new growth of minerals during flooding experiments for EOR purposes (Madland et al., 2011; Megawati et al., 2015; Minde, 2018; Wang et al., 2016).

Skovbjerg et al. (2012) demonstrated results on chalk from different locations and the interaction with clays and other minerals at nano-scale. The different mineral charges were interpreted to be useful for further research if EOR could be focused on these specific characteristics. Changing surface charge of the minerals of the reservoir rock would change wettability and may release more oil (Punternold, 2008). This research follows that specific approach.

1.3 The Object: Carbonate and Silicate Minerals

Different types of rocks and minerals have been used in AFM analyzes in this study to build a larger database for the use of AFM. Chalk is the main rock type used, derived from a variety of locations in Belgium and Denmark (Chapters 2.2.1-2.2.3). This peculiar rock type is the main study object for EOR experiments at UiS, as giant HC reservoirs are surprisingly located in chalk. During those flooding experiments (Chapter 2.3 Flooding Experiment), a new growth of minerals could be observed. These minerals are very small, mostly of sub-micron size, therefore ideal study objects for the AFM, and earlier for a variety of other applications (e.g. Borromeo et al., 2018; Minde et al., 2019; Zimmermann et al., 2017, 2015). The minerals to be expected and proven, resulting from numerous experiments, are mainly calcite, magnesite, quartz and clay minerals (e.g. Andersen et al., 2017; Korsnes et al., 2013; Megawati et al., 2015; Wang et al., 2016). To understand and pinpoint their characteristics in the experimental process, the study compares those data with international standards and other comparative material. The selected mineral standards which have been studied to gain a larger database for this technique, include: anorthite, fluorapatite, plagioclase, magnetite, ilmenite, dolomite, and calcite. All the sample preparations were carried out in the geological laboratory at UiS after the sample material were received by the researchers from the National IOR centre.

The samples (Chapter 2.1; Table 1) were gathered at different outcrops in Belgium and Denmark. Some of them were flooded while others were not, and they have different abundances of carbonate and non-carbonate minerals (Chapters 2.2.1-2.2.3). All chalk samples

were deposited during Cretaceous times and chosen due to their similarity of mechanical behavior to reservoir chalk from the North Sea (Collin et al., 2002; Neramoen et al., 2016; Surlyk et al., 2006).

1.4 The Rationale: The Relation Between Mineralogical Composition and Rock Mechanical Properties

In 1969, the first oil field on the Norwegian continental shelf was discovered. This oil field was called Ekofisk, which is still one of the largest fields in Norway. The reservoir rock in this area is chalk, a rock with high porosity and low permeability, which increases with fractures (Feazel and Farrell, 1988). Chalk was an uncommon reservoir rock until the discovery of this field (Feazel and Farrell, 1988). This type of reservoir rocks had previously only been known from Austin, USA, but not offshore. As the rock is easily compacted, it was never suspected that it could be a reservoir rock, but rather often a seal rock. The surprise was therefore enormous when Ekofisk presented chalk as the reservoir rock, and thus introduced petroleum engineering into the issue of why we find HC in chalk.

The relation between rock mechanics and minerals is paramount to understand the occurrence of HC in chalk and to minimize rock mechanical mechanisms during and after exploitation with subsidence effects. This is a great opportunity to implement EOR in these rather reactive reservoir rocks. AFM technology is a puzzle piece in the understanding of this relationship to develop more sophisticated fluids (Madland et al., 2011; Strand et al., 2006; Wang, 2018), polymers (Gjersdal, 2018), fracturing (Bredal, 2018) or other mechanisms of EOR (Zimmermann et al., 2017).

Chalk is a marine, fine-grained carbonate sedimentary rock formed by nano- and microfossils called coccolithophores (Figure 2). The individual coccolith particles ranges between 0.3 and 0.5 μm in size (Hjuler and Fabricius, 2009), often organized in ring-like structure (around 1-3 micron). Other microfossils the chalk contains are nanoliths and foraminifera. The coccolithophores lived in temperate sea water and when they died, they sunk to the seafloor. The deposition of several layers with coccolithophores and other fossils on the seafloor accumulates as ooze. The accumulation of ooze is slow with a rate of 1 to 6 cm per 1000 years (Garrison, 2010).

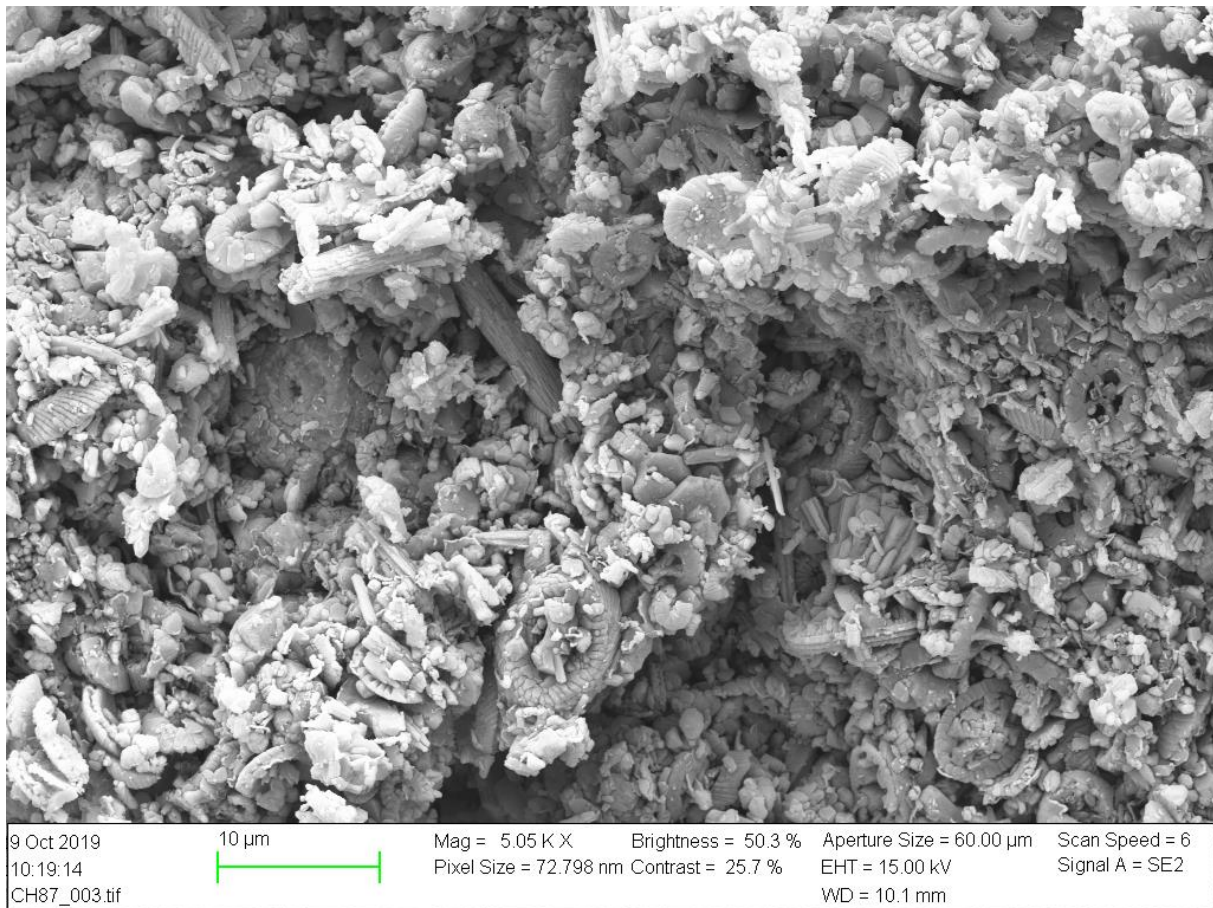


Figure 2 Coccolithophore in chalk flooded with synthetic sea water. (Kindly provided by Tine V. Bredal)

The chalk consists of mainly calcite (CaCO_3) but also some other minerals like quartz, opal, apatite, pyrite, dolomite, feldspar and different clay minerals depending on the facies and the geological framework may be deposited (Hjuler and Fabricius, 2009). Depending on the content of non-carbonates, the color of chalk varies, but is usually white to grey or beige. After Dunham's (1962) classification, the chalk, as a limestone, can be further classified as mudstone or pack-stone. Pure chalk is very soft and has a hardness of 3 on Mohs's hardness scale.

During the Cretaceous, the environment for the formation of carbonates and chalk was perfect as both the sea level and temperatures were high; high enough to call the period a greenhouse or even hothouse (Craig et al., 2009). The high temperatures were initiated by the paleogeographic distribution of continents and the occurrence of greenhouse gas producers related to plate tectonics as often seen after the breakup of a supercontinent, in this case Pangea (Craig et al., 2009; Eyles, 2008). Plate diversion caused the opening of the Atlantic Ocean (Scotese, 1991) and allowed simultaneously during sea level rise the formation of large epicontinental or marine basins where often chalk accumulation took place as a deep marine sediment. The warm climate triggered the melting of land-based ice, which again contributed

to the higher sea levels in this period. This resulted in a major transgression during this period which created optimal conditions for biological diversification. The high amount of marine organisms led to enormous accumulation of carbonate deposits and hence chalk formation. The fine-grained coccolith-rich mudstones were deposited in deep marine environments (Molenaar and Zijlstra, 1997). The sea level decreased from the Cretaceous until today which can be seen by less and less chalk deposition since the Cretaceous (Scholle, 1977), which coincides with lower temperature on Earth and the formation of large ice sheets. However, it seems very likely that anthropogenic influence disturbs this currently “normal” trend towards an icehouse.

2. Samples and Methodology

2.1 Overview of Samples

Chalk samples used for this study came from a variety of locations (Table 1) ranging from Upper Cretaceous to Cenozoic in age. The Chalk SK sample was prepared as both polished and unpolished, whereas the remaining samples, except the magnesite standard, were left unpolished (Chapter 2.4.2 Sample Preparation).

Table 1 Displaying an overview of the selected samples for this study.

Name of sample	Rock type	Flooded or not	Formation	Age
Chalk SK	Chalk	Not flooded	Stevns Klint	Maastrichtian
LTT1	Chalk	Flooded with MgCl ₂ , 1.5 years	Gulpen	Late Campanian to early Maastrichtian
OBSV18_1	Chalk	Flooded with NaCl	Saint Vaast	Upper Cretaceous
OBSV4_1	Chalk	Flooded with MgCl ₂	Saint Vaast	Upper Cretaceous
OBSV12	Chalk	Not flooded	Saint Vaast	Upper Cretaceous
OBSV12_6	Chalk	Flooded with sea water	Saint Vaast	Upper Cretaceous
Kaolinite	Kaolinite	Not flooded	Unknown	Cenozoic
MLTT	Chalk	Flooded with MgCl ₂ 2 years	Gulpen	Late Campanian to early Maastrichtian
ULTT	Chalk	Flooded with MgCl ₂ 3 years	Gulpen	Late Campanian to early Maastrichtian
Unflooded Liège	Chalk	Not flooded	Gulpen	Late Campanian to early Maastrichtian

2.2 Chalk

2.2.1 Liège: Gulpen Formation

One of the chalks used was deposited in the Gulpen Formation close to Liège, Belgium during late Campanian to early Maastrichtian (Molenaar and Zijlstra, 1997). This chalk sample was analyzed due to its mechanical behavior during reservoir simulation, hence comparable to chalk from Ekofisk (Collin et al., 2002). The Gulpen Formation chalk has a high carbonate content, approximately 95 %, whereas other minerals are mainly quartz, smectite and clinoptilolite (Hjuler and Fabricius, 2009).

2.2.2 Mons: Saint Vaast Formation

Another so-called analogue chalk, indicating chalks are supposed to be analogues to the reservoir chalk of the North Sea, are the rocks from the Saint Vaast Formation in the Mons basin (Belgium) with an Upper Cretaceous age (Nermoen et al., 2016). The samples are taken from Obourg quarry close to the town of Mons. Chalk from Saint Vaast Formation contains 95 % calcite whereas the other minerals are chlorite, quartz, iron oxides and pyrite.

2.2.3 Stevns Klint: Stevns Klint Formation

The chalk from the Stevns Klint Formation from the Upper Maastrichtian is found close to Copenhagen, Denmark. The chalk is a stratigraphic correlative of the Tor and Ekofisk formations in the North Sea (Surlyk et al., 2006). The chalk consists of 98-99 % carbonates and is the mineralogically cleanest chalk in this study (Megawati et al., 2015). Other occurring minerals are quartz, smectite and mica (Hjuler, 2007).

2.3 Flooding Experiment

The flooding experiments were done prior to this thesis (Abubeker, 2013; Geitle, 2013; Minde et al., 2019; Nermoen et al., 2015; Zimmermann et al., 2015) and the author has not performed them. A brief description of the experiments will follow, modified from Wang et al. (2016), as this gives the reader a broader understanding to the differences in the samples.

Chalk from different outcrops were sampled by taking large blocks that could be used for further analyzes. Back in the laboratory, cylindrical samples were drilled from large blocks and grinded into cylindrical cores of about the same size (ca. 7 cm long and 2.5 cm in diameter) from each outcrop. After the preparation, the cores were left to dry in a heating chamber for at

least 12 hours in 100°C. This was done to remove as much moisture as possible from the core before the dry mass could be determined. The drying conditions should not affect the calcite crystals. To find the saturated mass, the cores were first evacuated by vacuum and then saturated with distilled water. Using the dry mass and the saturated mass, the porosity can be determined. This experimental procedure was applied to all the cores that is flooded in this study. The set-up included tri-axial cells where the saturated cores were mounted. After the mounting of the cores, the confining pressure was increased to 0.5 MPa. Thereafter, the experiments were conducted according to the following stages:

1. The cores were flooded with three pore volumes (PVs) of distilled water at ambient temperature overnight. This was done to clean the sample and make sure all the salt precipitates were removed as this could affect the flooding tests. The geochemical properties of the core are not significantly altered by the flooding procedure.

2. A change in the flooding fluid was then performed, from distilled water to MgCl₂ brine and NaCl brine. This was done by attaching the piston cell into the flow loop. The flow rate was then set to one initial PV per day throughout the rest of the test.

3. Both the confining pressure and the pore pressure were increased to 1.2 MPa for MgCl₂ and 0.7 MPa for NaCl before the temperature was increased to 130°C. The pore pressure and temperature were both kept constant for the rest of the test.

4. By injecting hydraulic oil into the confining chamber, the confining pressure was increased from 1.2 MPa. The oil was injected at a constant flow rate. To slightly exceed friction of the piston, the piston pressure was set to 0.5 MPa during pressurization. The axial stress was then increased to be a bit above the radial stress. The confining pressure was increased until the stress - strain behavior of the rock became linear, i.e. when the rock started to deform plastically.

5. The axial deformation at creep conditions (constant temperature, stress, and pressure) was monitored during continuous flooding with both of the brines. The variation of confining pressure and pore pressure was within 0.1 MPa such that the effective stresses were stable throughout the test period.

Via a LabView programme, the pore pressure, confining pressure, piston pressure, hydraulic pressure difference, sample length and flooding time were logged continuously. The samples were first cleaned by injecting three PVs of distilled water, before dismantling the core. The

injection is performed to avoid precipitation of salts from the brines. After the dismantling, the saturated weight was measured and then the core was placed in a drying cabinet at 100°C. The core was weighed until the mass stayed constant. The cores were then cut into seven slices and used for geochemical analyzes and other analyzes.

2.4 Atomic Force Microscope (AFM)

An Asylum Research MFP-3D Origin AFM, located at Université Grenoble Alpes (France), was mainly used during this project. A Nanosurf NaioAFM is located at the University of Stavanger and has been used to compare with the topographic results from Grenoble¹. The main differences between the two machines are the chamber size and subsequently sample size (Chapter Sample Positioning). Another difference is the types of measurements the different AFMs can carry out. The MFP-3D Origin AFM can among other applications, measure in both, air and liquids using *contact mode*, *AC* (Alternating Current) *mode* and is able to carry out force measurements. The NaioAFM is able to be used for the same applications but cannot perform measurements in liquids. The size of the machine and equipment itself is also different; the NaioAFM is smaller and portable. However, the latter is more sensitive to noise and other disturbances in the surrounding environment, and thus, the measurements are more likely to be affected. The MFP-3D Origin in Grenoble is standing on a very special vibration table to minimize vibrations which has a significant impact on the results. The NaioAFM, on the other hand, has an integrated vibration isolation, which is less effective. One result of the study is the identification of this shortcoming, which will be corrected for to gain more effective analyzes at UiS. The NaioAFM locates single grains on a mount easier than the MFP-3D Origin AFM. Sample measurement, in turn, is twice as long with the NaioAFM than with the MFP-3D Origin AFM².

¹ However, due to Covid-19 and travel restrictions as well as total closure, the AFM at UiS was then used for all of the original work, and comparison has only been possible in a pilot state. This will be improved after the crisis is over; however, hampering the presented thesis.

² This affected also the thesis project, unfortunately; as the planned amount of samples having measured at UiS was not the number we have planned to perform, which would have been much more effective in Grenoble. University closure and the general lock-down also hampered the number and effectivity of the measurements.

2.4.1 The Application

An Atomic Force Microscope (Figure 3) with a resolution of nanometer analyzes the surface of a sample, for example a rock, a mineral, a cell, metal or DNA. The AFM uses a cantilever with a very sharp tip to scan over a sample surface. As the tip approaches the surface, attractive force between the surface and the tip causes the cantilever to deflect towards the surface. A laser beam is used to detect the cantilever deflections towards or away (up/down) from the surface. By reflecting the laser on the flat top of the cantilever, any cantilever deflection will cause slight changes in the direction of the reflected beam. A position sensitive photo diode can be used to track these changes and measure lateral and vertical motion. Thus, if an AFM tip passes over an elevated surface feature, the resulting cantilever deflection and the subsequent change in direction of the reflected laser beam is recorded by the photo diode (Figure 4). The AFM, by using a feedback loop, controls the height of the tip above the surface thus maintaining constant laser position.

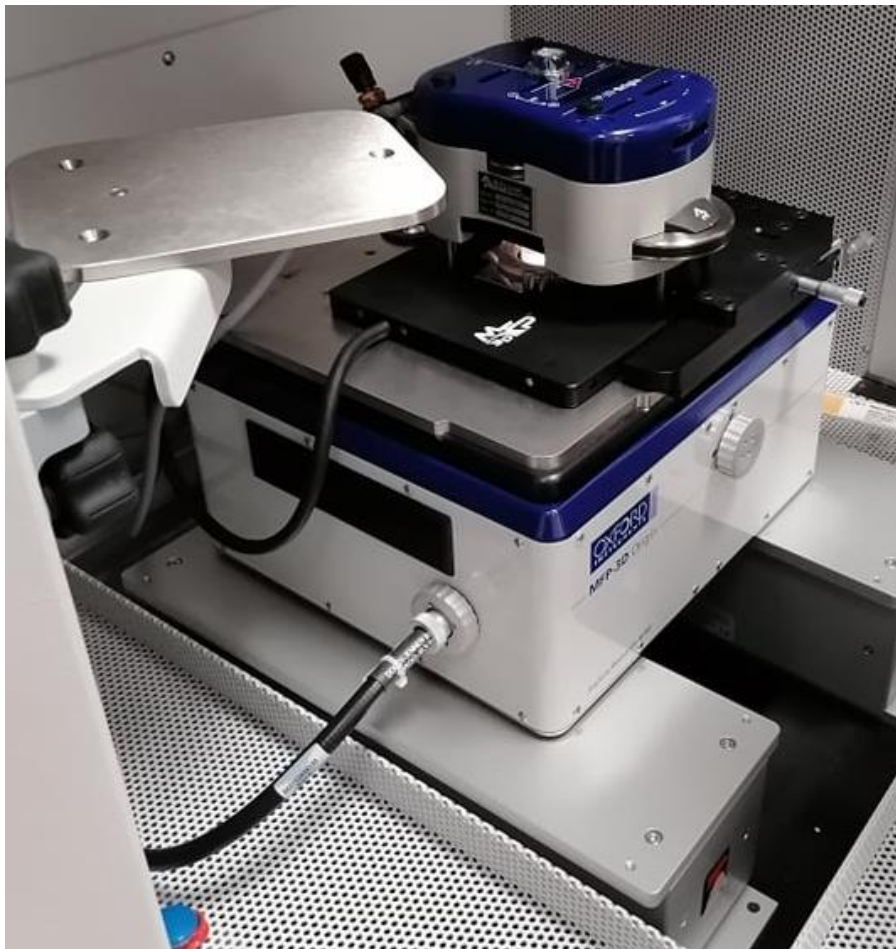


Figure 3 Atomic Force Microscope set-up in Grenoble placed on a special movement resistant table.

Therefore, the AFM can generate an accurate topographic map of the surface features. The information gathered are on micro- to nanometer scale and with atomic resolution, which makes the images more detailed than e.g. images from Scanning Electron Microscope (SEM). Another big difference to other microscopes is that the AFM also measures in Z direction, the height, whereas most alternative microscopes record images in 2D. The AFM can do measurements in air, liquid, vacuum and different gases (Butt et al., 2005).

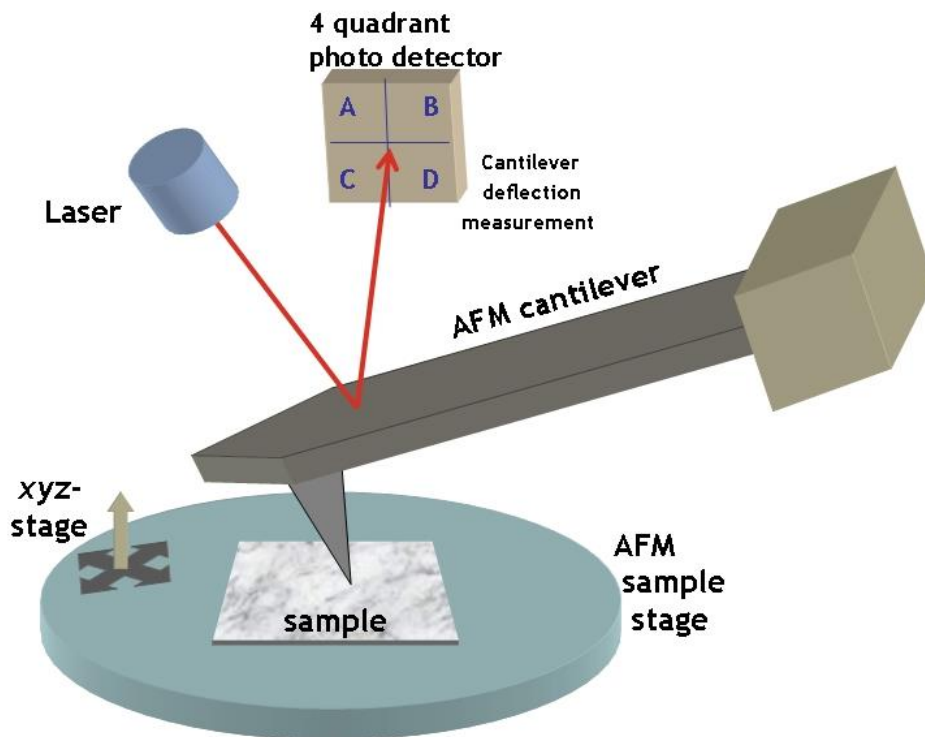


Figure 4 Schematic representation of the functioning principles of an AFM. (from “Nanotechnology - Wikibooks, open books for an open world,” 2018).

The AFM has several possible utilizations, where force measurements and topographic imaging were used in this thesis.

Imaging

Two different imaging modes were used, the *contact mode* and the *AC mode*, which is also called *tapping mode*. In *AC mode* or *tapping mode*, the cantilever oscillates at its resonance frequency close to or near the surface. The AC mode, named from alternating current, can also be executed in both air and liquid. If the goal is to observe dissolution or growth *in situ*, doing the measurements in liquid would be most effective. The force or oscillation of the cantilever does not need to be that extreme in liquid. This is important to have in mind before starting

measurements. AC mode works in some ways similarly to contact mode. Due to interaction between the tip and the sample, the oscillation changes when the tip approaches the surface of the sample. Hence, a damping effect of the cantilever oscillation takes place. Both the frequency and the amplitude of the oscillation experiences a reduction due to this effect. As in contact mode, the Z height is adjusted via the feedback loop, ensuring the tip is always at the same distance to the sample. In AC mode, the output images comprise three different parameters: height, amplitude, and phase. The amplitude image is similar to the deflection image and can be used for the same purposes as the latter (Figure 5) (Eaton and West, 2010). The phase image can characterize the difference between unlike materials based on a change in oscillation, but it is not necessarily possible to identify (in the sense of unambiguous) the different materials. Both phase and amplitude images detect the change in oscillation (Eaton and West, 2010).

In *contact mode*, the tip is in constant contact with the surface of the sample, being “dragged” over it. The *deflection/force* of the cantilever is constant while raster scanning. The mode can be performed in both air and liquid. The output from the contact mode with a constant force are two types of images: a height/topography image and a deflection image, where the deflection is also called error signal. When the cantilever is in a relaxed position, the Z actuator (Figure 4) is fully retracted. The difference output from the photo detector is zero when it is aligned to the laser beam which is centered. The cantilever is deflected from the zero-position if it is registered as a non-zero voltage. The zero-position means the center of the photo detector. Then a setpoint voltage has to be set, necessarily one that matches a certain deflection. The Z actuator is controlled by the Z feedback loop, which tries to keep the stated setpoint voltage. When there are changes in the deflection voltage compared to the setpoint, the Z actuator obviously changes. During the raster scanning, the Z feedback keeps the deflection constant. When the topography of the sample has abrupt changes, the Z feedback can over- or under-compensate. Hence, the deflection voltage is less or greater than the setpoint voltage and it extends or retracts the Z actuator, respectively. Therefore, the deflection is also called the error signal (Asylum Research, 2018). This output characteristics is helpful to detect minute details that will not be sensed in other output schemes, like the height and output schemes from other modes (Eaton and West, 2010). The contact mode is the fastest of the modes, as there is no summing of oscillation measurements required, which means the tip will be in full contact with the surface instead of the intermittent.

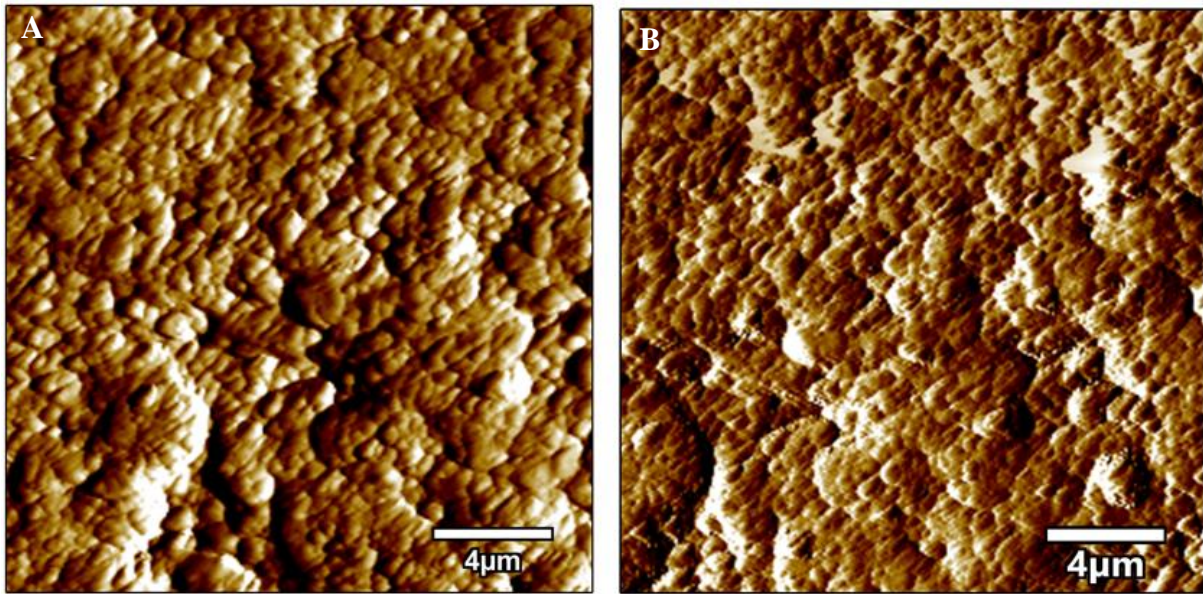


Figure 5 Comparing deflection image (A) and amplitude image (B) of the same area taken from the unpolished sample Chalk SK.

Force Spectroscopy Measurements

One of the other skills the AFM offers, is the ability to carry out force measurements. Force spectroscopy is used to study the interaction between the tip and the sample (Asylum Research, 2018; JPK instruments, 2020). Force measurements are carried out in contact mode, but the tip is only in contact with the surface in one single force measurement, while during topographic imaging the tip moves over a larger area of the surface. The difference between force measurements and topographic imaging is therefore the object of measurement. Using the latter, the interaction between the tip and the sample is measured. The output is a graph, called a force curve. A force curve (Figure 6) demonstrates how the cantilever and the tip is approaching the surface, it illustrates how both are interacting with the surface and when the tip retracts. Point B (Figure 6) is the point where the tip interacts with the surface, also called snap-in point. Here, either an attractive force or a repulsive force is working at the surface. The tip will touch the surface regardless, but with a positive lower error signal there are repulsive forces between the tip and the surface, and with a negative lower error signal there are attractive forces. At one point during the retraction, adhesion between the tip and the sample can be measured. This is the point when the tip is still attached to the surface and is in the process of detachment (point E in Figure 6). The force curve usually displays force or deflection (Y axis) *versus* the distance from the tip to the sample (X axis). If the graph displays deflection, the force (F) is obtained by multiplying the spring constant of the cantilever with the deflection of the cantilever.

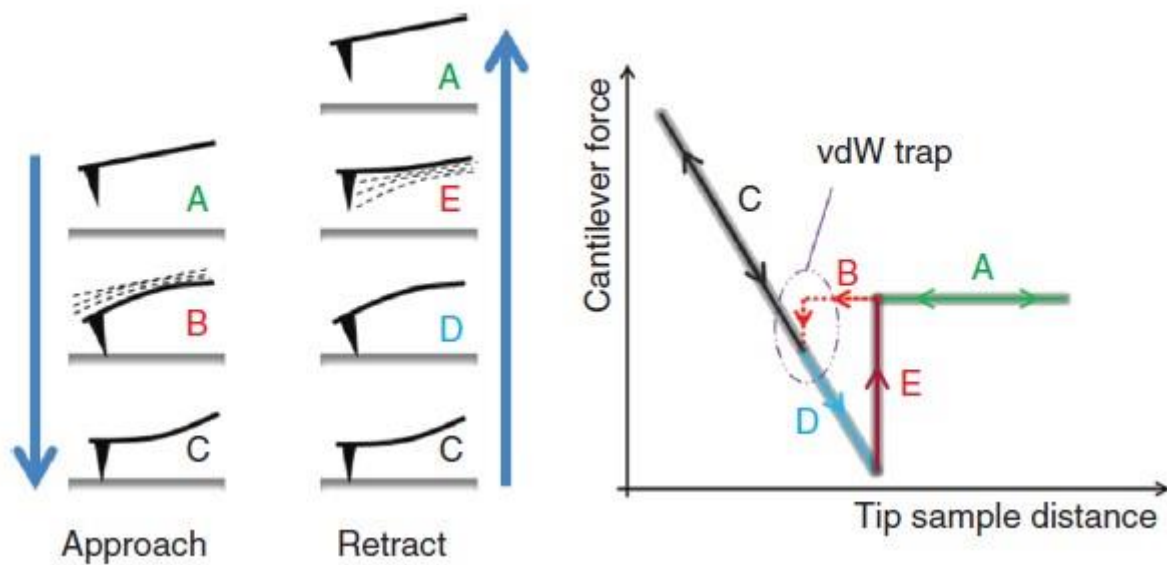


Figure 6 A standard force curve demonstrating the different steps of the cantilever approaching (point A-C) and retracting the sample. (from Javadpour et al., 2012).

There are differences in the force curve outputs from the MFP-3D Origin in Grenoble and the NaioAFM at UiS. An example of the different curves can be seen in Figure 7, with the curve from MFP-3D Origin to the left and from NaioAFM to the right. From MFP-3D Origin, the approach is the red line and the withdraw/retract is the blue line, whereas for the NaioAFM, the black line is the approach and the gray line is withdraw/retrace. The biggest difference is the Y-axis. Using the MFP-3D Origin, this axis displays force (measured in Newton) while NaioAFM measures the cantilever deflection/error signal (measured in Volt). This indicates that the MFP-3D Origin first measures the cantilever deflection, calibrate the cantilever spring constant, and then the software converts the output to force using Hooke's Law ($F=-kx$, where F is force, k is spring constant and x is distance). This has not been done with the NaioAFM due to limited expertise regarding software and application. Planned training courses were not able to carry out because of the crisis, and the force spectroscopy results from the different AFMs will therefore not be compared.

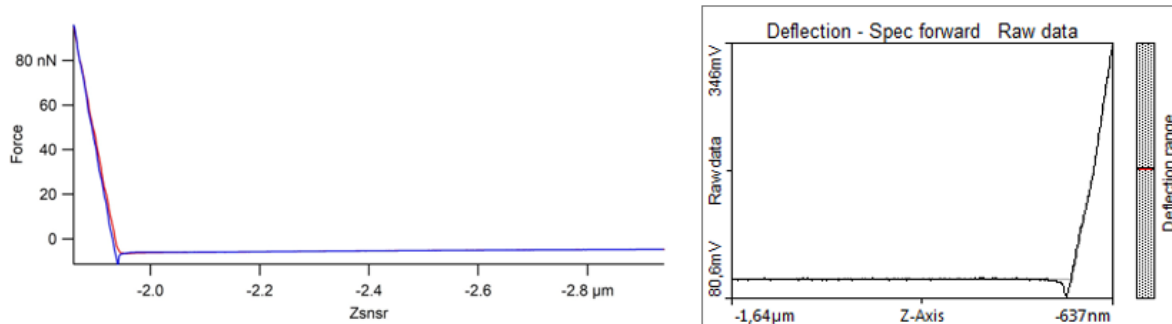


Figure 7 Demonstrating two different force curves from MFP-3D Origin (to the left) and from NaoAFM (to the right).

Preparation of the AFM

Before starting with measurements, the tip must be attached to the head of the AFM. This is done differently on each machine but in rather similar fashion on different models. The tip will be fixed with a simple screw (Figure 8), tightened sufficiently to prevent the tip from falling off. It is important not to force tightness as the tip breaks easily. This procedure is a meticulous process because of its tiny size. The tip must be placed in the middle (Figure 8) and straight, to receive the most effective measurements. The tips that have been used in this project are silicon tips, type PPP-CONTR-10 and PPP-NCHR-10 in Grenoble and type ACLA-10 in Stavanger.



Figure 8 Correctly placed tip (red circle) before placed on the head of the MFP-3D Origin AFM.

The tips are most effective while they are sharp. The more often tips have been used, the more rounded it gets, which may affect the measurements. Experienced researchers know when the tip needs to be changed based on the image quality (Figure 9), which is somewhat unsatisfying for a user starting with the method.

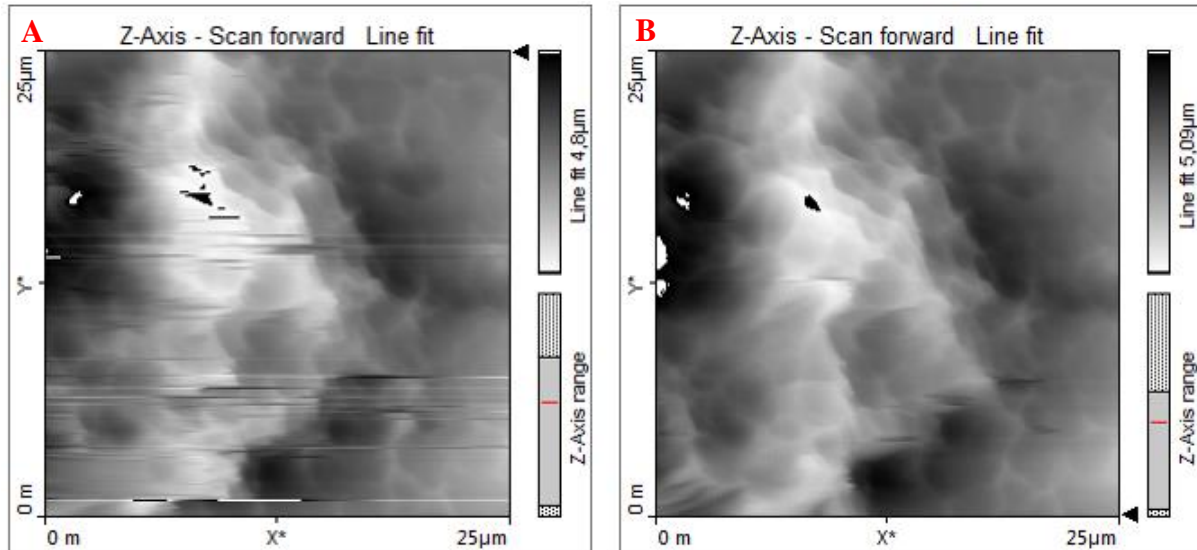


Figure 9 Illustrating an example of a poor quality height image (A) versus a good quality height image (B) using the NaioAFM at UiS.

Sample Positioning

Firstly, the sample is prepared in the laboratory and then placed on a glass plate in the AFM (Figure 10) with double sided tape to ensure it will move during measurements. The samples have to fit in the sample chamber in regard of its dimension. The samples used in this study in the application at Grenoble measured 2.5 cm in diameter with height up to 1 cm. In Stavanger, the diameter was similar, but the machine allowed only 1 mm in height, which is a serious restriction. The AFM at Université Grenoble Alpes (MFP-3D Origin) has a chamber that is large enough to take samples that are slightly larger than the ones in this study, but the height should be less than 1 cm to get the best quality on the images. However, even though the samples can be relatively large, the scanning area is smaller than 80 x 80 µm. Thus, there is no need to have large samples, but sample preparation may then be an issue cutting down sample sizes, however, that depends on the study objects. The AFM at UiS (NaioAFM) (Figure 11) can only take smaller sized samples. Nanosurf NaioAFM brochure (2019) state that the maximum sample size/height can be 12 mm/ 3.5 mm, whereas the maximum scan range is 70 µm, although the machine allows space for sample with a diameter of 25 mm, but then the measurements are

not possible in the middle of the sample as the head of the AFM is not possible to place properly. The size of the features that can be observed and detected with the AFM at UiS and in general, can be less than 100 nm, however the sample itself has to be large enough for it to be possible to distinguish the location of the sample under the head.

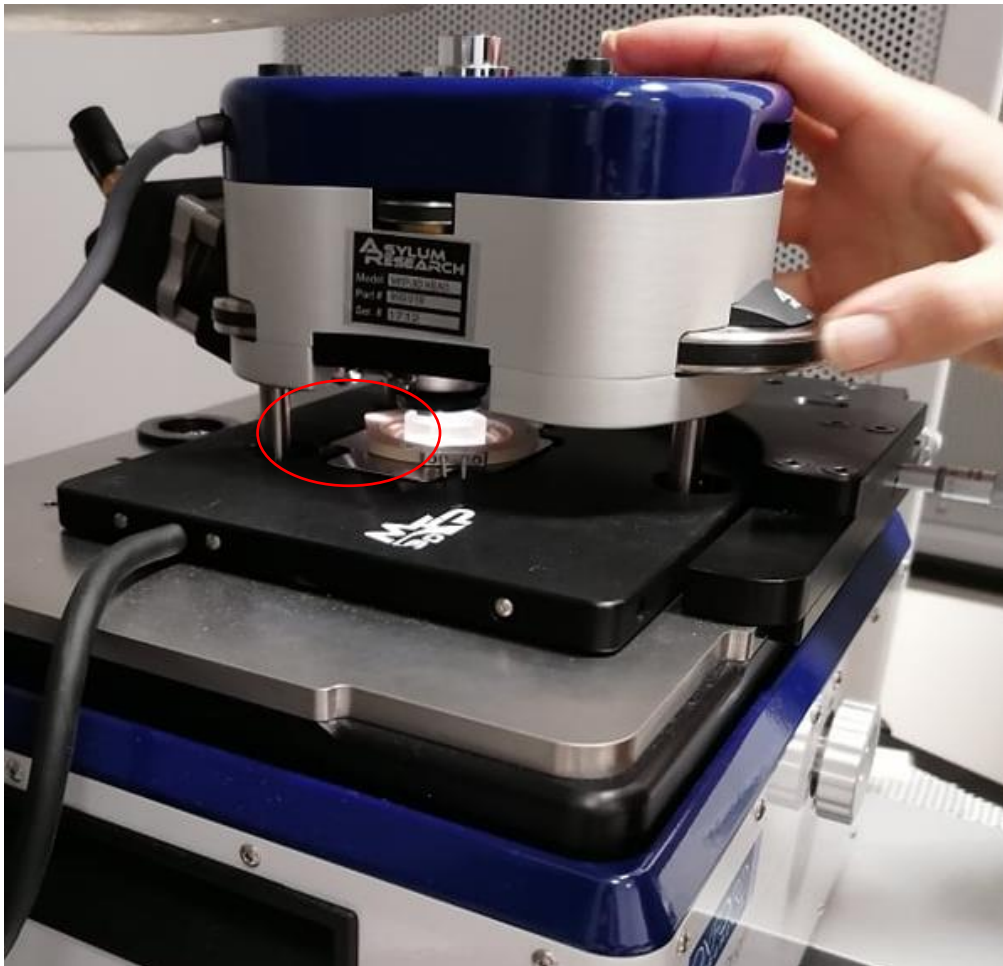


Figure 10 Sample placed on the sample holder (red circle) while adjusting the height of the legs of the head.

After the sample is placed on the sample holder, the head is put on top and then the legs are adjusted in height to make sure the tip is close enough to the surface of the sample. The deflection is set to 0, Z voltage to 75-80 volt and with these tips the sum (amount of light collected by the photodetector in volts) is usually around 6, before other parameters are adjusted within the software.

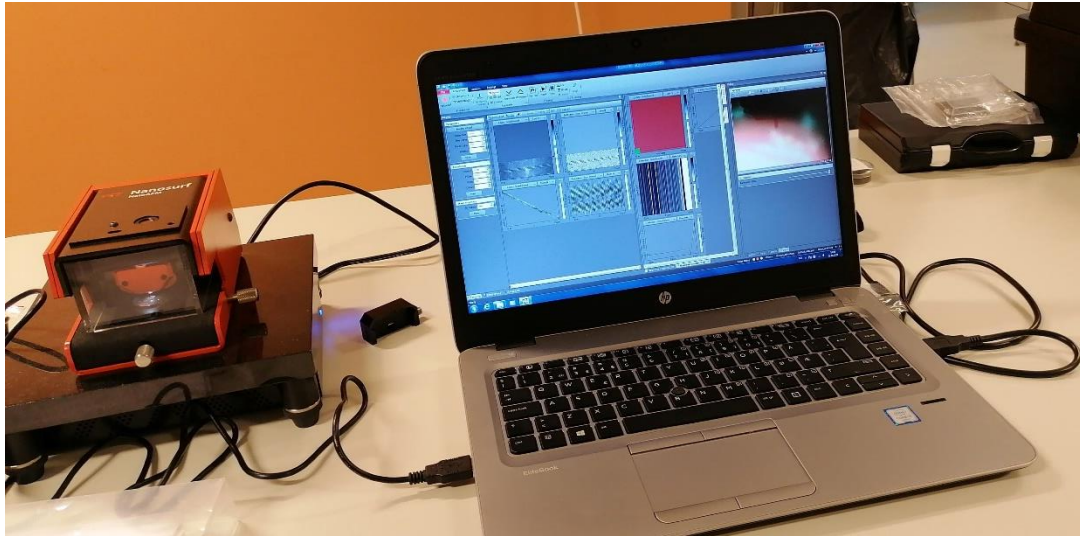


Figure 11 Set-up of the AFM at UiS. AFM to the left and software to the right.

Calibration of the Cantilever

The spring constant of the cantilever has to be calibrated using the thermal noise method before starting with force measurements at the AFM. This method is the most adequate for calibration in air and can be done rather efficient in the software with three steps (Asylum Research, 2018):

1. Correct for Virtual Deflection effects in the AFM hardware.
2. Calibrate InvOLS (Inverse Optical Lever Sensitivity, the relationship between the vertical cantilever motion and the cantilever deflection. This is measured in nm/V).
3. Then withdraw the tip and calibrate the tip spring constant by determine the thermal resonance frequency of the tip.

Measure Mechanism

AFM is time-consuming as 256 scan lines with 1 Hz (Hertz) scan frequency need around 4 minutes to be applied (MFP-3D Origin), more scan lines and lower scan frequency would extend the measuring time. If the sample surface is too large, the selection for a productive area for imaging and measurement could take time. However, the more time is invested, the images improve.

AFM analyzes are non-destructive, which is an enormous advantage when studying rather precious objects from archeological context, for instance. A sample can therefore be used several times, both in the same machine but also for other experiments prior and after the AFM study.

2.4.2 Sample Preparation

The sample preparation is for both applications, and in general, possibly one of the most important issues, but also the most difficult part when working with the AFM. Samples were prepared with both polished and fresh surfaces to be able to observe different properties of the study object. The samples were cut with an Accutom saw (Figure 12A) at UiS to get a fresh surface. One of the samples was then polished with a Struers Rotopol-35 polisher (Figure 12B) with the finest polishing of 1 micron polishing powder. It is important that the surface is as flat as possible to gain the best results. At the same time, the sample height is of importance, as described above (Chapter Sample Positioning), because the legs of the scanner head (Figure 13) are not longer than a few centimeters. The size of the sample should not be too large, as described, because the scan size of the AFM is usually only 80-150 μm and therefore not necessary but may be feasible during the preparation process. When carrying out experiments in liquid environments, the sample cannot be higher than a few millimeters.



Figure 12 Accutom saw (A) and Struers Rotopol-35 (B) are necessary to cut and polish the samples and mounts.



Figure 13 Scanning head of the AFM in unloaded position with the visible short legs.

Some standards of different minerals, which have been used in this study, were mounted as one single grain for each mineral on two different sized circular plastic plates using adhesive tape. With the help of Carl Zeiss Stemi DV4 binocular with LED illumination the mounting process was performed as it was possible to identify and mount the small grains (Figure 14). One grain

was taken out of each container and placed carefully on the tape with a straight micropick of 18.4 cm length. The grains were placed alphabetically by name to ensure effectivity during the analysis later. After all the grains have been placed, a cylindrical FixiForm was placed on the larger circle area. Epoxy resin mix was poured into the cylindrical form and then left to harden for at least 24 hours. The hardened mount could then be pressed out from the cylindrical form and subsequently polished on both sides: first by hand and then by machine, a Struers Rotopol-35 Figure 12B. One mineral, the magnesite, was already prepared before arriving at UiS. The preparation method is unknown, but it was set in epoxy and polished.

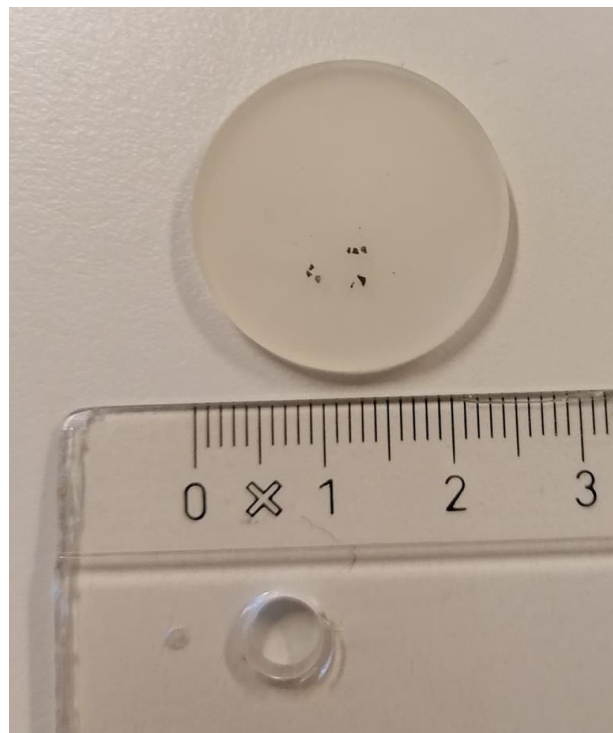


Figure 14 Displaying a mount with some of the mineral standards mounted.

A Gatan Model 601 Tuned piezo Cutting Tool (Figure 15) was used as another method to prepare samples. This instrument was used on thin sections of the chosen samples by drilling holes to collect small mini-cores which may be utilized for analyzes. First, a specimen table was placed on a hot plate (130°C) before applying wax. A glass plate was placed on top of the wax, before more wax was applied, followed by the chosen thin section. The construct had to cool down completely before continuing.



Figure 15 Set-up of the Gatan Model 601 Tuned piezo Cutting Tool. Hot plate in the front (with the specimen table on top), disc cutter back to the left and microscope back to the right.

The next step required positioning of the sample with the specimen table on a magnetic base under an optical microscope. The microscope allowed in determining the exact desired position of the location of the drilling hole. The specimen table was then carefully transferred to the platform of the cutter without changing the position of the sample.

The cutting of the thin section was carried out with a disc cutter. To perform this, firstly a slurry was made from cutting grit and water on top of the thin section, before the cutting tool was lowered into the slurry. The power of the cutting tool was turned on and the cutting process performed during adjusting the cutting rate to not harm the sample. The specimen table with the glass plate and thin section had to be reheated to be able to remove it from the wax. Final cleaning then allowed for the use in the AFM.

A third method was attempted to prepare samples. A Dremel mounted on a rack was going to cut out small circles of the thin section, but it was not stable enough and the glass broke, destroying the rest of the thin section. Hence, this method is by far too rough for the objective presented in this study and is not recommended.

Process steps which hamper the sample preparation

Contamination must be held to a minimum, preferably avoiding any contamination at all. There should be no touching of the surface of the sample as imaging would display this later on. Ideally, the sample should be stored in a closed container when not in use. The sample needs to be accurately fixed to a surface to prevent it from moving during the experiment. If it is not properly attached to the surface, the movement of the sample may lead to distortion in the image (Eaton and West, 2010). When the sample is fixed in epoxy, the use of double-sided tape to stick it to the glass plate or sample holder is, however, tested and found sufficient as seen in Figure 16.

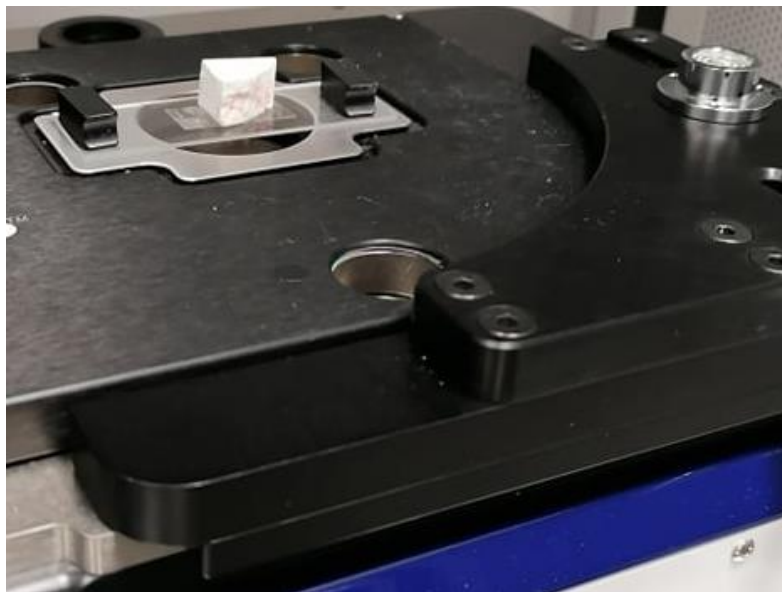


Figure 16 Sample placed on the glass plate, fixed with double sided tape.

3. Results

All the samples in this study have been prepared by the same method (Chapter 2.4.2 Sample Preparation). It is important to notice that there are differences in the output data sets and imaging qualities, as described from the different AFMs (MFP-3D Origin AFM (Grenoble) and NaioAFM (UiS)) (Chapter Measure Mechanism). In the samples measured in Grenoble, the exact measured location in the machine is not known, only approximately due to the larger

head. At UiS, the head is smaller and therefore it is easier to locate the different measured areas if this is needed for the objective of a study. The selected images in this chapter are chosen as a representative selection for each sample. More measurements can be found in Appendices 1 and 2. Few characteristics are below elucidated to avoid long explanation in captions and belong to the result section as they often are related to the fact of gaining a methodology for the use of the NaioAFM; which has never been operated besides in this pilot study, and hence, are “results”. The NaioAFM was mainly used unless specifically mentioned that it was the MFP-3D Origin.

3.1 Topography

The darkest colors in the images display lower seated features, those that are farther away from the observer, while lighter colors display features that are higher and therefore closer to the observer. This is the same for all the images from MFP-3D Origin AFM (Grenoble) throughout the thesis, whereas within the images from NaioAFM (UiS) darker colors indicate higher features and lighter colors reflect lower sitting ones.

3.1.1 Standards

A selected variation of minerals has been chosen to study in this thesis. Some were chosen due to their relevance for chalk while others to try to build a library with information of how the morphology and adhesion appears on the different minerals. Some of these standards were kindly provided by the Department of Mineral Sciences, Smithsonian Institution. These are NMNH 137041 Anorthite, NMNH 136321 Calcite, NMNH R10057 Dolomite, NMNH 104021 Fluorapatite, NMNH 96189 Ilmenite, NMNH 114887 Magnetite, NMNH R17701 Quartz. The rest were bought from IAGeo Limited.

Anorthite

Anorthite is a Ca-enriched plagioclase and from Figure 17 the features on the anorthite grain can be observed as rounded and smooth. The height image (Figure 17A) indicates only 443 nm height difference. The deflection image (Figure 17B) displays the features but also some noise due to the measurement environment. The features have different sizes ranging from 680 nm to 1.7 μm in length.

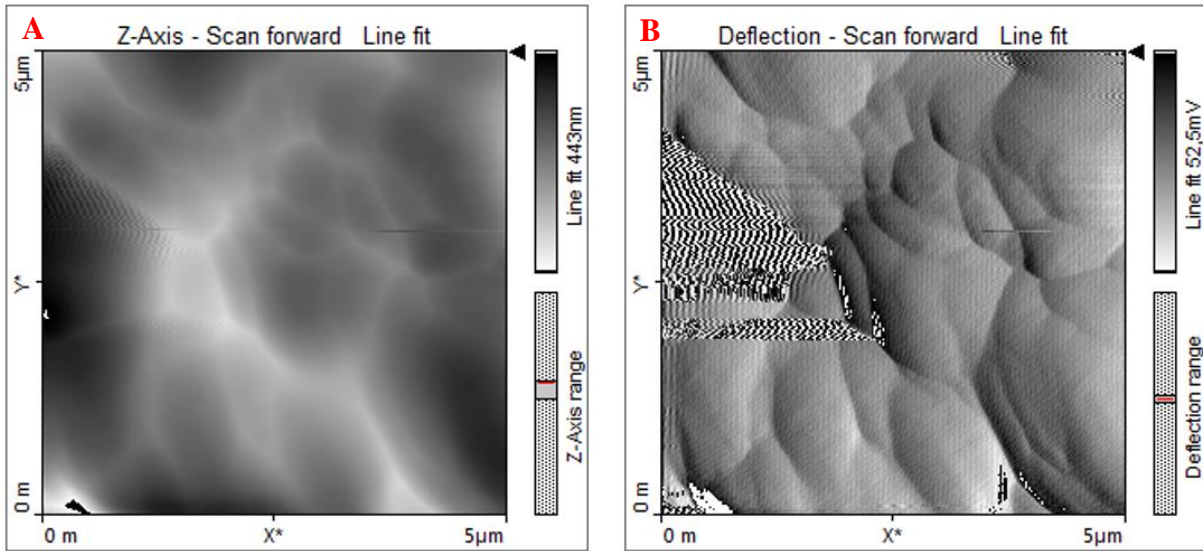


Figure 17 Demonstrating a standard anorthite with an area of $5 \mu\text{m}^2$. A) height image, B) deflection image. Noise to the left in the deflection image is due to the measurement environment.

From Figure 18, the height image (Figure 18A) indicates a slightly higher height difference, 457 nm, and the deflection image (Figure 18B) displays larger features than in the previous area. The largest feature here is $3.45 \mu\text{m}$ and the smallest around 474 nm . The features have the same shape as the previous area, rounded and some elongated geometries, with smooth edges and seem to follow a specific orientation from top left to bottom right.

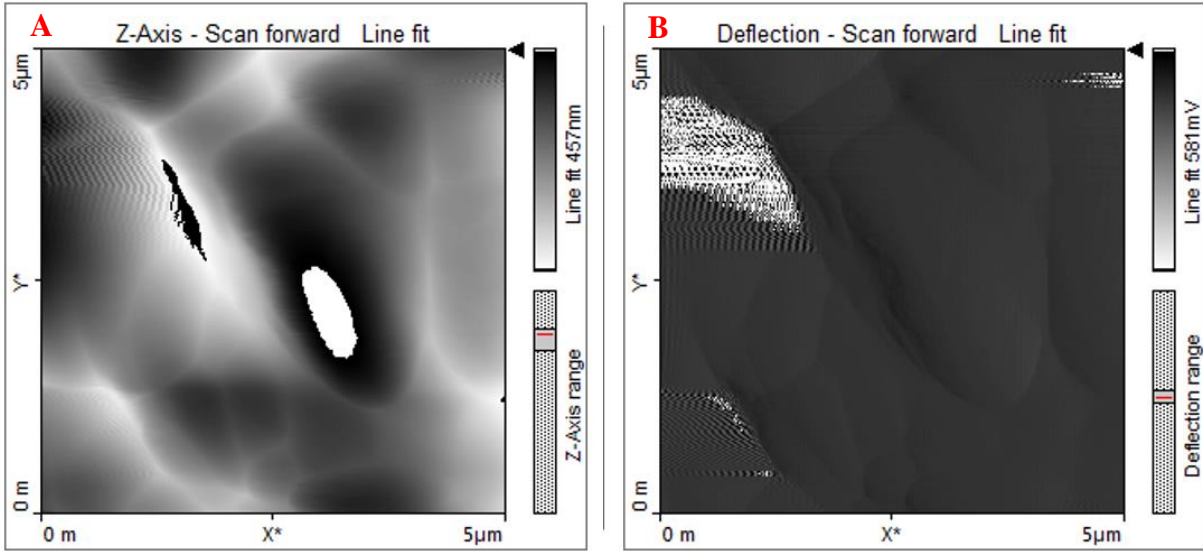


Figure 18 Illustrating a standard anorthite with an area of $5 \mu\text{m}^2$. A) height image, B) deflection image.

Calcite

Calcite is the main component in chalk and is therefore chosen as one of the minerals to be focused on within the standards. From Figure 19B, features can clearly be seen. These types of features have a rounded shape with smooth edges, differentiating in size from approximately $1\ \mu\text{m}$ to $2.8\ \mu\text{m}$. Some areas look flatter than the other areas, as marked with a red circle (Figure 19B). Both images display signs of noise caused possibly by an over-used tip due to several measurements without changing. It seems that the features lie close to each other with no interpretable mineralogical-based space in between, demonstrating the surface of the investigated calcite grain. The optical difference to the above shown anorthite is straight forward regarding size and orientation of the features.

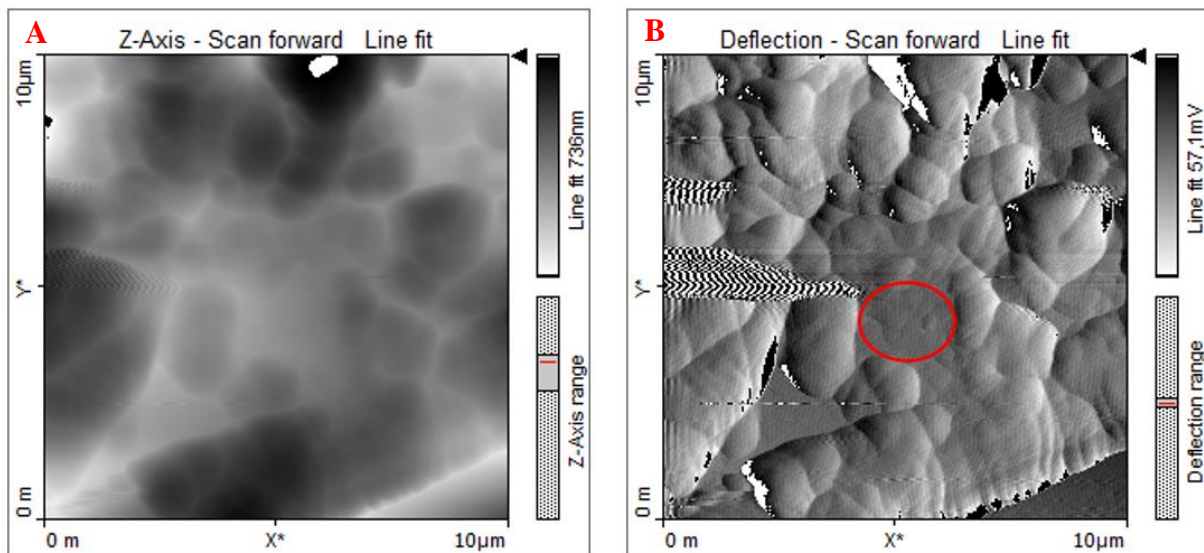


Figure 19 Standard calcite with an area of $10\ \mu\text{m}^2$. A) height image, B) deflection image. Red circle indicating a flatter surface than the surroundings.

Figure 20 has higher resolution than Figure 19 and displays an area of $5\ \mu\text{m}^2$. The rounded features with smooth edges are clearly seen, with the flatter surface located to the left in the deflection image (Figure 20B). The height difference is only 239 nm (Figure 20A) clearly displaying the highest features.

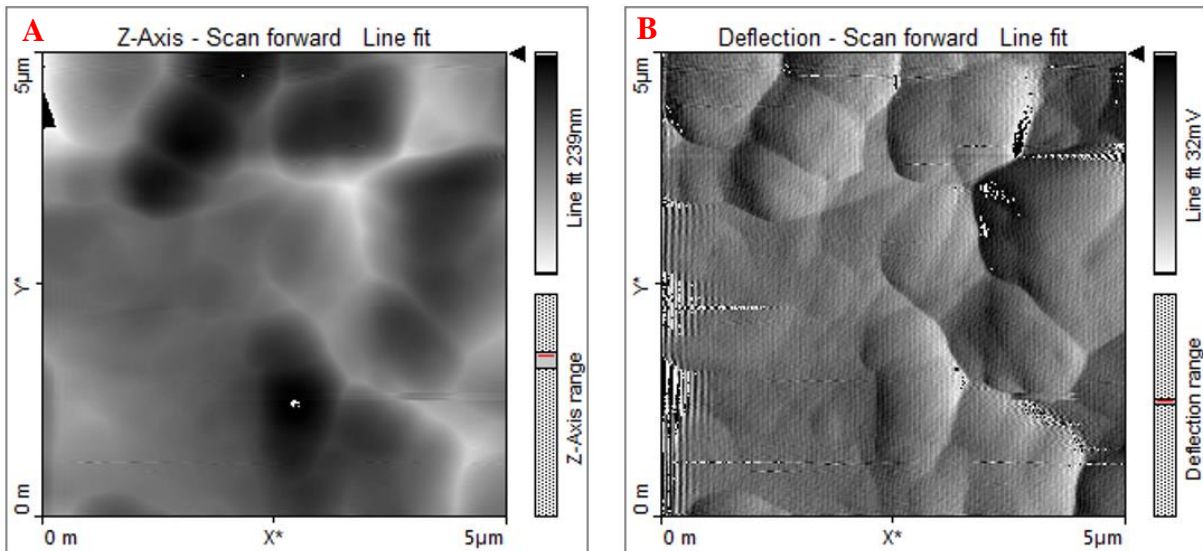


Figure 20 Displaying a standard calcite with an area of $5 \mu\text{m}^2$. A) height image, B) deflection image.

Dolomite

The dolomite grain in Figure 21 can be described as rounded features with smooth edges of different sizes. The size of the features ranges from 60 nm to $2.2 \mu\text{m}$. Some of the features lie together as one larger feature, whereas other lies by themselves. The features do not look oriented in a specific way and only two of the features are clearly higher than the rest (the darker areas in the height image, Figure 21A).

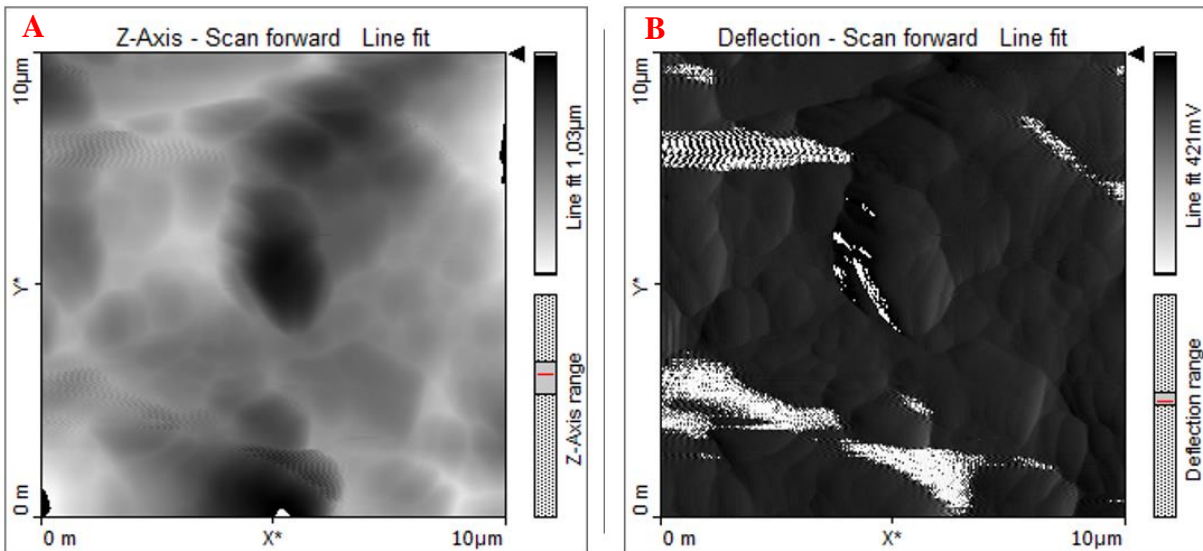


Figure 21 A standard dolomite grain with an area of $10 \mu\text{m}^2$. A) height image, B) deflection image.

Figure 22 has a higher resolution than the previous, zoomed in on the higher feature in the middle of the image of Figure 21. This higher feature is around 750 nm high and $3.5 \mu\text{m}$ long.

The shapes of the features are clearer in this image and seem to be segmented on a nano-sized scale. Overall, they appear rounded and the different sizes are also better to identify.

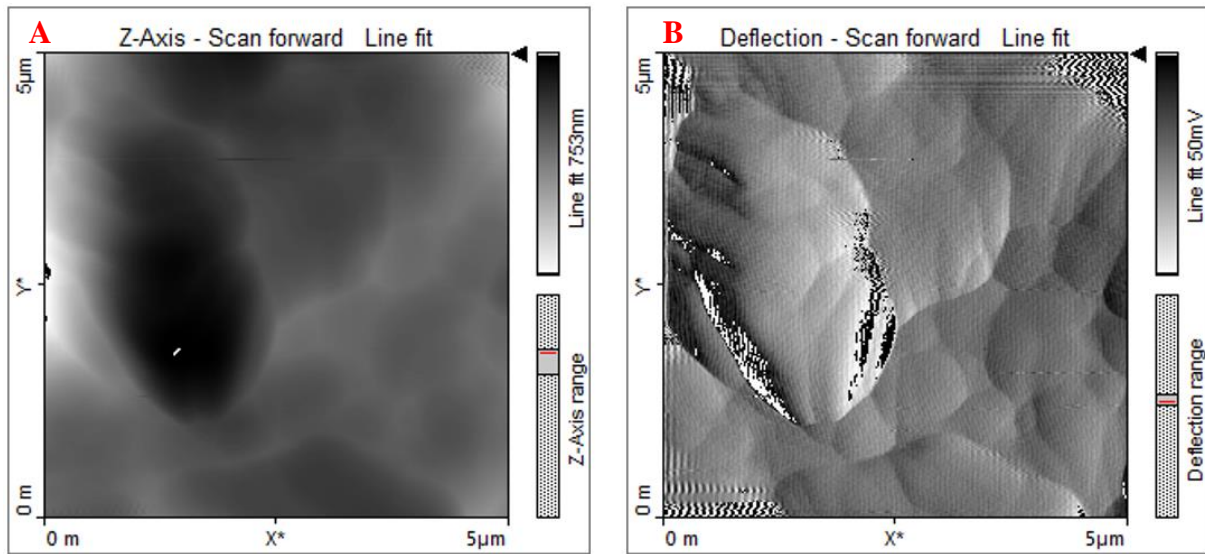


Figure 22 Imaging a standard dolomite with an area of $5 \mu\text{m}^2$. A) height image, B) deflection image.

Fluorapatite

From Figure 23 it is possible to see features in the fluorapatite grain slightly less rounded than e.g. the calcite (Figure 20). The edges of the features appear smooth and some of the features has a more triangular shape (red circle in Figure 23B) with more frequent and significant height differences than in the above presented minerals (Figures 17-22).

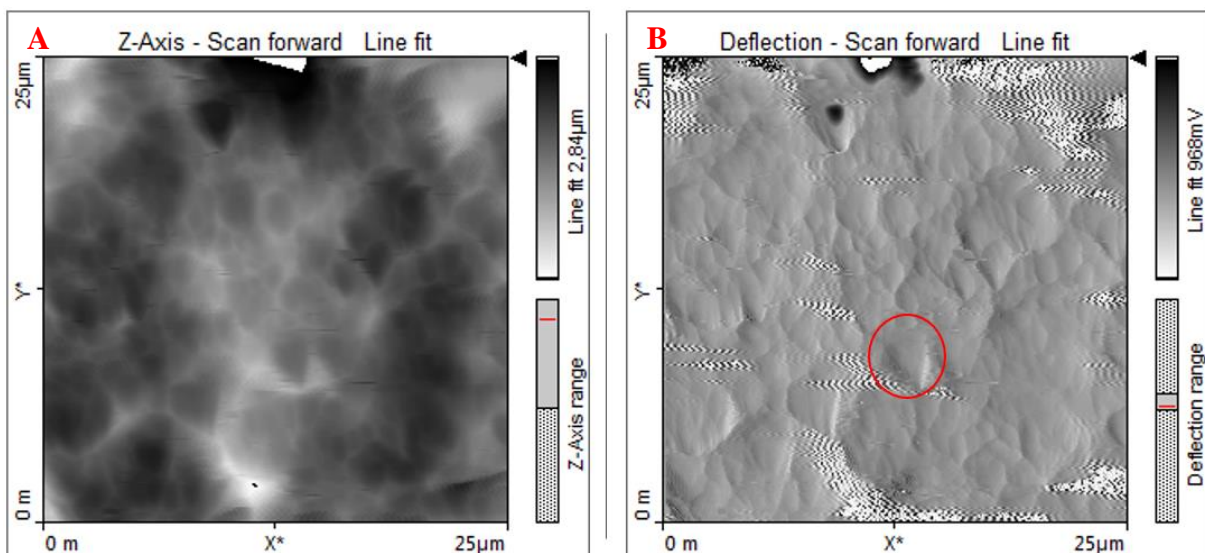


Figure 23 Standard fluorapatite with an area of $25 \mu\text{m}^2$. A) height image, B) deflection image. Red circle demonstrating a feature with a triangular shape.

Ilmenite

The features in the ilmenite grain (Figure 24) do not look equally rounded as in the previous minerals and have partly smooth edges. They have rather straight edges, but not sharp ones. Some features appear slightly rounded and elongated whereas others are more triangular with a clear cleavage texture, especially in the lower center of Figure 24B (red circle). The height difference is around $3\ \mu\text{m}$ which can be seen from the height image (Figure 24A), and it seems that the lowest points are too low for the tip to reach the bottom. This could not yet be observed and may be a characteristic for ilmenite.

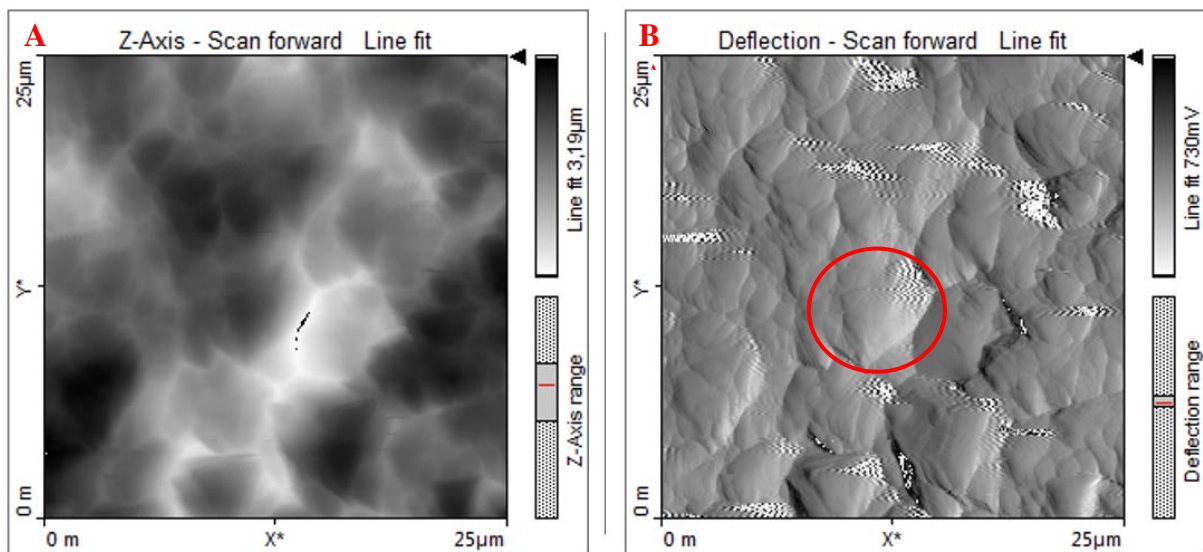


Figure 24 Illustrating an ilmenite standard with an area of $25\ \mu\text{m}^2$. A) height image, B) deflection image. Red circle indicating a triangular shaped feature.

Magnesite

The magnesite standard was polished as well as coated with carbon before measured. This has probably affected the measurements. The polishing is marked as straight lines in Figure 25, both in topography and deflection images, and some polishing dust remained. Due to the fact that this sample has been polished, it is not possible to exclude that the rather low topography (straddling 20 nm) is an effect of this process³. However, small rounded and only very slightly elongated features are visible, marked with a green circle in Figure 25B.

³ It needs to be mentioned that caused by the Corona-crisis, time was not available to produce an unpolished sample because of the time-consuming sample preparation process.

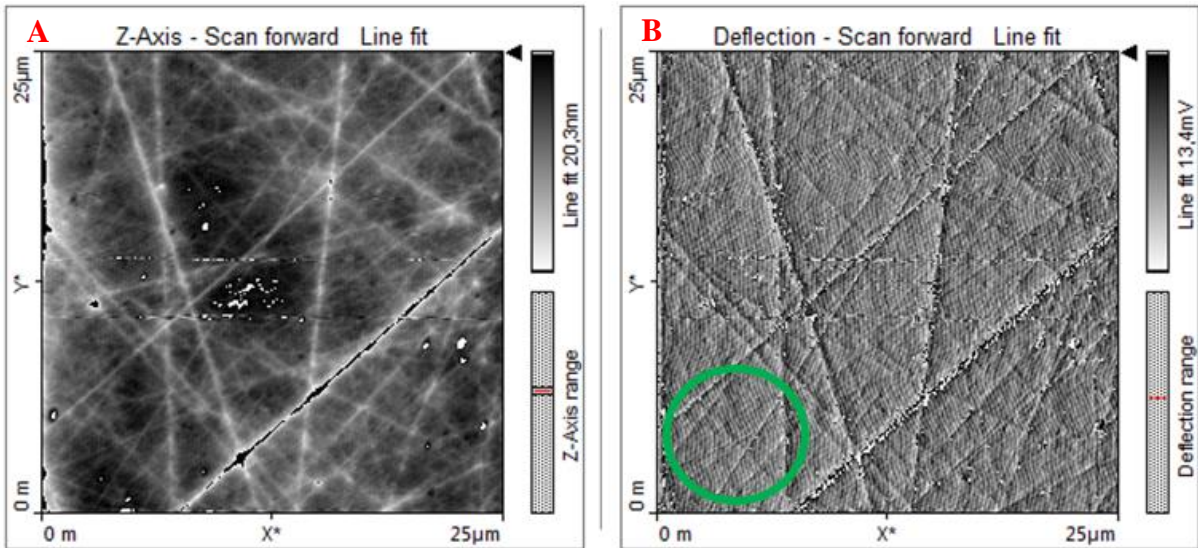


Figure 25 A magnetite standard with an area of $25 \mu\text{m}^2$ with a polished surface. A) height image, B) deflection image. Green circle illustrating some small, rounded features.

Magnetite

The features in Figure 26 can be described as some very rounded (Figure 26, center top) and some more square/rectangle shaped. There are no sharp edges, they all appear smooth. The area in the lower right corner (red circle in Figure 26B) looks flatter than other areas in the image. No clear stacking of features can be observed.

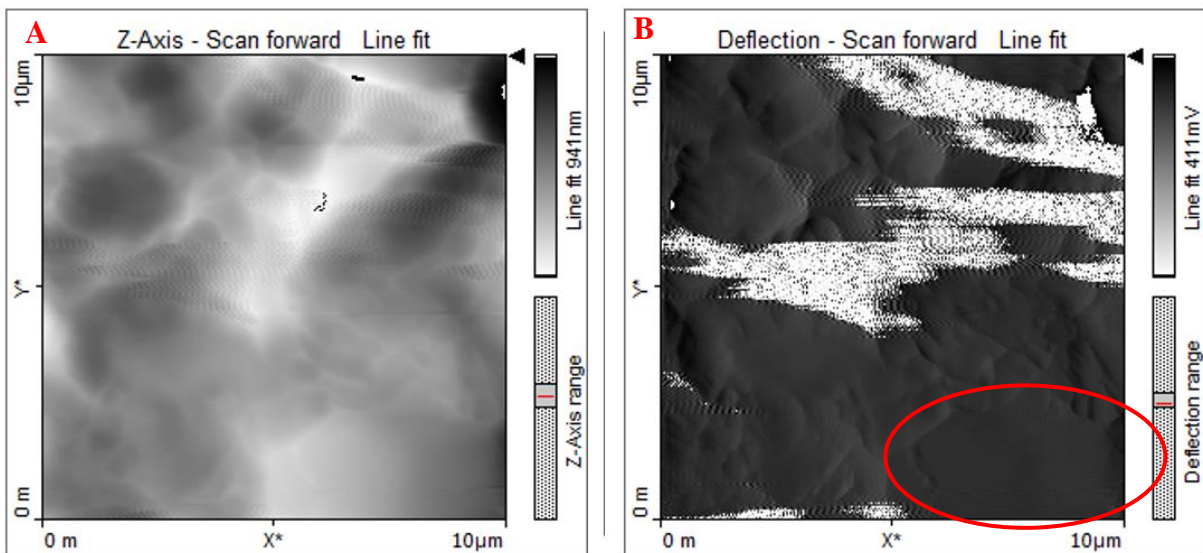


Figure 26 Displaying a magnetite standard with an area of $10 \mu\text{m}^2$. A) height image, B) deflection image. The red circle indicates a flatter area.

Plagioclase

Plagioclase is a Ca-rich feldspar variety, although it is not determined which variety is mounted here. In Figure 27 of this standard mineral grain, the main features appear rounded to elongated with smooth edges. Two major orientations seem to be visible. They appear to be mostly single features, not higher than 400 nm, partly comparable to anorthite in Figure 17.

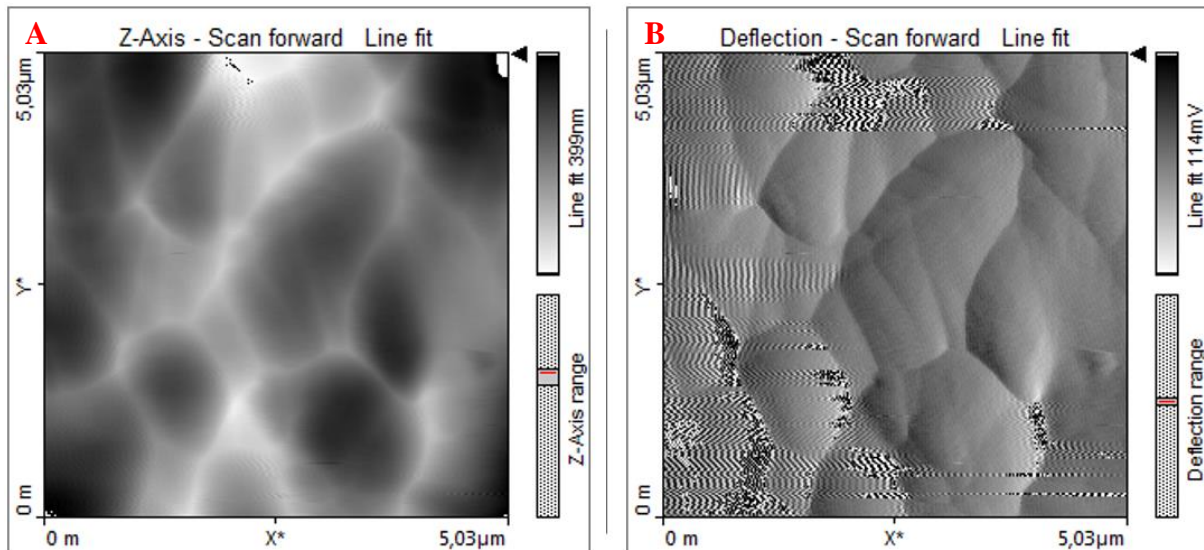


Figure 27 A plagioclase standard with an area of $5 \mu\text{m}^2$. A) height image, B) deflection image.

Quartz

The quartz features (Figure 28) look rounded and elongated of different sizes ranging from 50 nm to $3.45 \mu\text{m}$. The height difference (Figure 28A) indicates 956 nm height difference in the area, and are therefore very different from the plagioclase (Figures 17 and 27). Interestingly enough, most of the features seems to be characterized by roughly similar heights. Often it seems that larger features are sub-divided in smaller units, as well rounded or elongated, but never angular shaped.

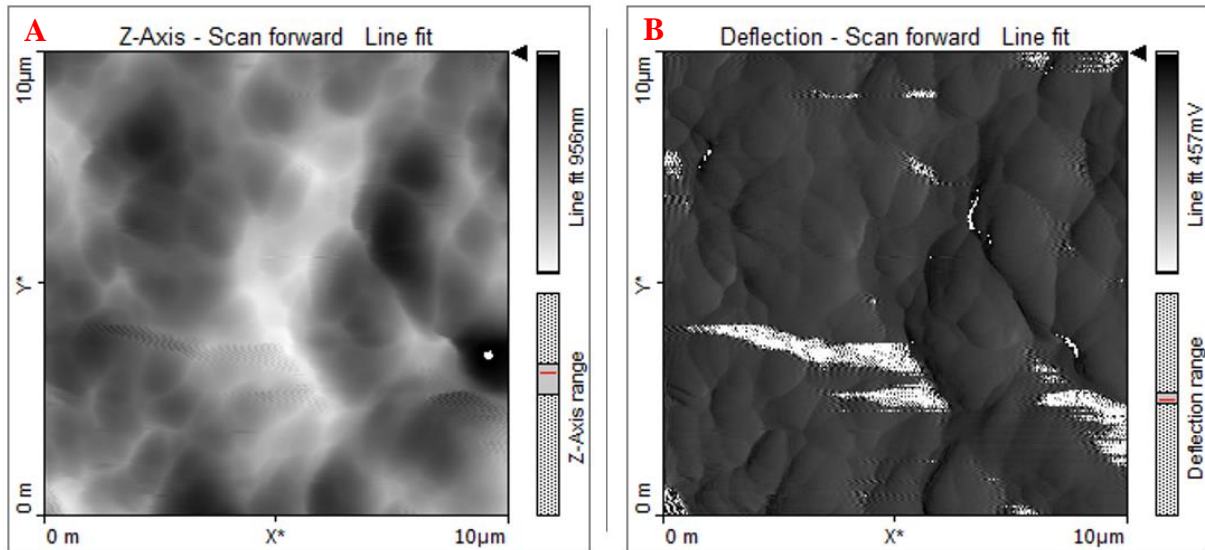


Figure 28 Demonstrating a quartz standard with an area of $10 \mu\text{m}^2$. A) height image, B) deflection image.

Zircon

The shapes of the observed features are mostly rounded, but not spherical in Figure 29. Obvious is the wide range of sizes and the rather “chaotic” texture with roughly three orientations; very different to the plagioclase, for example seen in Figure 27. The larger features on the surface of the zircon appear higher than the smaller ones. Some have one corner that is sharper than the rest where the edges appear smooth.

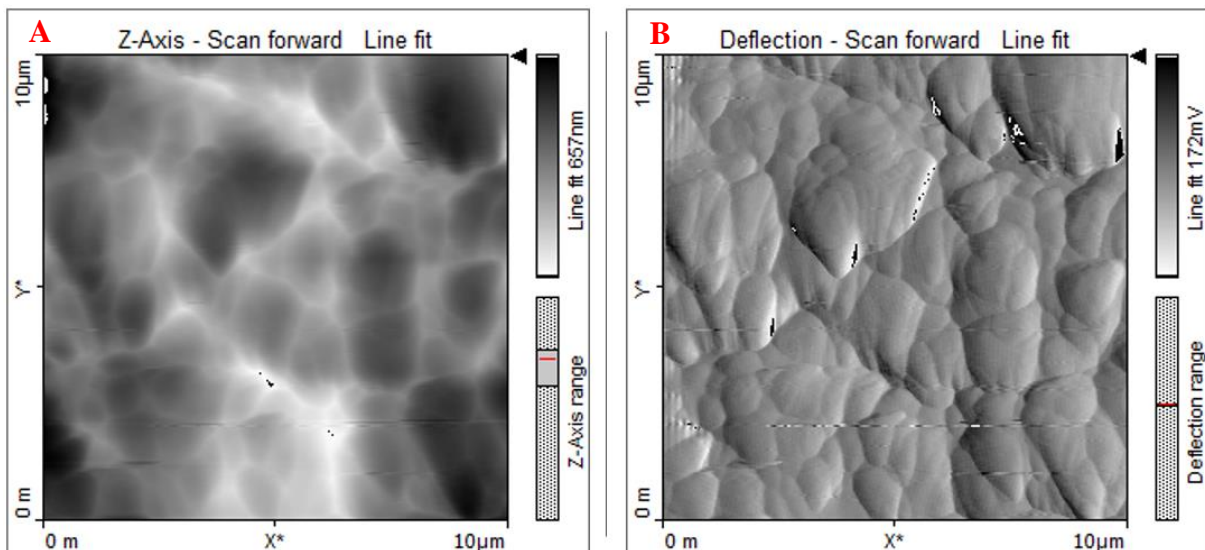


Figure 29 A zircon standard with an area of $10 \mu\text{m}^2$. A) height image, B) deflection image.

3.1.2 LTT1

Sample LTT1 (Chapter 2.1 Overview of Samples) was measured both in Grenoble and at UiS. The rock contains mostly calcite but also some non-carbonates. It was flooded for 1.5 years with MgCl_2 and MLA (Mineral Liberation Analyzer) images demonstrates that this particular part of the sample is affected by the flooding with new growth of secondary carbonate minerals (Minde et al., 2019). Almost all the calcite is replaced by magnesite, however some of the clay and calcite remained.

Grenoble – MFP-3D Origin

The difference from the lower and higher features can be seen in the height image (Figure 30A) to be 970 nm. Some lath-shaped particles can be observed (red arrows in Figure 30B) on top of the other, larger features, which had been, in turn, formerly identified as magnesite (Minde et al., 2019; Zimmermann et al., 2015). Similar appearing small elongated particles have also been observed by Skovbjerg et al. (2012) in Cretaceous unflooded chalk samples from Stevns Klint and Aalborg (Denmark). The shape of the larger features here are step-like and straighter, edgy features dominating the area, the edges are not rounded. This may be the cleavage with a preferred orientation of layers, while the lath-shaped particles are randomly distributed.

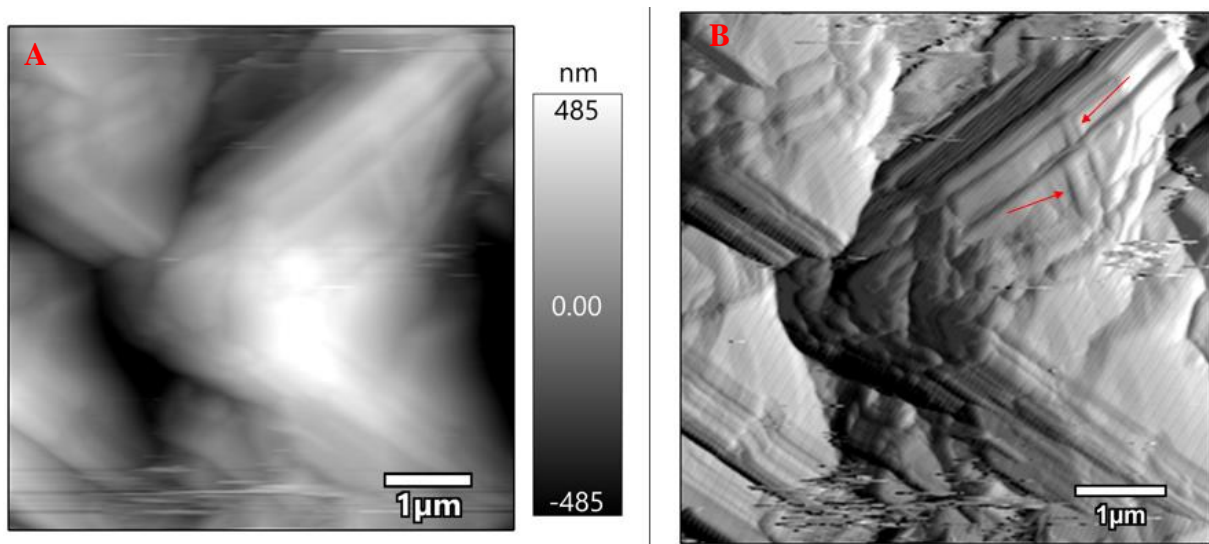


Figure 30 Displaying the first measured area of LTT1, scale bar is $1 \mu\text{m}$. A), height image, B) deflection image with red arrows indicating possible clay laths.

The height profile image (Figure 31A) demonstrates that there is an increasing height from one side of the feature to the other, taken where the feature displays a step-like layering which is more obvious in the deflection image (red line in Figure 31B).

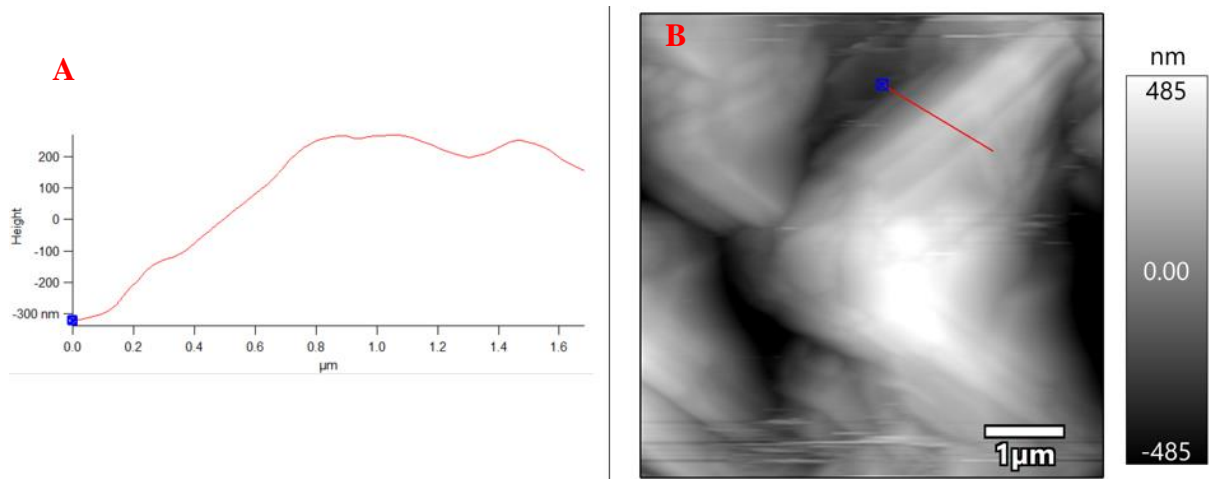


Figure 31 Demonstrating a height profile (A) over a selected line (red line in B) in the measured area. Scale bar is 1 μm .

The masked image (Figure 32) is approximately $1 \mu\text{m}^2$ and is taken within the step-like layer. Surface structures like roughness and nanoarchitecture plays a key role in determining the interactions of a material with its external environment, e.g. surface topography is a key determinant of wettability (Lafuma and Quéré, 2003; Wilson et al., 2011). The RMS (Root Mean Square) is used to display the distribution in the surface height and is more sensitive than average roughness. It is used to compute skew and kurtosis parameters and to calculate surface roughness. In fact, RMS and roughness gives the same information. The roughness of the surface is relatively high, 190 nm, meaning that the surface is not very smooth/flat. This makes sense as there is a height difference in the area. The roughness also has an effect on force curve measurements and for this reason the RMS has to be taken care of.

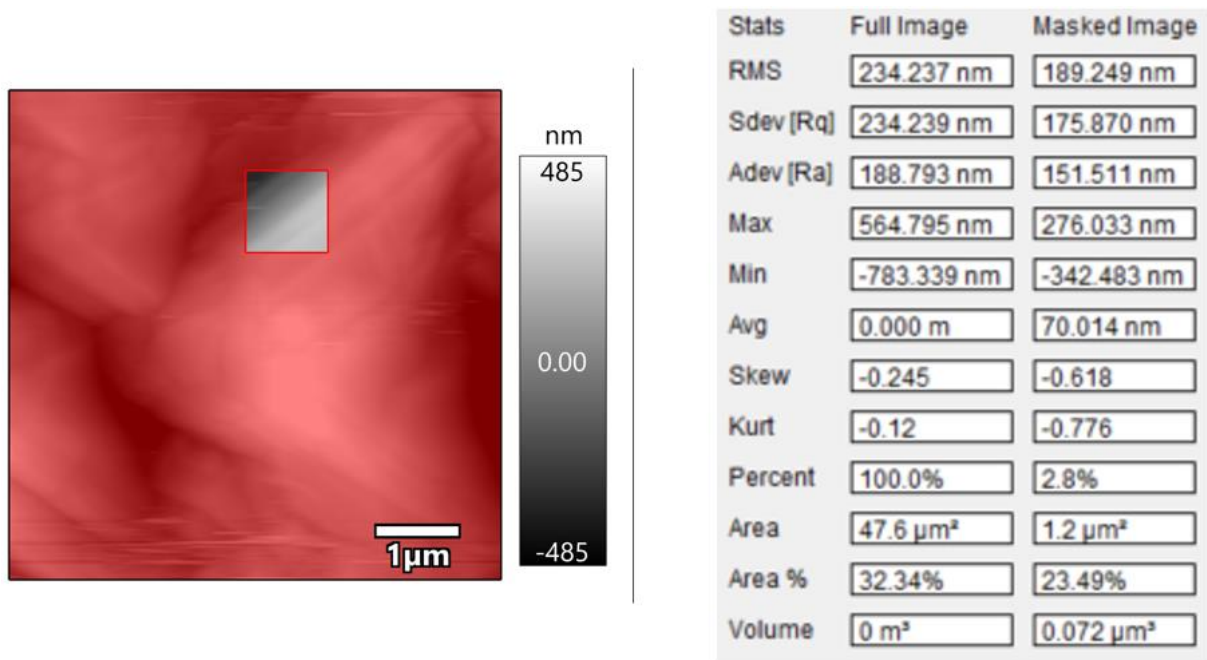


Figure 32 Calculating the roughness of the masked area (gray square in the left image) with the result in the table to the right.

The height difference in the image of Figure 33, which has a higher resolution than Figure 30 is 310 nm. In this area of the sample, more rounded features are observed in addition to the straight, step-like features. Small, elongated phases are absent here.

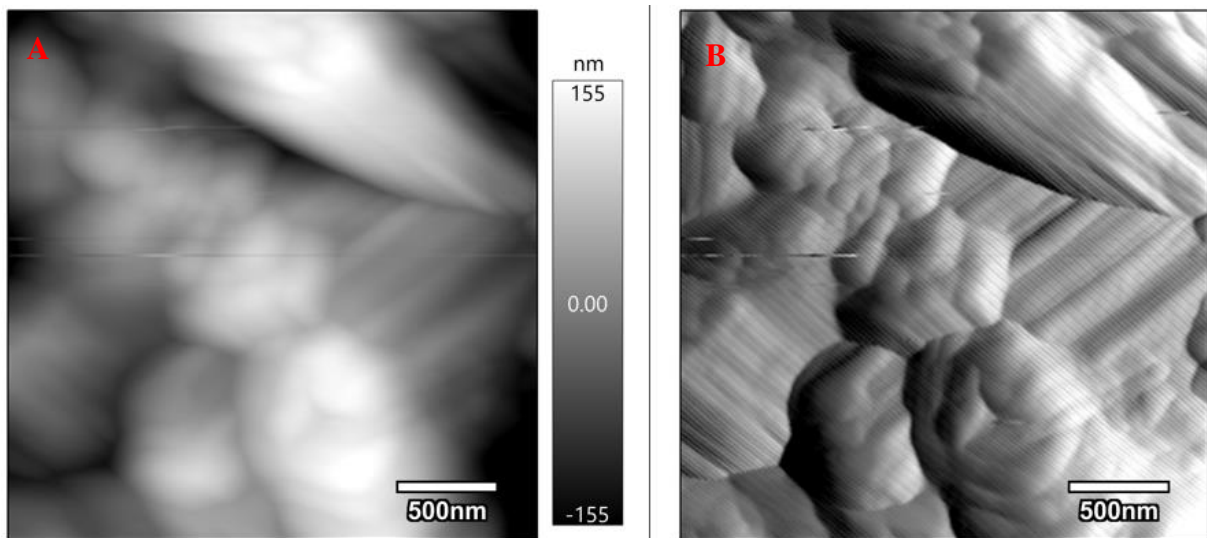


Figure 33 Displaying the second measured area from LTT1. A) height image, B) deflection image. Scale bar is 500 nm.

The height profile (Figure 34) implies that the round-edged features are attached on the flat and step-like surface. New grown magnesite may be a candidate, which has been observed at this

size (Minde et al., 2019). However, to identify minerals and differentiate between carbonate phases (calcite and magnesite) would be of tremendous importance for EOR research. It is out of the scope of this pilot study but a necessary follow-up research project.

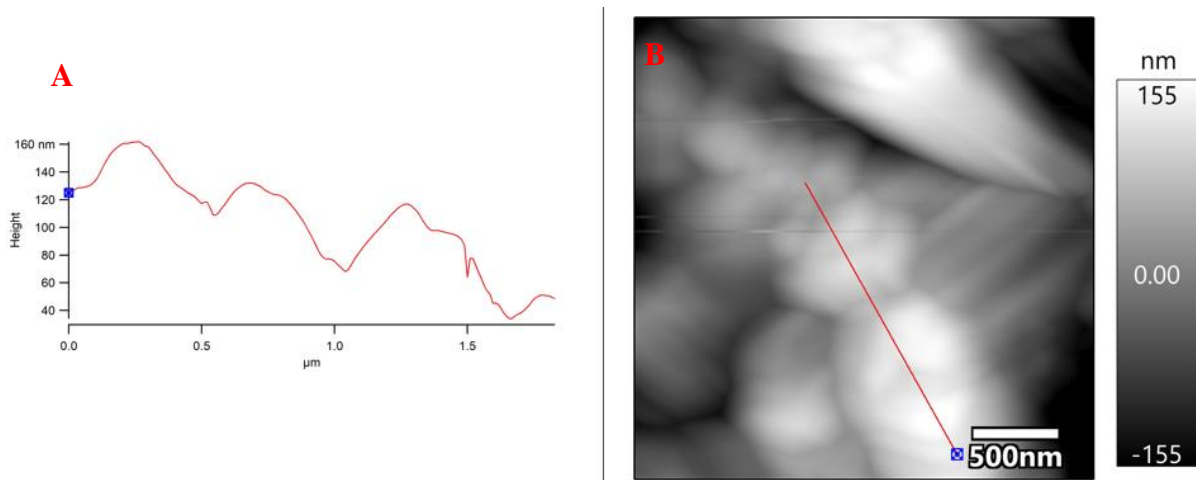


Figure 34 Illustrating a height profile (A) over a selected line (red line in B) in the measured area. Note the smaller scale bar with 500 nm compared to the former figures.

UiS - NaioAFM

This sample studied is from the same area of the flooded chalk but not identical because of size issues as described above (Chapter Sample Positioning). Minde et al. (2019) demonstrated that the sample is mainly characterized by abundant magnesite due to flooding, hence a secondary phase.

The resolution is slightly lower on this AFM and more sensitive to noises, as well as movement around the machine (Chapter 2.4 Atomic Force Microscope (AFM)). Due to this fact, noise is observed in the left part of Figure 35B. The features appear more rounded than those in the previous shown images of LTT1 from Grenoble, but at the same time slightly straighter in the features. The latter are strongly orientated and display another incision preference from top left to bottom right which is less penetrative.

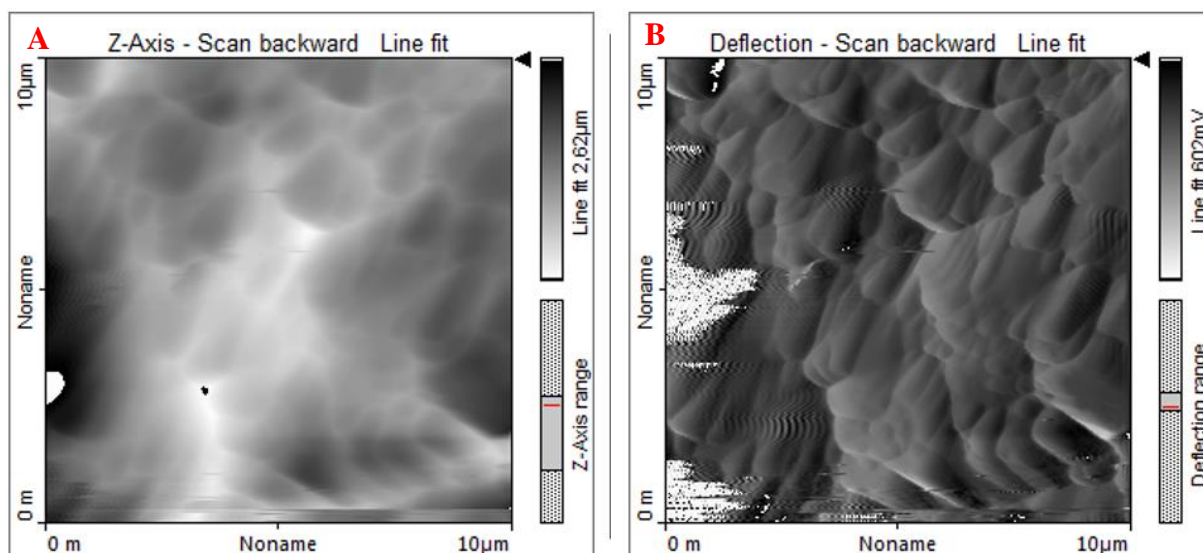


Figure 35 The first measured area in LTT1, UiS, area of $10 \mu\text{m}^2$. A) height image, B) deflection image.

In Figure 36 those features seem to be growing or are attached to a flatter surface, which is nearly completely masked by the mentioned features. The topography is much lower than in Figure 35 and the features smaller. Again, detailed analyzes of surface characteristics would be the next step to try to differentiate possible phases.

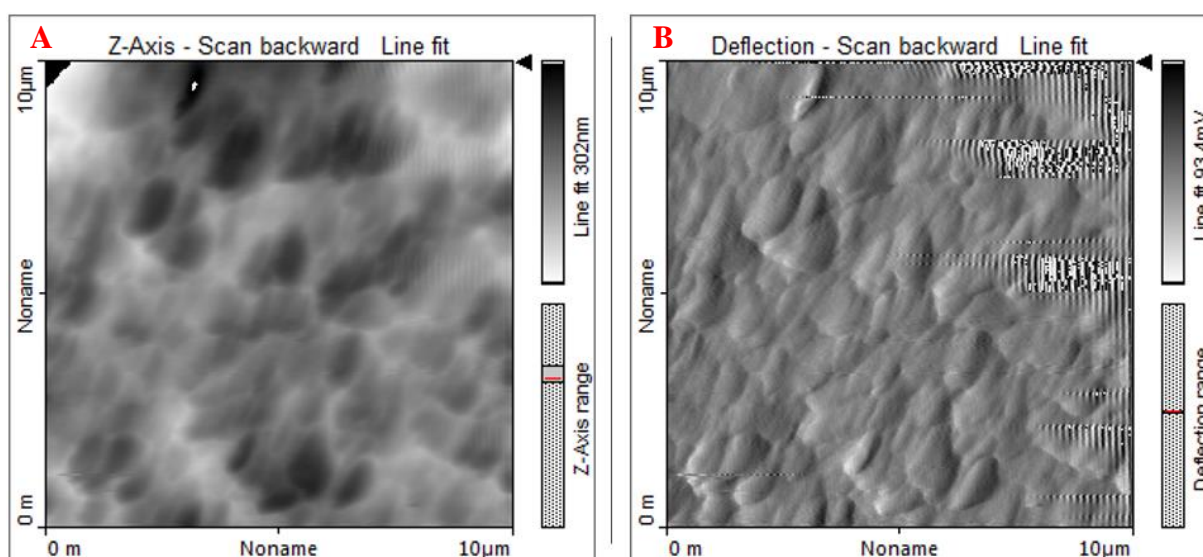


Figure 36 The second measured area in LTT1, UiS, area of $10 \mu\text{m}^2$. A) height image, B) deflection image.

Zooming into a specific area (Figure 37) is difficult as blurriness increase strongly, caused by the roundness of the tip possibly. Alternatively, the tip is not the ideal type for this sample. Nevertheless, the two orientation trends are well reflected, forming the elongated features.

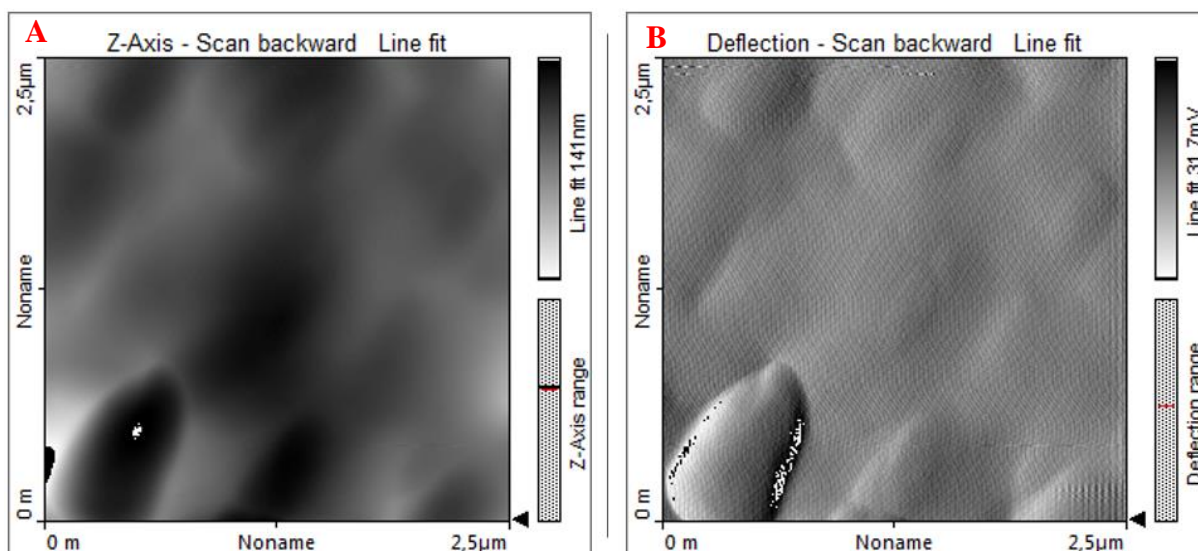


Figure 37 The third measured area in LTT1, UiS, area of $2.5 \mu\text{m}^2$. A), height image, B) deflection image.

3.1.3 MLTT

This rock sample is a chalk from Liège (Belgium), containing mostly calcite but also some non-carbonates. It was flooded for two years with MgCl_2 . MLA (Mineral Liberation Analyzer) data elucidate that this part of the sample has been recrystallized after flooding to approximately 50 % magnesite, while the other half is still calcite. The measurements are divided in this case in three parts: (i) measuring the calcite, (ii) measuring the transition zone where the sample most possibly contains clay and (iii) measuring the magnesite dominated area (Figure 9C in (Minde et al., 2019) explains and illustrates the different parts of MLTT).

Figure 38 demonstrates the area where calcite still dominates.

From the height image (Figure 38A) it is possible to observe a large difference from the lowest to the highest point, exceeding $2 \mu\text{m}$. The image clearly displays rounded features, which are overall well defined. These rounded features have approximately similar sizes and appear to be partly stacked, forming defined layer-like textures; however, different from LTT1 in Figure 30. This stacking was also not observed in the calcite standard (Figure 19), but the well-defined orientation exists.

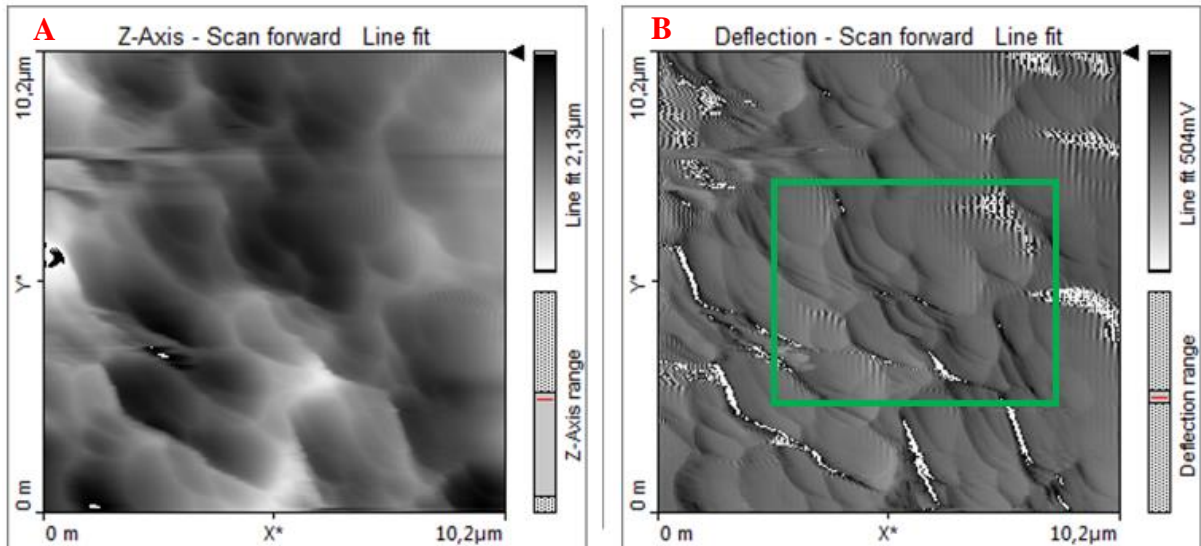


Figure 38 Displaying the calcite-rich area of MLTT with a size of $10 \mu\text{m}^2$. A) height image, B) deflection image. Green box marks roughly area of Figure 38.

When zooming in (green box in Figure 38), noise effect kicked in (Figure 39B), as described above. The reason for this may be more details in the zoomed-in-image, which could have caused this overflow of data. However, the shapes are still similar to those in Figure 38 and in the middle of the image, there seem to be a slope where the features are stacked on top of each other, like a possible cleavage.

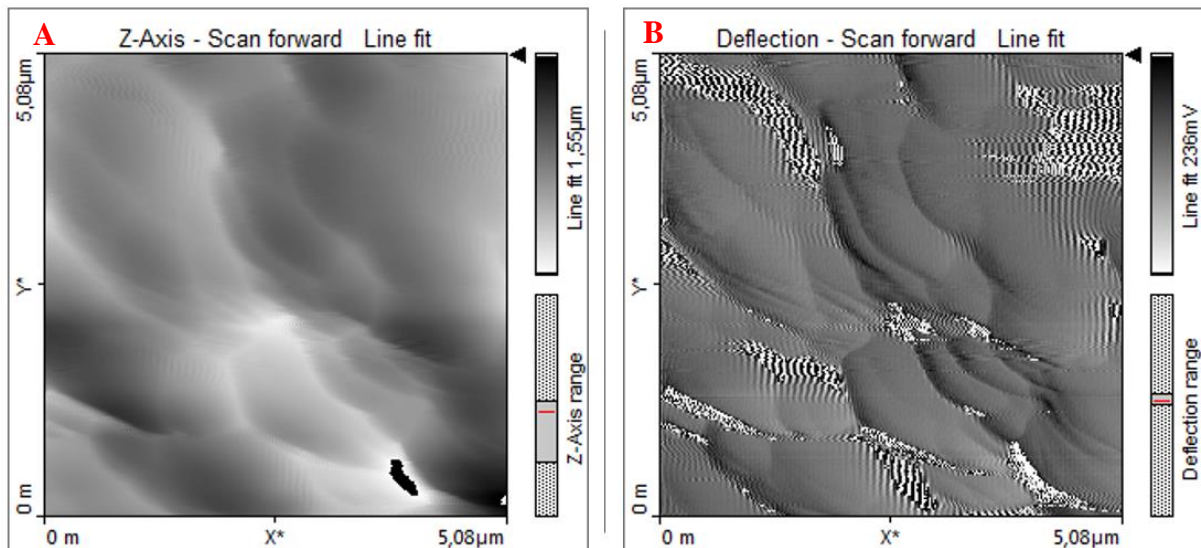


Figure 39 Zoomed-in area of MLTT, calcite part, of $5 \mu\text{m}^2$ (green box in Figure 37). A) height image, B) deflection image.

This second part of the MLTT sample was interpreted to be containing abundant clay minerals (Minde et al., 2019), as this is the transition zone between the calcite and the magnesite. The resolution of the AFM makes it very difficult to exactly locate the sampled area.

The features in the red circle (Figure 40B) appears to be stacked like the calcite in the first part of this sample. The shape of the other features in the area appears rounded, however there is a lot of noise which may be due to the tip not feasible for this measurement, which can cause the features to appear this way. The surface topography illustrates typical features observed in standards of calcite, dolomite, or magnesite (Figure 19, Figure 21 and Figure 25).

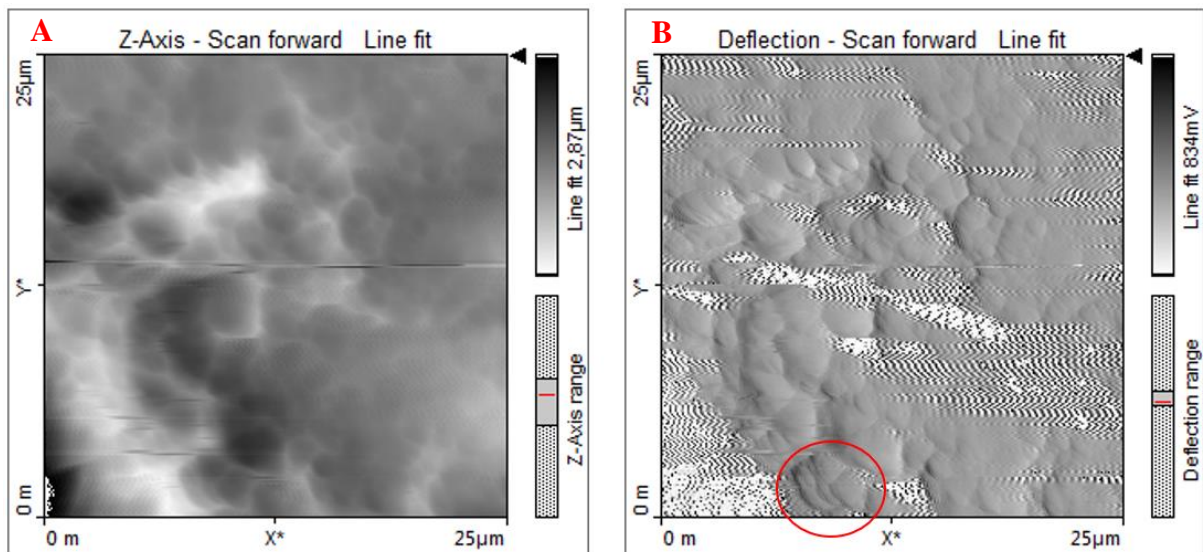


Figure 40 The first measured area of MLTT, clay part, of $25 \mu\text{m}^2$. A) height image, B) deflection image, red circle indicating stacked features.

Some similarities from Figure 39 can be seen in this image, however the features seem here (Figure 40 and Figure 41) larger and less defined than in the former area (Figure 37 and Figure 38). They are also lower, approximately half the height, but this characteristic is not calibrated and additionally the topography differs partly from area to area.

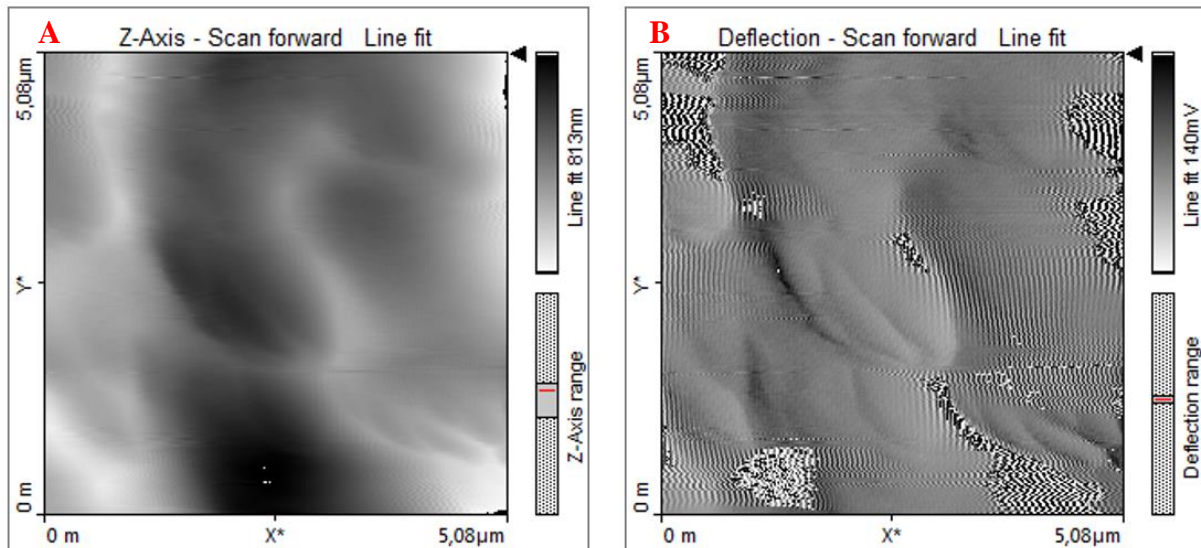


Figure 41 The second measured area of MLTT, clay part, of $5 \mu\text{m}^2$. A) height image, B) deflection image.

The last sample area of sample MLTT locates the highest amount of secondary magnesite. This means that the area is strongly affected by the flooding.

Figure 42 displays the sample area to be rather homogeneous, in terms of size and form, as well as the same morphology and topography all over the sampled area. It has rounded edges and approximately 600 nm height difference. In the zoomed-in image of Figure 42 noise can be registered, most likely as a result of the tip is not hitting the surface of the sample and thus cannot image in this area.

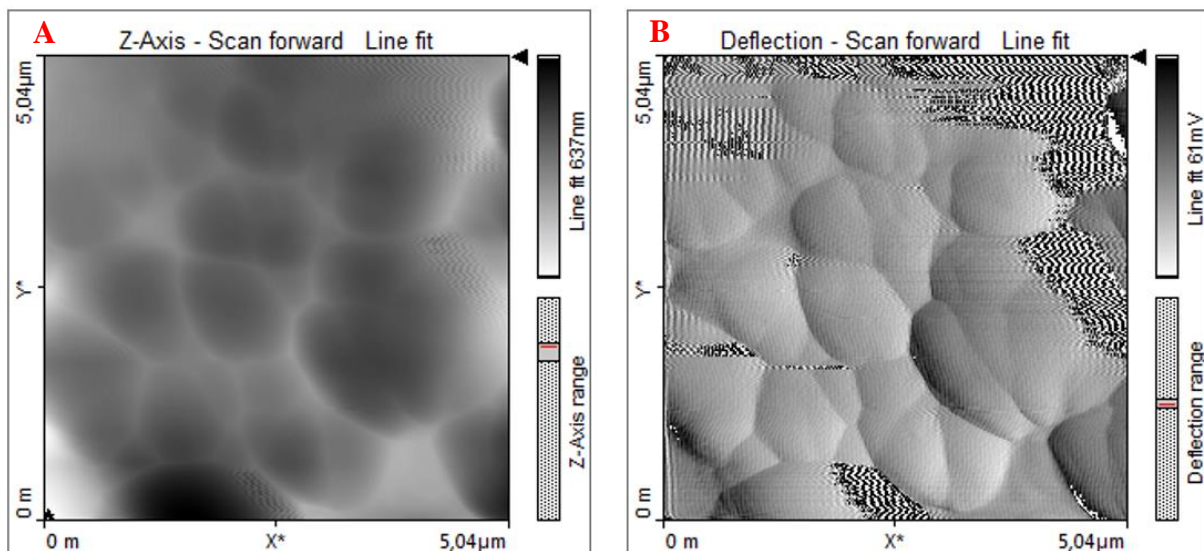


Figure 42 The first measured area in MLTT, magnesite part, of $5 \mu\text{m}^2$. A) height image, B) deflection image.

Nevertheless, in Figure 43, some areas (red circles) displays stacked features comparable to Figure 39 and more than in the previous image (Figure 42). There is still a lot of noise. The features do not have the same rounded shape as in Figure 42, but the edges are still rounded. Stacking may be related to the magnification and the angle between the tip and the morphology.

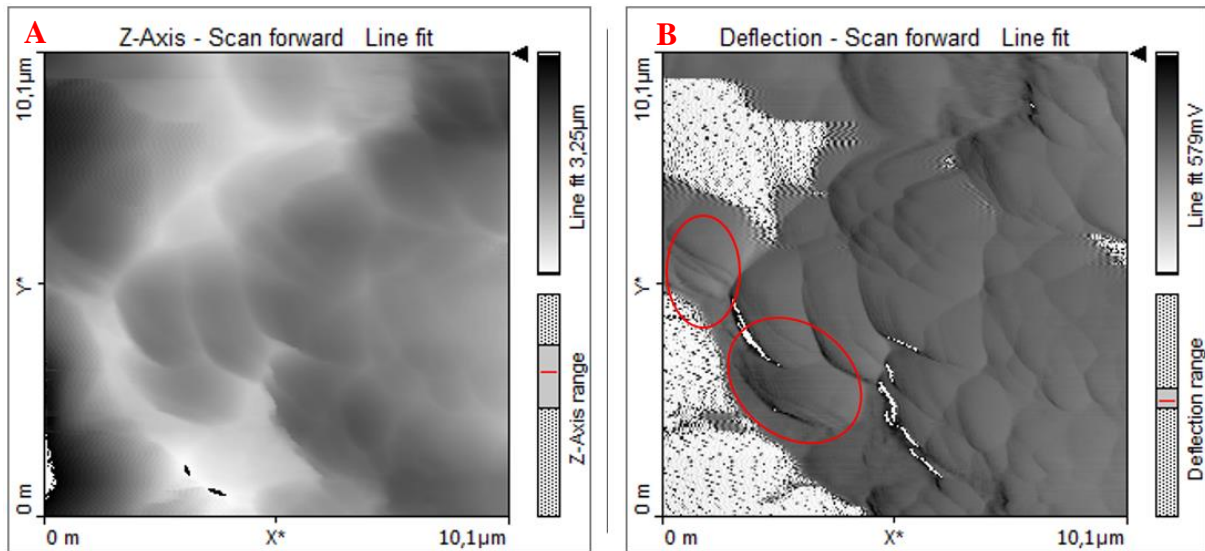


Figure 43 Illustrating the second measured area in MLTT, magnesite part, of $10 \mu\text{m}^2$. A) height image, B) deflection image with stacking features in the red circles.

3.1.4 ULTT

The sample is chalk from Liège (Belgium), originally containing mostly calcite and some non-carbonates. The core where the sample is from has been flooded for as long as three years with MgCl_2 , replacing nearly completely the calcite in the original sample with secondary magnesite (Minde et al., 2019).

The features in ULTT demonstrate the best defined stacked-like texture thus far, even in lower resolution. From the deflection image (Figure 44B) it seems that the step-like layering does not differ significantly in height, which may be an effect of the observation angle (Figure 44A). Elongated and rounded features are rare in this area using $10 \times 10 \mu\text{m}$.

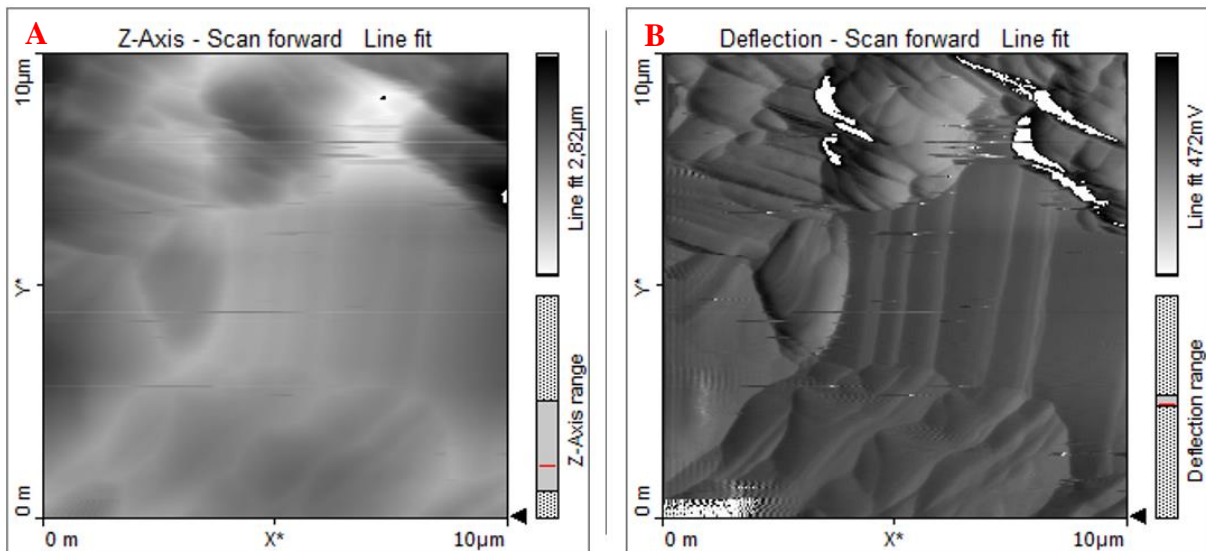


Figure 44 Demonstrating the first measured area in ULTT of $10 \mu\text{m}^2$. A) height image, B) deflection image.

Another image of the area (Figure 45) is somewhat more blurry but displays very interesting characteristics. Deep incising areas which define in some parts the stacked texture (yellow circle in Figure 45A), and the majority of the features have the same height. Some of the features seems to have a smooth “depression” (red circles in Figure 45B), which is lower than the rest of the surface of a specific layer. This might be a secondary effect on top of the stacked texture. In the two red circles the line can be interpreted as sharp and straight boundary within a layer.

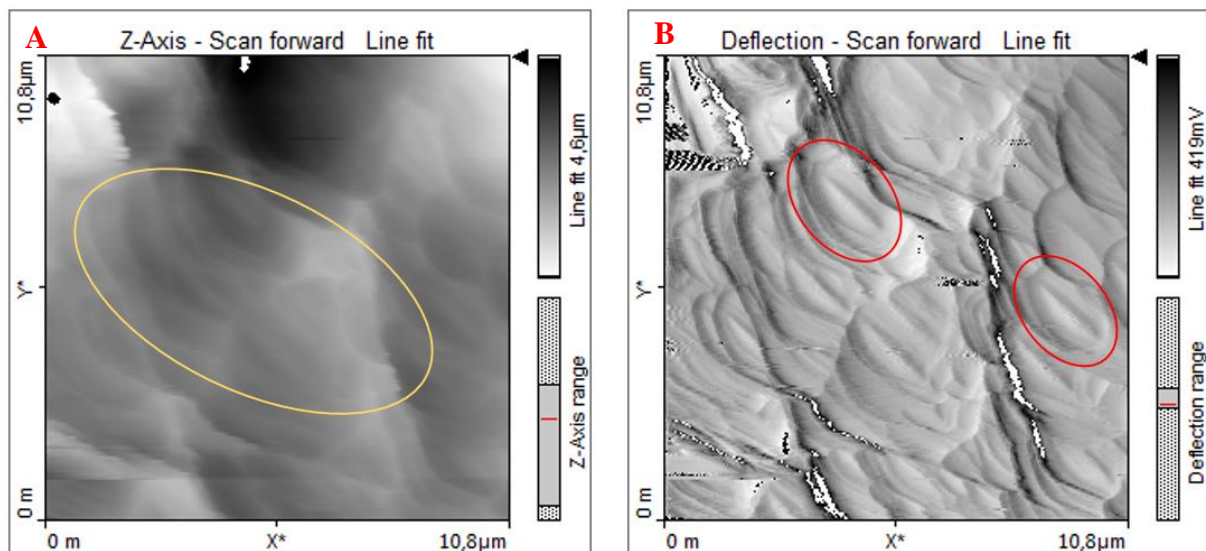


Figure 45 The second measured area in ULTT, $10 \mu\text{m}^2$. A) height image with the yellow circle indicating a stacking pattern, B) deflection image red circles displaying features with a little “depression”.

Rounded edges on the features are abundant in the area of the image of Figure 46. Height differences are vast, and the left part of the image seems to display a larger elongated “range” of topography, unseen thus far up to nearly $3.7\ \mu\text{m}$. This points to a rather inhomogeneous growth pattern.

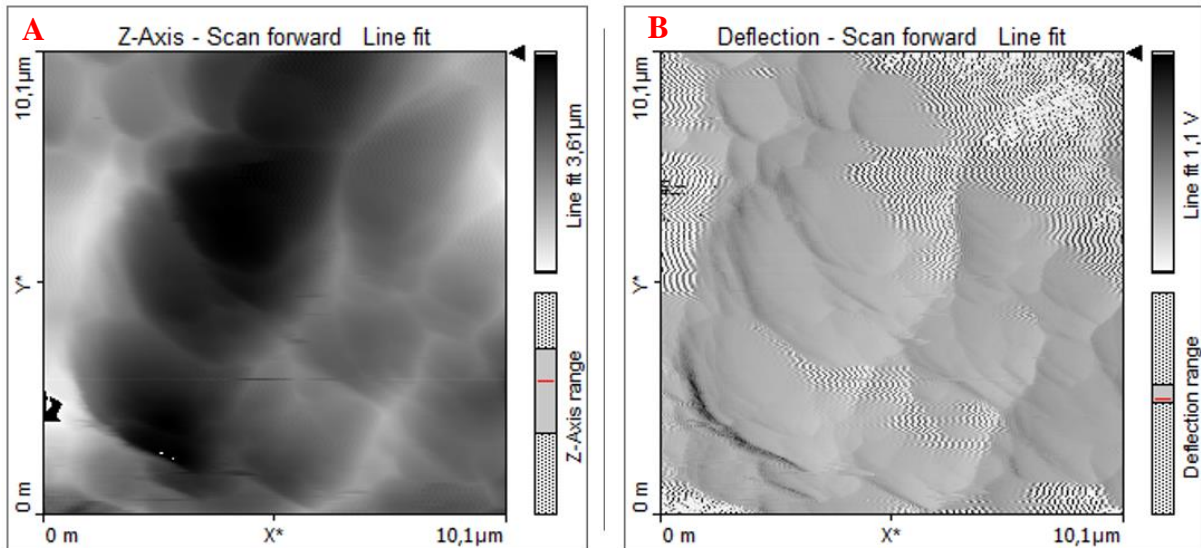


Figure 46 Imaging a third measured area from ULTT of $10\ \mu\text{m}^2$. A) height image, B) deflection image.

Figure 47 displays a 3D image of the same image as seen in Figure 46, which also displays the elongated “micro-mountain range” feature. The imaging of the stacked texture with a specific dip and strike together with the incisions in between the stacked layers is marvelous. Interesting and a necessary subsequent study would be the analysis of the incised areas and why they exist depending on changes in chemistry or if they are related to crystallographic parameters.

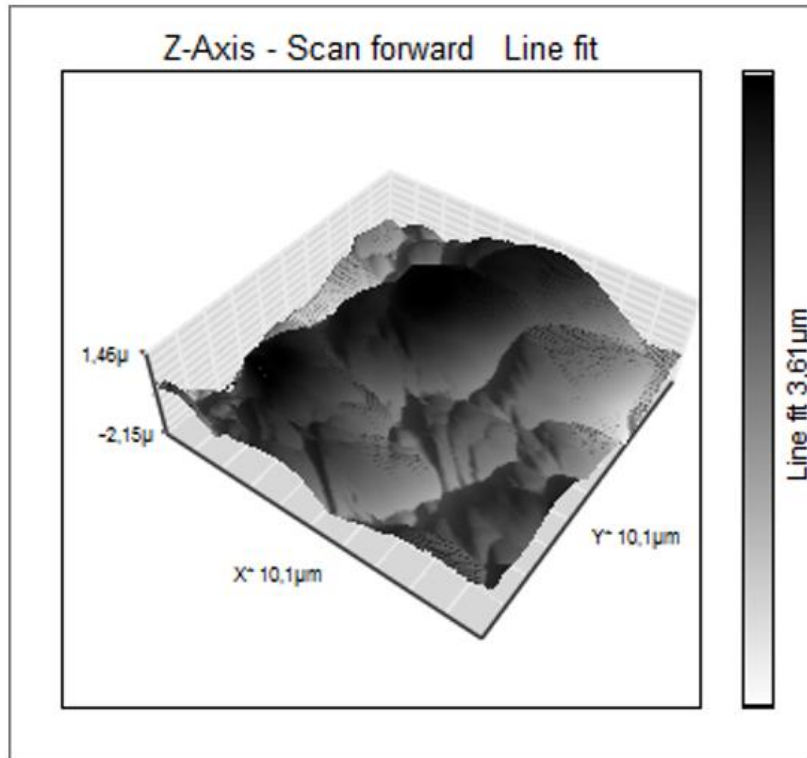


Figure 47 3D image of the height from Figure 45 in ULTT, size of 10 x 10 μm in x- and y-direction.

3.1.5 OBSV4_1 – MFP-3D Origin

This sample is a chalk from Mons basin (Belgium) and is not a clean chalk as it consists of 5 % non-carbonates. The sample has also been flooded with MgCl₂ but for a shorter amount of time (several weeks) than LTT1, MLTT and ULTT. Only a few parts of the sample was affected by this process, replacing just some of the calcite with magnesite (Bredal, 2018).

The deflection image (Figure 48B) indicates a feature which is definitely a part of a coccolithophore that is also visible in the height image. The fossil has a size of 4-5 μm and displays some smooth edges as an effect of the flooding but its texture is still preserved.

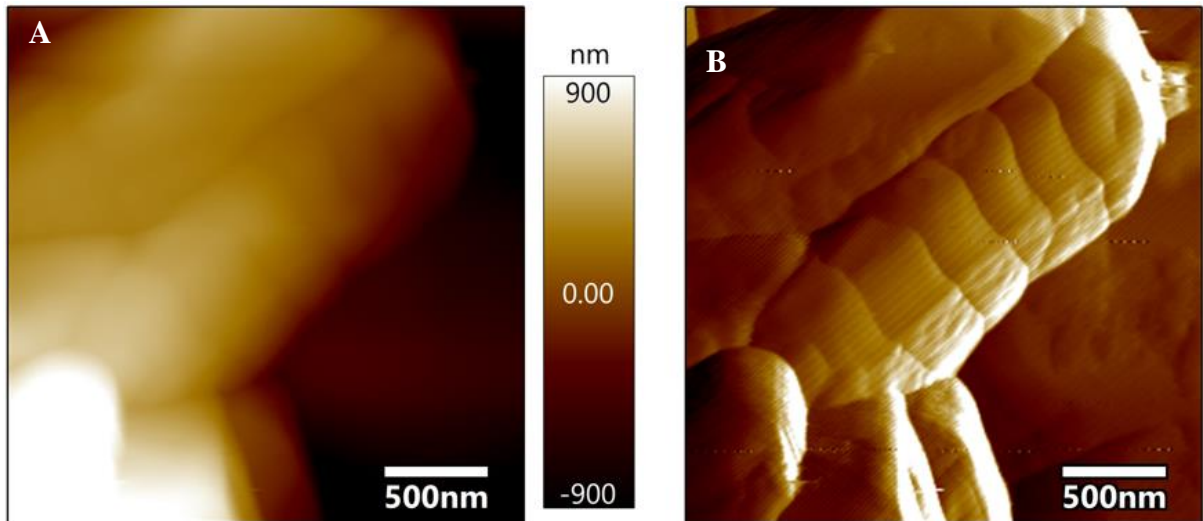


Figure 48 First measured area of OBSV4_1 with a possible coccolith. A) height image, B) deflection image. Scale bar is 500 nm.

The red circle in Figure 49 indicates which part of the coccolithophore that may have been sampled. This current sample is unflooded, but the part from Figure 48 looks unflooded and this is therefore a good example of how it looks in SEM.

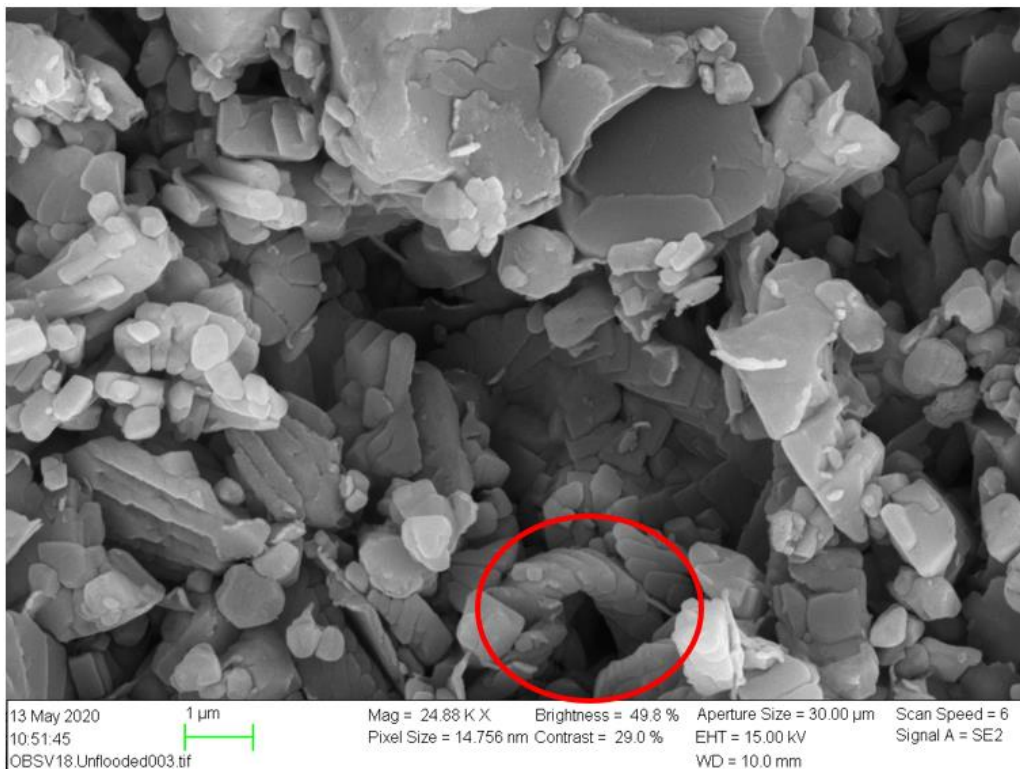


Figure 49 SEM image of part of a coccolithophore (red circle) in an unflooded chalk sample with a scale bar of 1 μm . (Kindly provided by Tine Bredal.)

The height profile (Figure 50) over the area indicates that the fossil has a height difference of approximately 1 μm from one side to the other or it is inclined down into a pore.

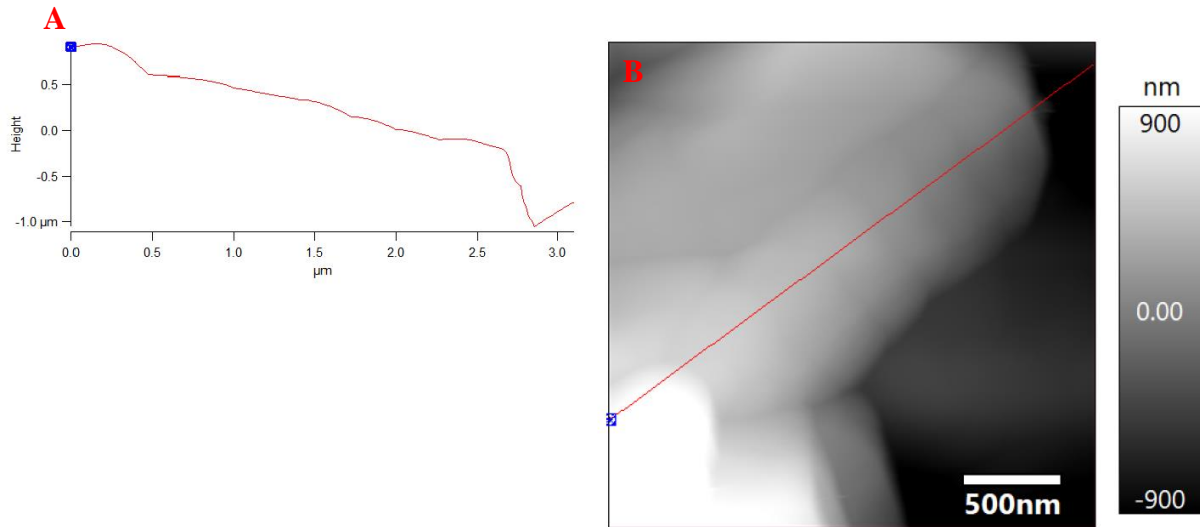


Figure 50 Illustrating a height profile (A) over a selected line (red line in B) in the measured area. Scale bar is 500 nm.

The height image (Figure 51A) displays approximately 2 μm height difference, where the assumed fossil is the highest feature. This area may be a micropore within the tested chalk. In the deflection image (yellow circle in Figure 51B), a feature on top of the flat surface can be observed. This is assumed to be the same kind of feature as in LTT1 (Figure 30), only with a different shape. Similarly shaped object have been recognized by Skovbjerg et al. (2012) and interpreted to be clay particles based on the growing on top of a flatter surface; the latter property could not be determined within this thesis.

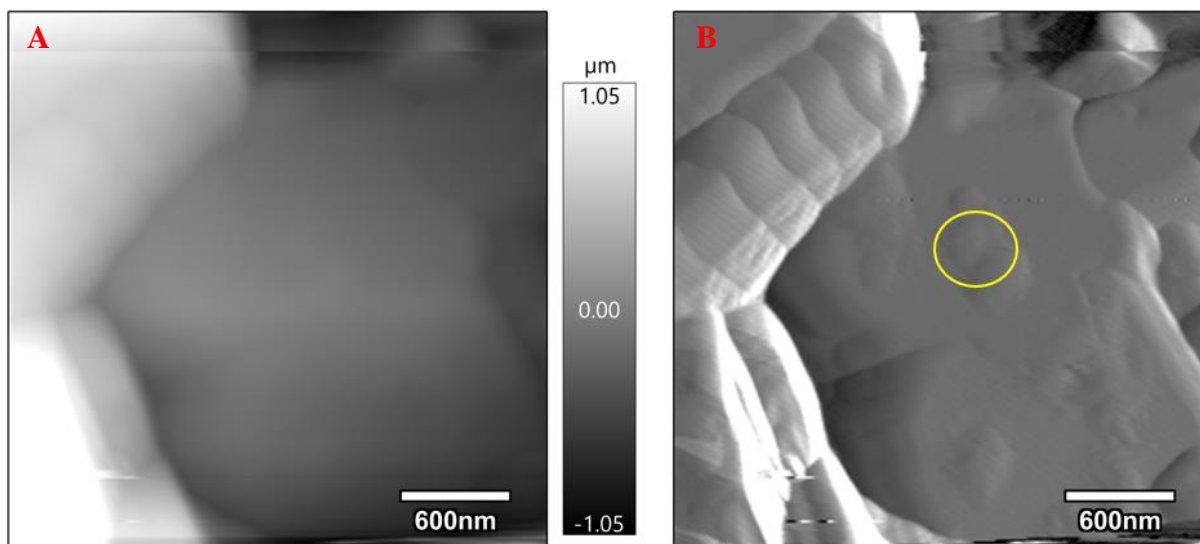


Figure 51 Displaying a second measured area from OBSV4_1. A) height image, B) deflection image with an assumed clay particle in the yellow circle. Scale bar is 600 nm.

In this sample, that specific overgrowing feature has a more rounded shape than in LTT1 (Figure 30) and is c. 400 nm long and 100 nm wide. Figure 52 confirms, spectacularly, that it is a new grown phase as there is a clear height difference compared to the surrounding area. The height of the feature can be estimated to be approximately 200 nm (Figure 52A)

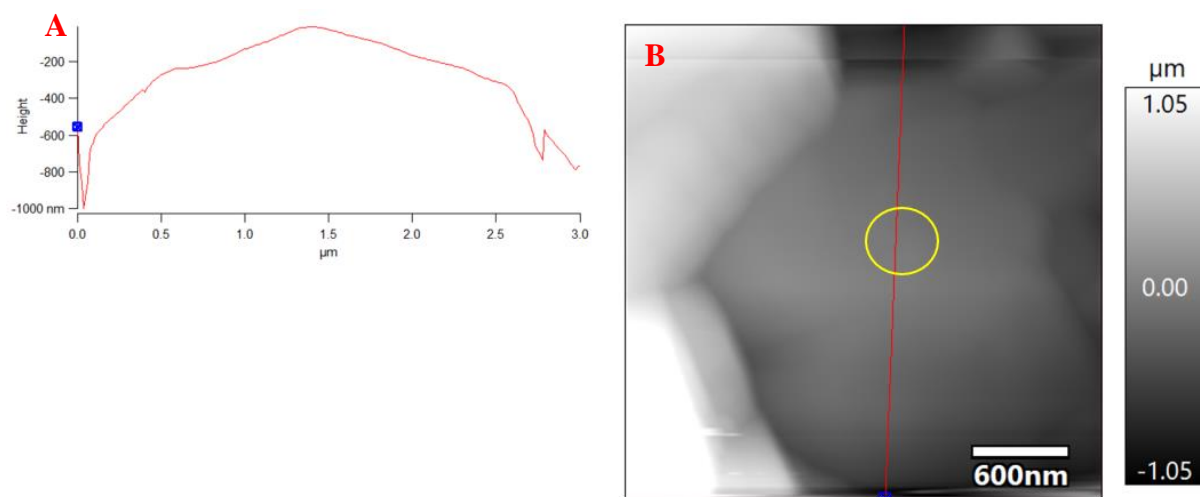


Figure 52 Illustrating a height profile (A) over a selected line (red line in B) in the measured area. Scale bar is 600 nm.

The 3D image of this specific area (Figure 53) gives an indication of the exact location and the extension of this topographic feature. The assumed coccolith (red circle) rules over the other features. The flat area where the described phase has seeded may be an inorganic crystal (yellow circle), either primary or secondary, located in a pore and the topographic feature, seems that

similar ones are neighboring the one analyzed in detailed, is positioned in the central area of the flat surface. Again, detailed studies in the future need to determine the chemical composition or crystallographic structure of these features to identify a different mineral than calcite.

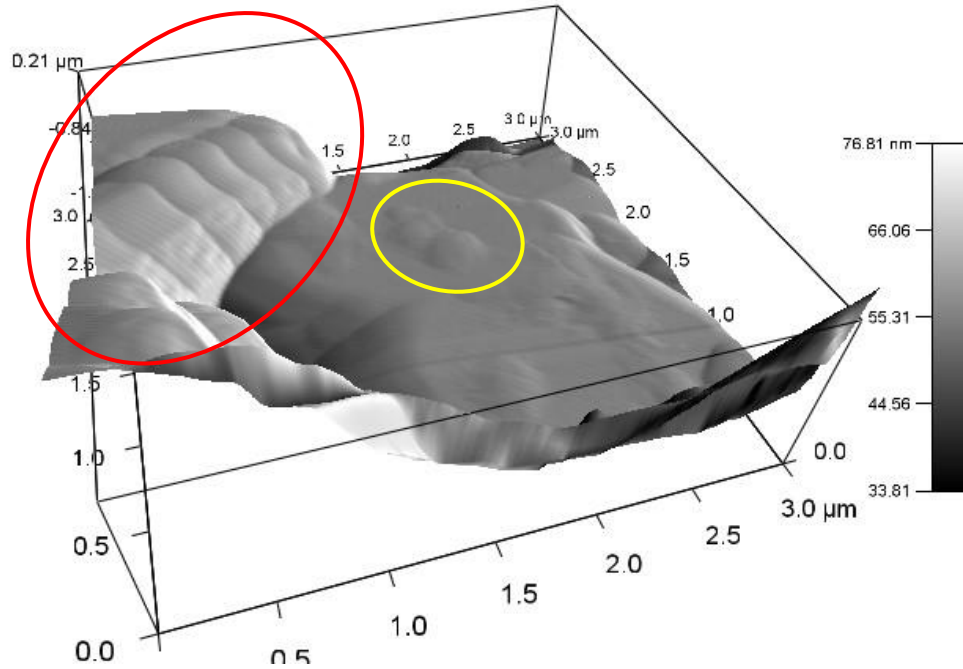
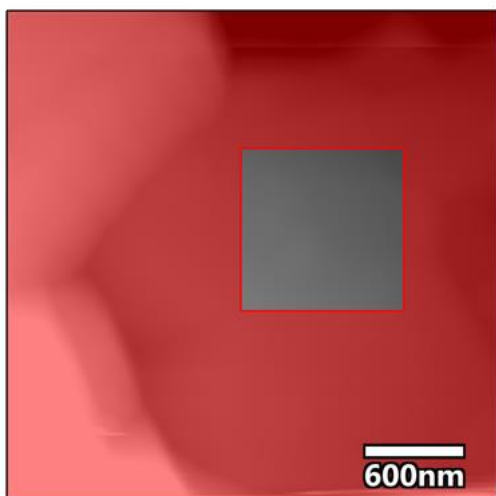


Figure 53 3D image of the height from Figure 50. The assumed clay particle can be seen in the yellow circle and the assumed coccolith in the red circle. Size is 3*3 μm in x- and y-direction.

The calculated roughness (see explanation in 3.1.2) in the masked area, $1\mu\text{m}^2$, (gray square in Figure 54) is high ($1.073\mu\text{m}$), but does not have a strong difference from the calculated high of the entire image ($1.048\mu\text{m}$). This indicates that the surface is not smooth or flat in this area, confirming the feature has grown on the flat surface.



Stats	Full Image	Masked Image
RMS	1.048 μm	1.073 μm
Sdev [Rq]	624.817 nm	82.178 nm
Adev [Ra]	439.157 nm	68.246 nm
Max	1.513 μm	-886.104 nm
Min	-2.300 μm	-1.300 μm
Avg	-841.850 nm	-1.070 μm
Skew	1.33	-0.198
Kurt	2.59	-0.519
Percent	100.0%	11.0%
Area	17.2 μm^2	1.0 μm^2
Area %	90.76%	5.143%
Volume	-7.6 μm^3	-1.1 μm^3

Figure 54 Calculating the roughness of the masked area (gray square in the left image) with the result in the table to the right.

3.1.6 OBSV12_6 – MFP-3D Origin

This sample is also a chalk from the Mons basin (Belgium) which has been flooded with sea water. It is the outlet-part of the core, meaning that if any precipitation has taken place in the core, the outlet is the last part to be affected.

The amplitude image (Figure 55A) displays an area with a relatively flat surface, which is definitely a small carbonate mineral (500 nm) with a feature (50 nm) growing on the surface marked with a red circle in Figure 55A. This sample has similarities in terms of shape and size to those observed in OBSV4_1 (Figure 51). The minute feature is even visible in the height image (Figure 55B), which also demonstrates the rather flat and texture-less crystal surface where the small phase is attached to. The phase image (Figure 55C) (Chapter Imaging) is able to illustrate if there are different minerals in the selected area. By using this specific magnification, the area seems to be homogeneous. The lighter colors in Figure 55C, dark in the height image (Figure 55B), seem to appear due to a pore or hole, which may have resulted in the tip not reaching the bottom of the hole.

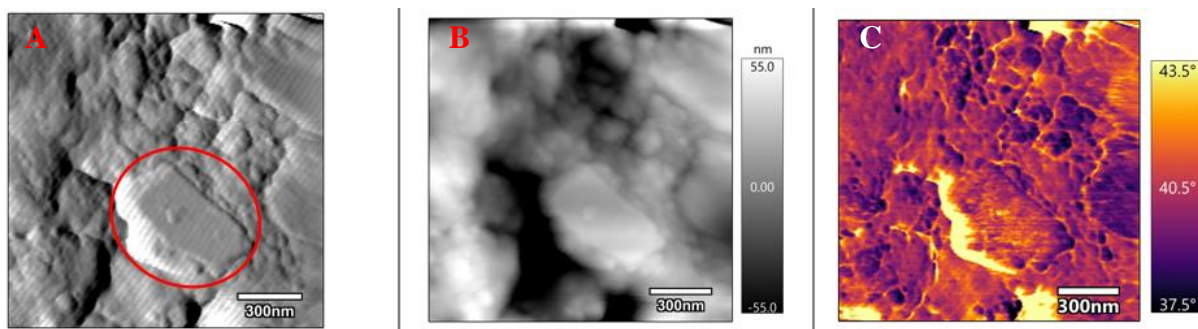


Figure 55 One measured area from sample OBSV12_6 demonstrating amplitude image (A, red circle indicating possible clay particle), height image (B) and phase image (C). Scale bar is 300 nm.

The height image (Figure 56A) of another area in OBSV12_6 indicates 170 nm height difference in the sampled area, but it might be that in the darkest locations, the tip has not reached the bottom; therefore this effect. A feature can be observed in the deflection image (red circle in Figure 56B), probably clay, but could be another small mineral phase (50 nm) as well, like new grown magnesite. The shape is slightly elongated, but as well curved, untypical for the features observed earlier in Figure 51. The phase marked with a blue circle seems to be a primary mineral with a very different surface than the main mineral between the two colored circles. This material is characterized by rounded features, which are hard to distinguish and may resemble carbonate, possible calcite (Figure 20).

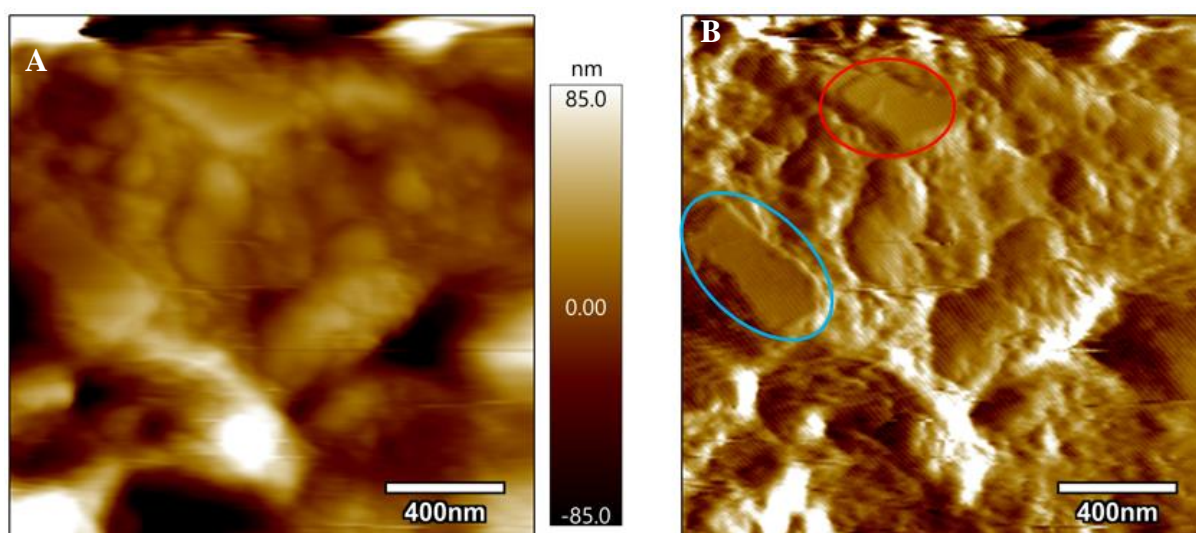


Figure 56 A second measured area in OBSV12_6. A) height image, B) deflection image (red circle includes a very small phase, possibly a clay mineral; blue circle indicating a relatively flat feature). Scale bar is 400 nm.

From the height profile (Figure 57) it can be seen that the two flat surfaced features described above (Figure 55) are higher than the area around. They both have a height of approximately 40 nm, which may be caused by their hardness. However, it is necessary to apply other identification methods to determine the phases.

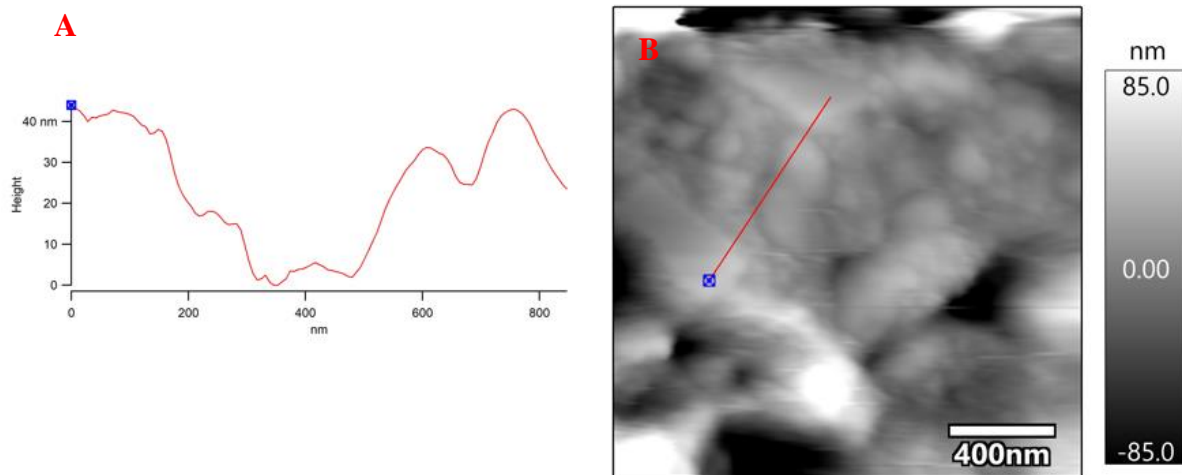


Figure 57 Illustrating a height profile (A) over a selected line (red line in B) in the measured area from Figure 55. Scale bar is 400 nm.

A feature is observed in all of the images in Figure 58. The feature is elevated (200-300 nm) on both sides and may be a remnant of a fossil or a more resistant structure. Alternatively, it may be a newly grown phase in the rock. The phase image (Figure 58C) indicates a possible comparable composition of the different parts of the area, but the unknown feature seems to have a lighter color than the surroundings. The height image (Figure 58B) illustrates an overall height difference of 810 nm. The amplitude image (Figure 58A) displays the shape of the different features, with most of them appearing rounded and only few more angular. These shapes are of different sizes, the rounded ranges from approximately 18 nm to 50 nm, and the angular ones are around 62 nm. Overgrowing the angular shapes are some very small features, maybe clay minerals or other phases. Nevertheless, this demonstrates the extreme attractive potential of the AFM to discover phases, further work is needed to characterize those for identification or similar phases.

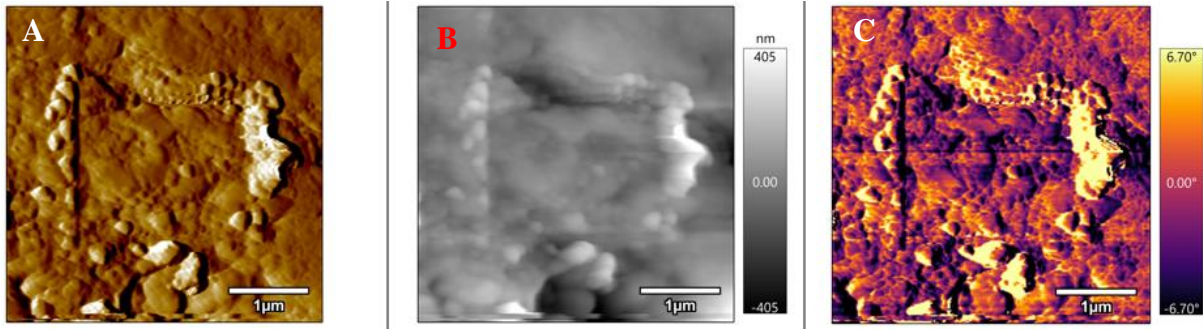


Figure 58 A second measured area from sample OBSV12_6 displaying amplitude image (A), height image (B) and phase image (C). All images indicate signs of an unknown feature in the middle of the image. Scale bar is 1 μm .

3.1.7 OBSV12 – MFP-3D Origin

The rock sample is a chalk from Mons basin (Belgium), it is not flooded nor polished.

The images in Figure 59 illustrates an area of around 15 μm , with a height difference (Figure 59A) of maximum 490 nm. The dark/light area to the right (red circles) in Figure 59A and B respectively may be caused by an area too deep for the tip to reach.

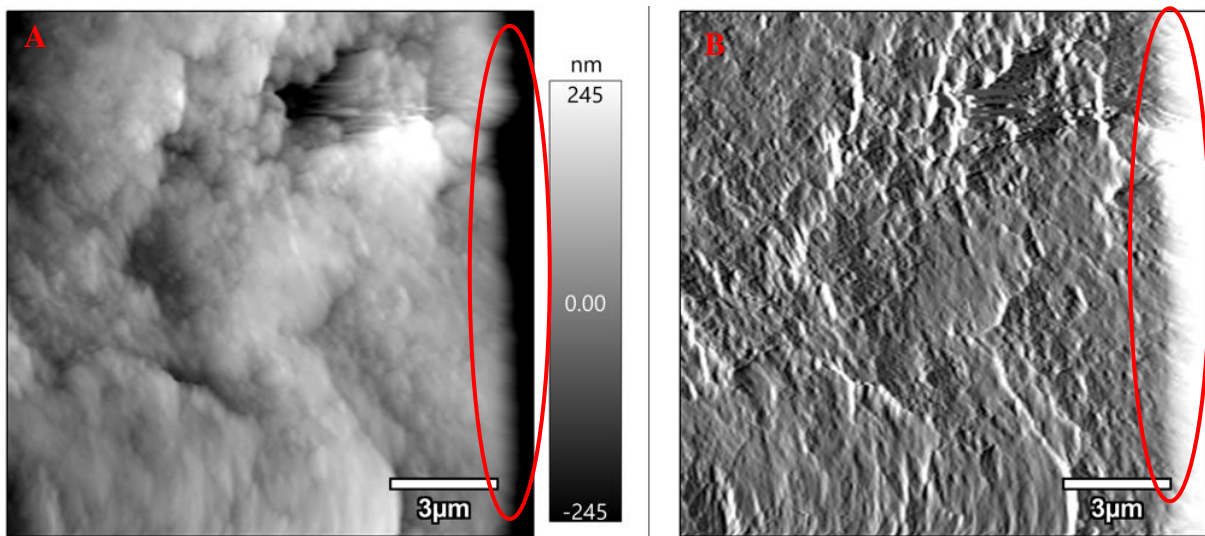


Figure 59 Displaying a measured area from sample OBSV12. A) height image, B) deflection image. The red circles indicate a deep area. Scale bar is 3 μm .

The height profile (Figure 60) illustrates different height all over the measured area. It indicates differences from -150 nm up to 150 nm over this particular line.

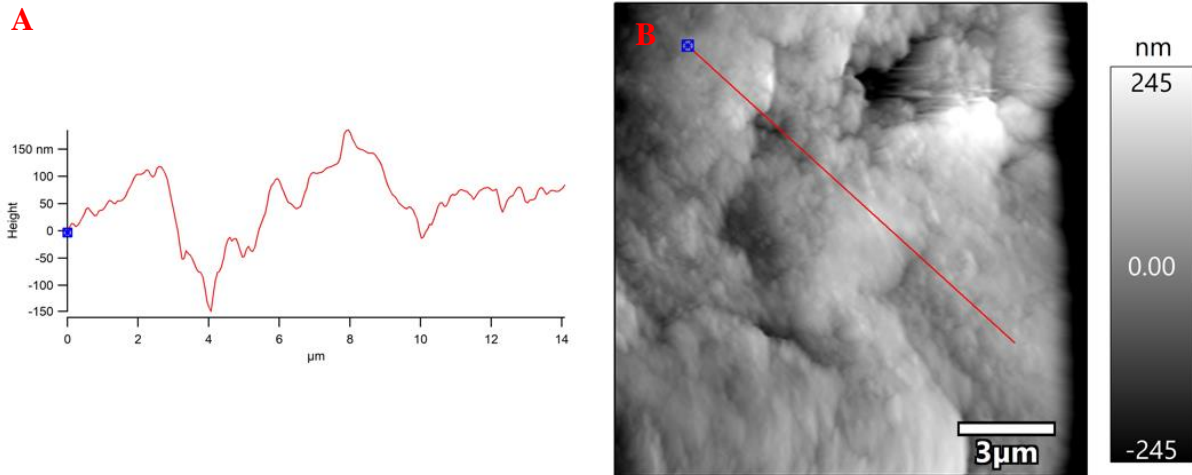


Figure 60 Illustrating a height profile (A) over the area from Figure 59 (red line in B). Scale bar is 3 μm .

All of the images from this area demonstrates the same kind of features, which may imply that this is all carbonate. Some images with a smaller area were measured, but no useful output has been gained.

3.1.8 OBSV18 – MFP-3D Origin

This chalk sample is from Mons basin (Belgium) and has been flooded with NaCl, which has most likely reacted inert with the rock (Andersen et al., 2017; Wang et al., 2016).

Figure 61 displays a height image (Figure 61A) and deflection image (Figure 61B), both reflecting signs of the sample moving during the measurement. This can be seen in the top part of both images, where it is “fuzzy”. The deflection image also displays some imaging artifacts or noise in the lower right corner. The features have smooth edges, which can be seen in both the deflection image and the 3D image of the height (Figure 62). An unknown feature is observed in the blue circle in Figure 61B where this is a coccolithophore beyond doubt.

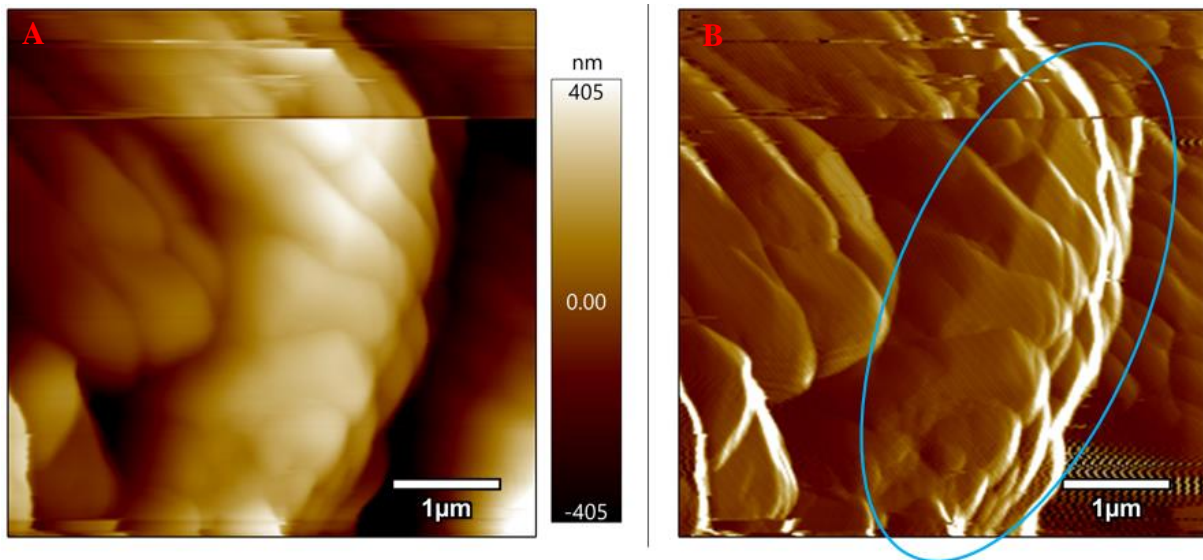


Figure 61 Displays a measured area from OBSV18. A) height image, B) deflection image, blue circle indicating an unknown feature. Scale bar is 1 μm .

This part of a coccolithophore is perfectly imaged in the 3D image on Figure 62. In the center of the fossil at the left corner of the image, cement or other organic or inorganic carbonate fragments are visible. The edges of this feature are also smooth and rounded and it is even possible to observe the different angles of the compartments of the coccolithophore in relation to each other. This helps in identification and interpretation of microfossils of this type (Saruwatari et al., 2011).

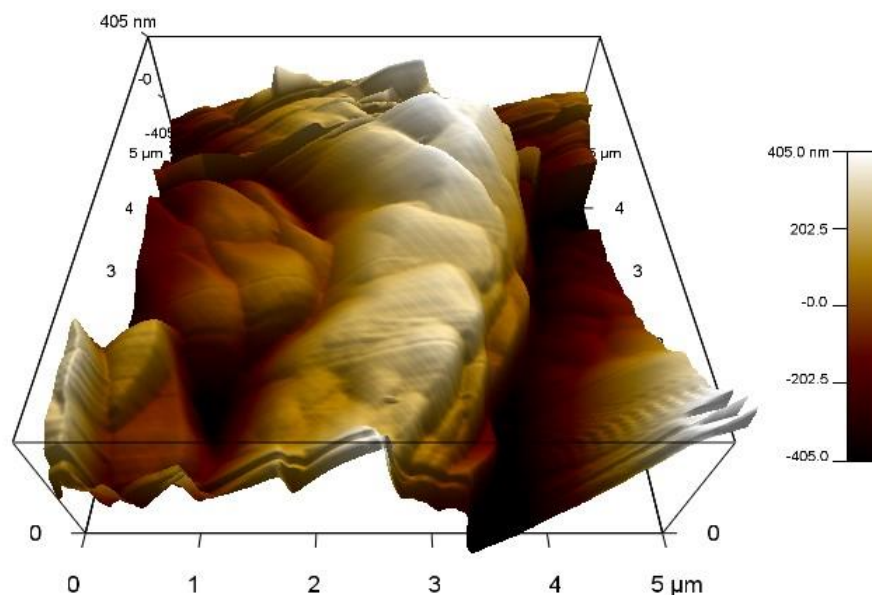


Figure 62 3D image of the height from Figure 61 indicating a coccolithophore in the middle. Area measures 5 x 5 μm in x- and y-direction.

In Figure 63, a flat surface of a coccolithophore (circa 2 μ m) images a new grown elongated phase of around 400 nm in length. It is relatively flat as it cannot be seen in the height image (Figure 63A), only in the deflection image (Figure 63B), which is a very interesting observation. Flooding with NaCl, as mentioned, would not change the mineralogy and rock mechanics of chalk significantly (Wang et al., 2016), and hence suggests that this feature is primary.

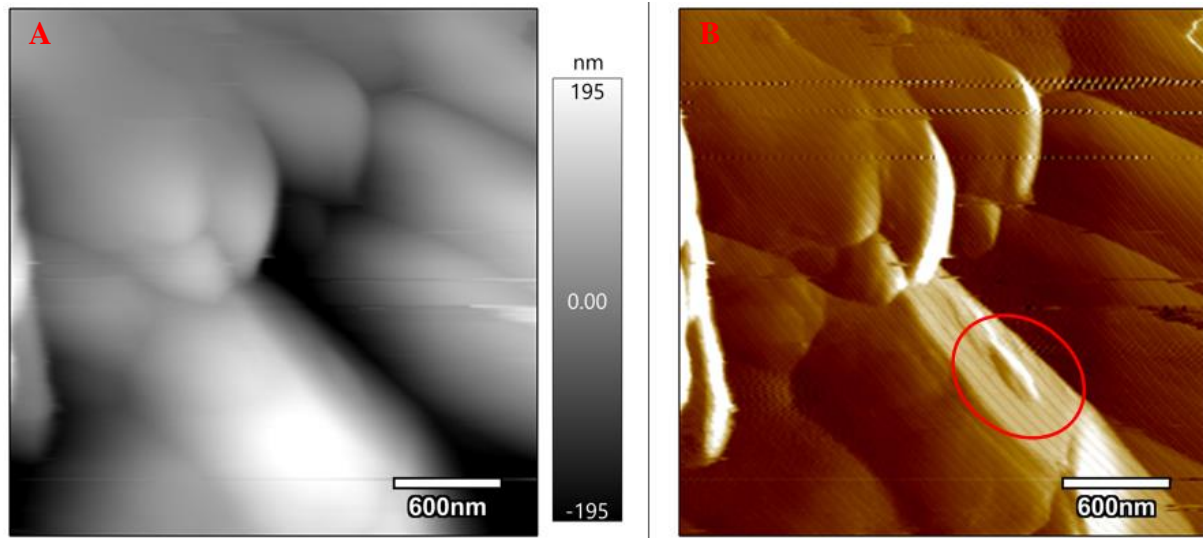


Figure 63 Demonstrating another measured area from OBSV18. A) height image, B) deflection image, red circle indicating an unknown particle. Scale bar is 600 nm.

The features observed in Figure 64 looks even more rounded than the previous ones, although these large units are again parts of a coccolithophore. Some height differences (Figure 64A) are obvious and reflect fantastically the boundaries in between the fossil segments from another angle than in Figure 50B, for instance. The roughness has been calculated on the lower feature (Figure 65), and the very low RMS of 19.126 nm indicates that this part of the surface is rather smooth and flat.

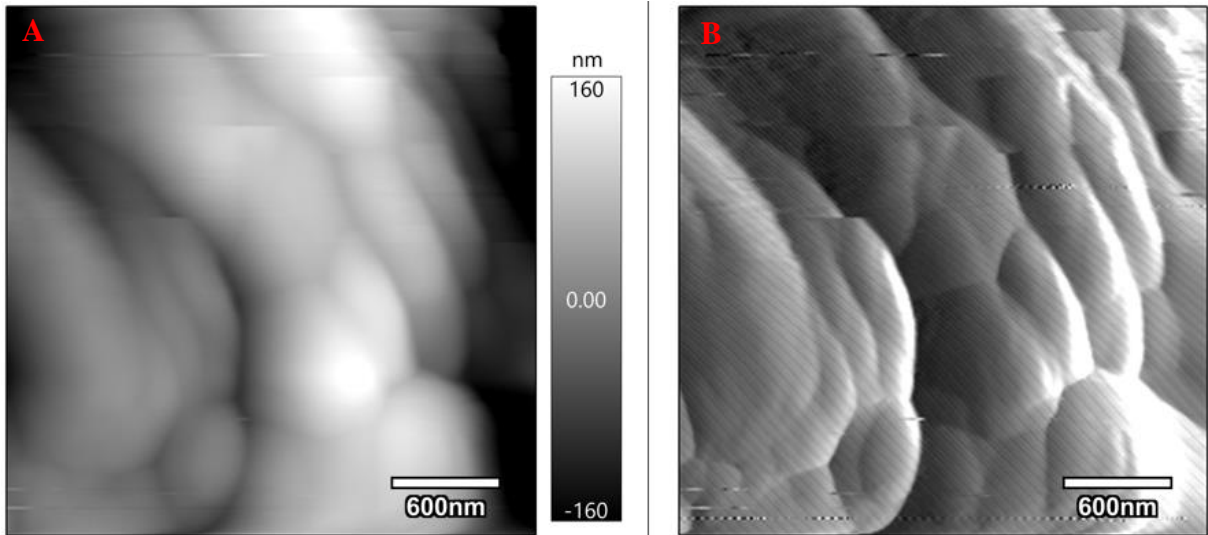


Figure 64 A third measured area from OBSV18. A) height image, B) deflection image. Scale bar is 600 nm.

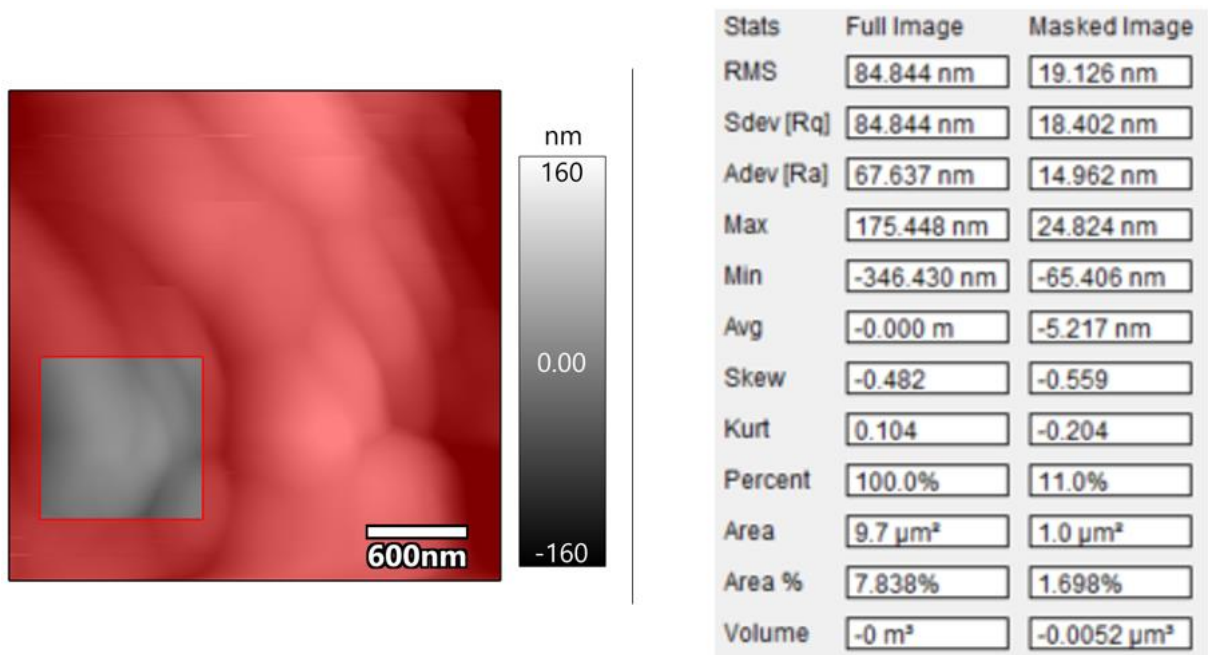


Figure 65 Calculating the roughness of the masked area (gray square in the left image) with the result in the table to the right.

3.1.9 Chalk SK – MFP-3D Origin

This rock sample is the cleanest in terms of its carbonate content and is an unflooded chalk from Stevns Klint (Denmark). The majority of the studied samples area unpolished. This sample, however, was both polished and unpolished (Chapter 2.4.2 Sample Preparation) to be able to identify if there are any differences and how the results are affected by the two different preparation methods to know which type of preparation benefits this type of study.

Unpolished sample

From Figure 66, rounded features with smooth edges can be clearly observed. The height difference is 310 nm, and both, the low features, possibly a pore, and the higher features are imaged. It seems that the features all have similar structure, smaller features with rounded edges shaping larger elongated components as observed in carbonates above (Figure 19, Figure 21 and Figure 25).

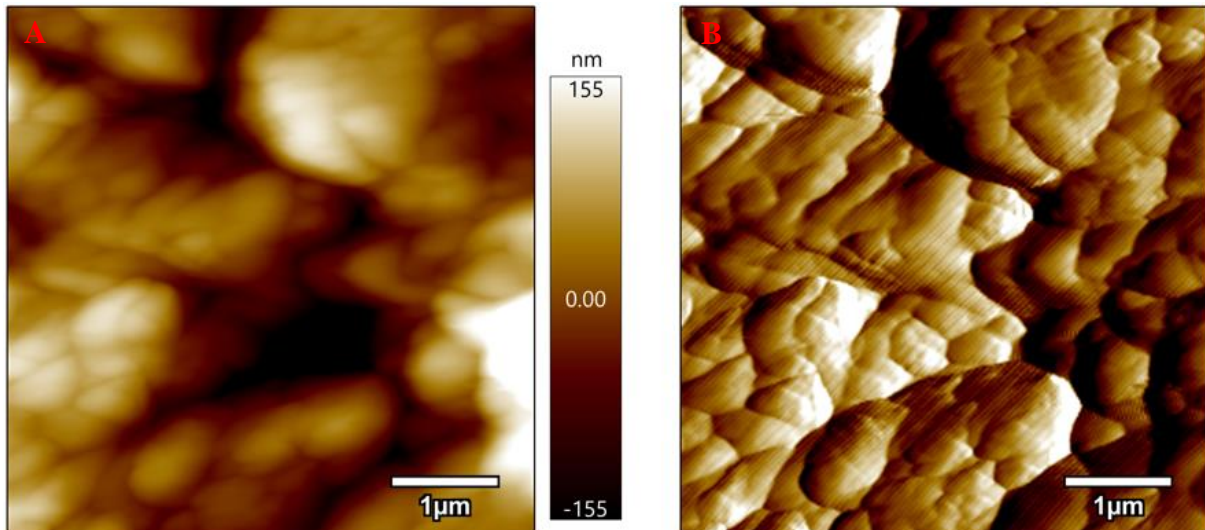


Figure 66 Illustrating one of the measured areas from the unpolished sample Chalk SK. A) height image, B) deflection image. Scale bar is 1 μm .

Figure 67 displays an amplitude image (Figure 67A), a height image (Figure 67B) and a phase image (Figure 67C). The height image indicates 360 nm height difference in the area with a long part being the lowest (the darkest area). From the amplitude and the phase images it is feasible to suspect that this part is a pore. The phase image displays similar colors in the entire area, indicating that it contains the same phases which makes sense, as it is almost only calcite in the sample. The right part of the area seems a bit elevated in comparison to the left side, observable in both the amplitude and the height image. The amplitude image displays the rounded features with smooth edges which has been seen in other areas of the sample as well.

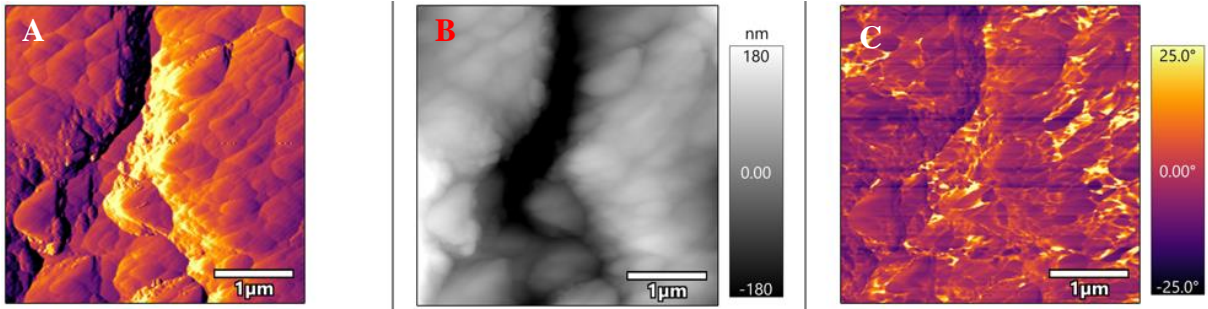


Figure 67 A second measured area from the unpolished sample of Chalk SK, demonstrating amplitude image (A), height image (B) and phase image (C). Scale bar is 1 μm .

Polished sample

From Figure 68 it is hard to distinguish any features on the surface of the sample. The height image (Figure 68A) indicates only 58 nm height difference, which is less than the other samples. Both the height image and the deflection image display signs from the polishing, both lines and leftover minute dust. They are white in the height image and appears like small grains in the deflection image.

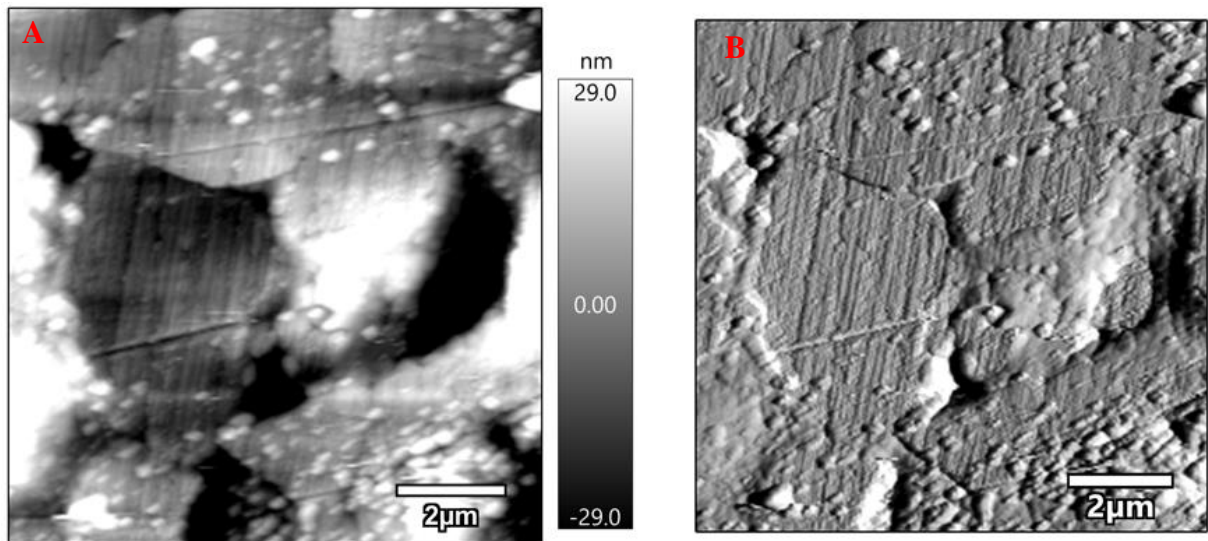


Figure 68 A measured area from the polished sample of Chalk SK, demonstrating signs of polishing dust and stripes. A) height image, B) deflection image. Scale bar is 2 μm .

The roughness has been calculated (Figure 69) over an area of 1 μm^2 , and the surface is smooth as the RMS is only 15 nm.

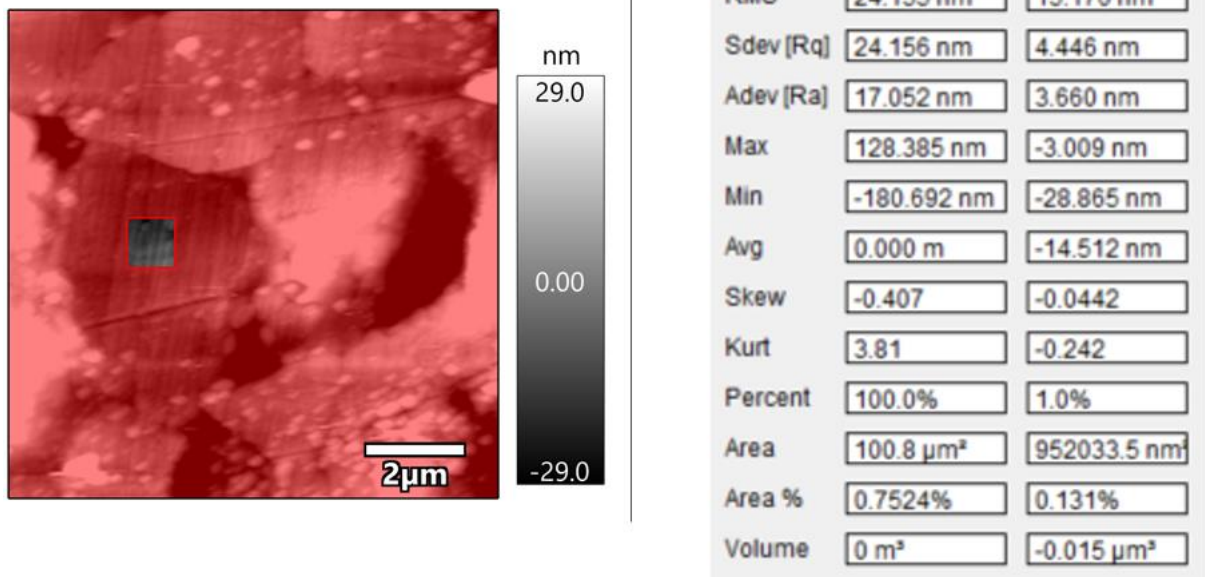


Figure 69 Calculating the roughness of the masked area (gray square in the left image) with the result in the table to the right.

The difference in the polished and unpolished preparation is very clear to observe (Figure 70) and therefore polished samples are, for this type of study very difficult to interpret. With a polished sample it is harder to differentiate minerals and materials by looking at the surface in the AFM.

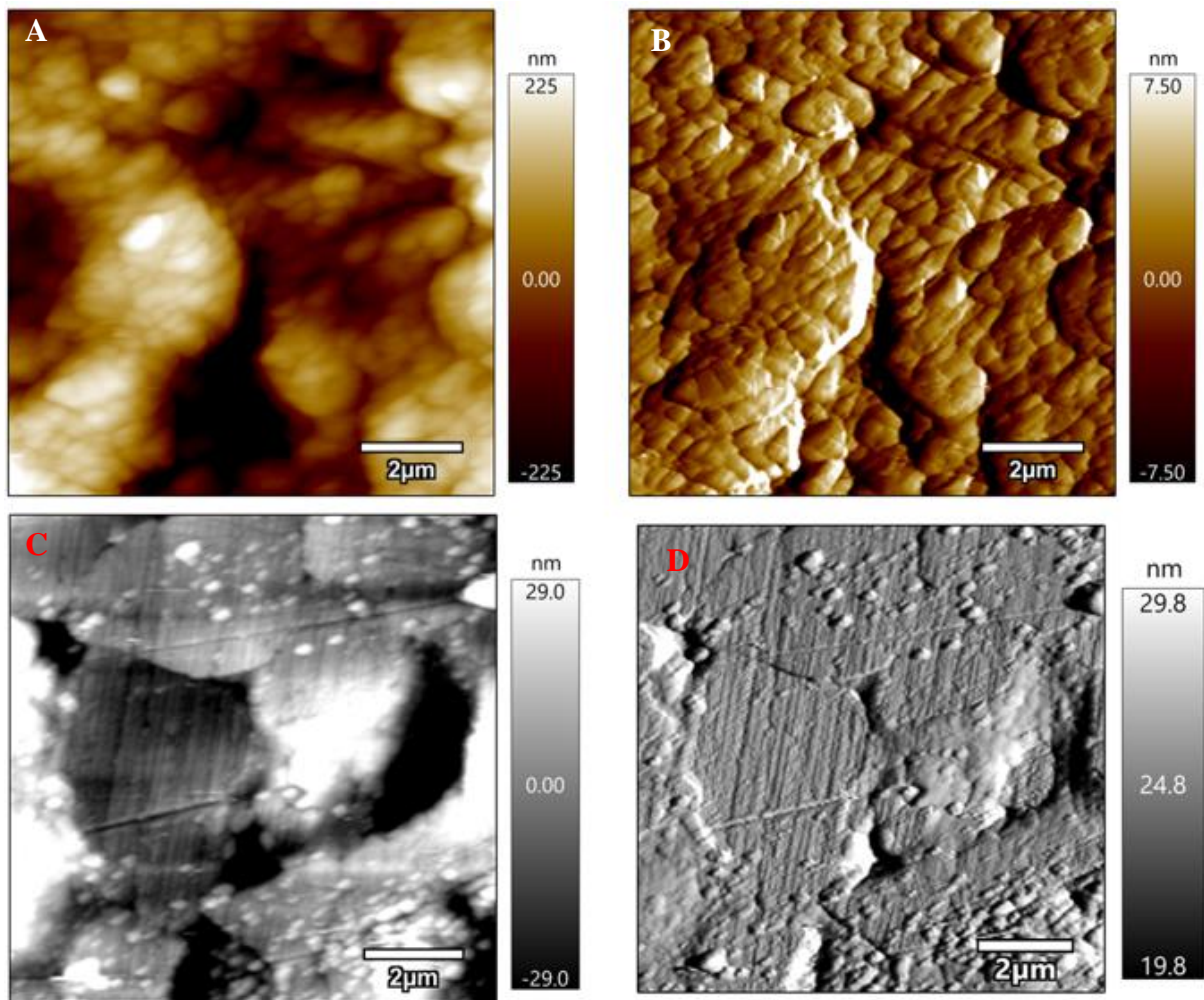


Figure 70 Demonstrating the difference between unpolished (A and B) and polished (C and D) sample of Chalk SK. Scale bar is 2 μm.

3.1.10 Unflooded Liège

The rock sample is a chalk from Liège (Belgium), and it is unflooded.

The height image (Figure 71A) indicates a large height difference of 3.41 μm. The features have some similarities to MLTT (calcite part) (Figure 38 and Figure 39), and in this case a coccolithophore is imaged which disappears into view direction and the surrounding matrix is mainly representing the left part of the sampled area. Rounded features, close to the larger stacked area, are loose and broken coccolithophore fragments composed of calcite (Figure 71B). The image has been affected by the surrounding noise and disturbances in the room when taking the measurements.

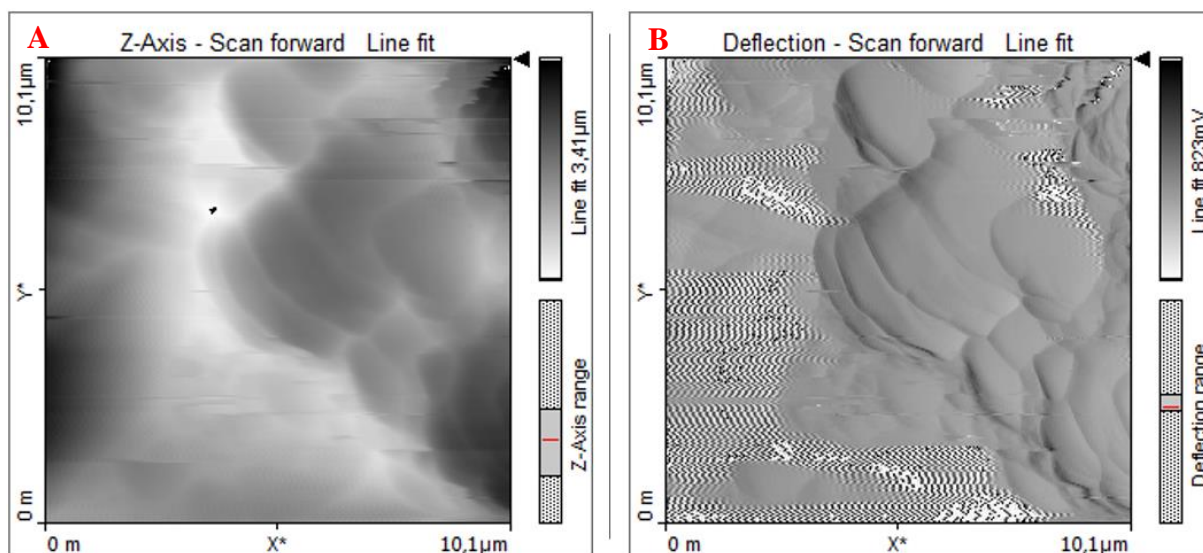


Figure 71 Displaying a measured area from the Unflooded Liège sample with height image (A) and deflection image (B). Area of $10 \mu\text{m}^2$.

The features in Figure 72 can be observed as rounded and smooth, lying next to each other, together forming the topography of the calcite (Figure 19).

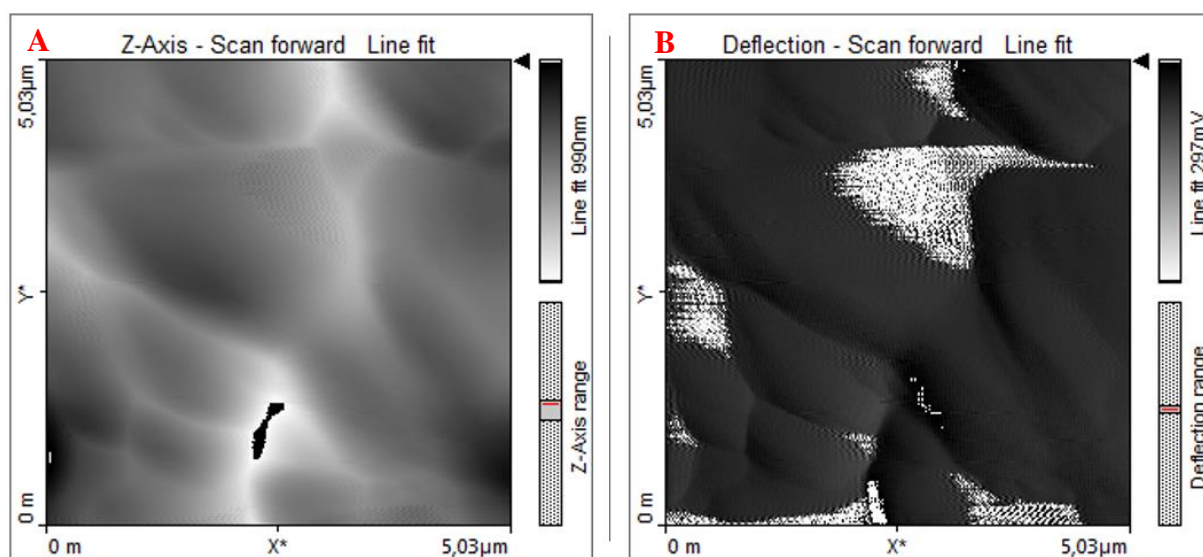


Figure 72 Another measured area from the Unflooded Liège sample with height image(A) and deflection image (B). Area of $5 \mu\text{m}^2$.

3.1.11 Kaolinite – MFP-3D Origin

This sample is taken from a rock sample, which is pure kaolinite. This sample, along with almost all the others, is unpolished to make sure the features does not disappear. In Figure 73, the crystal shape of kaolinite can be observed with angular corners and a platy cleavage stacking appearance. The kaolinite usually has a hexagonal shape (Zbik, 1998), however the shape

observed in this image can also occur. Moreover, it seems not to be a complete image, a certain cutting angle may have masked the real crystal form. The crystal in Figure 73 has a size of about 700 nm in length and 400 nm in width. In the two top crystals (red circles) in the deflection image, the typical structure of phyllosilicates can be observed with its platy-stacked character. A sampling with higher resolution and less noise would be needed to have a more detailed image.

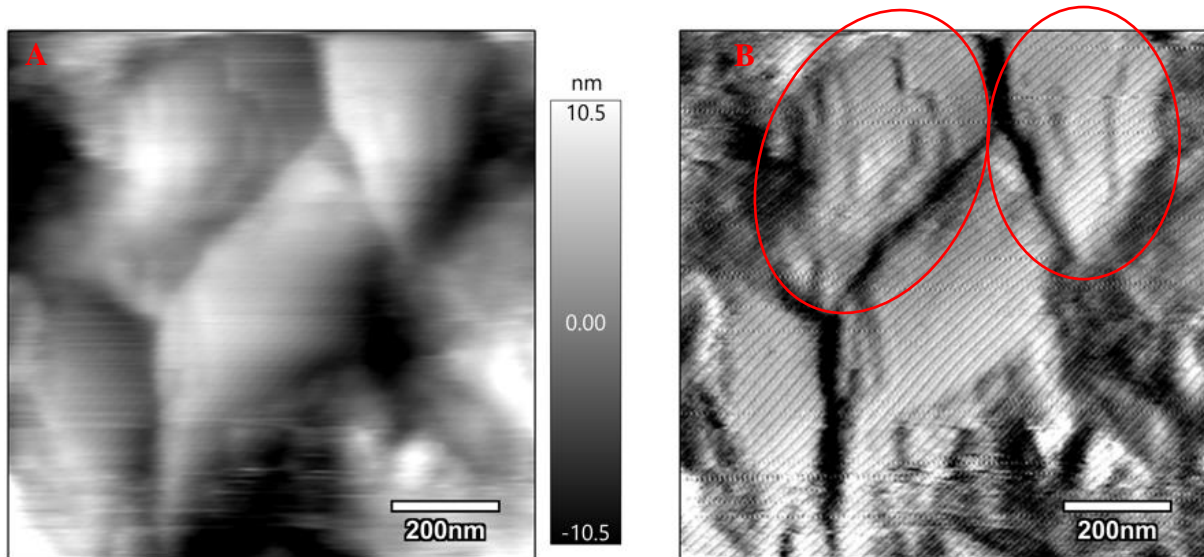


Figure 73 A measured area from the kaolinite sample displaying crystal structure, red circles indicating typical structure of phyllosilicates. A) height image, B) deflection image. Scale bar is 200 nm.

The height image (Figure 74A) indicates a larger hole/pore in the lower middle of the area. In the deflection image (Figure 74B), it is imaged as a relatively flat surface. It is uncertain if the tip has reached the bottom of the pore or not. The shape of the pore from the deflection image is believed to be almost the same as the crystal in the previous area (Figure 73). The height image also indicates 1 μm height difference all over the area, and it is possible to observe that the features on the left side are a bit raised than the features on the right side. These features are more blocky than the chalk samples and it is possible to see the typical phyllosilicate structure. The red circle in the deflection image indicates a smaller crystal than the surroundings.

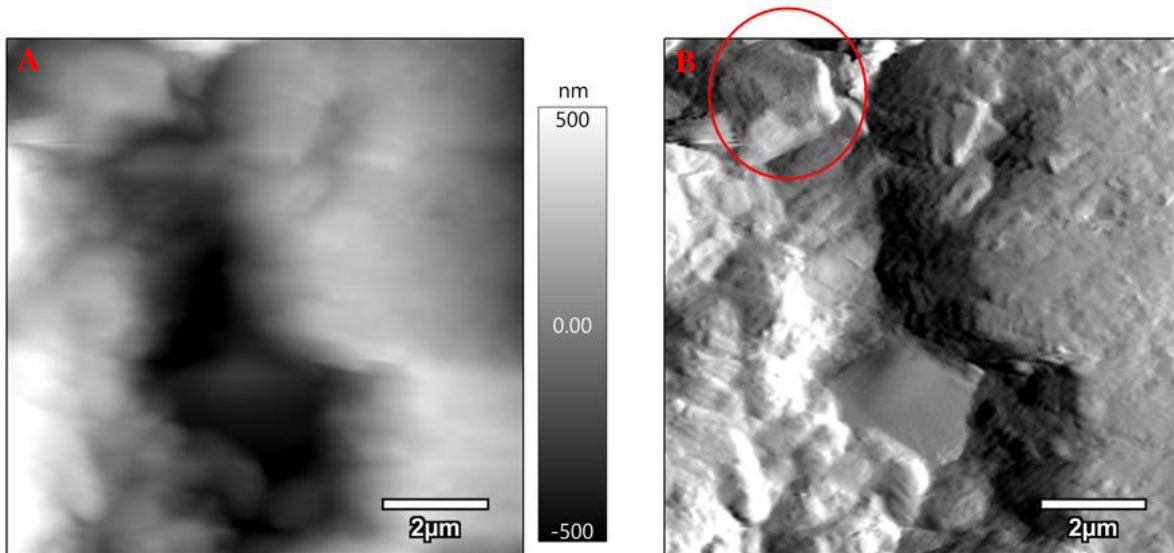


Figure 74 Demonstrating another measured area in the kaolinite sample. A) height image, B) deflection image, red circle indicating a similar shape as the crystal in Figure 73. Scale bar is 2 μm .

Figure 75 displays a height profile over the lowest area in the image, the assumed pore. The height difference from the highest feature to the bottom of the pore is 1 μm , while from the lower side to the right, the difference is 800 nm.

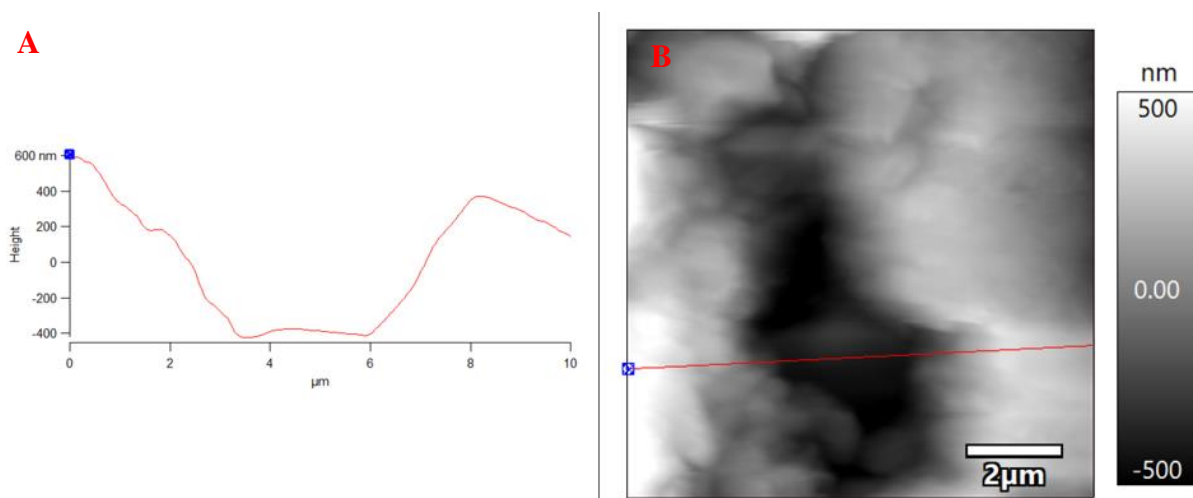


Figure 75 Illustrating a height profile (A) over the area from Figure 59 (red line in B). Scale bar is 2 μm .

The calculated roughness (Figure 76) indicates a rather rough surface.

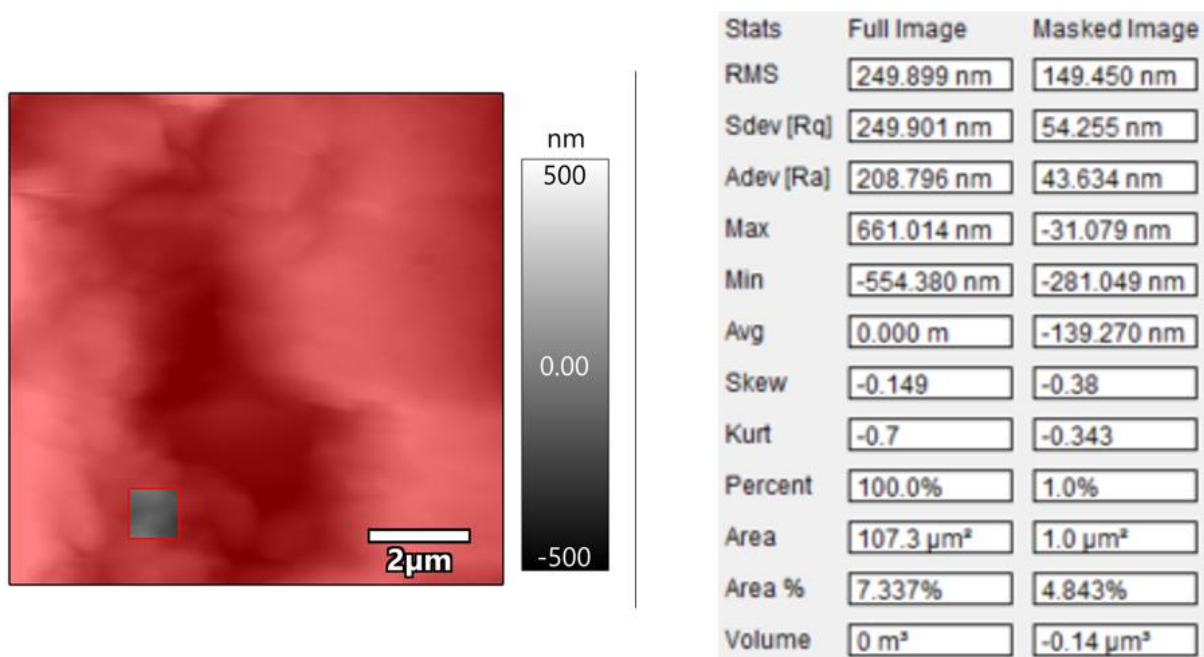


Figure 76 Calculating the roughness of the masked area (gray square in the left image) with the result in the table to the right pointing to high roughness, indicating that the surface is not smooth.

3.2 Force Spectroscopy

Force curves were not measured for all samples as this is a totally unknown field with the AFM at UiS and requires much more time than the Corona crisis allowed. Nevertheless, it was possible to carry out some preliminary studies on standard samples. Two samples (OBSV4_1 and OBSV12) were measured for force spectroscopy in Grenoble, prior to the Corona crisis, as a main goal for the first approach to the AFM. A second trip was cancelled; therefore, a pilot study is presented. The field of force spectroscopy is not only for this study but also novel for the samples investigated. Please note the theoretical explanation in Chapter Force Spectroscopy Measurements.

3.2.1 Standards

Anorthite

The areas (Figure 77A-B and Figure 78A-B) on the standard anorthite mineral has been measured to range between -170 mV and -12.5 mV as the lowest error signal, and between 344 mV and 415 mV as the highest.

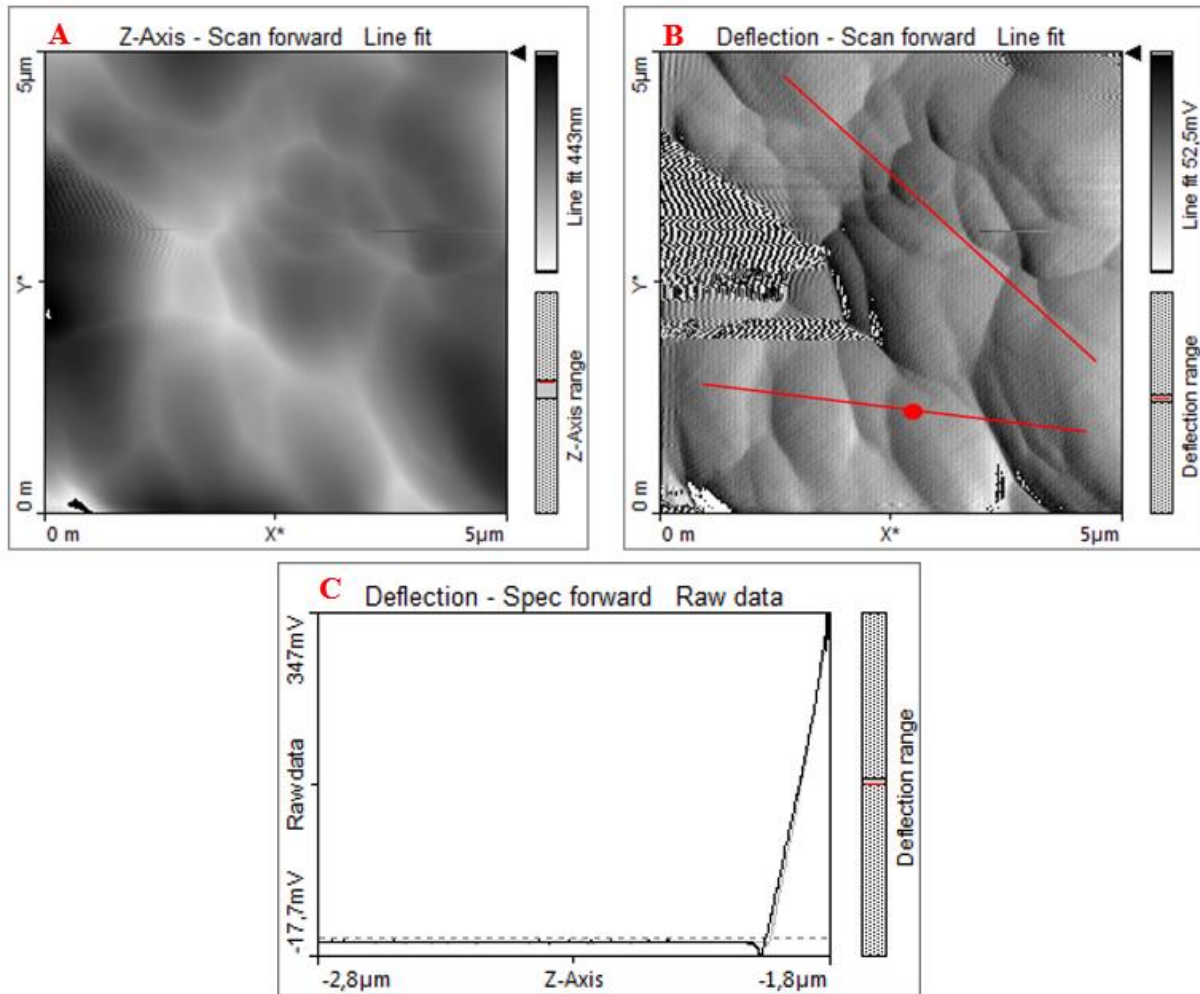


Figure 77 Illustrating a measured area of the anorthite with the respective force curve from the red point on the marked line in B. A) height image, B) deflection image indicating where the selected force curve is marked as a red point, C) the selected force curve indicating attractive force.

The negative values indicate an attractive force in the area (Figure 77C and Figure 78C). The point of snap-in of the tip varies from $-5.04 \mu\text{m}$ to -997 nm .

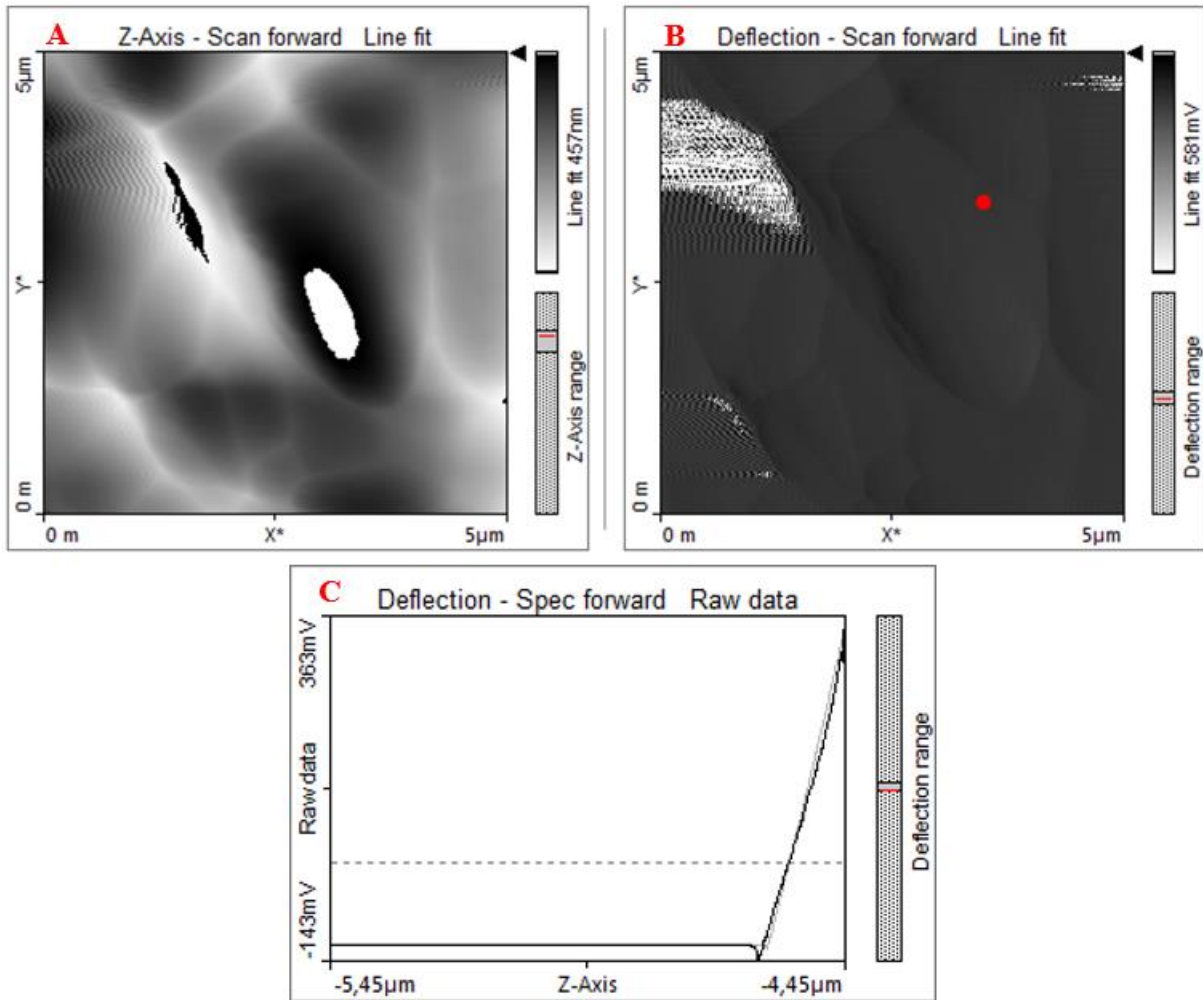


Figure 78 Displaying another measured area of the anorthite with the respective force curve from the red point in B. A) height image, B) deflection image indicating where the selected force curve is marked as a red point, C) the selected force curve indicating attractive force.

Calcite

Two areas (Figure 79A-B and Figure 80A-B) of the calcite mineral grain has been measured for force curves, both having an attractive force (Figure 79C-E and Figure 80C-E).

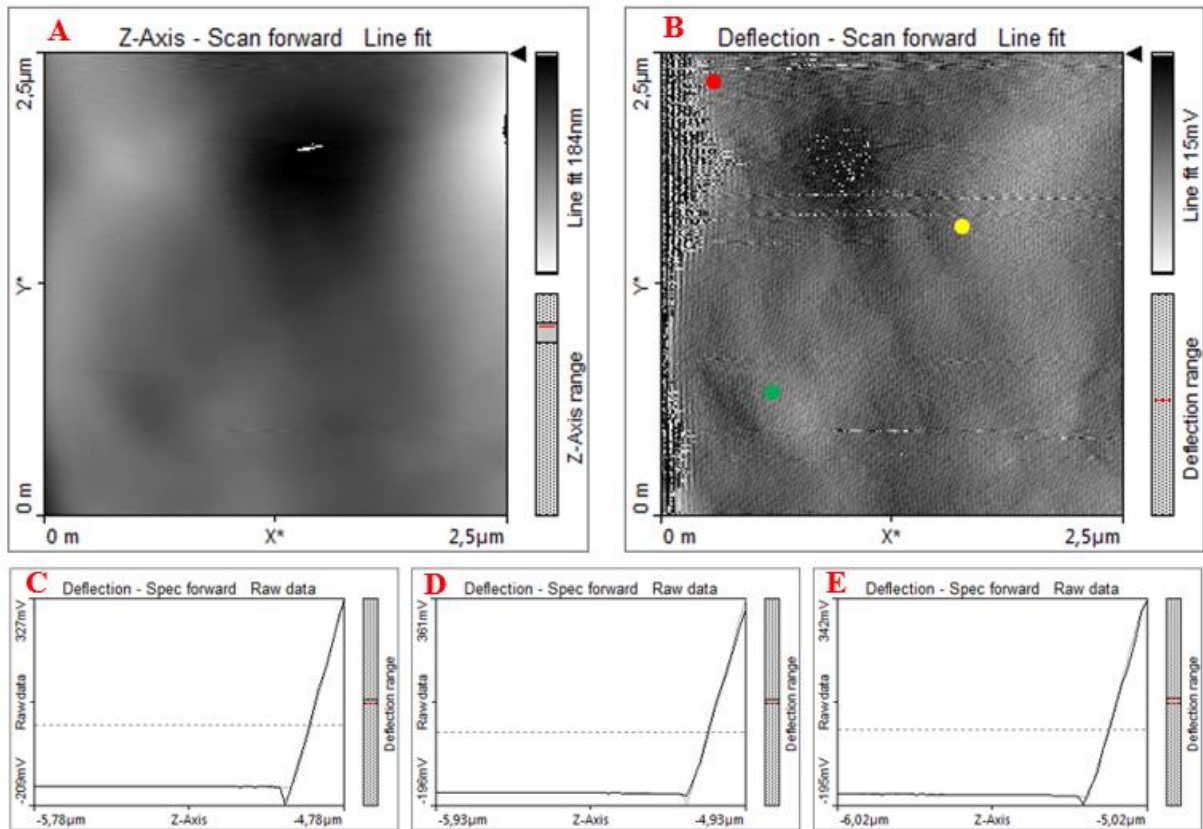


Figure 79 Demonstrating a measured area of the calcite with the respective force curves from the red, yellow, and green circles in B. A) height image, B) deflection image displaying where the selected force curves are marked with red, yellow and green circles, C) the selected force curve indicating attractive force from red circle, D) selected force curve indicating attractive force from yellow circle, E) selected force curve indicating attractive force from green circle.

The error signal was measured to be between -222 mV and -80.6 mV at the lowest, and 322 mV to 556 mV at the highest. The point of snap-in differs from -5.41 μm to -4.78 μm.

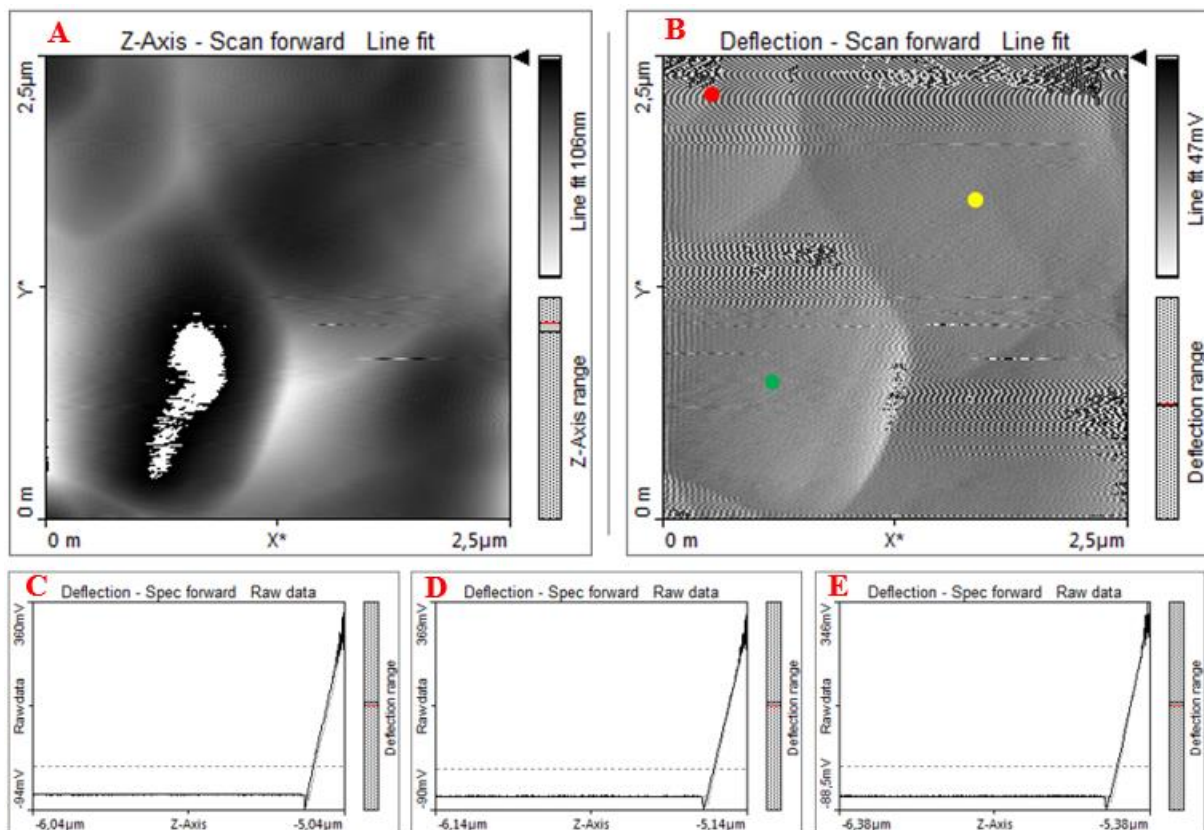


Figure 80 Illustrating another measured area of the calcite with the respective force curves from the red, yellow, and green circles in B. A) height image, B) deflection image displaying where the selected force curves are marked with red, yellow and green circles, C) the selected force curve indicating attractive force from red circle, D) selected force curve indicating attractive force from yellow circle, E) selected force curve indicating attractive force from green circle.

Dolomite

Force curves has only been measured in one area (Figure 80A-B) of the dolomite mineral grain, and it implies an attractive force (Figure 81C). The error signal was measured to range between -82.7 mV and -69.9 mV at the lowest while the highest is 322 mV to 442 mV. The point of snap-in varies from -4.66 μm to -4.17 μm .

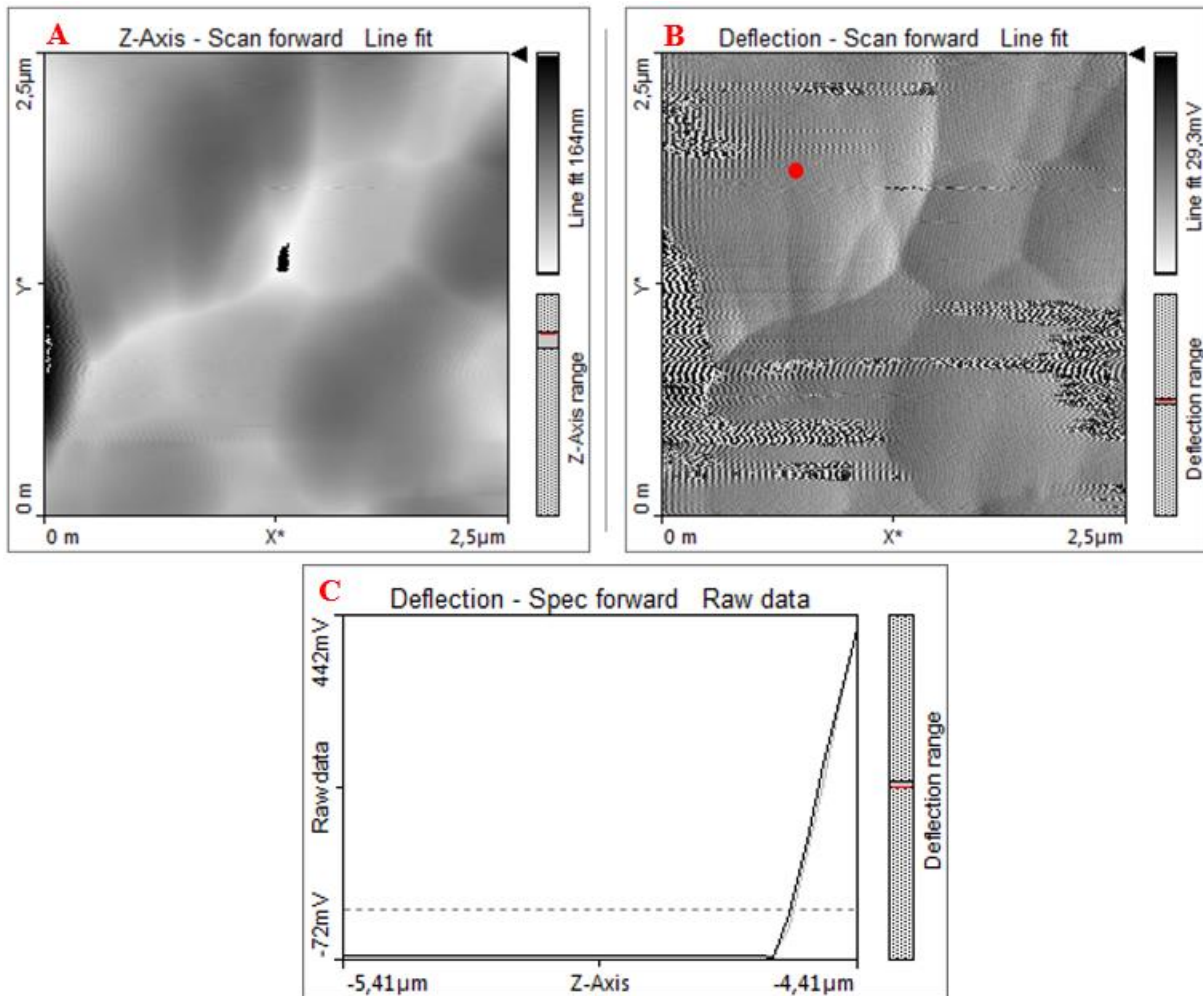


Figure 81 Displaying a measured area of the calcite with the respective force curve from the red point in B. A) height image, B) deflection image displaying where the selected force curve is marked as a red point, C) the selected force curve indicating attractive force.

Fluorapatite

Only one area (Figure 82A-B) of the fluorapatite grain has been measured for force curves, indicating a repulsive force (Figure 82C). The error signal varies from 14 mV to 22.3 mV as the lowest whereas the highest is 94.9 mV to 500 mV. The point of snap-in ranges from - 2.43 μm to -1.08 μm .

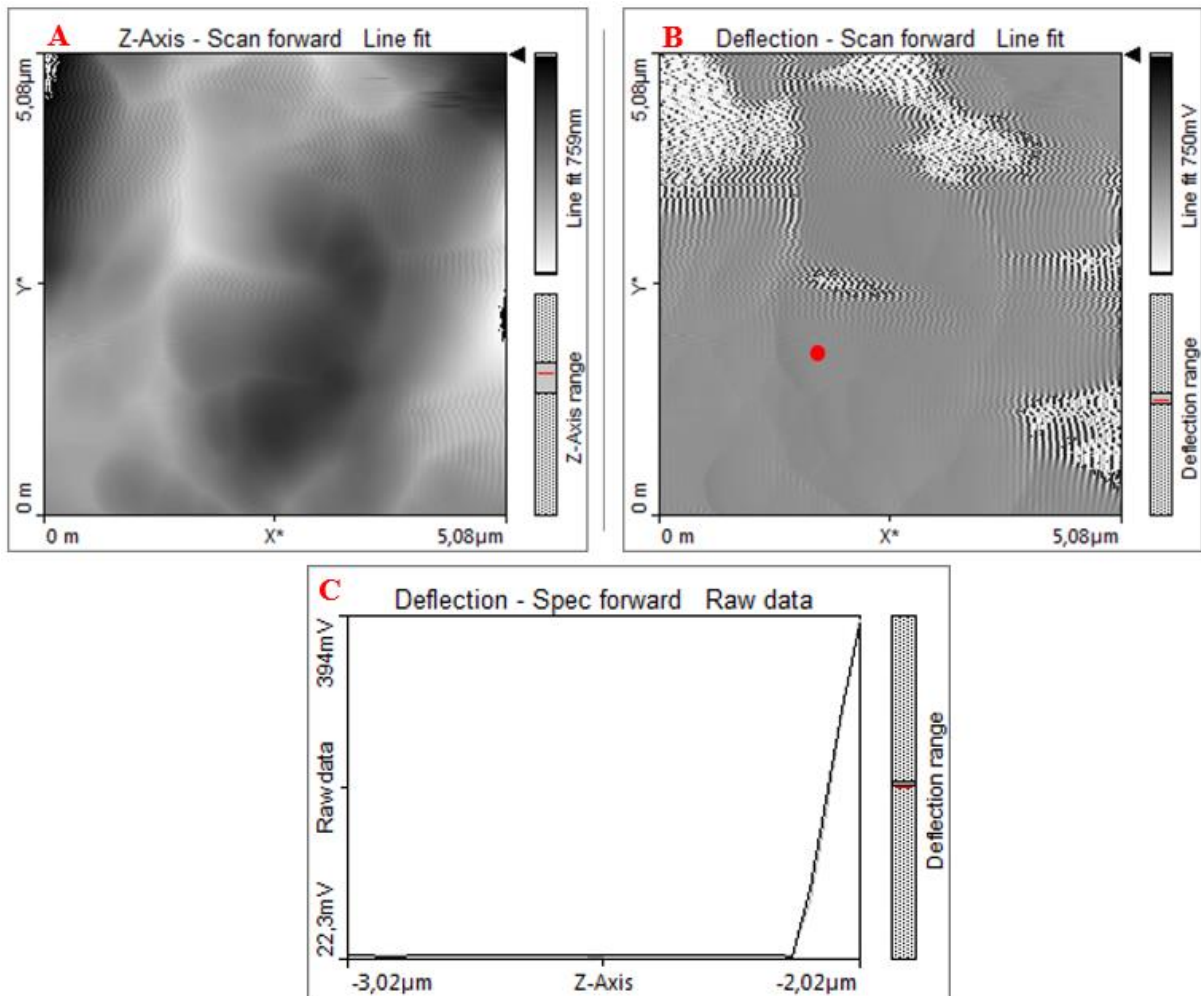


Figure 82 Illustrating a measured area of the fluorapatite with the respective force curve from the red point in B. A) height image, B) deflection image displaying where the selected force curve is marked as a red point, C) the selected force curve indicating repulsive force.

Ilmenite

Two different areas (Figure 83A-B and Figure 84A-B) on the ilmenite mineral grain has been measured, one area had a repulsive force (Figure 83C) while the other had an attractive force (Figure 84C).

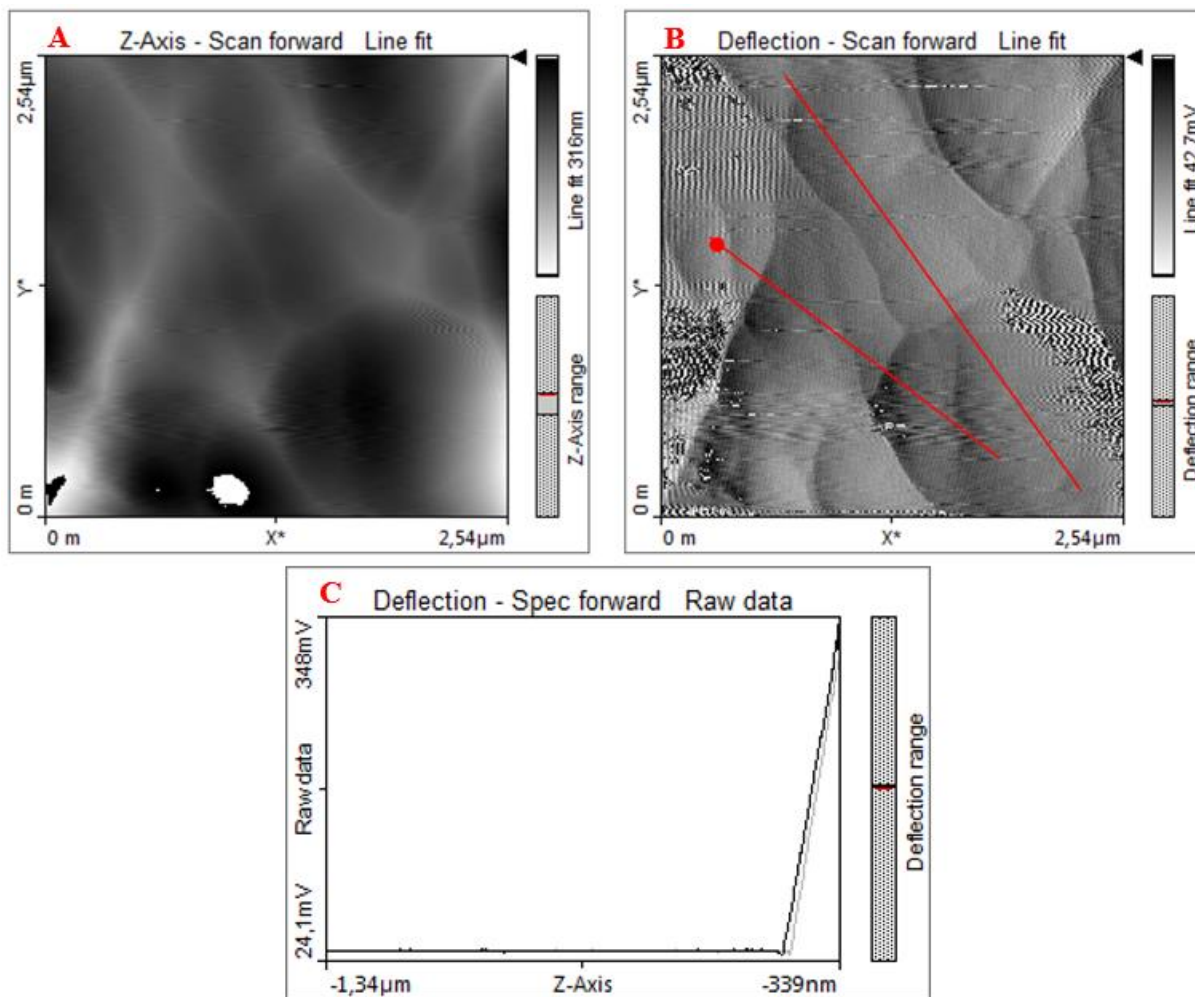


Figure 83 Demonstrating a measured area of the ilmenite with the respective force curve from the red point in B. A) height image, B) deflection image displaying where the selected force curve is marked as a red point on the red line, C) the selected force curve indicating repulsive force.

In the repulsive force area, the error signal was measured to be between 7.32 mV and 25.3 mV as the lowest and 347 mV to 546 mV as the highest, while in the attractive force area the lowest was between -106 mV and -59.8 mV and the highest is 345 mV to 480 mV.

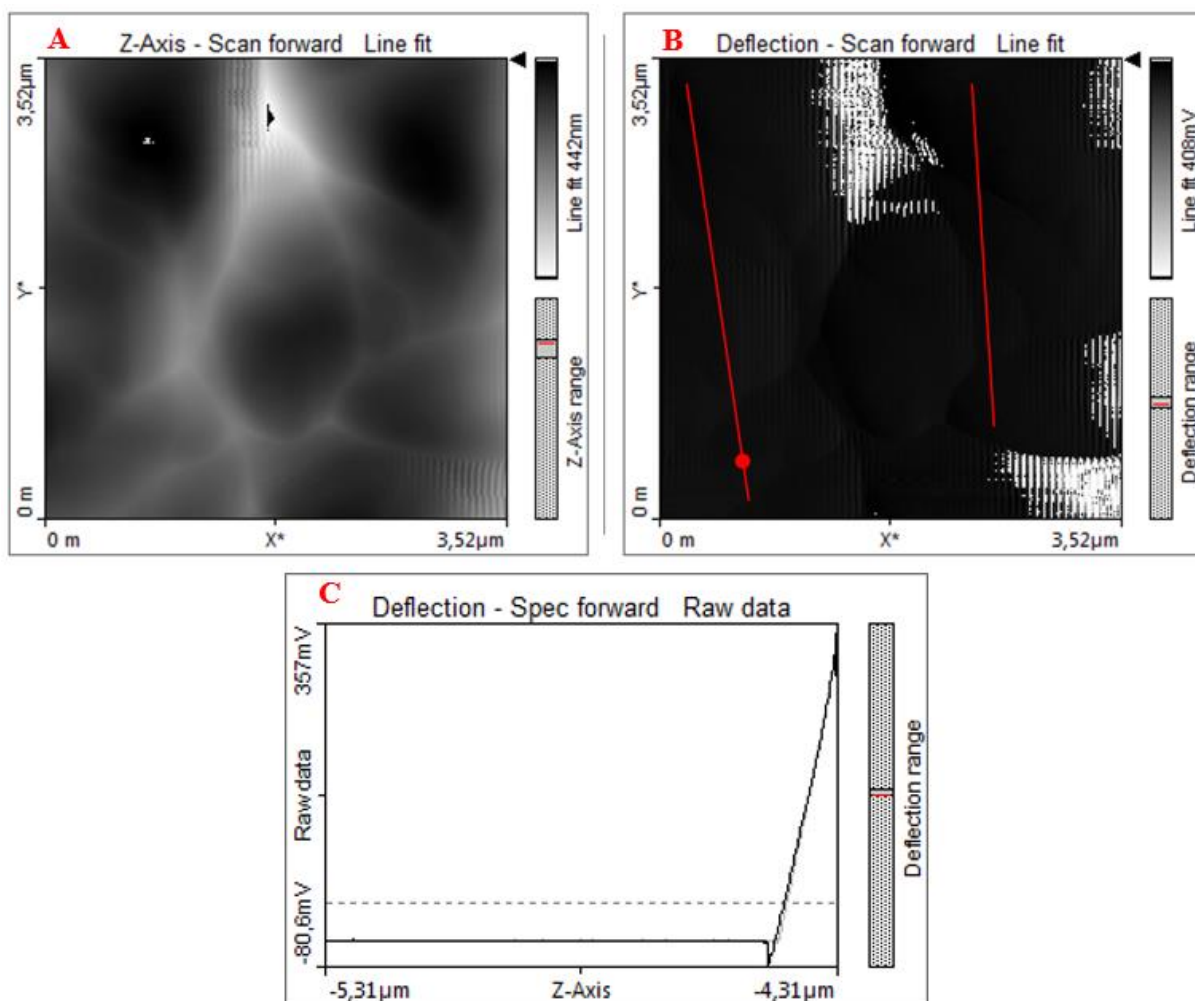


Figure 84 Displaying another measured area of the ilmenite with the respective force curve from the red circle in B. A) height image, B) deflection image illustrating where the selected force curve is marked as a red circle on the red line, C) the selected force curve indicating attractive force.

In the repulsive force area, the point of snap-in ranges between -707 nm and -25.6 nm, whereas in the attractive force area, the point of snap-in varies between -4.54 μm and -4.01 μm.

Magnesite

On the magnesite mineral grain, four areas have been measured, two being displayed here, (Figure 85A-B and Figure 86A-B), and only one of them had an attractive force. In the attractive force area (Figure 85C), one of the curves had a repulsive force (Figure 86C).

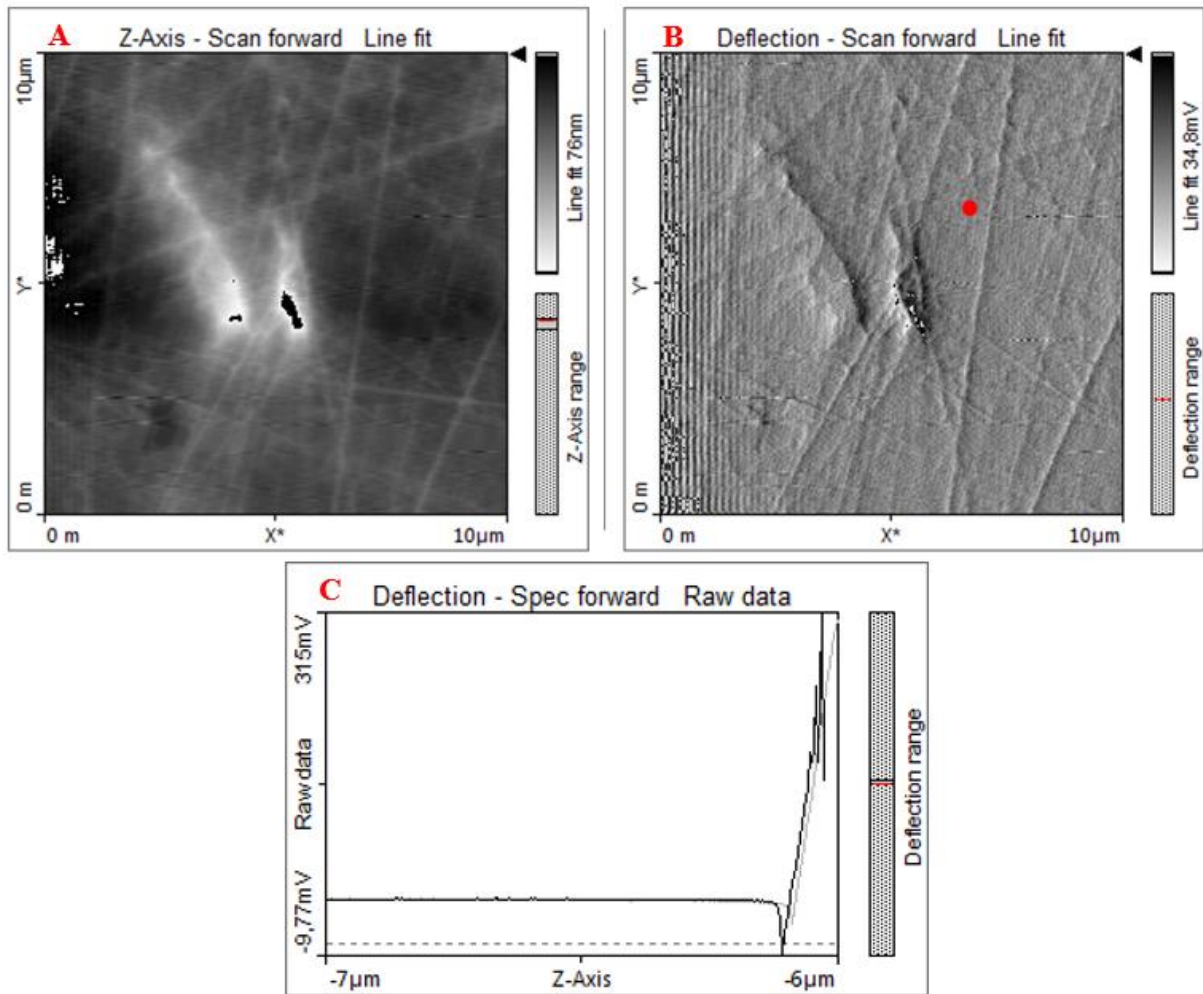


Figure 85 Displaying a measured area of the magnesite with the respective force curve from the red circle in B. A) height image, B) deflection image illustrating where the selected force curve is marked as a red circle, C) the selected force curve indicating attractive force.

The attractive force differs from -35.4 mV to -5.19 mV as the lowest error signal and 315 mV to 692 mV as the highest, while the repulsive force area ranges between 28.4 mV and 193 mV as the lowest and 329 mV to 551 mV as the highest. The snap-in point of the attractive force area was $-6 \mu\text{m}$ to $-5.91 \mu\text{m}$ and in the repulsive force areas it was $-1.16 \mu\text{m}$ to -404 nm .

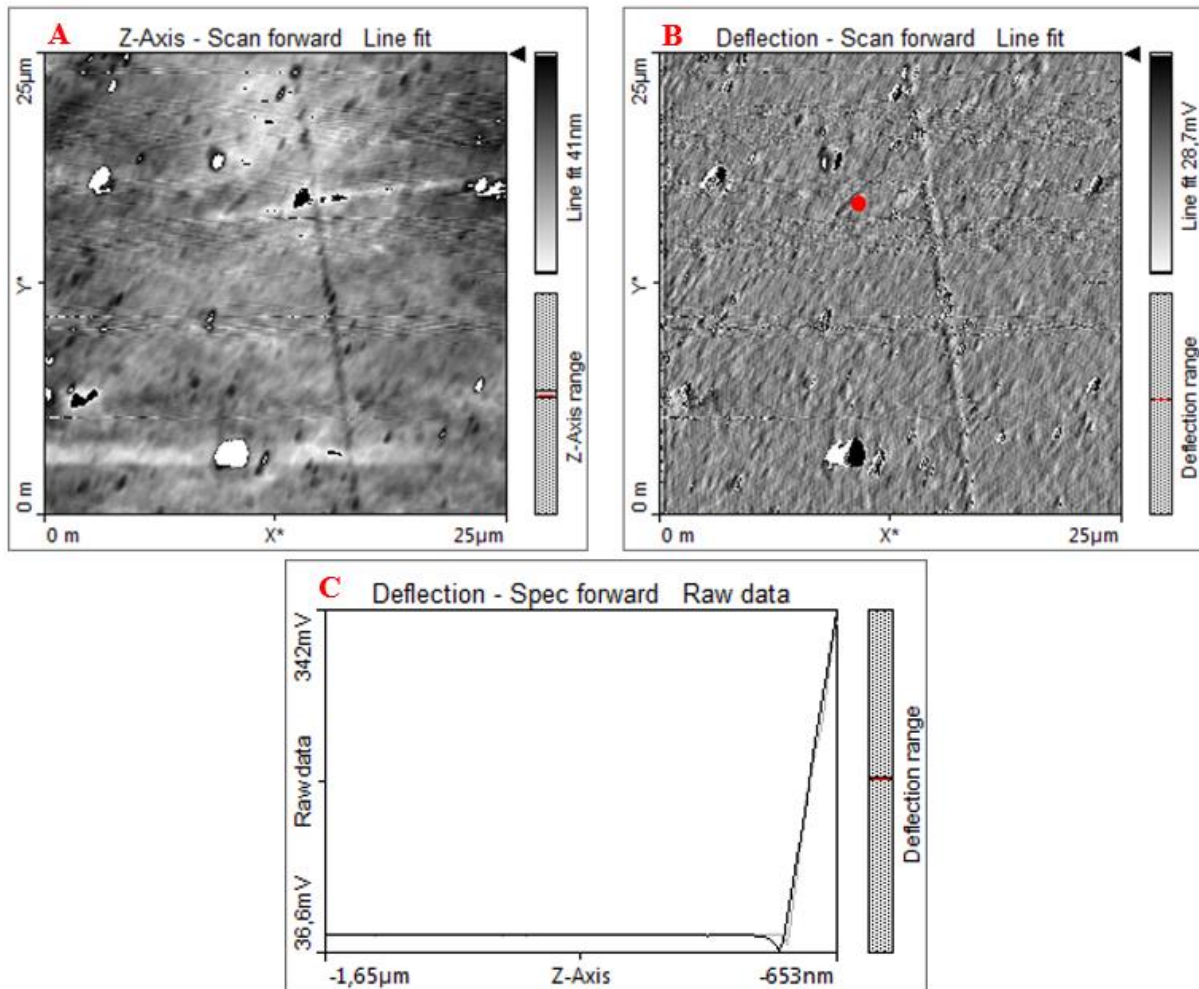


Figure 86 Illustrating another measured area of the magnetite with the respective force curve from the red circle in B. A) height image, B) deflection image illustrating where the selected force curve is marked as a red circle, C) the selected force curve indicating repulsive force.

Magnetite

Overall, the magnetite mineral grain (Figure 87A-B and Figure 88A-B) has an attractive force, with only three curves of repulsive force. The attractive force curves (Figure 87C) range between -71.7 mV and -1.53 mV as the lowest error signal while the highest is 327 mV to 650 mV. Here, the point of snap-in of the tip to the surface differs between -3.18 μm and -188 nm.

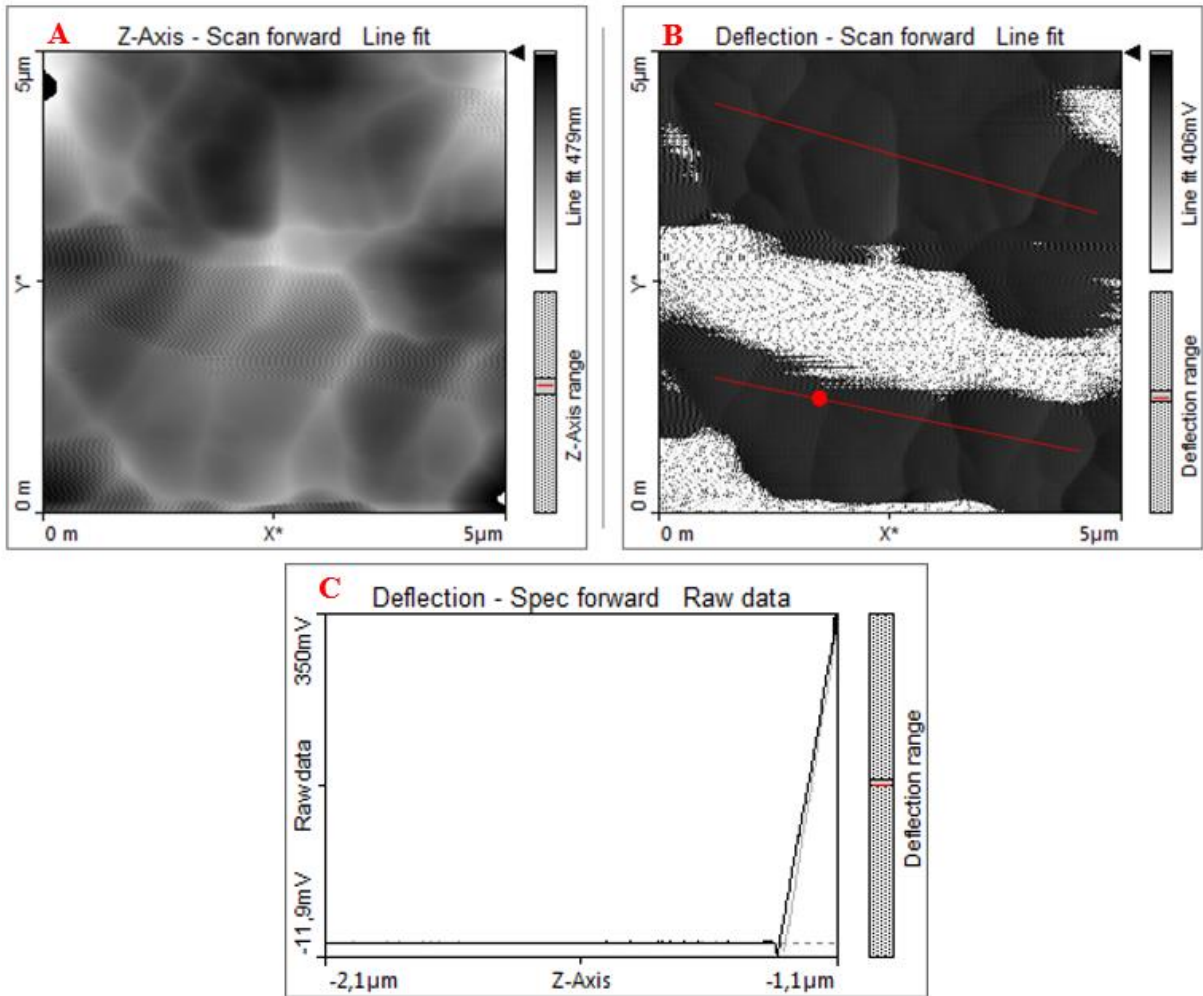


Figure 87 Demonstrating a measured area of the magnetite with the respective force curve from the red point in B. A) height image, B) deflection image illustrating where the selected force curve is marked as a red point on the red line, C) the selected force curve indicating attractive force.

In the repulsive force area (Figure 88C), the lowest error signal has been measured to vary between 2.14 mV and 3.05 mV while the highest is 327 mV to 371 mV. The snap-in point of the tip was between -770 nm and -188 nm for the three curves.

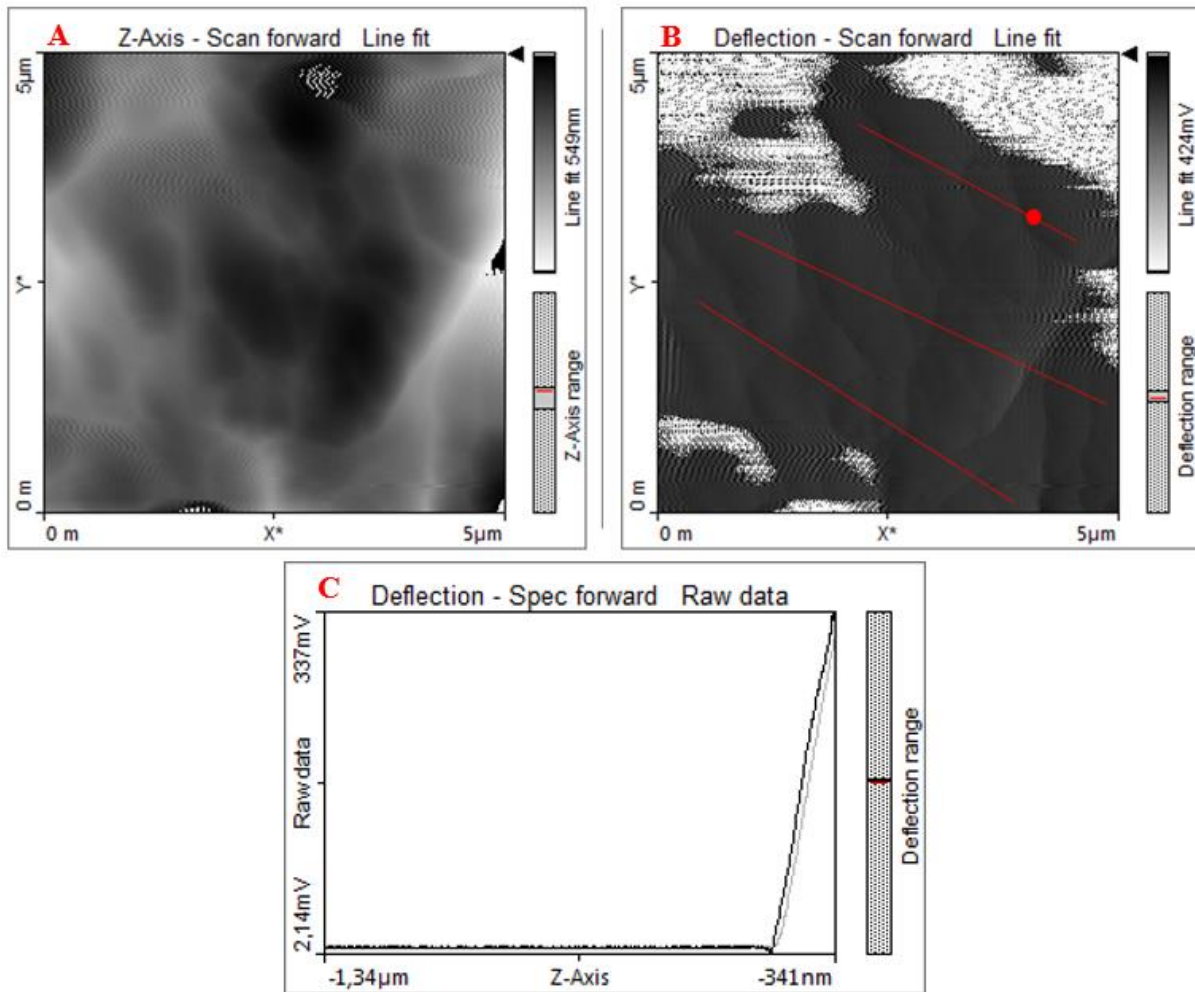


Figure 88 Displaying another measured area of the magnetite with the respective force curve from the red point in B. A) height image, B) deflection image displaying where the selected force curve is marked as a red point on the red line, C) the selected force curve indicating repulsive force.

Plagioclase

The measured area (Figure 89A-B) of the plagioclase mineral grain has a repulsive force (Figure 89C) with an error signal ranging from 1.83 mV to 16.8 mV as the lowest, to 333 mV to 615 mV as the highest. The point of the snap-in between the tip and the surface was between $-2.25 \mu\text{m}$ and $-1.68 \mu\text{m}$.

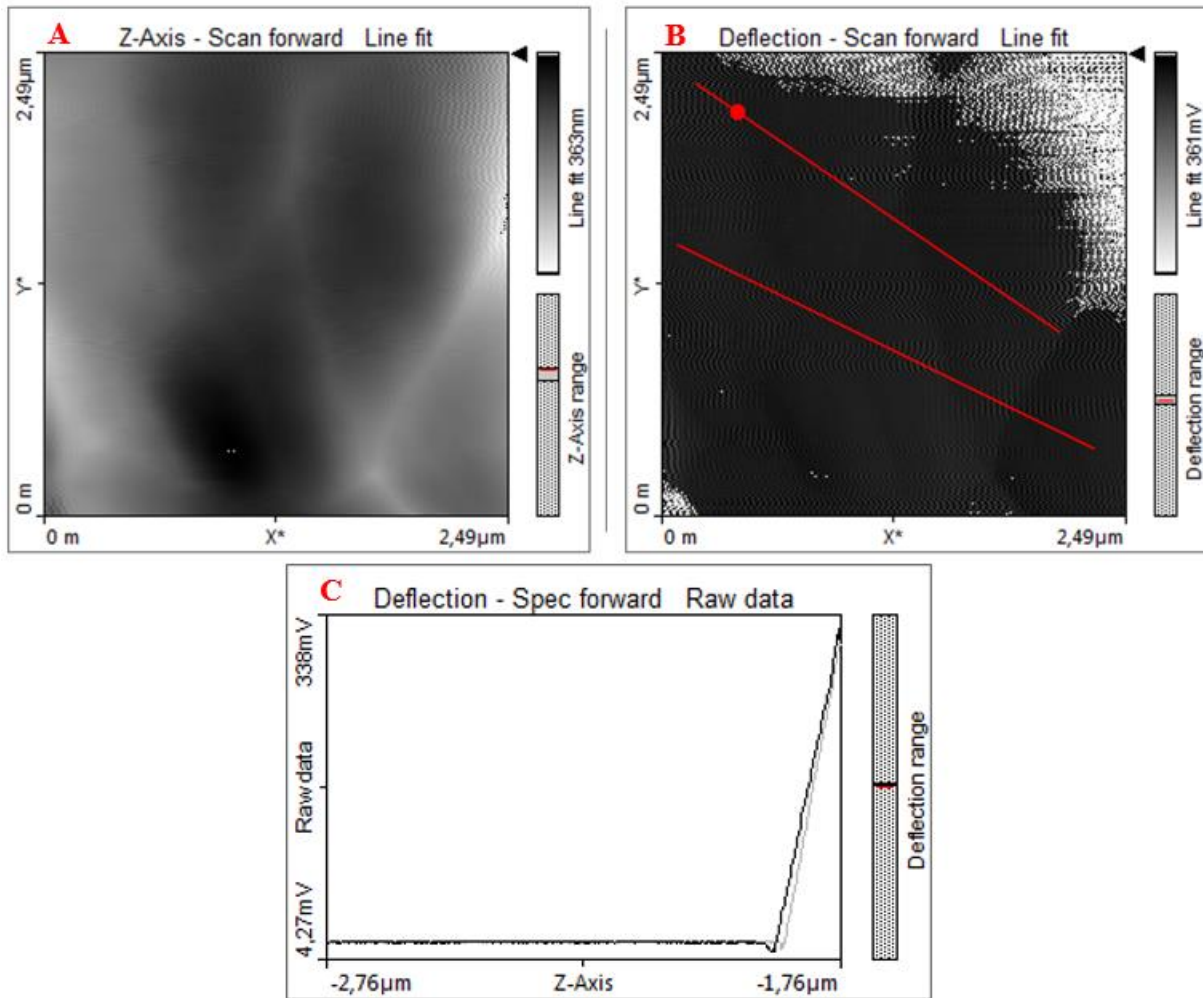


Figure 89 Illustrating a measured area of the plagioclase with the respective force curve from the red point in B. A) height image, B) deflection image displaying where the selected force curve is marked as a red point on the red line, C) the selected force curve indicating repulsive force.

Quartz

The measured area (Figure 90A-B) of the quartz mineral grain differs between both repulsive (Figure 90C) and attractive (Figure 90D) forces. The error signal in the attractive forces was measured to be between -8.24 mV and $-305 \text{ } \mu\text{V}$ as the lowest and between 350 mV and 487 mV as the highest. In the repulsive forces the lowest was measured to be $916 \text{ } \mu\text{V}$ to 3.05 mV and the highest between 344 mV and 522 mV . The snap-in point of the tip in the attractive force area was -818 nm to -507 nm , while in the repulsive force area it was -725 nm to -543 nm .

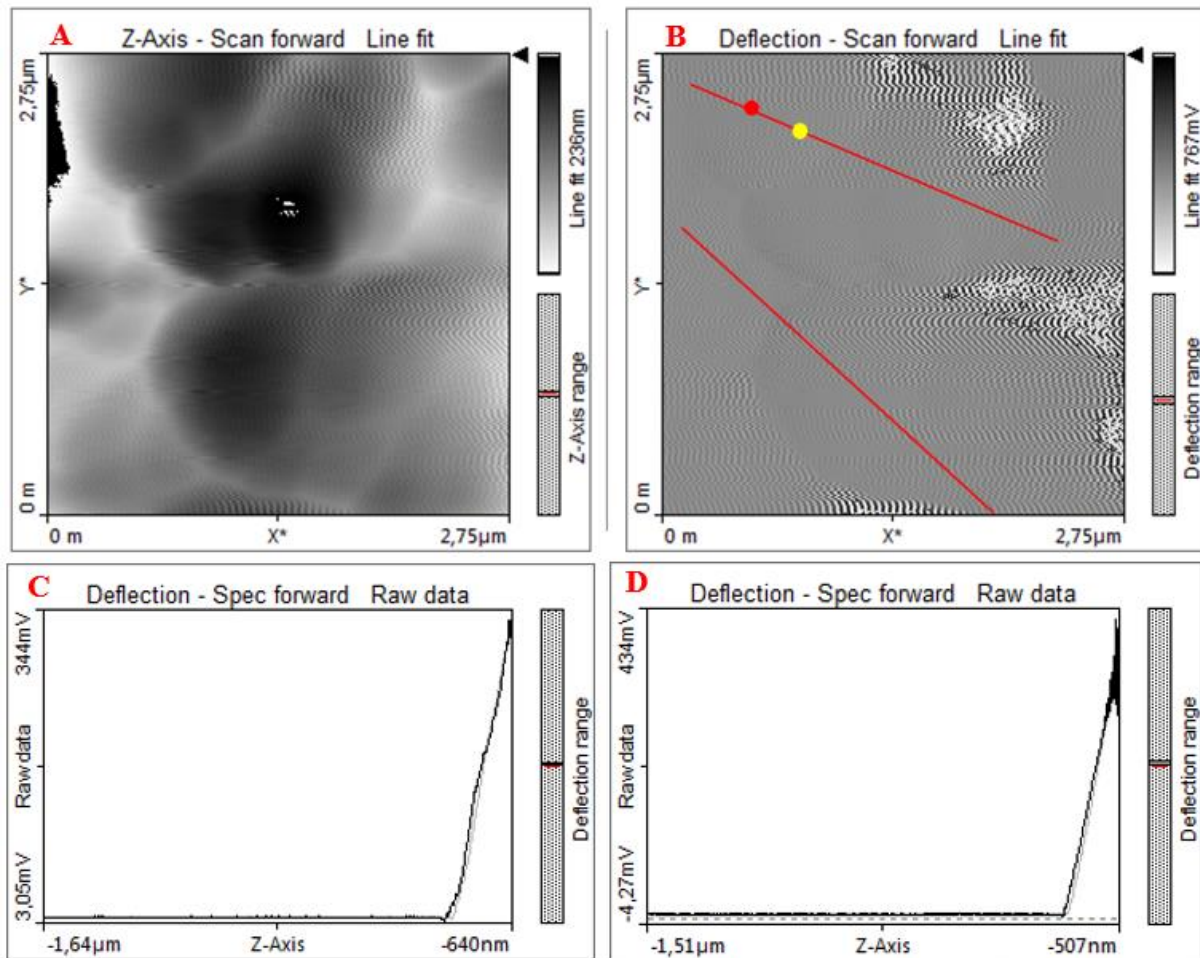


Figure 90 Displaying a measured area of the quartz with the respective force curves from the red and yellow circles in B. A) height image, B) deflection image illustrating where the selected force curves are marked with red, and yellow circles on the red line, C) the selected force curve indicating repulsive force from the red circle, D) the selected force curve indicating attractive force from the yellow circle.

3.2.2 MLTT

The areas in most of the images in MLTT (Figure 91A-B, Figure 92A-B, Figure 93A-B and Figure 94A-B) that were taken in the calcite part (Chapter 3.1.3 MLTT for explanation) seems to have a too big height difference to be able to make force curves from the area. Thus, a lot of curves had to be cut out from the study.

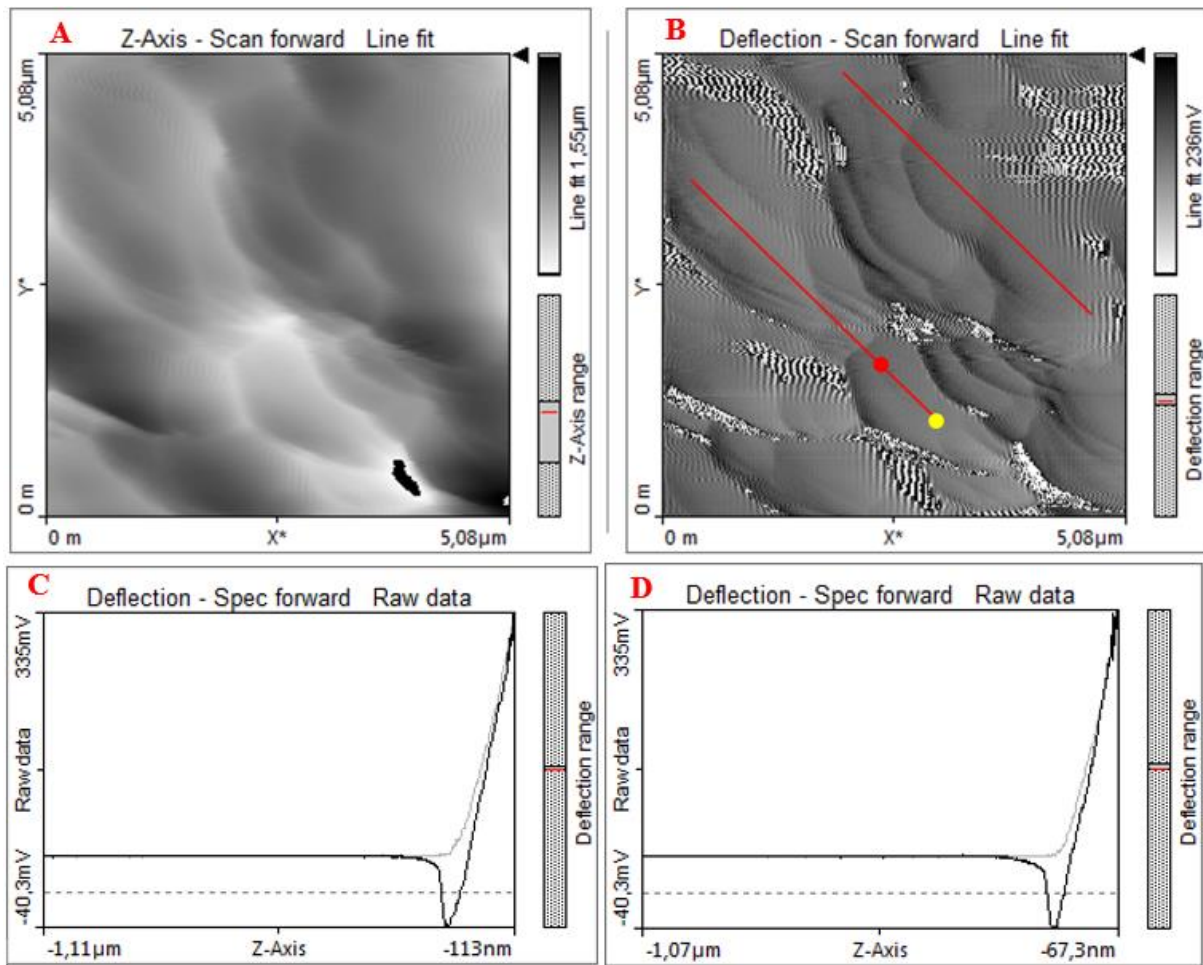


Figure 91 Demonstrating a measured area of MLTT calcite part with the respective force curves from the red and yellow circles in B. A) height image, B) deflection image displaying where the selected force curves are marked with red, and yellow circles on the red line, C) the selected force curve indicating attractive force from the red circle, D) the selected force curve indicating attractive force from the yellow circle.

However, the curves that could be used indicated both repulsive and attractive forces in the rock. The attractive force (Figure 91C-D, Figure 92C-E, Figure 93C-D) ranges from -73.5 mV to -25.3 mV in the lowest error signal while the highest varies between 327 mV and 689 mV.

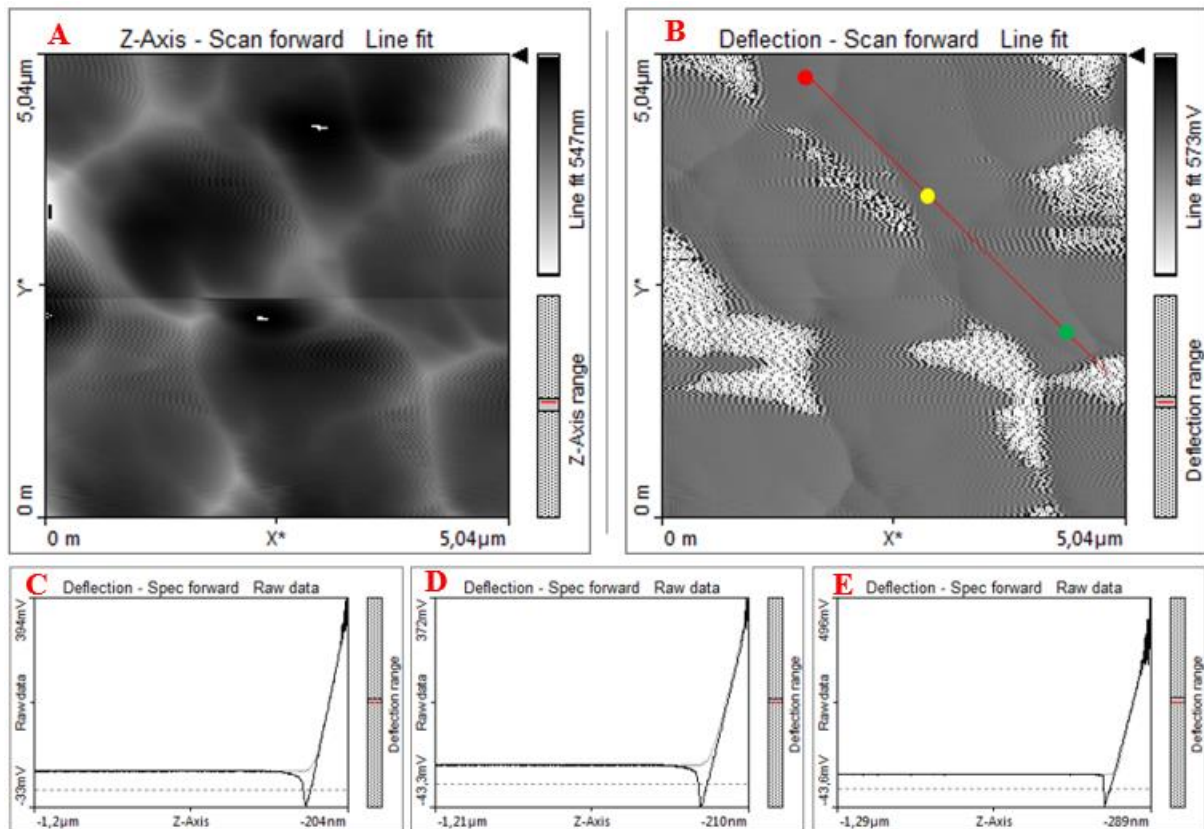


Figure 92 Illustrating another measured area of MLTT calcite part with the respective force curves from the red and yellow points in B. A) height image, B) deflection image illustrating where the selected force curves are marked with red, yellow, and green points on the red line, C) the selected force curve indicating attractive force from the red point, D) the selected force curve indicating attractive force from the yellow point, E) the selected force curve indicating attractive force from the green point.

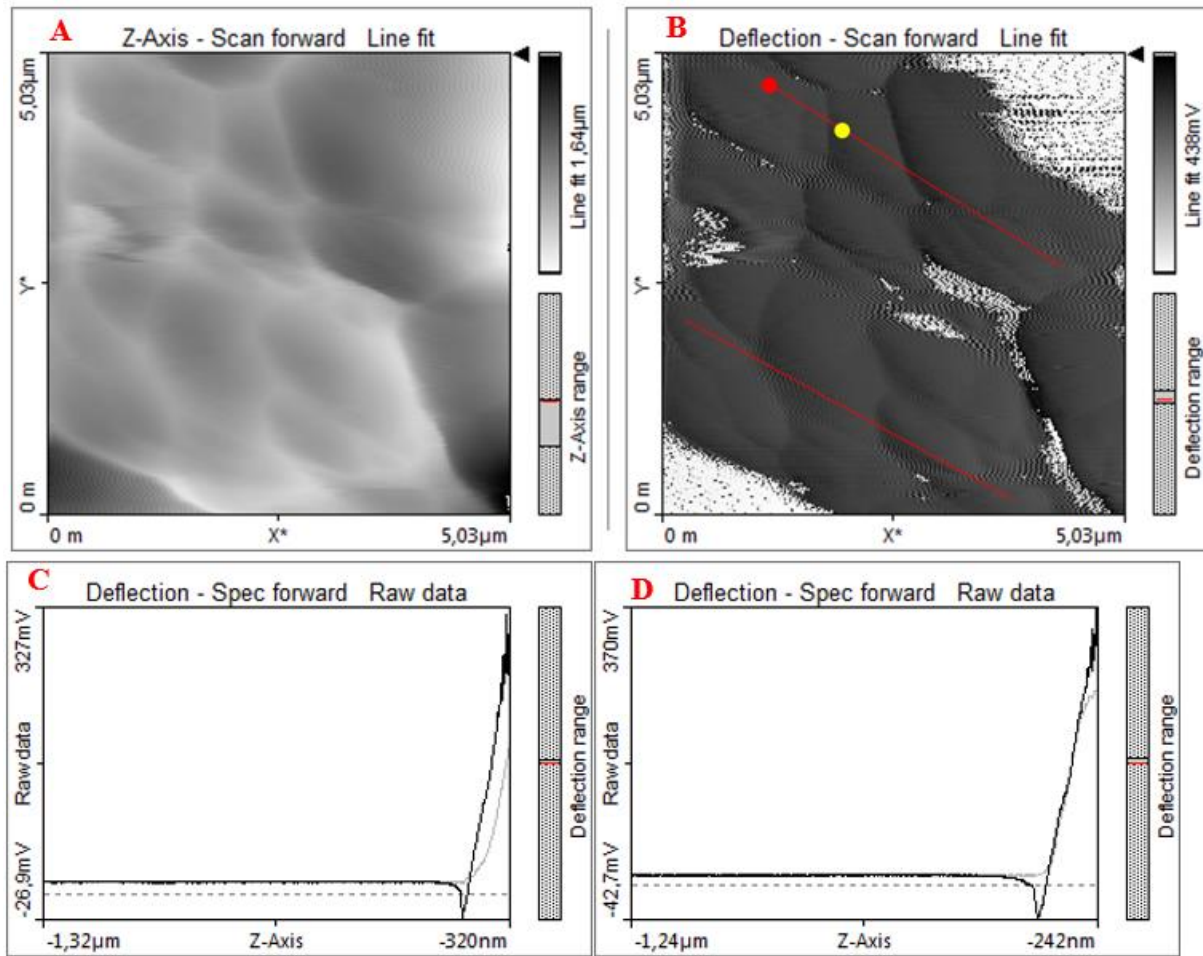


Figure 93 Displaying a third measured area of MLTT calcite part with the respective force curves from the red and yellow circles in B. A) height image, B) deflection image displaying where the selected force curves are marked with red, and yellow circles on the red line, C) the selected force curve indicating attractive force from the red circle, D) the selected force curve indicating attractive force from the yellow circle.

The repulsive force (Figure 94C-E) varies from 11 mV to 52.8 mV as the lowest and 348 mV to 496 mV as the highest. The snap-in point of the tip to the surface was -337 nm to -74.8 nm for the attractive force and -1.5 μm to -51.5 nm for the repulsive force.

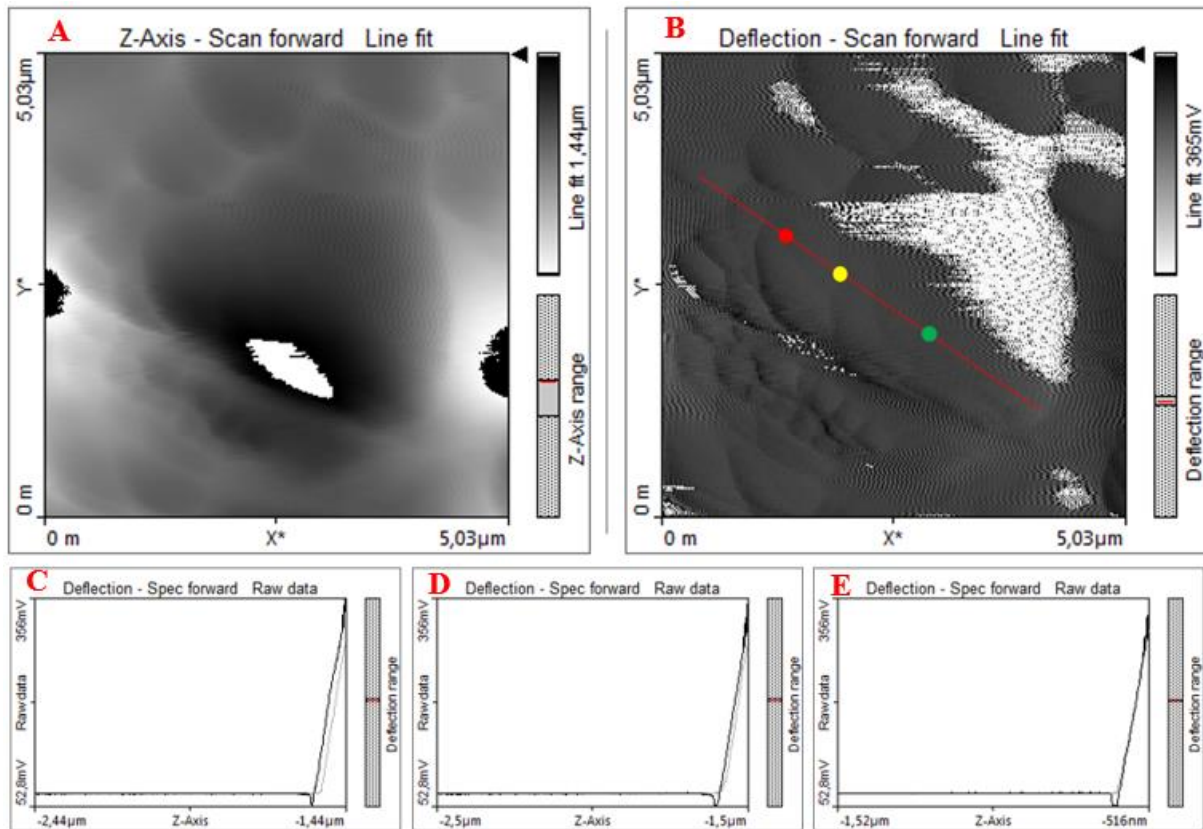


Figure 94 Demonstrating a fourth measured area of MLTT calcite part with the respective force curves from the red and yellow circles in B. A) height image, B) deflection image illustrating where the selected force curves are marked with red, yellow, and green circles on the red line, C) the selected force curve indicating repulsive force from the red circle, D) the selected force curve indicating repulsive force from the yellow circle, E) the selected force curve indicating repulsive force from the green circle.

Both of the measured areas (Figure 95A-B, Figure 96A-B) in the magnesite part (Chapter 3.1.3 MLTT for explanation) of sample MLTT was in attractive force areas (Figure 95C-E and Figure 96C).

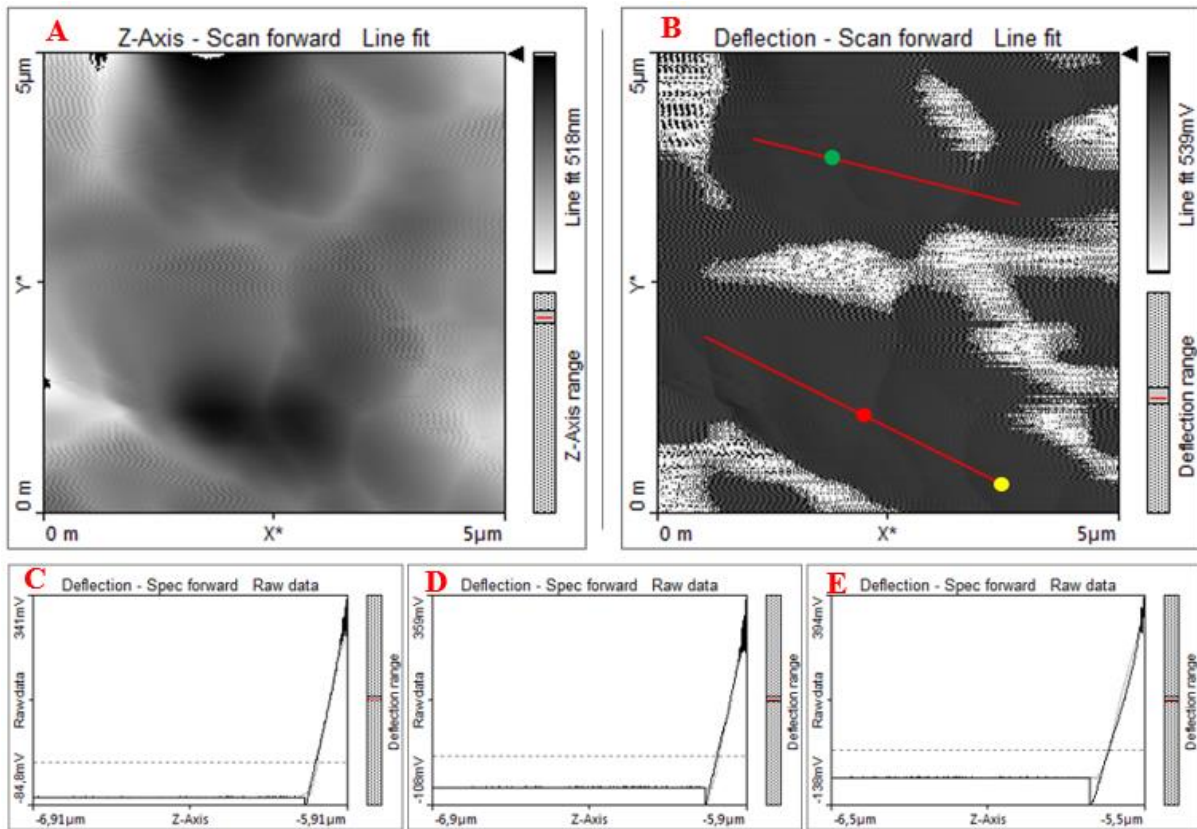


Figure 95 Illustrating a measured area of MLTT magnesite part with the respective force curves from the red, yellow, and green points in B. A) height image, B) deflection image displaying where the selected force curves are marked with red, yellow, and green points on the red line, C) the selected force curve indicating attractive force from the red point, D) the selected force curve indicating attractive force from the yellow point, E) the selected force curve indicating attractive force from the green point.

The error signal differs from -146 mV to -12.5 mV on the lowest, and 337 mV to 611 mV on the highest. The point of snap-in of the tip was measured to be between -5.94 μm and -3.79 μm .

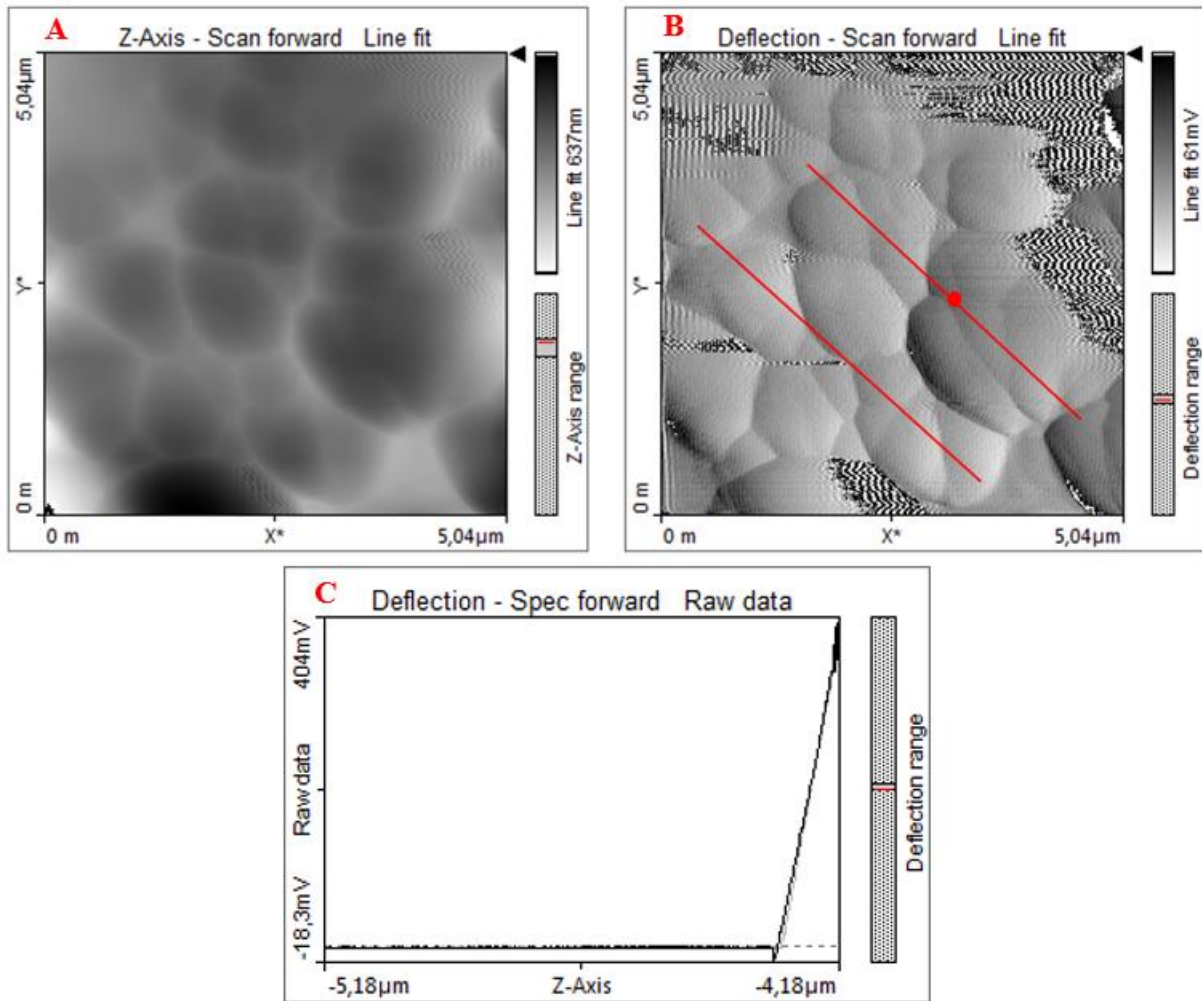


Figure 96 Displaying another measured area of MLTT magnesite part with the respective force curve from the red circle in B. A) height image, B) deflection image demonstrating where the selected force curve is marked as a red circle on the red line, C) the selected force curve indicating attractive force.

3.2.3 ULTT

In the sample ULTT, which is flooded with $MgCl_2$ for three years, three areas (Figure 97A-B, Figure 98A-B and Figure 99A-B) has been measured for force curves.

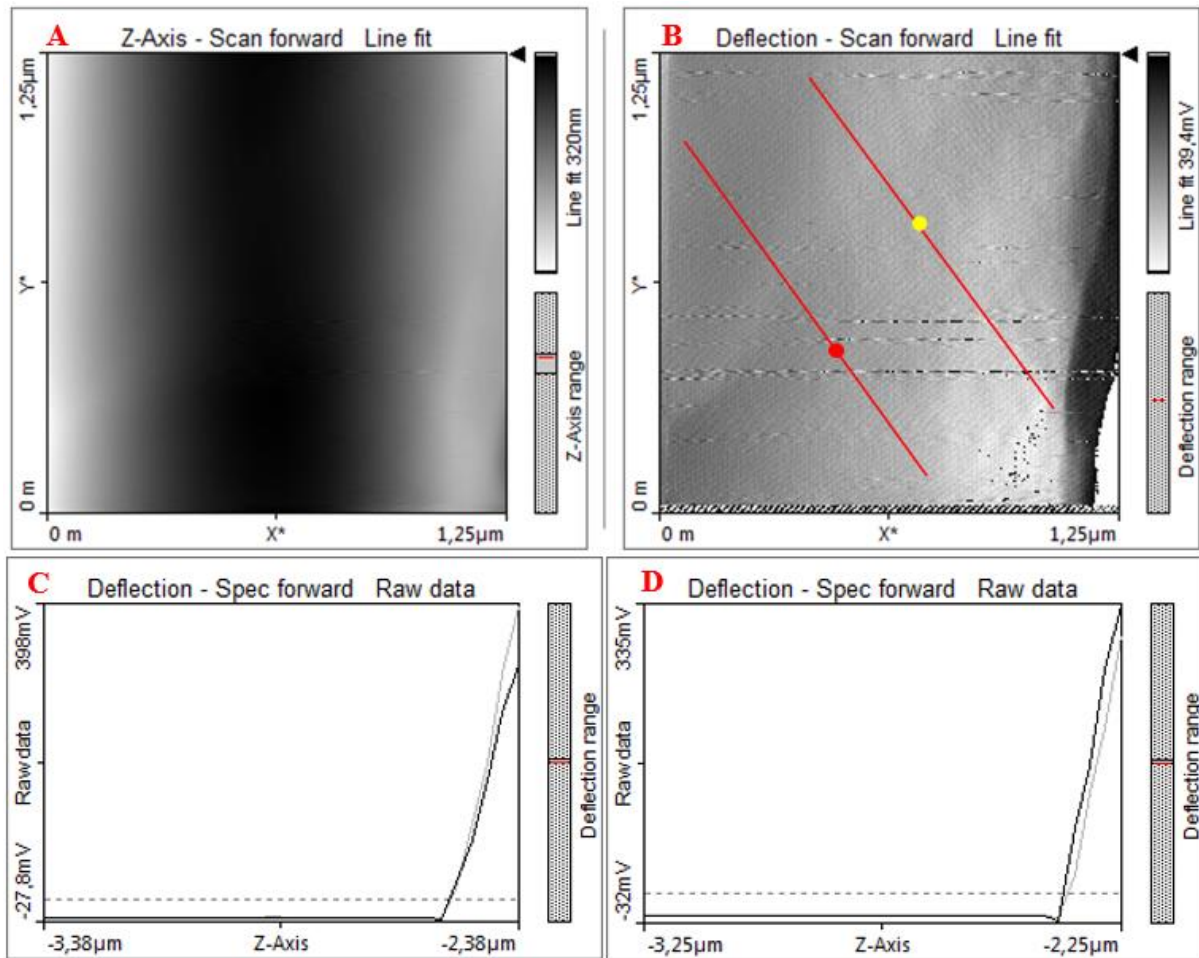


Figure 97 Demonstrating a measured area of ULTT with the respective force curves from the red and yellow circles in B. A) height image, B) deflection image demonstrating where the selected force curves are marked with red, and yellow circles on the red lines, C) the selected force curve indicating attractive force from the red circle, D) the selected force curve indicating attractive force from the yellow circle.

One area demonstrates attractive forces, the other repulsive forces and the third area indicates an overlay of both forces. In the areas with attractive force (Figure 97C-D), the error signal was measured to be -39.4 mV to -1.53 mV at the lowest whereas the highest was 208 mV to 558 mV. The repulsive force area (Figure 98C, Figure 99C-D) illustrates error signal of 1.22 mV to 51 mV at the lowest and 324 mV to 589 mV at the highest.

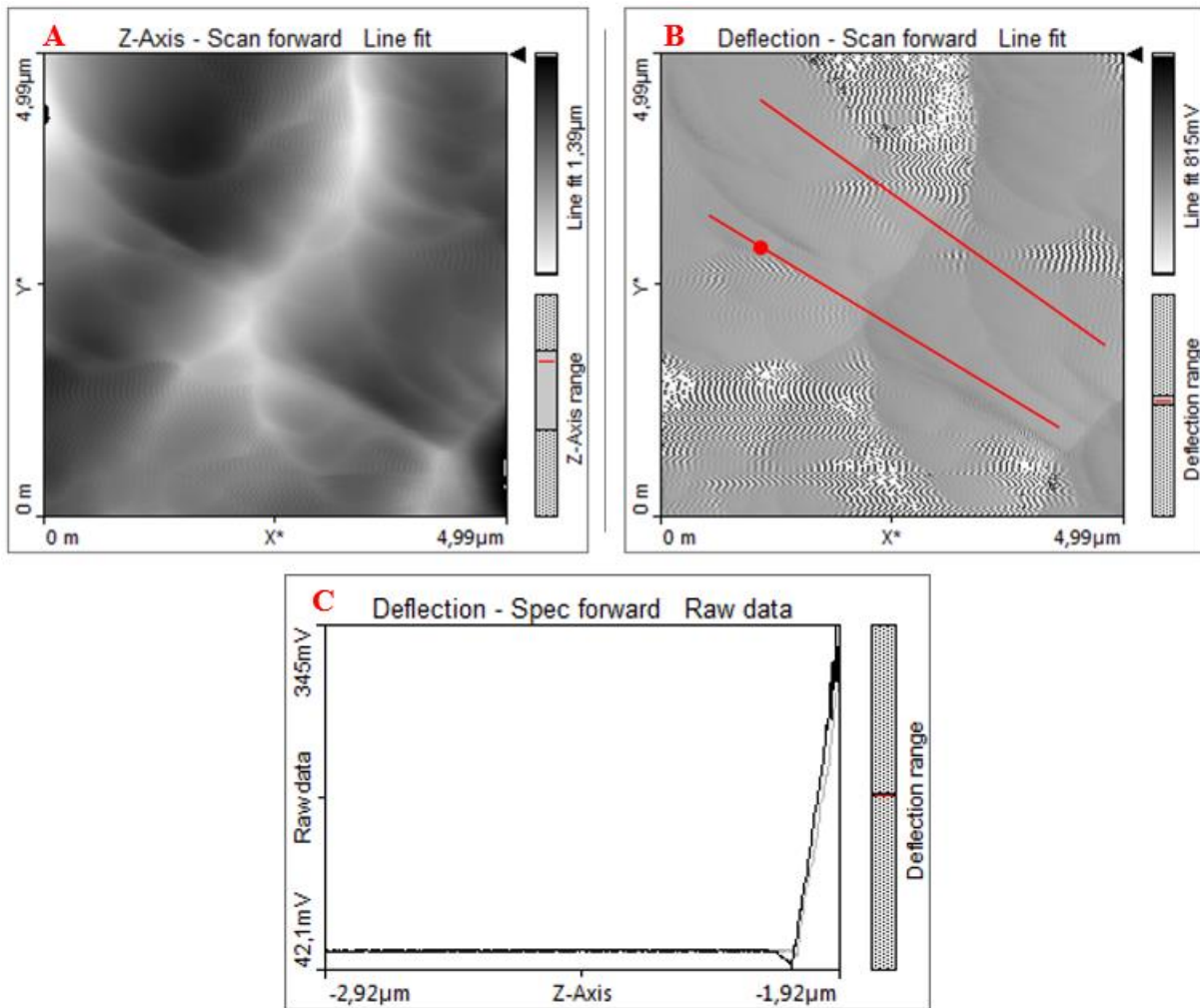


Figure 98 Displaying another measured area of ULTT with the respective force curves from the red circle in B. A) height image, B) deflection image demonstrating where the selected force curves are marked with red circle on the red line, C) the selected force curve indicating repulsive force from the red circle.

The point of snap-in of the tip to the surface in the attractive force area was $-3 \mu\text{m}$ to $-1.41 \mu\text{m}$ while in the area of repulsive force, the point of snap-in was between $-3.43 \mu\text{m}$ and -91 nm .

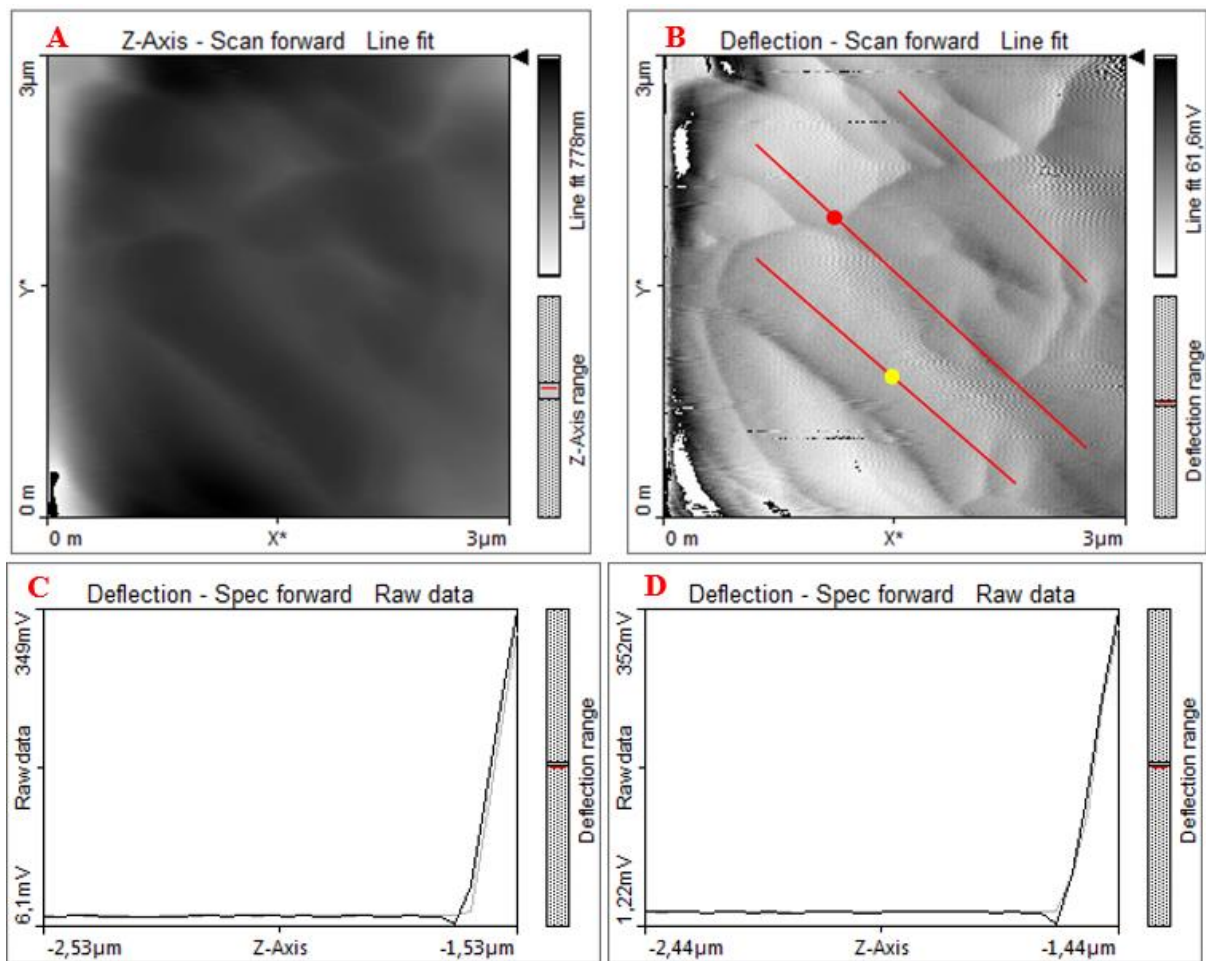


Figure 99 Illustrating a third measured area of ULTT with the respective force curves from the red and yellow circles in B. A) height image, B) deflection image displaying where the selected force curves are marked with red, and yellow circles on the red lines, C) the selected force curve indicating repulsive force from the red circle, D) the selected force curve indicating repulsive force from the yellow circle.

3.2.4 OBSV4_1 – MFP-3D Origin

The sample OBSV4_1 has been measured in Grenoble on the MFP-3D Origin, which gives the force curve output in Force *versus* Distance (Zsnsr) (Chapter Force Spectroscopy for more details on the differences). In general, the measured area (Figure 100A-D) indicated little to no adhesion. The pixels in Figure 100B and D indicates every spot the tip has touched the surface, here 10 x 10 spots all over the sampled area.

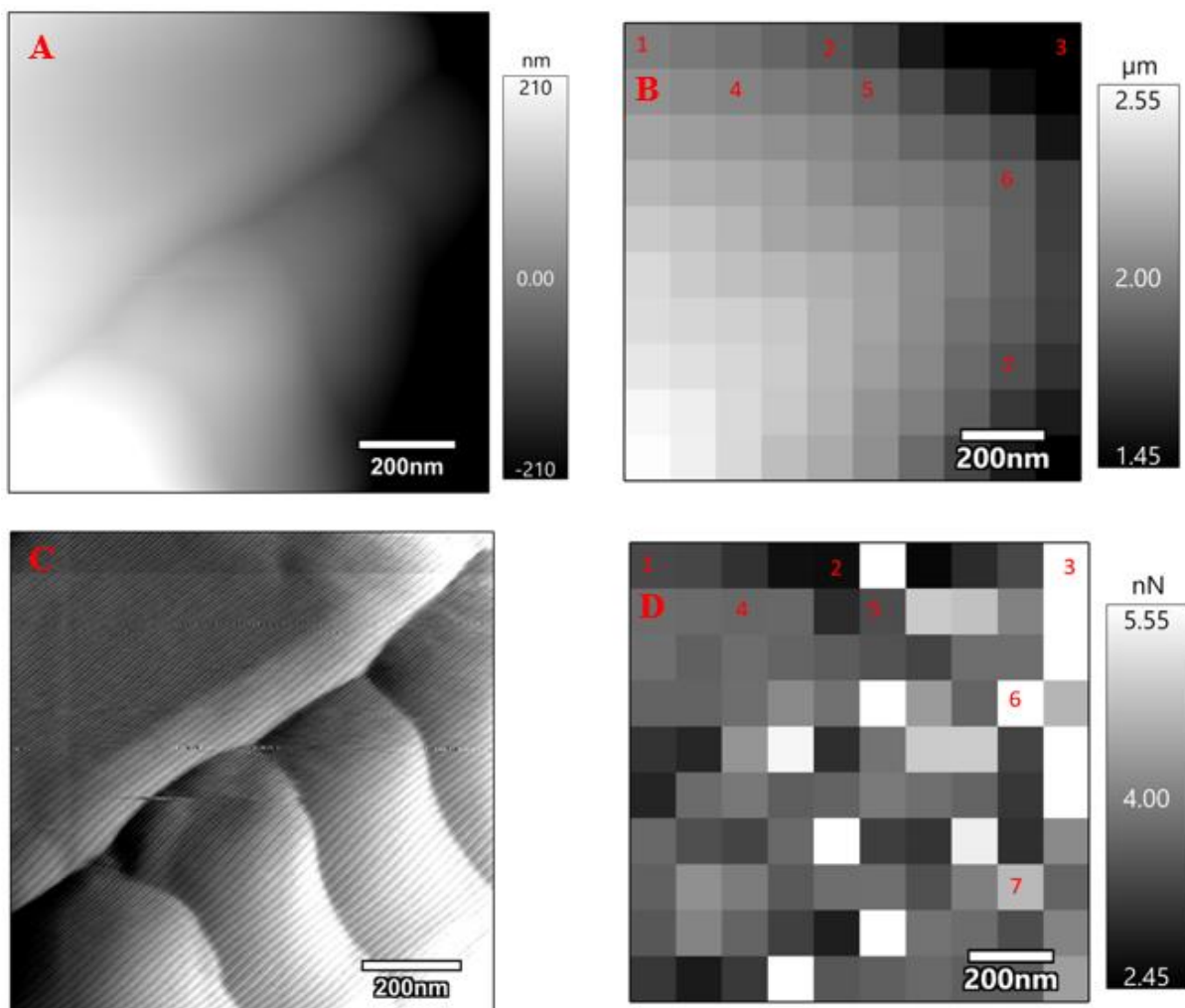


Figure 100 Displaying the measured area in OBSV4_1. A) height image, B) force map from the height image, C) deflection image, D) adhesion map. Numbers in B and D indicating which curve number it is. Scale bar is 200 nm.

Curve number 1 (Figure 101A) indicates no adhesion and only curve number 6 (Figure 101C) reveals a little adhesion, approximately 2 nN. The point of snap-in of the tip to the surface varies from $-2.1 \mu\text{m}$ to $-1.1 \mu\text{m}$. Curve number 3 (Figure 101B) and the area around demonstrates different behavior than the rest of the area because the trace and retrace do not match.

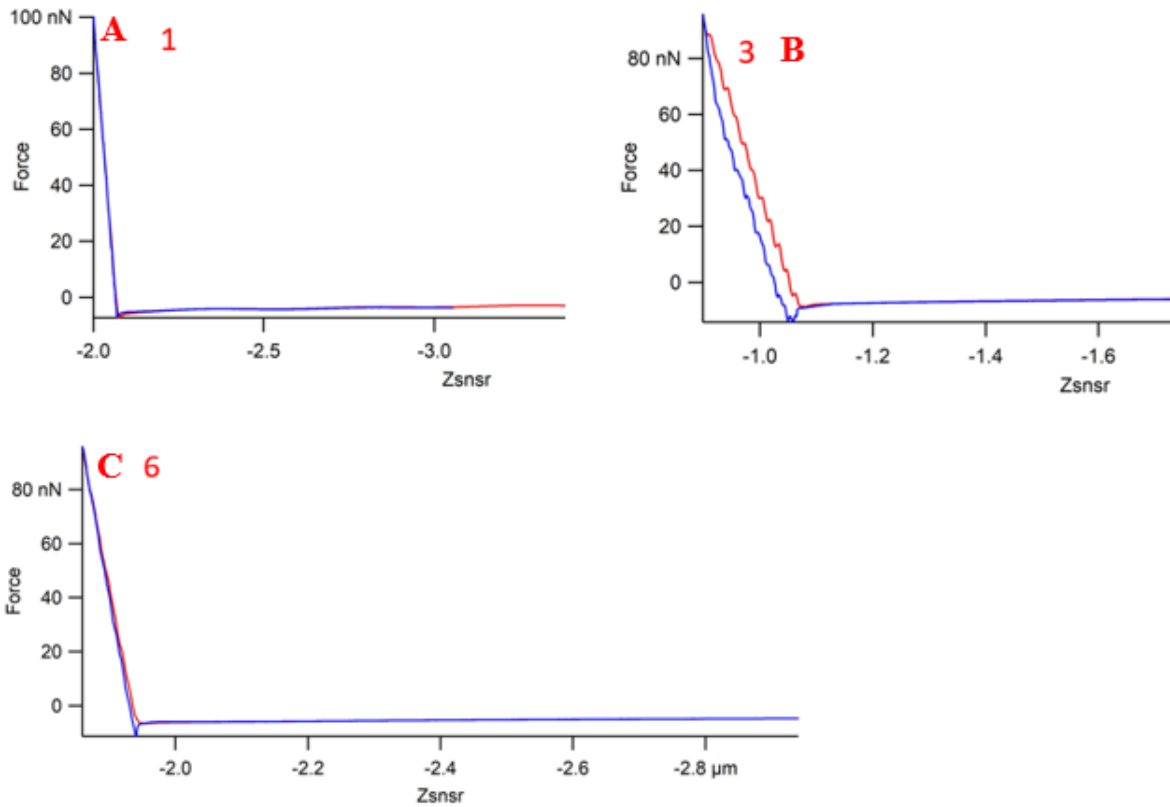


Figure 101 Displaying measured force curves from sample OBSV4_1 in the area in Figure 100. A) force curve number 1 with no adhesion, B) force curve number 3 displaying mismatch of trace and retrace curves, C) force curve number 6 with a little adhesion. See Figure 100 B and D for location of the curves and Chapter Force Spectroscopy Measurements for explanation of the lines.

3.2.5 OBSV12 – MFP-3D Origin

Two areas have been measured in this sample in Grenoble on the MFP-3D Origin, both areas indicating signs of adhesion. In the first area (Figure 102A-E), the adhesion differs from around 7 nN to 50 nN and the snap-in point of the tip to the surface was around $-2.7 \mu\text{m}$ to $-1.1 \mu\text{m}$.

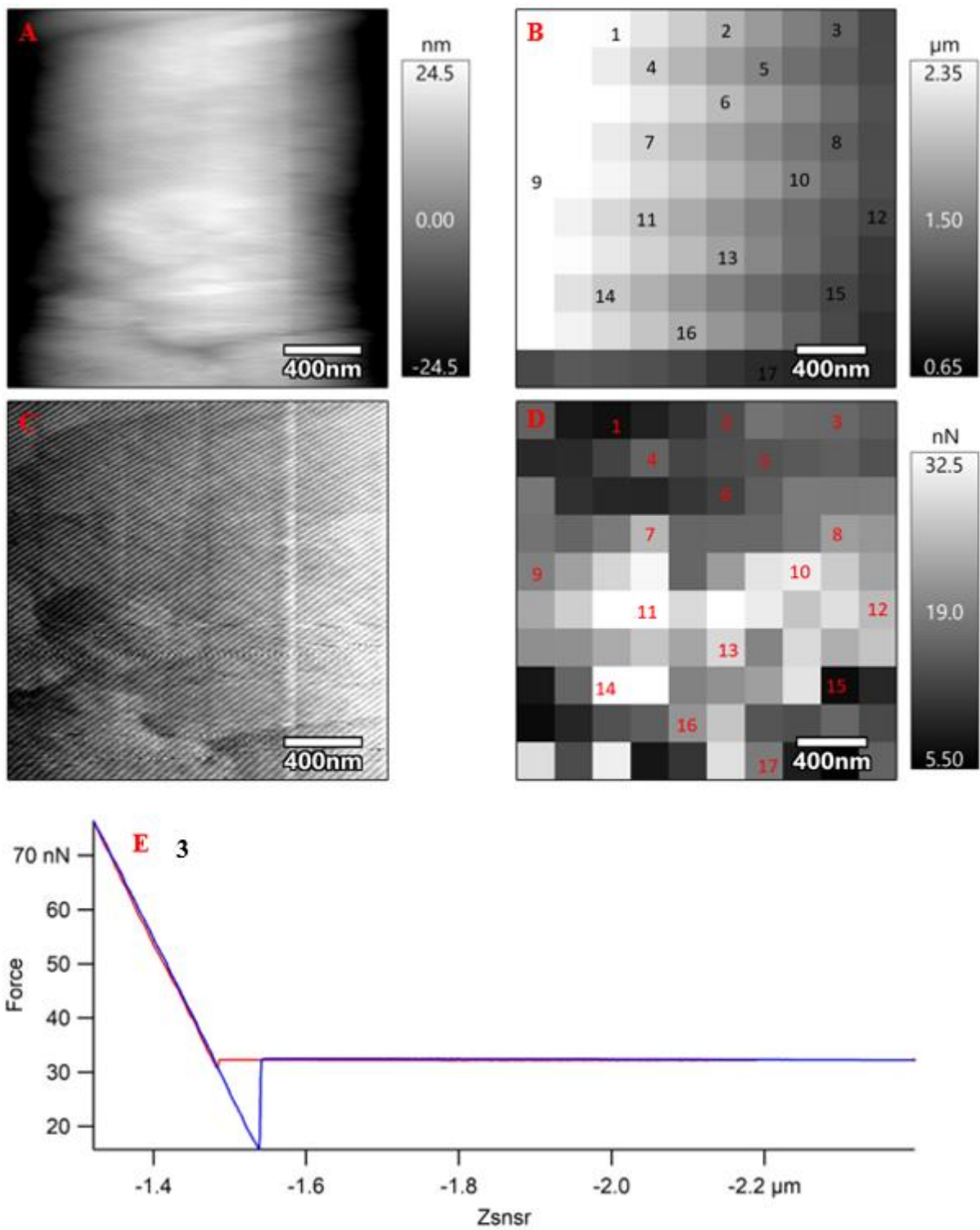


Figure 102 Demonstrating a measured area in OBSV12 with one representative force curve. A) height image, B) force map of the height, C) deflection image, D) adhesion map, E) a representative force curve displaying adhesion. Scale bar is 400 nm.

The second area (Figure 103A-E) displayed similar behavior as the first area. The adhesion ranges from around 15 nN to around 50 nN in this area, while the point of snap-in ranges between -2.6 μm and -1.5 μm .

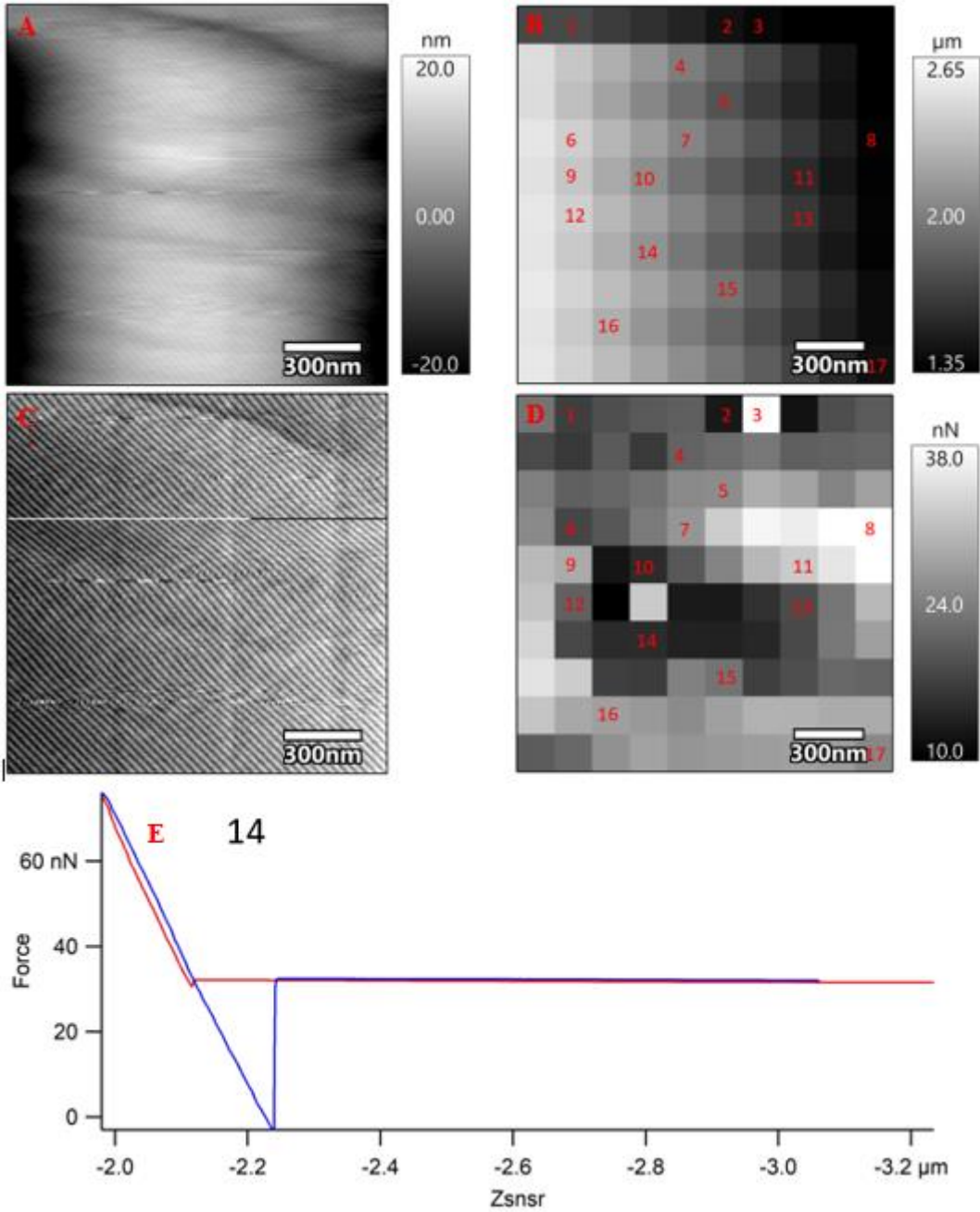


Figure 103 Illustrating another measured area in OBSV12 with one representative force curve. A) height image, B) force map of the height, C) deflection image, D) adhesion map, E) a representative force curve illustrating adhesion. Scale bar is 300 nm.

3.2.6 Unflooded Liège

Three areas have been measured for force curves in the uncoated and unflooded Liège sample. One of these areas demonstrated too large height difference for the tip to actually touch the

surface while measuring the curves, hence, the curves needed to be discarded and are not shown here.

The two other areas measured (Figure 104A-B and Figure 105A-B) were usable, one area indicating repulsive force (Figure 104C-E) and the other attractive force (Figure 105C-E).

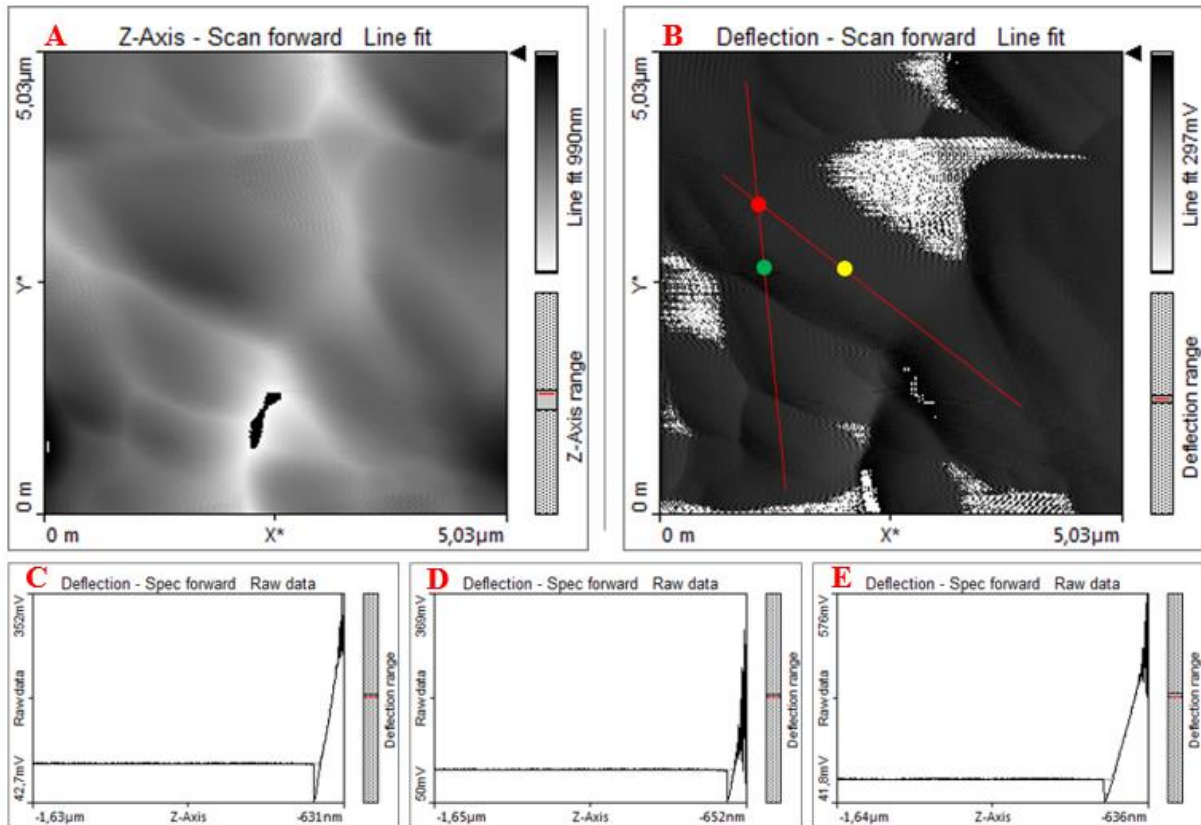


Figure 104 Demonstrating a measured area of Unfolded Liège with the respective force curves from the red, yellow, and green points in B. A) height image, B) deflection image displaying where the selected force curves are marked with red, yellow, and green points on the red lines, C) the selected force curve indicating repulsive force from the red point, D) the selected force curve indicating repulsive force from the yellow point, E) the selected force curve indicating repulsive force from the green point.

The error signal in the area with attractive force ranges between -90.3 mV and -31.3 mV at the lowest and 337 mV to 433 mV at the highest, while in the repulsive area it is 23.2 mV to 90.3 mV at the lowest and 344 mV to 627 mV at the highest. The snap-in point of the tip to the surface was between -4.49 μm and -4.24 μm in the area with attractive force and between -731 nm and -232 nm for the area with repulsive force.

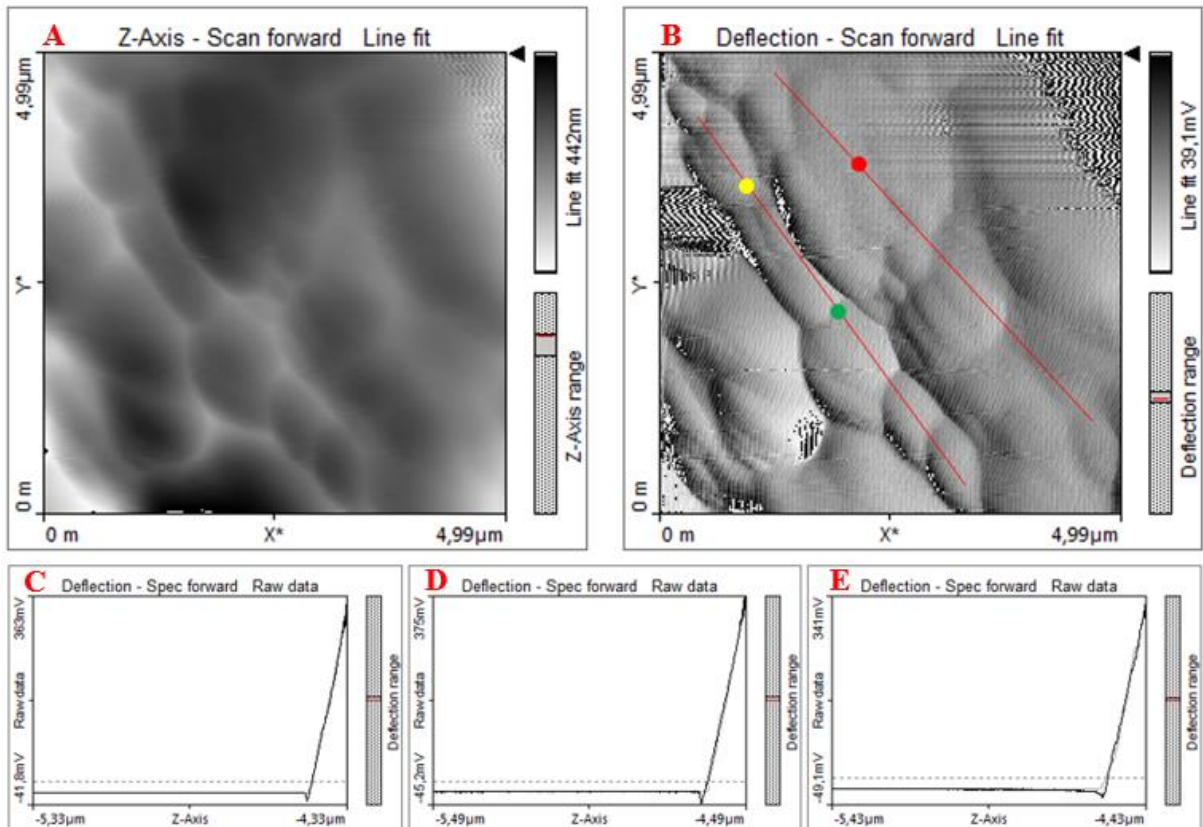


Figure 105 Illustrating another measured area of Unflooded Liège with the respective force curves from the red, yellow, and green points in B. A) height image, B) deflection image demonstrating where the selected force curves are marked with red, yellow, and green points on the red lines, C) the selected force curve indicating attractive force from the red point, D) the selected force curve indicating attractive force from the yellow point, E) the selected force curve indicating attractive force from the green point

The same sample from the unflooded Liège was then coated with a layer of carbon to monitor if there were any differences notable. Four areas have been measured where three display both, repulsive and attractive forces (Figure 106A-B), while the fourth only indicates attractive forces. The error signal from the force curves indicates that the attractive forces (Figure 106C) varies from $-305 \mu\text{V}$ to -2.44 mV at the lowest and from 342 mV to 526 mV at the highest. The error signal from the force curves implying repulsive force (Figure 106D) ranges between 1.53 mV and 14.3 mV as the lowest and 339 mV to 572 mV as the highest. In the repulsive force area, the snap-in point of the tip ranges between $-2.1 \mu\text{m}$ and -909 nm whereas in the attractive force area it varies from $-2.11 \mu\text{m}$ to -892 nm .

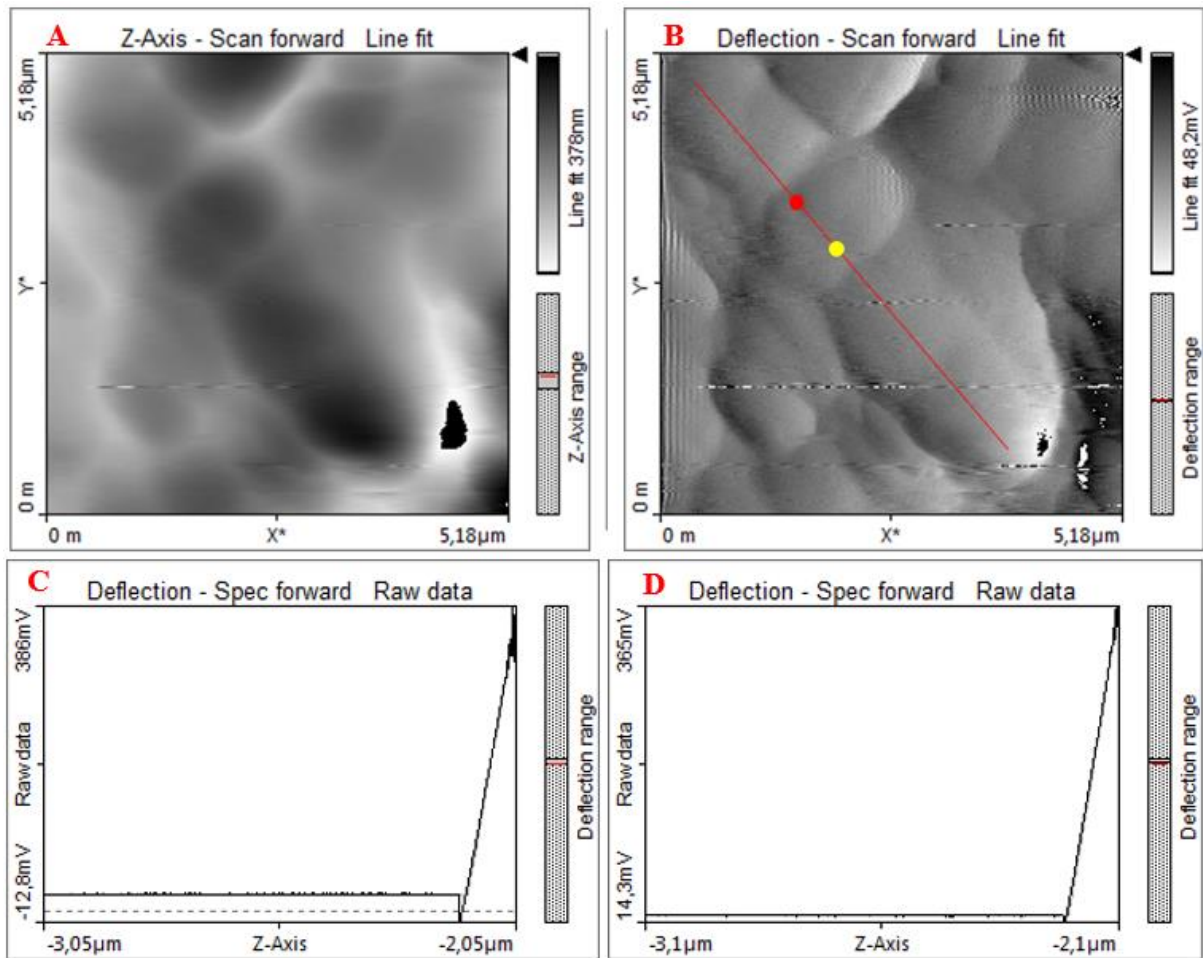


Figure 106 Displaying a measured area of Unflooded Liège with the respective force curves from the red and yellow circles in B. A) height image, B) deflection image illustrating where the selected force curves are marked with red, and yellow circles on the red line, C) the selected force curve indicating attractive force from the red circle, D) the selected force curve indicating repulsive force from the yellow circle.

3.3 Compilation of the results

The topography results are compiled in Table 2 with the main collected information from Chapter 3.1 Topography. The magnesite standard and sample Chalk SK (polished) are polished and does not illustrate any features.

Table 2 Compiling the topography results. Samples with “-“ in mineral growth and dissolution are not flooded and there will therefore not be precipitation nor dissolution here. Samples marked “Grenoble” have been measured on MFP-3D Origin, whereas the rest on NaioAFM at UiS.

Mineral/ Sample	Shape of features	Edges	Mineral growth	Dissolution
Anorthite	Rounded	Smooth	-	-
Calcite	Rounded	Smooth	-	-
Dolomite	Rounded	Smooth	-	-
Fluorapatite	Less rounded, some triangular shape	Smooth	-	-
Ilmenite	Less rounded, some triangular shape	Mainly straight	-	-
Magnesite	-	-	-	-
Magnetite	Rounded and square	Smooth	-	-
Plagioclase	Rounded	Smooth	-	-
Quartz	Rounded	Smooth	-	-
Zircon	Rounded	Smooth to sharp	-	-
LTT1	Step-like, straight, edgy, rounded	Straight and smooth	Magnesite	Calcite
MLTT (calcite)	Rounded, some stacking	Smooth	Not observed	Not observed
MLTT (clay)	Rounded	Smooth	Not observed	Not observed
MLTT (magnesite)	Rounded to elongated, some stacking	Smooth	Not observed	Not observed
ULTT	Step-like layering, some rounded	Straight and smooth	Magnesite	Not observed
OBSV4_1 (Grenoble)	Fossil	Smooth	Not observed	Not observed
OBSV12_6 (Grenoble)	Elongated to curved and rounded to angular	Smooth to sharp	Magnesite?	Not observed
OBSV12 (Grenoble)	Not much visible	Not much visible	-	-
OBSV18 (Grenoble)	Fossil and rounded	Smooth to straight	Unknown	-
Chalk SK (unpolished, Grenoble)	Rounded and elongated	Smooth		
Chalk SK (polished, Grenoble)	-	-	-	-
Unflooded Liège (Uncoated)	Rounded, fossil fragments	Smooth	-	-
Kaolinite (Grenoble)	Crystal-shape	Straight	-	-

The fore spectroscopy results are compiled in Table 3 with all the collected information from the force spectroscopy with a better overview of the different forces. See Chapter Force Spectroscopy Measurements for explanation of adhesion, repulsive force, and attractive force. The repulsive and attractive forces are written in mV, while adhesion is in nN and the point of snap-in is in μm for all minerals and samples. All samples have been prepared the same way (Chapter 2.4.2 Sample Preparation), however sample Unflooded Liège have been measured both without and with a layer of carbon coating. Samples OBSV4_1 and OBSV12 were measured in Grenoble on MFP-3D Origin, while the others on NaoAFM at UiS.

Table 3 Demonstrating the force spectroscopy results compiled in a table.

Mineral/ Sample	Repulsive force lowest error signal (mV)	Repulsive force highest error signal (mV)	Repulsive force snap-in point (μm)	Attractive force lowest error signal (mV)	Attractive force highest error signal (mV)	Attractive force snap-in point (μm)	Adhesion (nN)
Anorthite	-	-	-	-170 to -12.5	344 to 415	-5.04 to -0.997	-
Calcite	-	-	-	-222 to -80.6	322 to 556	-5.41 to -4.78	-
Dolomite	-	-	-	-82.7 to -69.9	322 to 442	-4.66 to -4.17	-
Fluorapatite	14 to 22.3	94.9 to 500	-2.43 to -1.08	-	-	-	-
Ilmenite	7.32 to 25.3	347 to 546	-0.707 to -0.025	-106 to -59.8	345 to 480	-4.54 to -4.01	-
Magnesite	28.4 to 193	329 to 551	-1.16 to -0.404	-35.4 to -5.19	315 to 692	-6 to -5.91	-
Magnetite	2.14 to 3.05	327 to 371	-0.770 to -0.188	-71.7 to -1.53	327 to 650	-3.18 to -0.188	-
Plagioclase	1.83 to 16.8	333 to 615	-2.25 to -1.68	-	-	-	-
Quartz	0.916 to 3.05	344 to 522	-0.725 to -0.543	-0.916 to -1.22	350 to 487	-0.818 to -0.507	-
MLTT (calcite)	11 to 52.8	348 to 496	-1.5 to -0.0515	-73.5 to -25.3	327 to 689	-0.337 to -0.0748	-
MLTT (magnesite)	-	-	-	-146 to -12.5	337 to 611	-5.94 to -3.79	-
ULTT	1.22 to 51	324 to 589	-3.43 to -0.091	-39.4 to -1.53	208 to 558	-3 to -1.41	-
OBSV4_1 (Grenoble)	-	-	-	-	-	-2.1 to -1.1	0 to 2
OBSV12 (Grenoble)	-	-	-	-	-	-2.7 to -1.1	7 to 50
Unflooded Liège (Uncoated)	23.2 to 90.3	344 to 627	-0.731 to -0.232	-90.3 to -31.3	337 to 433	-4.49 to -4.24	-
Unflooded Liège (coated)	1.53 to 14.3	339 to 572	-2.1 to -0.909	-0.305 to -2.44	342 to 526	-2.11 to -0.892	-

4. Discussion

4.1 Topography

Reviewing the information from the topography of the different mineral standards, most of the minerals have rounded features of different sizes with smooth edges. The magnesite was polished, giving no feasible topography results, a lesson also learnt for this type of study. The magnetite displayed both rounded and square-like shapes, however the edges were still smooth. Both fluorapatite and ilmenite displayed features less rounded than the other mineral standards, some were more triangular shaped, similar to the kaolinite sample. It appears that carbonate minerals are smooth and elongated shaped, never imaging straight boundaries or shapes. This may be a good hint when distinguishing minerals in flooded chalk to monitor new growth of non-carbonate minerals. It might be possible to differentiate fluorapatite or ilmenite from the other minerals studied. However, these features are not systematic and reasons for the topographic appearances need to be investigated, which is not the focus of this study. Besides, samples are often not strongly homogeneous, yet it is questionable if the measured or sampled area are actually representative for the whole object or not. Again, further studies need to be applied within this field, as it seems, thus far, topography alone cannot be a parameter to distinguish minerals.

Both LTT1 (measurements done in Grenoble) and one area in ULTT expose similar topography and structures due to the flooding with $MgCl_2$. The step-like features in Figure 30 and Figure 44 appear similar, and is assumed to be magnesite. Magnesite is a new grown phase in the flooded chalk. It is possible that AFM studies on extremely fresh minerals display sharper edges than those with certain ages or exposed to weathering besides other geological processes. If new grown minerals, here magnesite, is possible to identify using this type of method, then quantification efforts would be very important in the future. Magnesite, however, in MLTT does not demonstrate the sharp edges, possibly because of erosion during the flooding process. Such mechanism will have a very strong effect on these very small-scale analyzes.

LTT1 also has one area (Figure 33) where the features appear more rounded and consists of several smaller features, which may point to dissolution of calcite. Megawati et al. (2011) discovered that the dissolution of calcite can change the morphology of the grain, e.g. to a rounder shape. Figure 45 and Figure 46 demonstrates a smooth “depression” and repetitive layered structures, respectively. Whereas the layered structures could be a sign of classic precipitation, the rounded edges and the smooth “depression” could be a sign of dissolution.

Most of the time during the flooding, when equilibrium is nearly reached or the flow rate is not significantly high, in some regions precipitation will occur and in some other areas, prevalent dissolution.

In LTT1 (Figure 30), OBSV4_1 (Figure 51), OBSV12_6 (Figure 55) and OBSV18 (Figure 63) lath-shaped features are observed, and more rounded shaped-features that appears to be growing on top of a relatively flat surface of another phase, most probably coccolithophore fragments. Skovbjerg et al. (2012) have also observed this in chalk samples from Stevns Klint and Aalborg (Denmark). They concluded this type of feature to be clay. But to be sure for all of these observed features, further investigations is needed by using TERS (Tip-Enhanced Raman Spectroscopy)-nano Raman (Borromeo et al., 2018), TEM (Transmission Electron Microscopy) or HIM-SIMS (Helium-Ion Microscopy with Secondary Ion Mass Spectrometry) techniques (Minde et al., 2019) to decipher the crystallography and/or chemistry of those nano-sized minerals.

Topographic studies can very well identify different phases when the samples are known, like in this study. The comparisons to standards help in terms of the identification but is not unambiguous. Flooded chalk will contain new grown minerals and these small phases are possible to identify. This approach is easier on larger flat areas than in areas that are rather chaotic and inhomogeneous, e.g. the matrix of the chalk samples. Nevertheless, the high magnification allows a detailed insight into those firstly geometric features and then enables possible identification. More research is required in this area to gain systematic data sets which was impossible to generate during the Corona crisis. The results are though very promising.

Polished *versus* unpolished samples

The clean chalk sample from Stevns Klint (Chalk SK) was prepared using two different methods, as one polished and one unpolished sample for topographic studies. This was done to be able to determine which type of preparation is best suitable for the purposed described in this project. Figure 70 compares the unpolished and the polished samples, demonstrating large differences in the topography. As predicted, the polished sample displays no topography at all, as this has been polished away. Due to this, it would be impossible differentiate minerals and materials. The unpolished sample is the best fit for this purpose, as the surface is needed to understand the sample.

4.2 Force Spectroscopy

Within this research project, a number of force curves were taken in areas with large height differences, which has been a novel approach for chalk samples in the EOR research field. However, large height differences increase the chances of not receiving complete feasible results, due to the tip not being able to hit the surface of the sample while measuring. This infers that a lot of the curves had to be ignored, but measurements have been carried out for 9 minerals and 5 samples.

The samples which gave reasonable results reflected, when applying force spectroscopy, some very interesting systematics with a high potential of further research. Within this pilot study, the minerals anorthite, calcite and dolomite, as well as the rock sample MLTT (magnesite part) all reveal attractive forces in the measured areas while the minerals fluorapatite and plagioclase only displays repulsive forces. Other phases, e.g. ilmenite, magnesite, magnetite, and quartz exhibit both attractive and repulsive forces in the measured areas. This is most likely due to different surface charge of different minerals and materials (Table 3).

The attractive forces have a large range in the mineral standards at the minimum V from -222 mV to -619 μ V, demonstrating large variations in all the measured samples (Table 3 and e.g. Figure 77, Figure 81, Figure 87 and Figure 97). The repulsive forces in the mineral standards range at the minimum V from 916 μ V to 193 mV, also indicates large variations in the measured samples (Table 3 and e.g. Figure 82, Figure 89, Figure 94 and Figure 104). The lowest and the highest are from different minerals for both attractive and repulsive forces (Table 3). The variations in both the repulsive and attractive forces, may be derived from humidity and meniscus effects or by different surface roughness (pers. communication Bahareh Zareeipolgardani). These are parameters that can have an influence on the forces on the surface of the same mineral/material.

Different minerals or organic matter may explain the different forces on the rock surface, and possible different pHs or ionic forces. The attractive force could also be due to electrostatic forces of the surface. In general, but not always, the samples with attractive forces snaps in from a further distance than the samples with repulsive forces.

Adhesion to surfaces is related to wettability in hydrocarbon-rich rocks where it plays a major role, and different brines alter the wettability of the rocks (Li et al., 2018). Reservoir carbonate rocks are preferred when they are water-wet and not oil-wet. Adhesion, however, cannot be measured directly within these analytical approaches on the NaioAFM, but attractive or

retractive forces are in a way related to these characteristics. The MFP-3D Origin could measure the adhesion, but this was only done for two samples. Hence, AFM methodology can possibly deliver an estimate for adhesion, which in turn would be already a significant advance in research for EOR.

Both samples, OBSV12 and OBSV4_1, are from the same chalk formation in Belgium, respectively unflooded and flooded. The flooded sample displays lower adhesion than the unflooded. Sample OBSV4_1 expose little to no adhesion in the measured area, however the most interesting force curve is number 3 (Figure 101B). In this curve, a mismatch in the trace and retrace curves can be observed, which is most likely due to a softer material in this area. The darker area around curve number 3 in the height force map (Figure 100B) has the same behavior, indicating a softer material in this area. The low adhesion in the sample could be due to the flooding with $MgCl_2$ when this fluid may have manipulated the surfaces by thin layers of new grown phases. Unflooded OBSV12 displays signs of adhesion, varying from 7 nN to 50 nN in the two measured areas.

It seems that either attractive or repulsive forces, or the identification of both, may be a possibility of distinguishing minerals. This factor is related to adhesion, which in turn can be interpreted by using the analytical power of the AFM as described. Within an area in flooded chalk, where new grown magnesite shall be differentiated from quartz, these distinguishing characteristics may be employed, which would be already an advance to other highly complex, time-consuming and expensive methodologies (Zimmermann et al., 2017). Both MLTT (calcite part), ULTT and Unflooded Liège disclose both, repulsive and attractive forces in the measured areas in this study, while MLTT (magnesite part) only reveals attractive forces. However, the magnesite mineral standard reveal both, repulsive and attractive forces. The reason for this is unknown and it will need further measurements and interpretations to gain more knowledge regarding this issue.

However, force spectroscopy is an effective approach for the described research study on flooded chalk where magnesite grows within calcite, and few clays as well as quartz phases. Thus far, only highly sophisticated and time consuming, as well as expensive methodologies, e.g. nanoSIMS or FIB-SEM (Focused Ion Beam-Scanning Electron Microscopy) for TEM studies were able to gain this distinction (Minde et al., 2019; Zimmermann et al., 2015). Research may deliver a prediction of which minerals will dissolve and precipitate when flooding chalk with different brines. The AFM is a potential tool to help foresee possible changes of wettability when substitute the minerals or provoke new growth of others, for

instance through flooding. Therefore, to study wettability and effectivity of EOR processes AFM technology may have a large potential.

Coated *versus* uncoated samples

The sample Unflooded Liège was measured for force spectroscopy without and with carbon coating to gain information regarding possible effects caused by coating. The measurements were not done in the exact same area, which is a nearly impossible task due to the small size of the sampling area but was definitely very close. This was known because of the intensive study of the sample and therefore the good knowledge of the details within the sample. Both samples demonstrated force curves of attractive and repulsive forces, meaning that the coating probably does not affect the force results. However, this is only based on one sample and is not necessarily representative for other samples. After the Corona crisis this will be intensified and systematic developed.

4.3 Reliability of Data

As this study is a pilot research project mainly introducing absolutely novel analytical approaches to chalk and related minerals involved in EOR experiments and research (e.g. Borromeo, 2018; Kallestén, 2015; Minde, 2018; Wang, 2018) it was possible to identify a number of pitfalls and issues.

Sample preparation has been discussed and commented upon coating and polishing or not, given above. Furthermore, knowing when to change the tip or area of measurement is crucial to get good results. If the tip gets worn out, it needs to be changed but only experience can establish this.

Rough surfaces are obviously a general issue, but polishing cannot be proposed for this types of studies as presented in this study (Figure 25, Figure 68, Figure 69 and Figure 70, and Chapters 3.1.1 Standards (magnesite) and 3.1.9 Chalk SK – MFP-3D Origin). This allows only small areas to be analyzed. The advantage with most of the samples used in this project and in general in EOR experiments, has been that most of them are studied beforehand and information about new mineral growth, for instance, exists. This is helpful when AFM can add the location and sizes, shapes as well as contact areas of and between the new growth and the primary phases. These observations can be carried out by other methods as well (e.g. FIB-SEM for TEM or nanoSIMS; Minde et al., 2019; Zimmermann et al., 2017) but is extraordinary time

consuming and costly, while AFM studies are quick, easy, and very economic. With SEM and TEM, the composition of the grains can be determined, which cannot be done with the AFM. Together, these tools can complement each other perfectly.

Noise in the topographic images will usually be a part of the results due to the sensitivity of the AFM and the positioning of the machine. A “clean room” with no dust, no other machines nearby, no movements etc. will reduce the risk of noise.

The sample preparation for the AFM is also paramount, as this sets the foundation for the results. If there is a lot of contamination on the sample surface, this will also affect the results. If the surface is not sufficiently flat (without using polishing technique for the research presented), the results might not be usable due to the tip not reaching all points. A polished surface will, however, give no topographic information. In this study, the preparation of the samples included casting the sample in epoxy, and the epoxy could penetrate through the pores of the rock and affect the results. This also requires more detailed studies in the nearest future to test effects of sample preparation.

In this study, the measurements have all been acquired in air, both the images and the force curves. Doing measurements in liquid has been proven to remove the uncertainty due to capillary force and meniscus effect. This has been planned within this thesis, but the Corona crisis did not allow for those measurements as they are quite time consuming.

5. Conclusion

Different mineral standards and chalk samples have been examined with an AFM to investigate the potential of this methodology in the field of EOR. Chalk samples, both before and after flooding, have been used, to be able to observe which primary and secondary minerals existed or have grown, or which minerals may have been affected by dissolution during the flooding. Two of the available abilities of the AFM have been applied, topography measurements and force spectroscopy.

Topographic analyzes of the mineral standards indicate similarities in the morphology and topography for most of the minerals. In general, the minerals have rounded features with smooth edges with some exceptions in three of the minerals (fluorapatite (Figure 23), ilmenite (Figure 24), and magnetite (Figure 26)). One of them (magnesite) did not display features due to polishing. One of the rock samples (Chalk SK polished) was also polished and did not reveal

any features due to the topography being polished away. The different rock samples display some similarities and some differences on the surface, mainly differences between the magnesite and calcite in the samples. The minerals may behave dissimilarly in different samples due to age or geological processes, like diagenesis and/or weathering. Despite the differences, it is difficult to differentiate the different minerals only based on the topography and morphology. However, the measurements give a closer snapshot to the minerals and can deliver better images with higher resolution of the newly grown or dissolved minerals in the rock than some other methodologies. This allows to locate the mineral changes, a very useful information for the interpretation of EOR research approaches.

Force spectroscopy was used to carry out force curves from each mineral and sample in the study. There were various results generated from those curves, when attractive and repulsive forces were observed. Unfortunately, most of the minerals and rocks exhibit signs of both forces, which hampers a differentiation of them based on the force curves. Furthermore, there was a large range in the error signal in each of the measurements, affecting the interpretation. Deciding which mineral is observed is thus far not possible based solely on the force curves, but further studies will be carried out after the Corona crisis, and more knowledge will be earned to allow such a differentiation, which would be a very important tool for mineralogical research and especially for EOR research.

In conclusion, based on the measurements and knowledge gained throughout this pilot research study, the AFM together with other machines and studies will improve the potential in the field of EOR to a great extent as AFM can add valuable further information. However, as mentioned, more detailed knowledge of a variety of processes is also needed, for instance to understand the relation between the force curves and wettability. Nevertheless, the results presented in this project were promising and when a systematic study would generate the necessary data for this crucial parameter of HC-rich rocks, the tool would be superb. This implies more detailed knowledge of the sample preparation to allow easier and more feasible measurements in future research.

6. References

- Abdallah, W., Buckley, J.S., Carnegie, A., Edwards, J., Herold, B., Fordham, E., Graue, A., Habashy, T., Seleznev, N., Signer, C., Hussain, H., Montaron, B., Ziauddin, M., 2007. Fundamentals of wettability. *Oilfield Review* 19, 44–61.
- Abubeker, E., 2013. Water weakening of chalks - comparison of intact and fractured cores. University of Stavanger, Norway.
- Andersen, P.Ø., Wang, W., Madland, M.V., Zimmermann, U., Korsnes, R.I., Bertolino, S.R.A., Minde, M., Schulz, B., Gilbricht, S., 2017. Comparative Study of Five Outcrop Chalks Flooded at Reservoir Conditions: Chemo-mechanical Behaviour and Profiles of Compositional Alteration. *Transp Porous Med* 121, 135–181. <https://doi.org/10.1007/s11242-017-0953-6>
- Asylum Research, 2018. Asylum Research Applications Guide.
- Borromeo, L., 2018. Raman spectroscopy applied to the mineralogical analysis of flooded chalk. University of Stavanger, Faculty of Science and Technology, Department of Energy Resources, Stavanger.
- Borromeo, L., Toccafondi, C., Minde, M.W., Zimmermann, U., Andò, S., Madland, M.V., Korsnes, R.I., Ossikovski, R., 2018. Application of Tip-Enhanced Raman Spectroscopy for the nanoscale characterization of flooded chalk. *Journal of Applied Physics* 124. <https://doi.org/10.1063/1.5049823>
- Bredal, T., 2018. Micro- and nano-analyses of fracture-filling after flooding on-shore chalk with different IOR fluids. University of Stavanger, Faculty of Science and Technology, Department of Energy Resources.
- Burkett, V., 2011. Global climate change implications for coastal and offshore oil and gas development. *Energy Policy, Clean Cooking Fuels and Technologies in Developing Economies* 39, 7719–7725. <https://doi.org/10.1016/j.enpol.2011.09.016>
- Butt, H.-J., Cappella, B., Kappl, M., 2005. Force measurements with the atomic force microscope: Technique, interpretation and applications. *Surface Science Reports* 59, 1–152. <https://doi.org/10.1016/j.surfrep.2005.08.003>
- Chatterjee, S., Gadad, S.S., Kundu, T.K., 2010. Atomic force microscopy: A tool to unveil the mystery of biological systems. *Reson* 15, 622–642. <https://doi.org/10.1007/s12045-010-0047-z>
- Collin, F., Cui, Y.J., Schroeder, C., Charlier, R., 2002. Mechanical behaviour of Lixhe chalk partly saturated by oil and water: experiment and modelling. *Int. J. Numer. Anal. Meth. Geomech.* 26, 897–924. <https://doi.org/10.1002/nag.229>
- Craig, J., Thurow, J., Thusu, B., Whitham, A., Abutarruma, Y., 2009. Global Neoproterozoic petroleum systems: the emerging potential in North Africa. Geological Society, London, Special Publications 326, 1–25. <https://doi.org/10.1144/SP326.1>
- Dunham, R.J., 1962. Classification of Carbonate Rocks According to Depositional Textures, in: Ham, W.E. (Ed.), *Classification of Carbonate Rocks*. American Association of Petroleum Geologists Memoir, pp. 108–121.
- Eaton, P., West, P., 2010. *Atomic Force Microscopy*, 1 edition. ed. Oxford University Press, Oxford ; New York.

- Eyles, N., 2008. Glacio-epochs and the supercontinent cycle after ~3.0 Ga: Tectonic boundary conditions for glaciation. *Palaeogeography, Palaeoclimatology, Palaeoecology* 258, 89–129. <https://doi.org/10.1016/j.palaeo.2007.09.021>
- Feazel, C.T., Farrell, H.E., 1988. Chalk From the Ekofisk Area, North Sea: Nanofossils + Micropores = Giant Fields. *Society for Sedimentary Geology* 1 & 2.
- Garrison, T., 2010. *Oceanography: an invitation to marine science*, 7th ed. ed. Brooks/Cole Cengage Learning, Belmont, Calif.
- Geitle, K., 2013. Chemically induced compaction in fractured and intact chalk cores. University of Stavanger, Norway.
- Gjersdal, S., 2018. TEM, SEM and optical microscopy analyses of Berea sandstone cores flooded with sodium silicate polymers for IOR purposes. University of Stavanger, Faculty of Science and Technology, Department of Energy Resources.
- Green, D.W., Willhite, G.P., 1997. *Enhanced Oil Recovery*. Society of Petroleum Engineers, Richardson, UNITED STATES.
- Hermansen, H., Landa, G.H., Sylte, J.E., Thomas, L.K., 2000. Experiences after 10 years of waterflooding the Ekofisk Field, Norway. *Journal of Petroleum Science and Engineering* 26, 11–18. [https://doi.org/10.1016/S0920-4105\(00\)00016-4](https://doi.org/10.1016/S0920-4105(00)00016-4)
- Hjuler, M.L., 2007. Diagenesis of Upper Cretaceous onshore and offshore chalk from the North Sea area. DTU Environment.
- Hjuler, M.L., Fabricius, I.L., 2009. Engineering properties of chalk related to diagenetic variations of Upper Cretaceous onshore and offshore chalk in the North Sea area. *Journal of Petroleum Science and Engineering* 68, 151–170. <https://doi.org/10.1016/j.petrol.2009.06.005>
- Javadpour, F., Moravvej Farshi, M., Amrein, M., 2012. Atomic-Force Microscopy: A New Tool for Gas-Shale Characterization. *Journal of Canadian Petroleum Technology* 51, 236–243. <https://doi.org/10.2118/161015-PA>
- JPK instruments, 2020. A practical guide to AFM force spectroscopy and data analysis.
- Kallestén, E., 2015. *The North Sea reservoir chalk characterization*. University of Stavanger, Norway.
- Korsnes, R.I., Madland, M.V., Zimmermann, U., Haser, S., Audinot, J.N., Gysan, P., Schulz, B., Gutzmer, J., Hiorth, A., 2013. Neofomed Dolomite in Flooded Chalk for EOR Processes. Presented at the 75th EAGE Conference and Exhibition incorporating SPE EUROPEC 2013, London, UK. <https://doi.org/10.3997/2214-4609.20130890>
- Lafuma, A., Quéré, D., 2003. Superhydrophobic states. *Nature materials* 2, 457–60. <https://doi.org/10.1038/nmat924>
- Li, Z., Xu, Z., Ayirala, S., Yousef, A., 2018. SmartWater Effects on Wettability, Adhesion and Oil Liberation in Carbonates. Presented at the Abu Dhabi International Petroleum Exhibition & Conference, Society of Petroleum Engineers. <https://doi.org/10.2118/193196-MS>
- Madland, M.V., Hiorth, A., Omdal, E., Megawati, M., Hildebrand-Habel, T., Korsnes, R.I., Evje, S., Cathles, L.M., 2011. Chemical Alterations Induced by Rock–Fluid Interactions When Injecting Brines in High Porosity Chalks. *Transp Porous Med* 87, 679–702. <https://doi.org/10.1007/s11242-010-9708-3>

- Megawati, M., Andersen, P., Korsnes, R., Evje, S., Hiorth, A., Madland, M.V., 2011. The Effect of Aqueous Chemistry pH on the Time-Dependent Deformation Behaviour of Chalk- Experimental and Modelling Study.
- Megawati, M., Madland, M.V., Hiorth, A., 2015. Mechanical and physical behavior of high-porosity chalks exposed to chemical perturbation. *Journal of Petroleum Science and Engineering* 133, 313–327. <https://doi.org/10.1016/j.petrol.2015.06.026>
- Minde, M.W., 2018. Mineral Replacements in Flooding Experiments Linked to Enhanced Oil Recovery in Chalk.
- Minde, M.W., Madland, M.V., Zimmermann, U., Egeland, N., Korsnes, R.I., Nakamura, E., Kobayashi, K., Ota, T., 2019. Mineralogical alterations in calcite powder flooded with MgCl₂ to study Enhanced Oil Recovery (EOR) mechanisms at pore scale. *Microporous and Mesoporous Materials* 109402. <https://doi.org/10.1016/j.micromeso.2019.03.050>
- Molenaar, N., Zijlstra, J.J.P., 1997. Differential early diagenetic low-Mg calcite cementation and rhythmic hardground development in Campanian-Maastrichtian chalk. *Sedimentary Geology* 109, 261–281. [https://doi.org/10.1016/S0037-0738\(96\)00064-4](https://doi.org/10.1016/S0037-0738(96)00064-4)
- Nanosurf, 2019. NaioAFM — The leading compact AFM - Nanosurf Brochure.
- Nanotechnology - Wikibooks, open books for an open world [WWW Document], 2018. URL <https://en.wikibooks.org/wiki/Nanotechnology> (accessed 7.20.20).
- Nermoen, A., Korsnes, R.I., Aursjø, O., Madland, M.V., Kjørslevik, T.A.C., Østensen, G., 2016. How Stress and Temperature Conditions Affect Rock-Fluid Chemistry and Mechanical Deformation. *Front. Phys.* 4. <https://doi.org/10.3389/fphy.2016.00002>
- Nermoen, A., Korsnes, R.I., Hiorth, A., Madland, M.V., 2015. Porosity and permeability development in compacting chalks during flooding of nonequilibrium brines: Insights from long-term experiment. *Journal of Geophysical Research: Solid Earth* 120, 2935–2960. <https://doi.org/10.1002/2014JB011631>
- Philibert, C., 2017. Renewable Energy for Industry, IEA insight series. Paris.
- Punternvold, T., 2008. Waterflooding of carbonate reservoirs: EOR by wettability alteration. University of Stavanger, Norway.
- Saruwatari, K., Tanaka, Y., Nagasawa, H., Kogure, T., 2011. Crystallographic variability and uniformity in Cretaceous heterococcoliths. *European Journal of Mineralogy* 23, 519–528. <https://doi.org/10.1127/0935-1221/2011/0023-2129>
- Scholle, P.A., 1977. Chalk Diagenesis and Its Relation to Petroleum Exploration: Oil from Chalks, a Modern Miracle? *AAPG Bulletin* 61, 982–1009. <https://doi.org/10.1306/C1EA43B5-16C9-11D7-8645000102C1865D>
- Scotese, C.R., 1991. Jurassic and Cretaceous plate tectonic reconstructions. *Palaeogeography, Palaeoclimatology, Palaeoecology* 87, 493–501.
- Skovbjerg, L.L., Hassenkam, T., Makovicky, E., Hem, C.P., Yang, M., Bovet, N., Stipp, S.L.S., 2012. Nano sized clay detected on chalk particle surfaces. *Geochimica et Cosmochimica Acta* 99, 57–70. <https://doi.org/10.1016/j.gca.2012.05.037>
- Strand, S., Høgnesen, E.J., Austad, T., 2006. Wettability alteration of carbonates—Effects of potential determining ions (Ca²⁺ and SO₄²⁻) and temperature. *Colloids and Surfaces A: Physicochemical and Engineering Aspects* 275, 1–10. <https://doi.org/10.1016/j.colsurfa.2005.10.061>

- Surlyk, F., Damholt, T., Bjerager, M., 2006. Stevns Klint, Denmark: Uppermost Maastrichtian chalk, Cretaceous–Tertiary boundary, and lower Danian bryozoan mound complex. *Bulletin of the Geological Society of Denmark* 54, 48.
- Wang, W., 2018. Geological and engineering aspects of chemo-mechanical compaction during flooding experiments on high-porosity chalks: chemo-mechanical behaviour and compositional changes based on comparative study of five outcrop chalks. University of Stavanger, Faculty of Science and Technology, Department of Energy Resources, Stavanger.
- Wang, W., Madland, M.V., Zimmermann, U., Neramoen, A., Korsnes, R.I., Bertolino, S.R.A., Hildebrand-Habel, T., 2016. Evaluation of porosity change during chemo-mechanical compaction in flooding experiments on Liege outcrop chalk. *Special Publication - Geological Society of London* 435, 217–234. <https://doi.org/10.1144/SP435.10>
- Wilson, M.A., Koutelou, E., Hirsch, C., Akdemir, K., Schibler, A., Barton, M.C., Dent, S.Y.R., 2011. Ubp8 and SAGA Regulate Snf1 AMP Kinase Activity. *Molecular and Cellular Biology* 31, 3126–3135. <https://doi.org/10.1128/MCB.01350-10>
- Zbik, M., 1998. Nanomorphology of Kaolinites: Comparative SEM and AFM Studies. *Clays and Clay Minerals* 46, 153–160. <https://doi.org/10.1346/CCMN.1998.0460205>
- Zimmermann, U., Madland, Merete.V., Minde, M., Borromeo, L., Egeland, N., 2017. Tools to Determine and Quantify Mineralogical Changes During EOR Flooding Experiments on Chalk, in: Abu Dhabi International Petroleum Exhibition & Conference. Presented at the Abu Dhabi International Petroleum Exhibition & Conference, Society of Petroleum Engineers, Abu Dhabi, UAE. <https://doi.org/10.2118/188297-MS>
- Zimmermann, U., Madland, M.V., Neramoen, A., Hildebrand-Habel, T., Bertolino, S.A.R., Hiort, A., Korsnes, R., Audinot, J.-N., Grysan, P., 2015. Evaluation of the compositional changes during flooding of reactive fluids using scanning electron microscopy, nano-secondary ion mass spectrometry, x-ray diffraction, and whole-rock geochemistry. <https://doi.org/10.1306/12221412196>

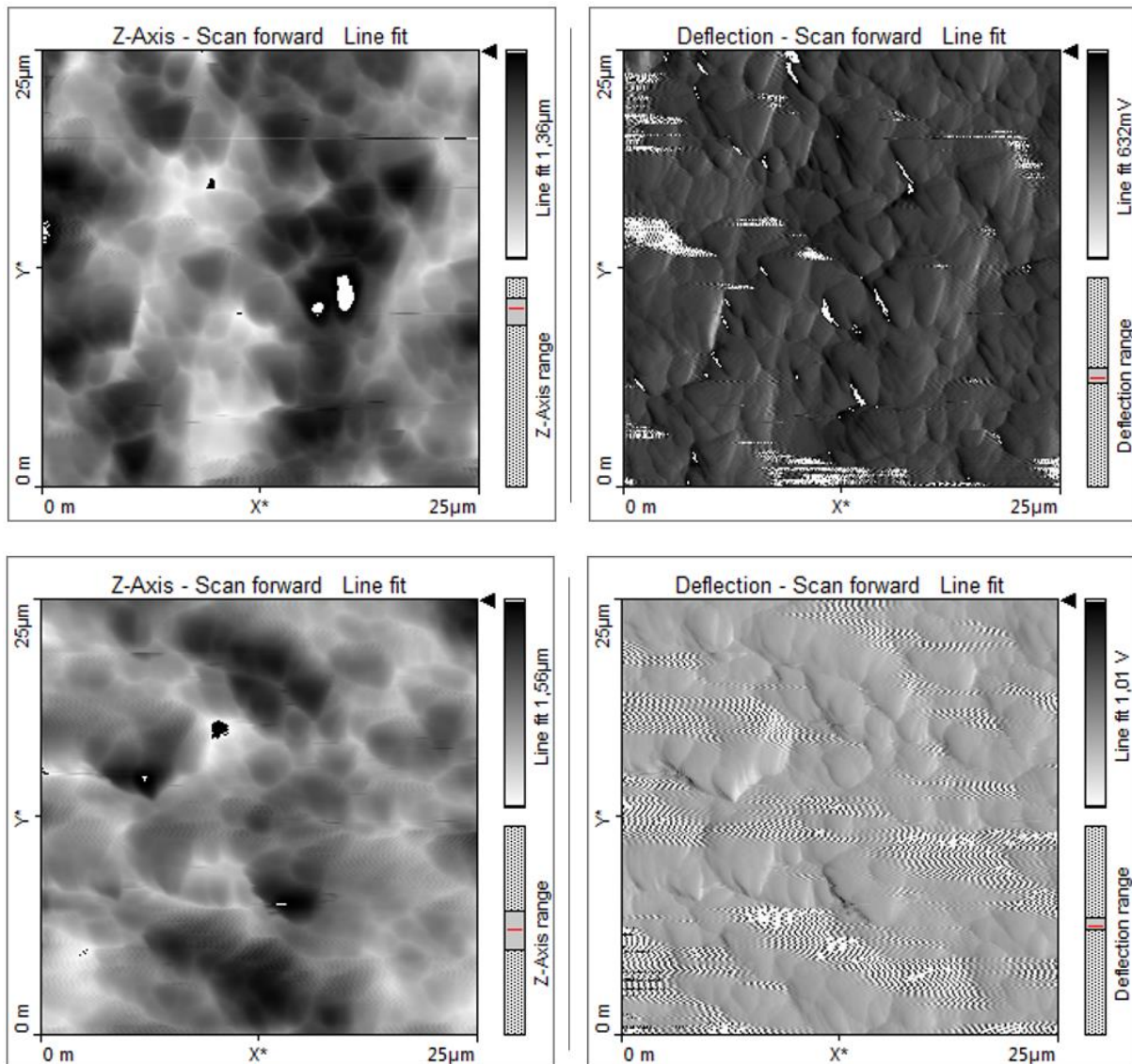
7. Appendix

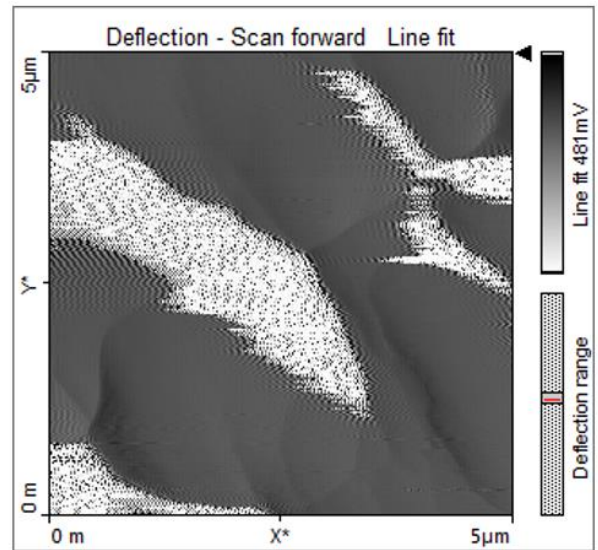
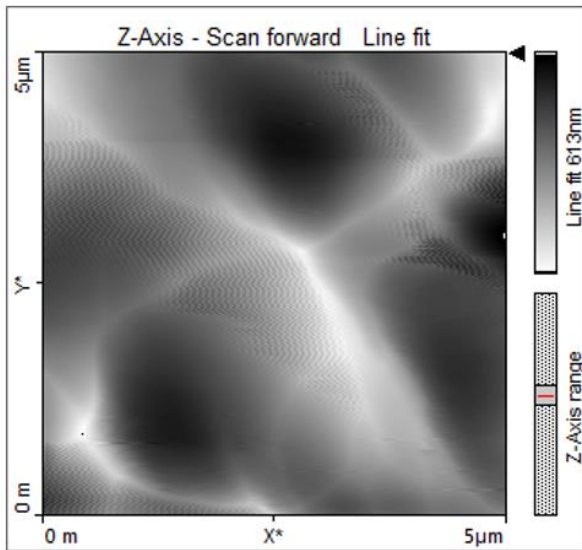
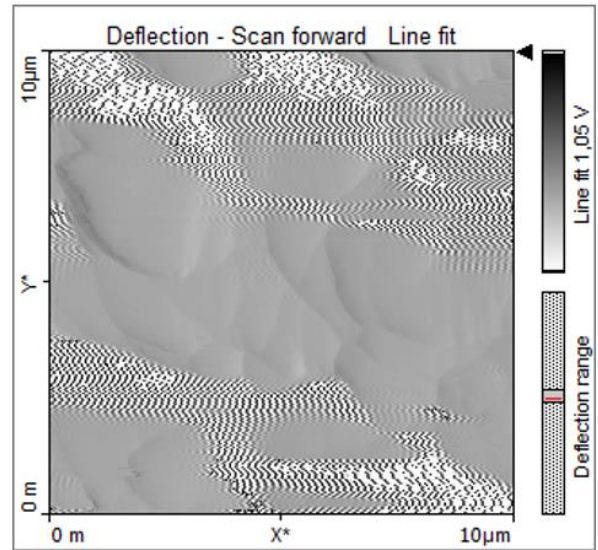
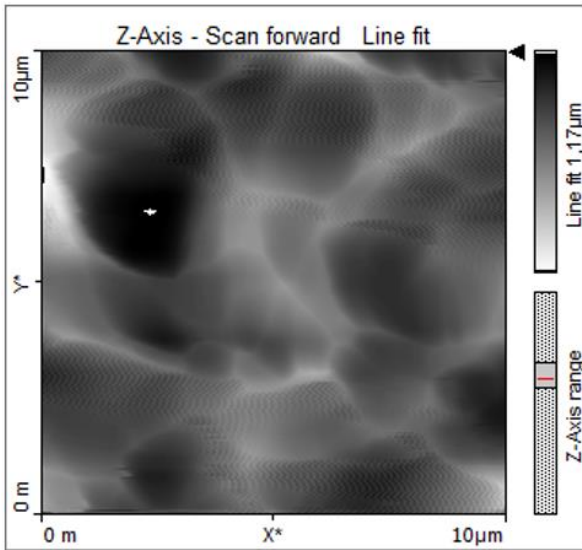
Appendix 1 Topography

Height image to the left and deflection image to the right where there are two images. Amplitude image to the left, height image in the middle and phase image to the right where there are three images.

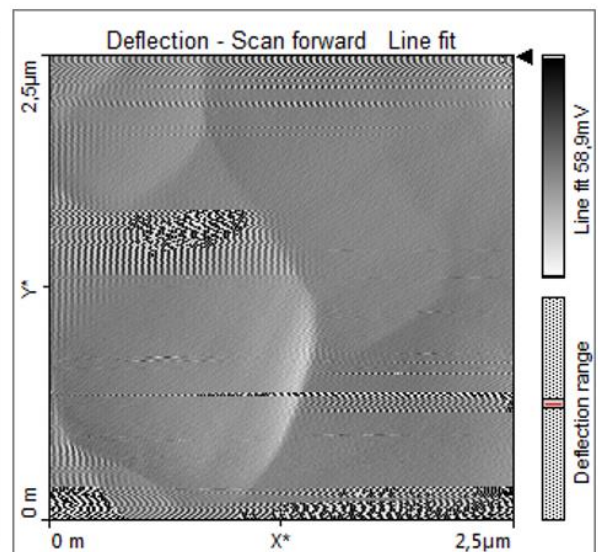
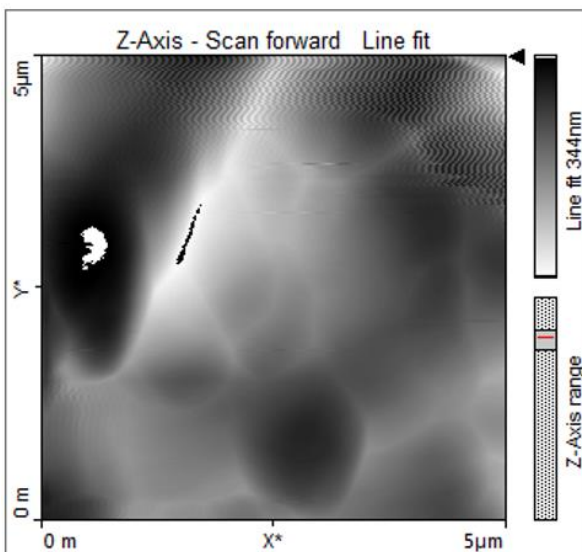
Standards

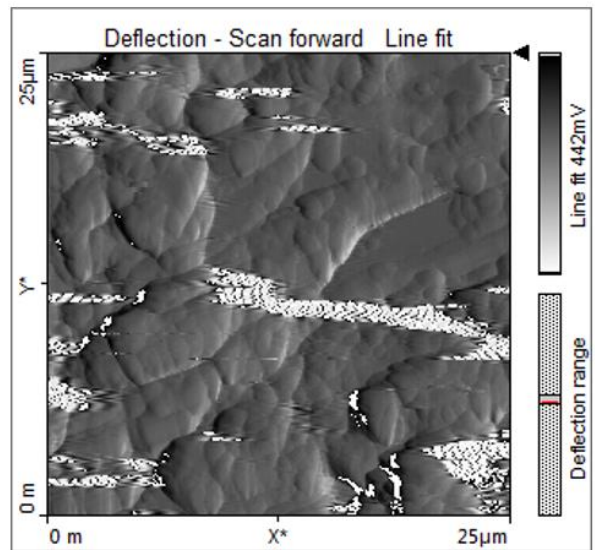
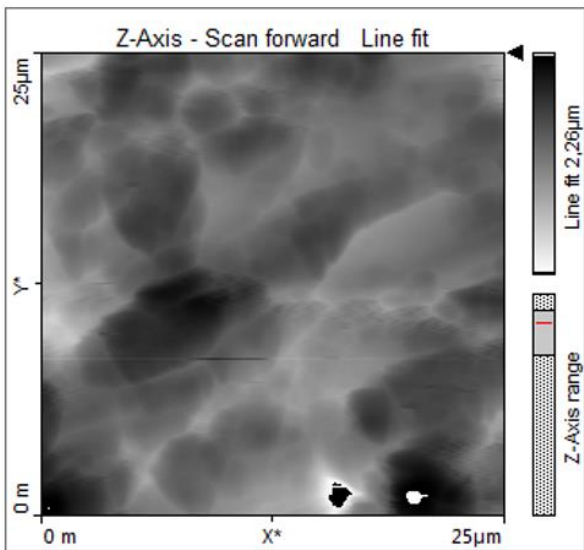
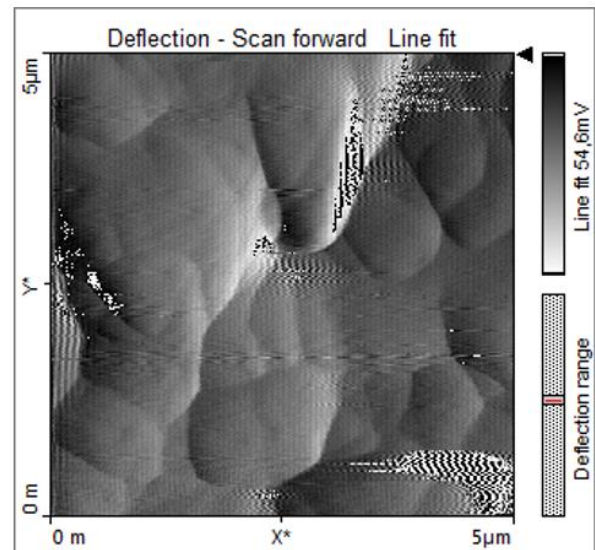
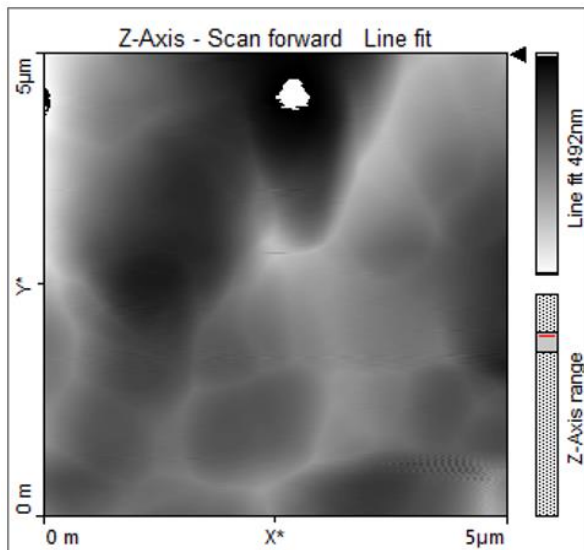
Anorthite



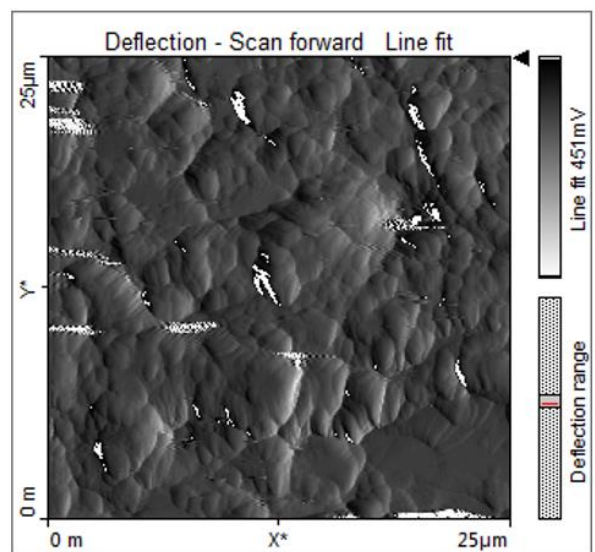
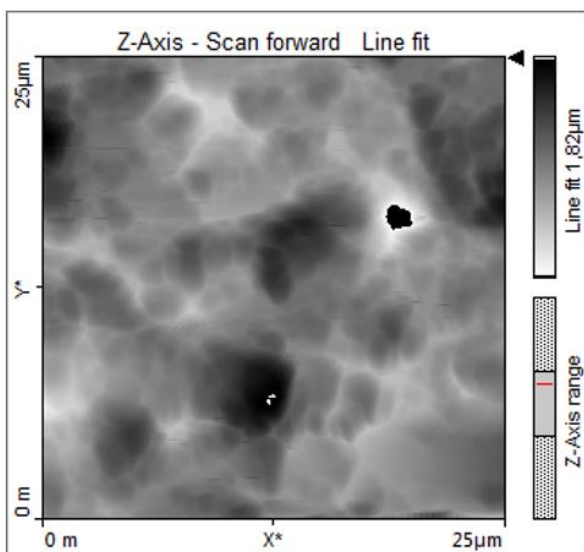


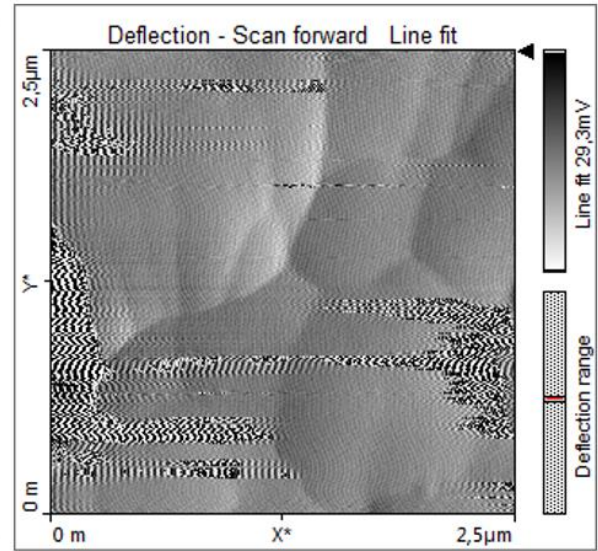
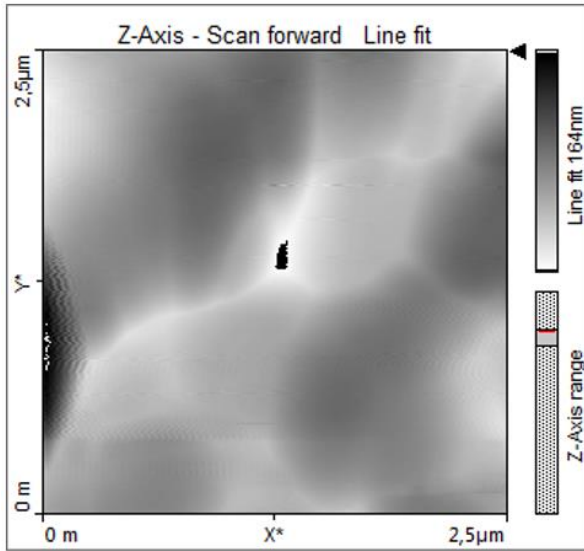
Calcite



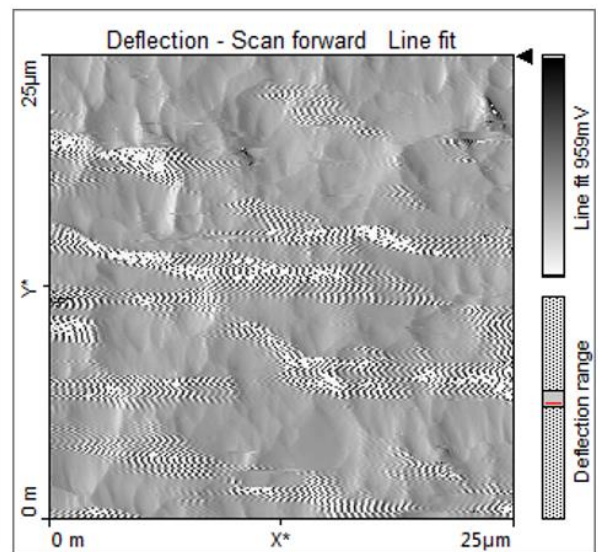
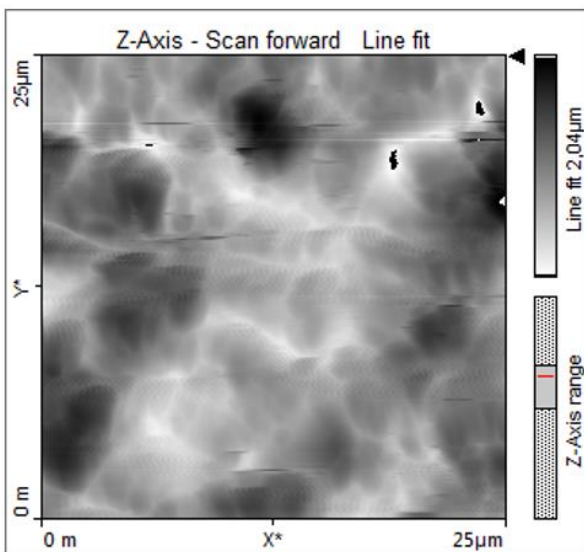
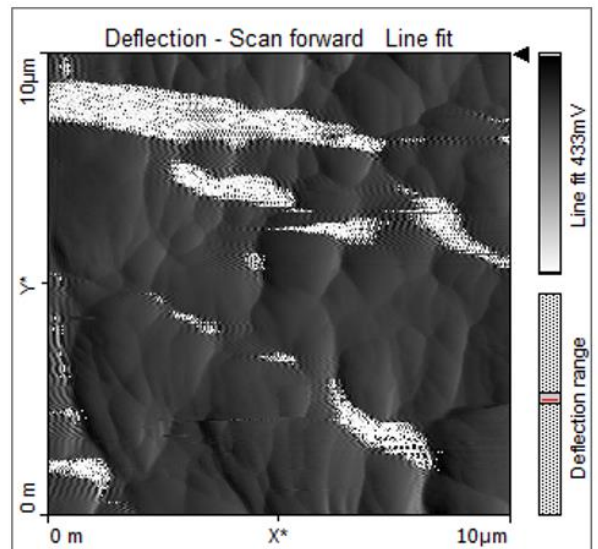
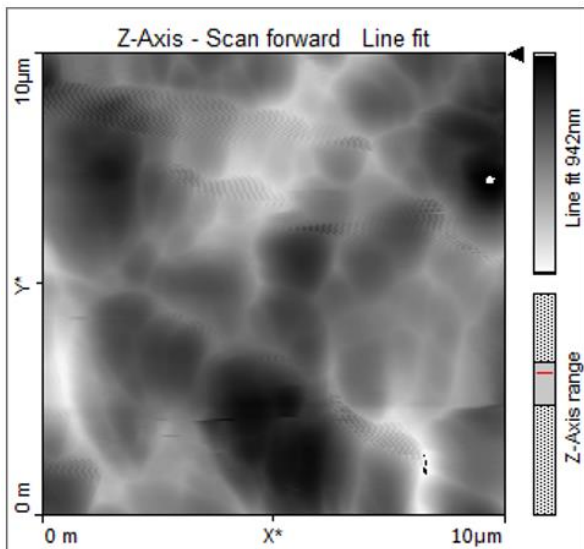


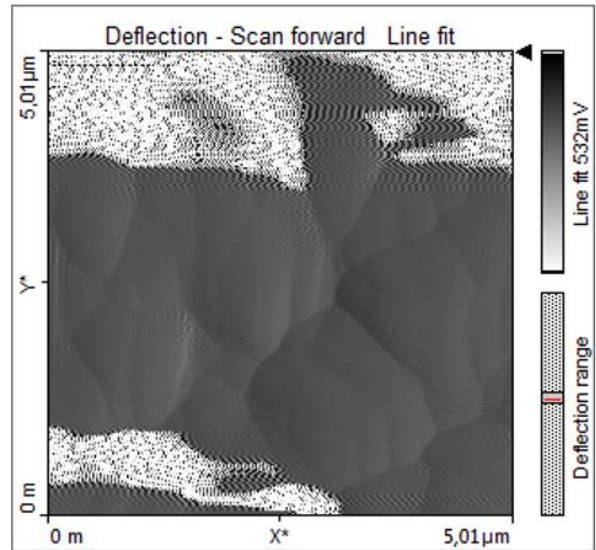
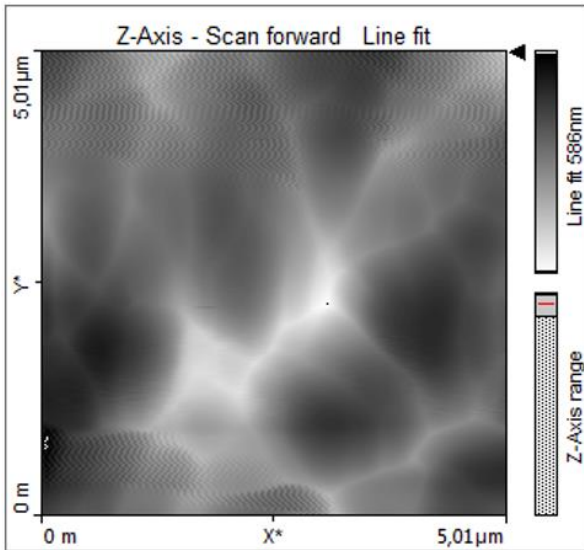
Dolomite



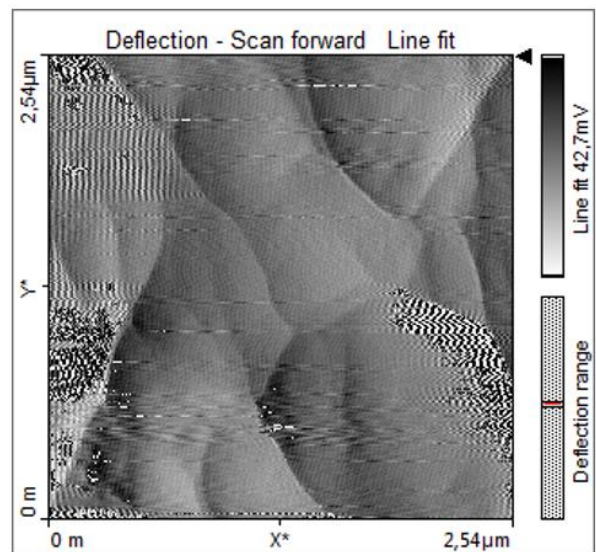
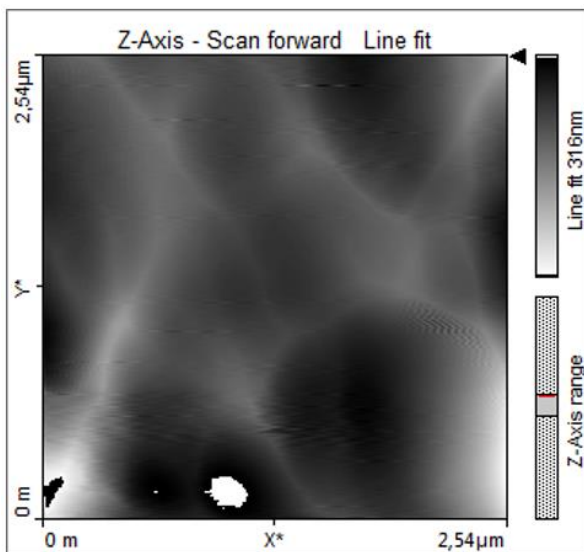
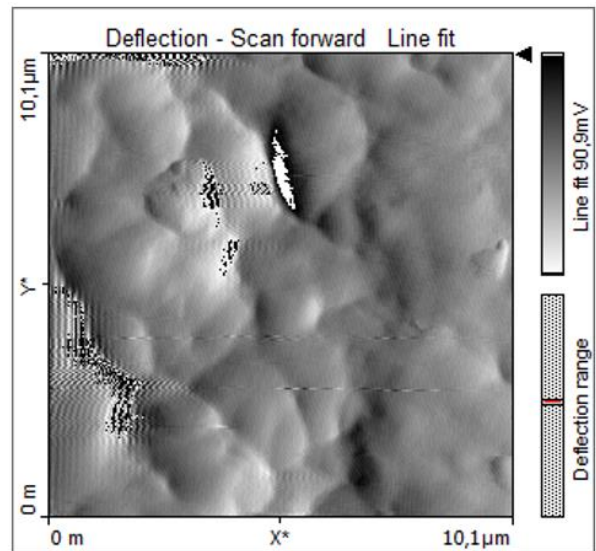
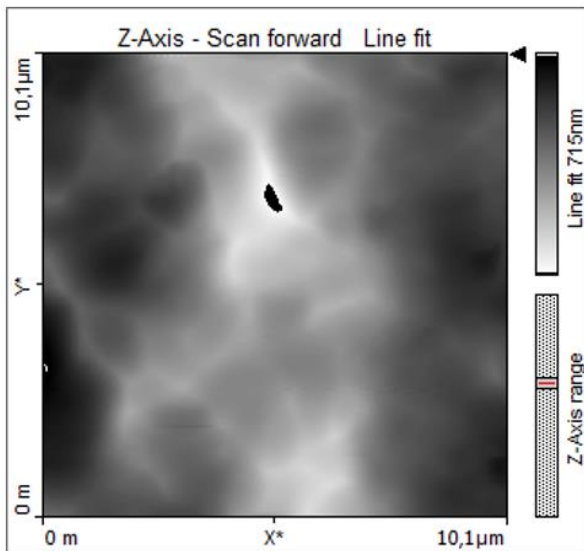


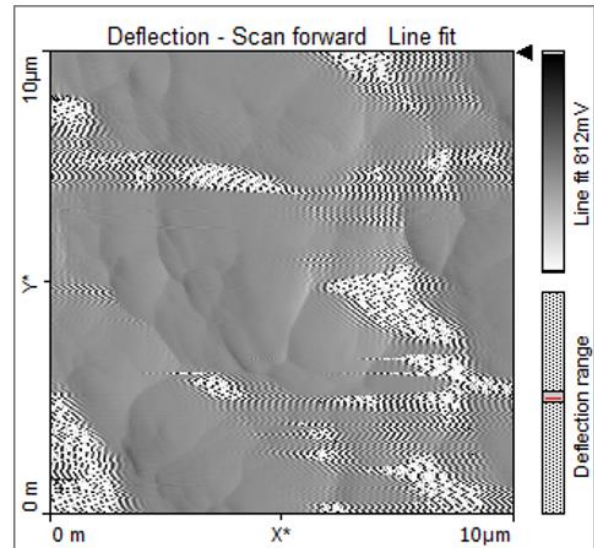
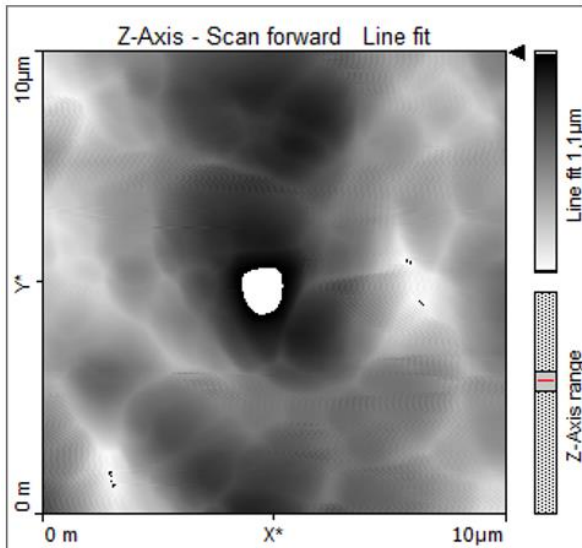
Fluorapatite



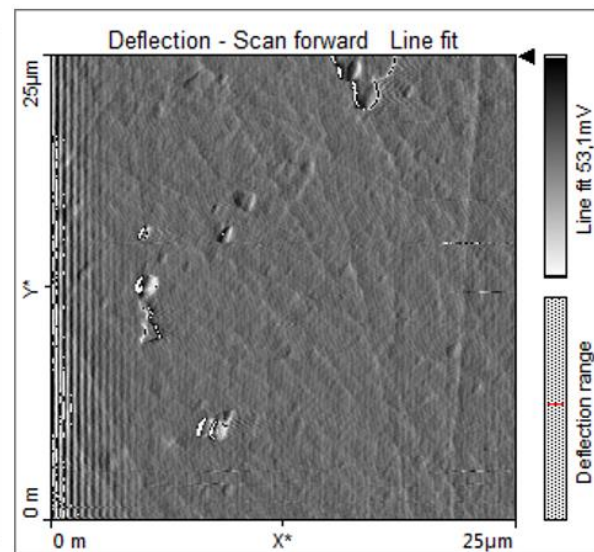
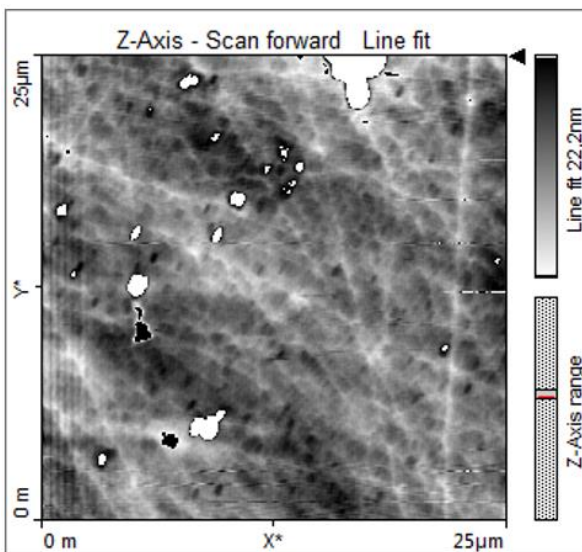
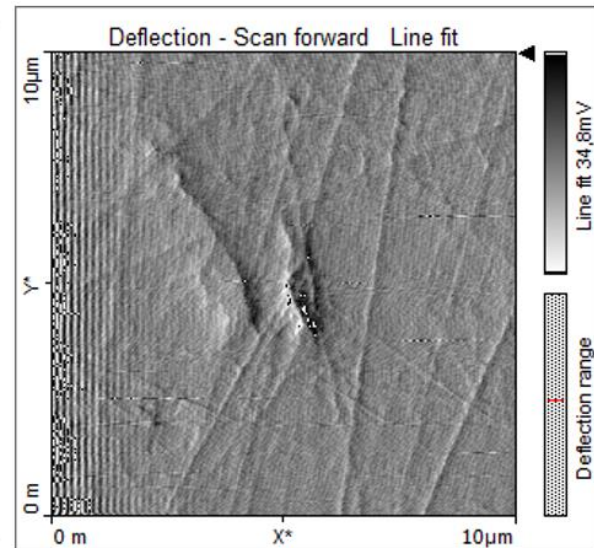
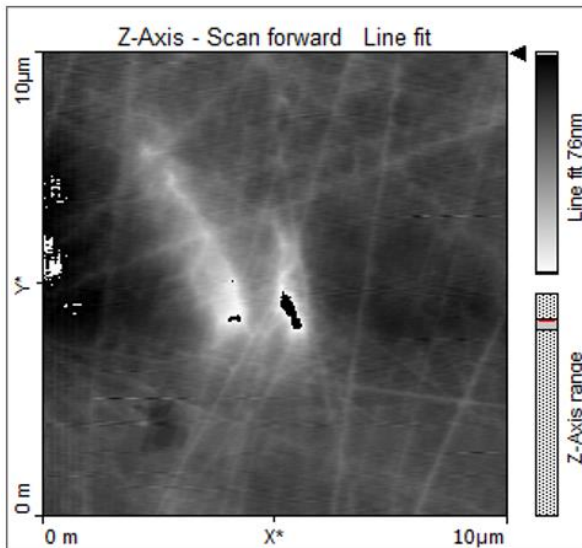


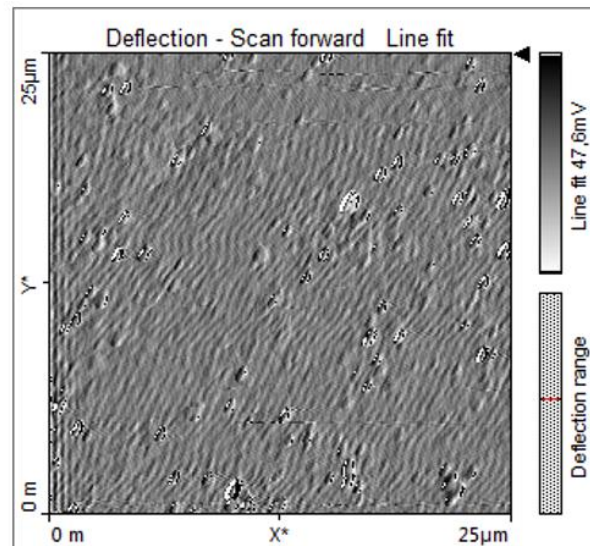
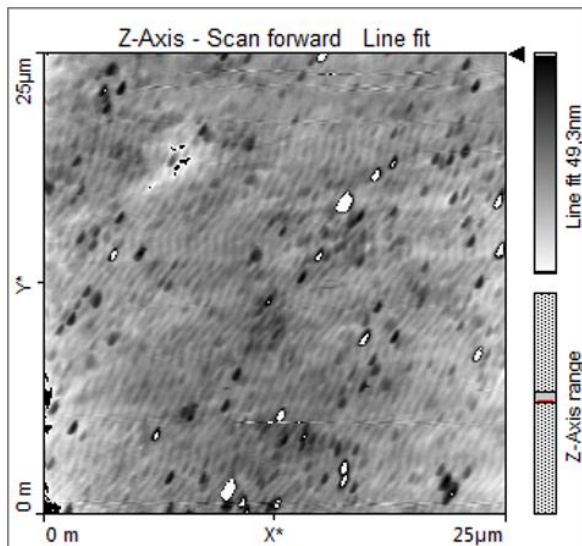
Ilmenite



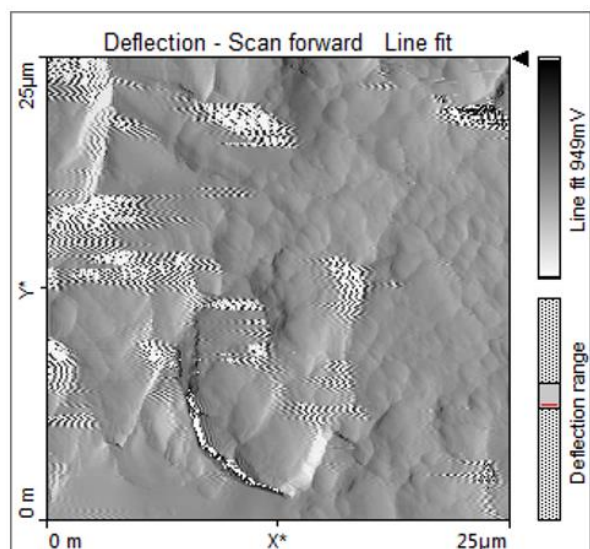
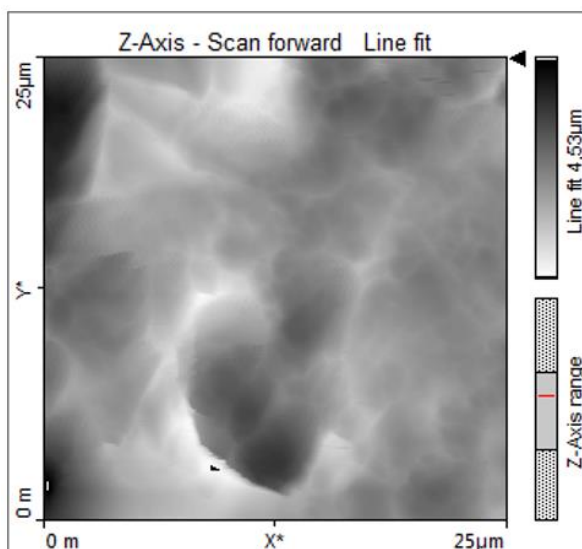
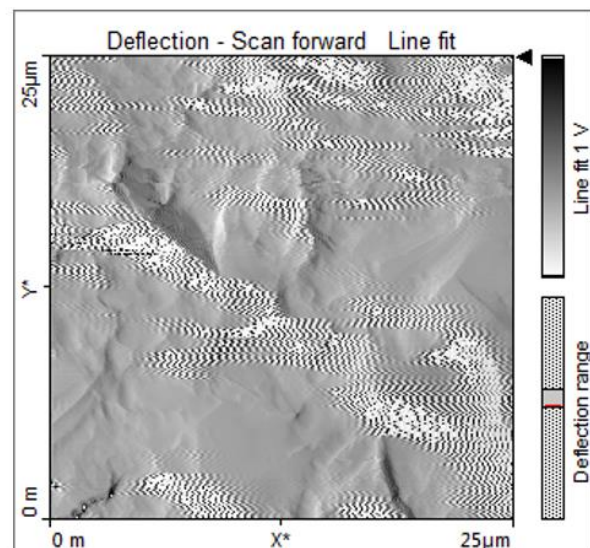
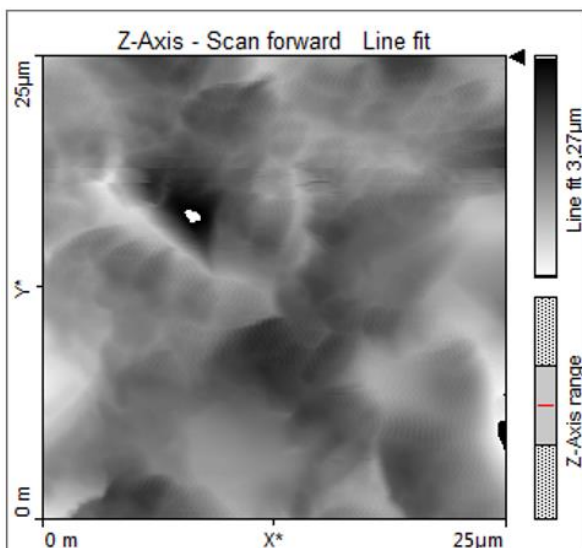


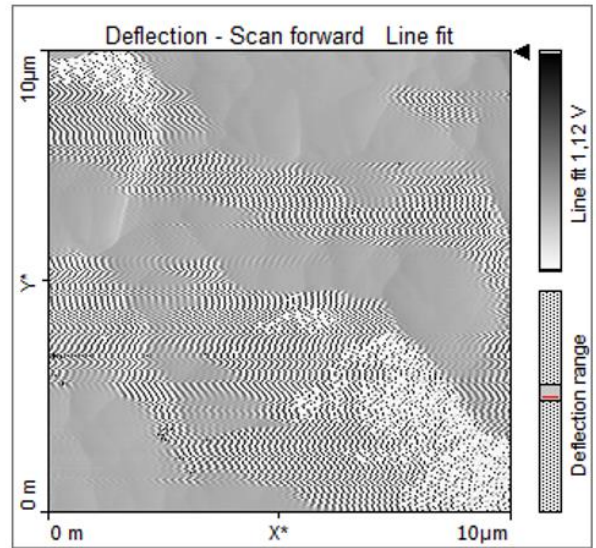
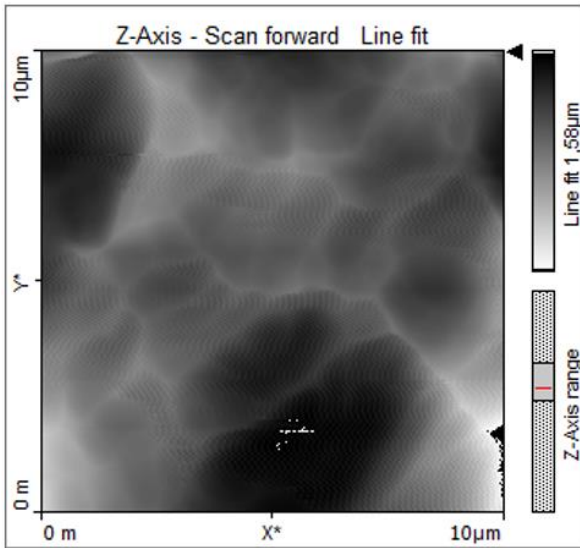
Magnesite



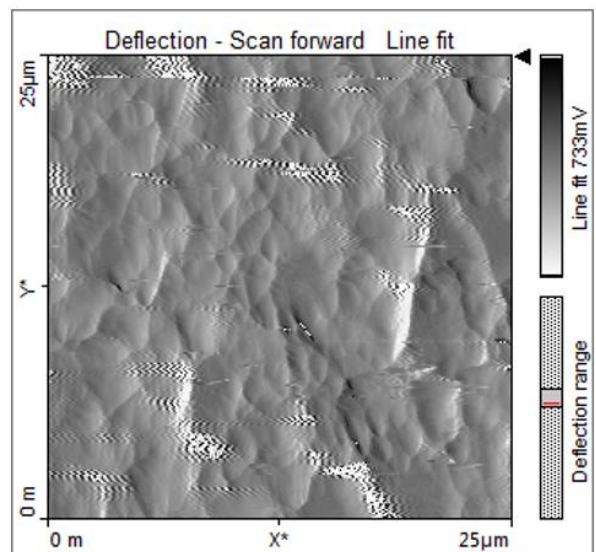
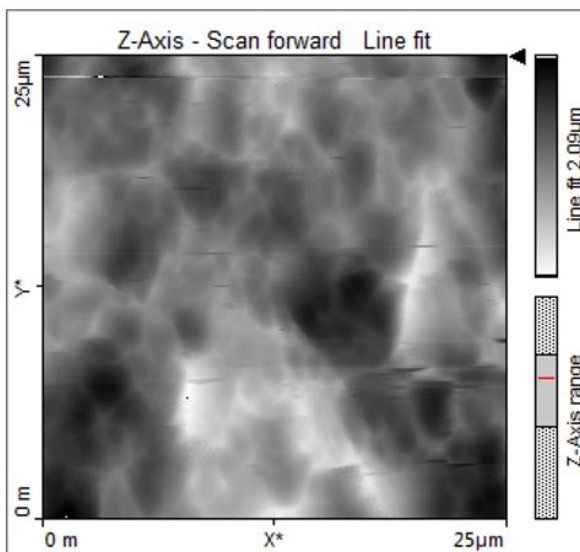
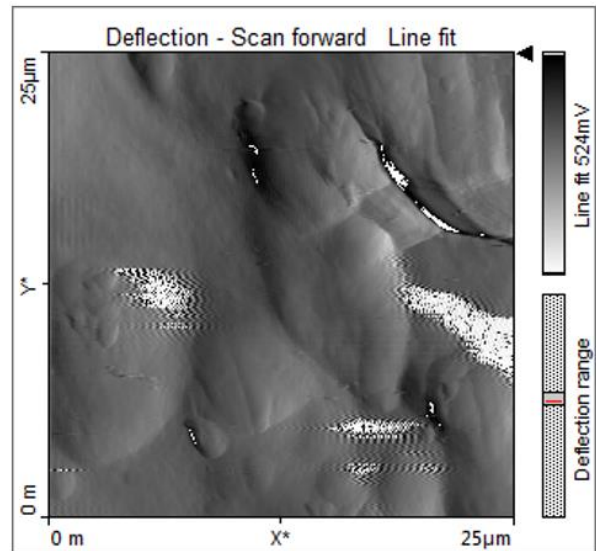
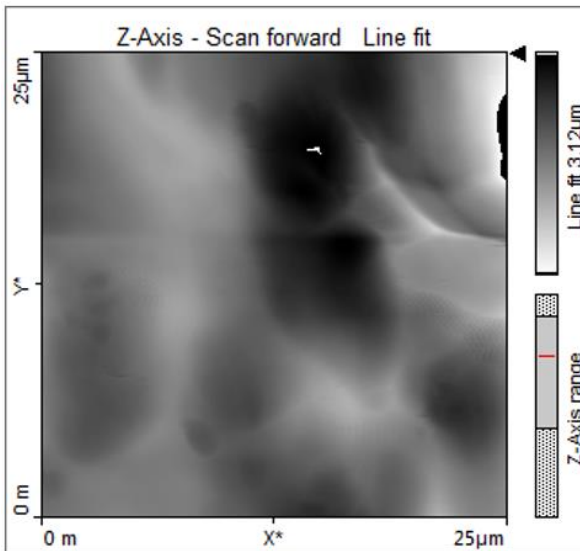


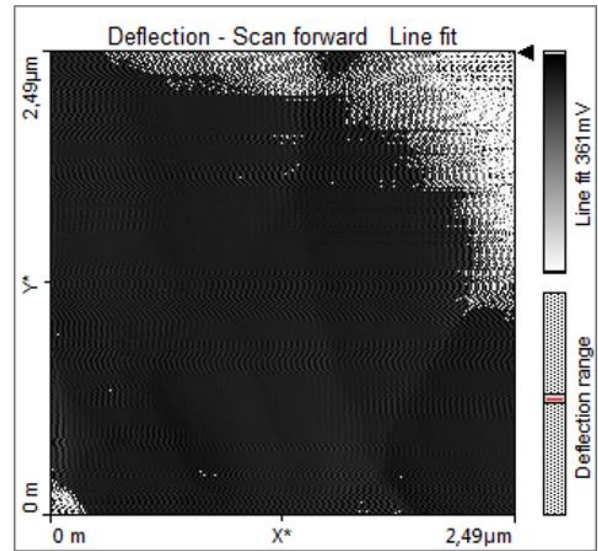
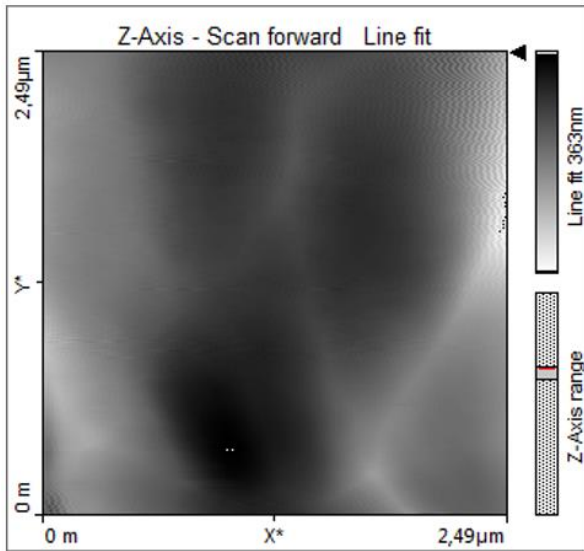
Magnetite



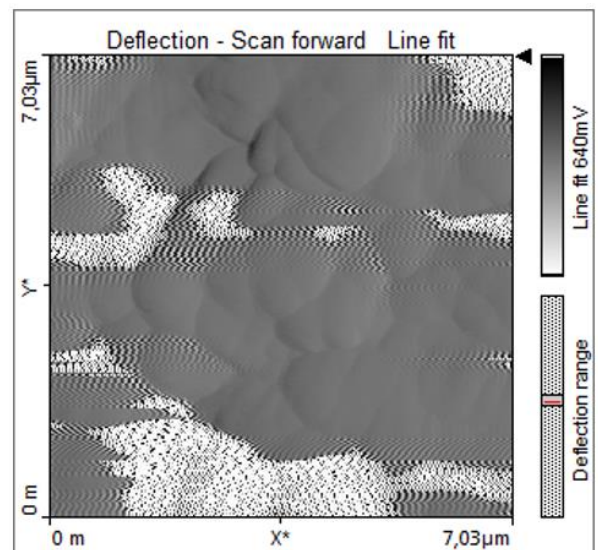
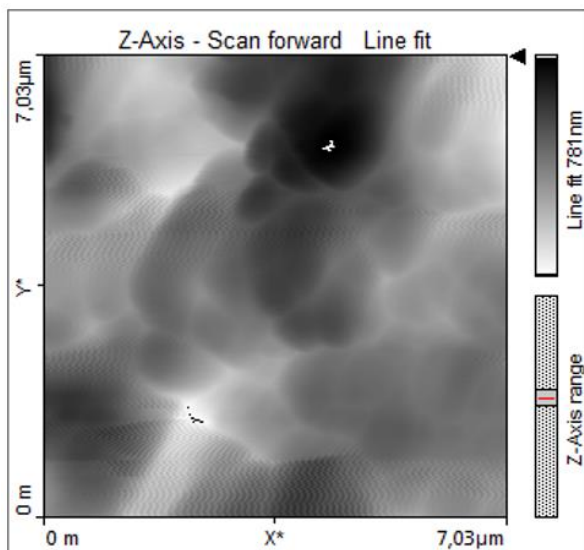
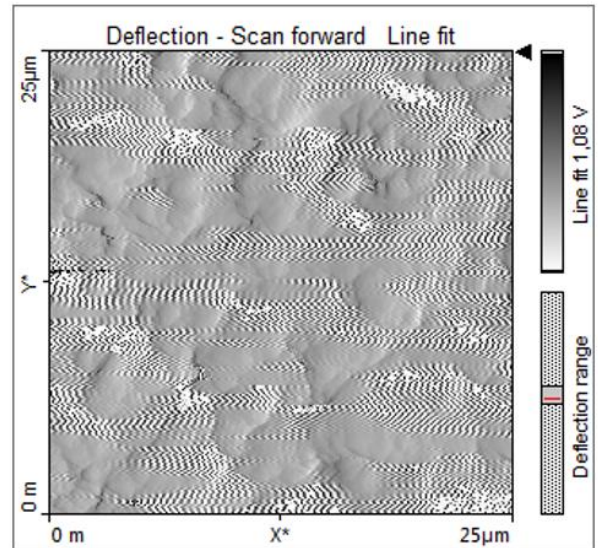
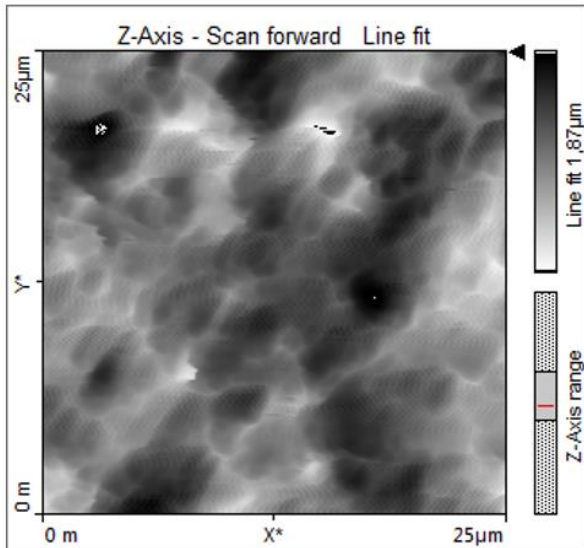


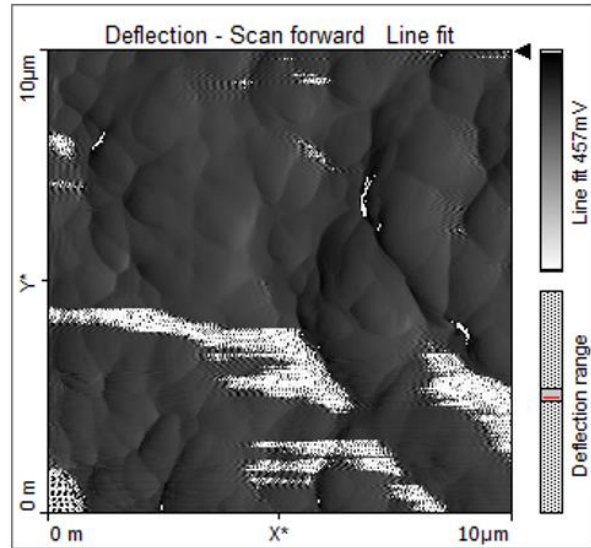
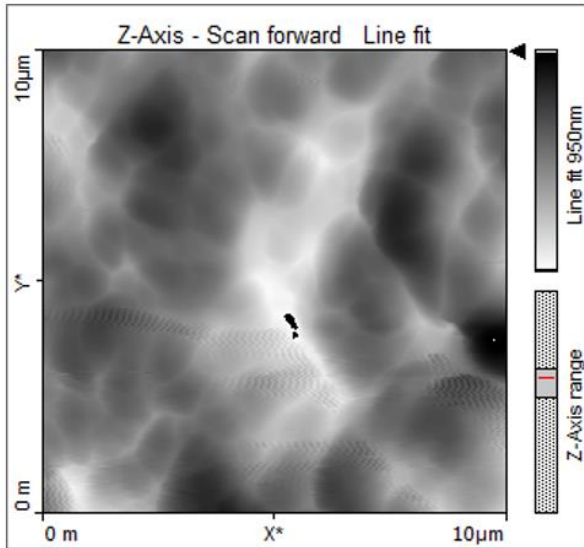
Plagioclase



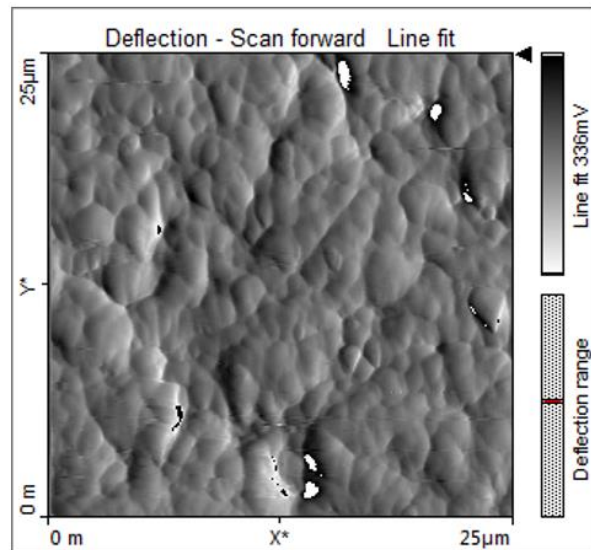
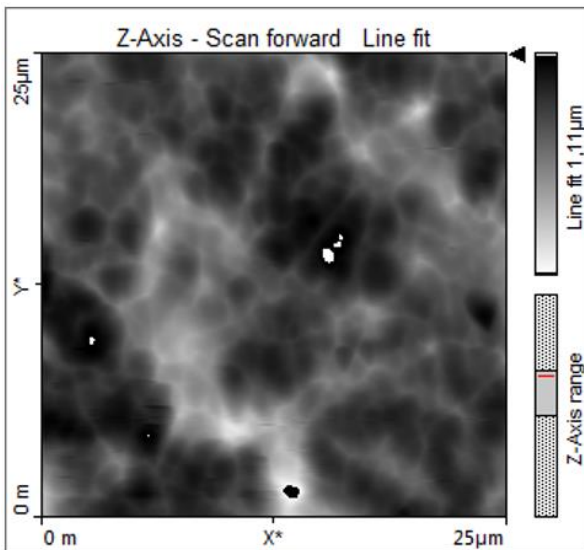
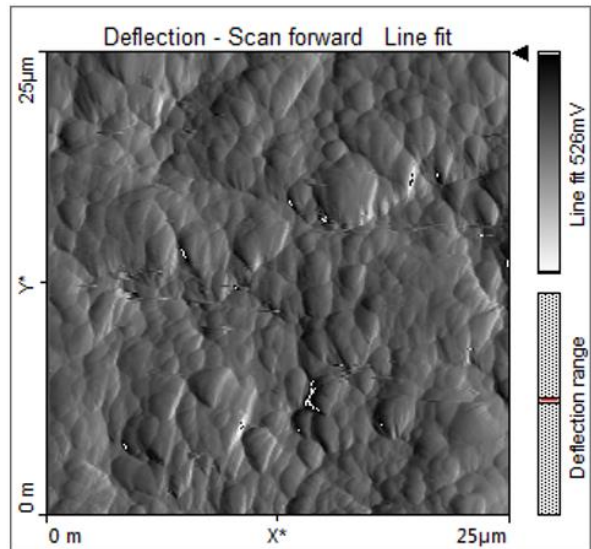
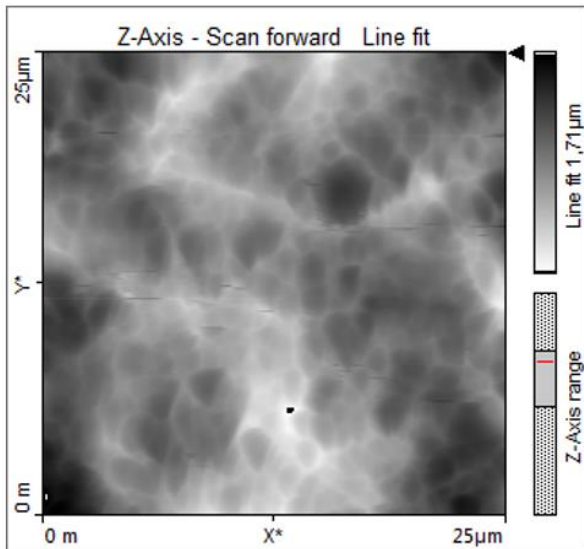


Quartz



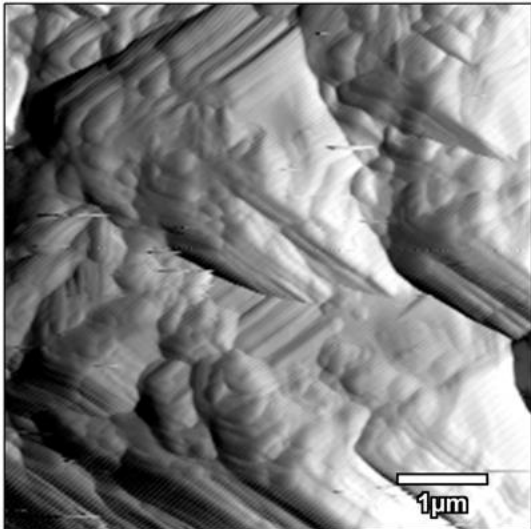
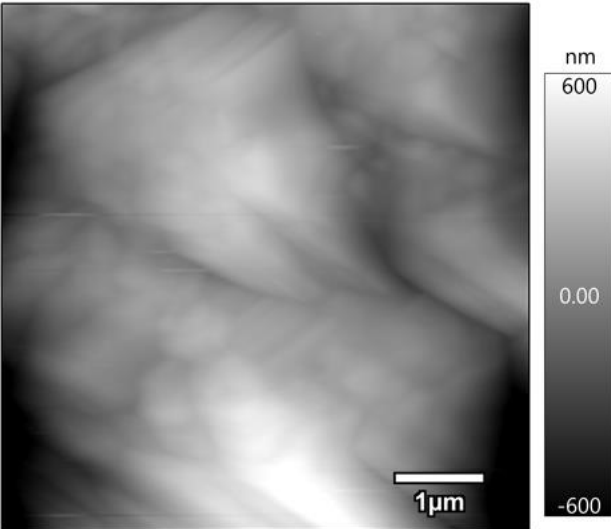
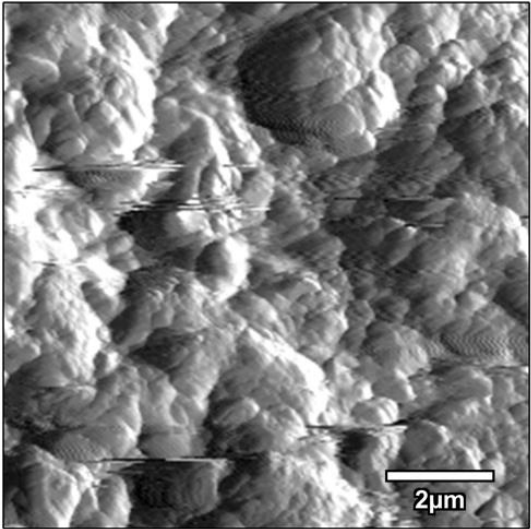
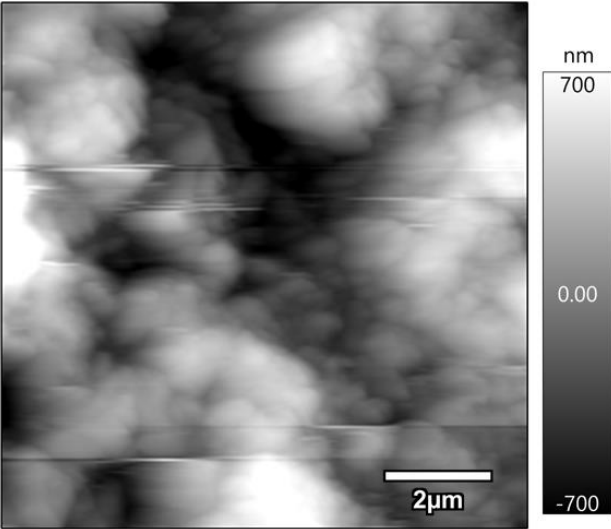


Zircon

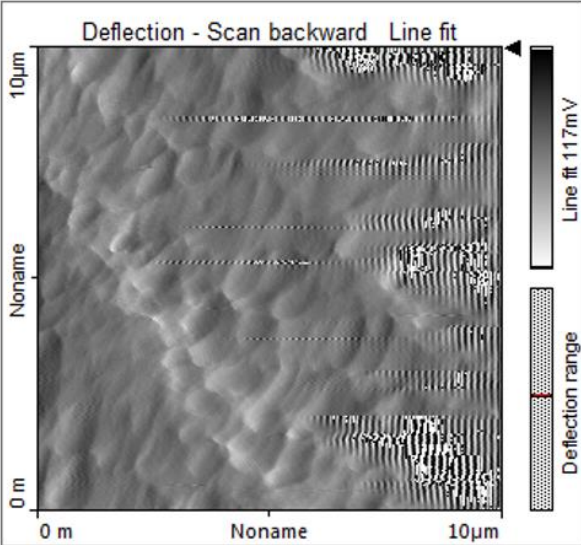
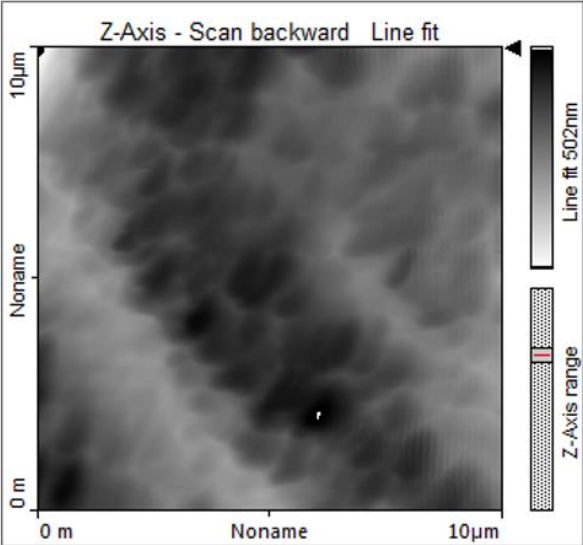


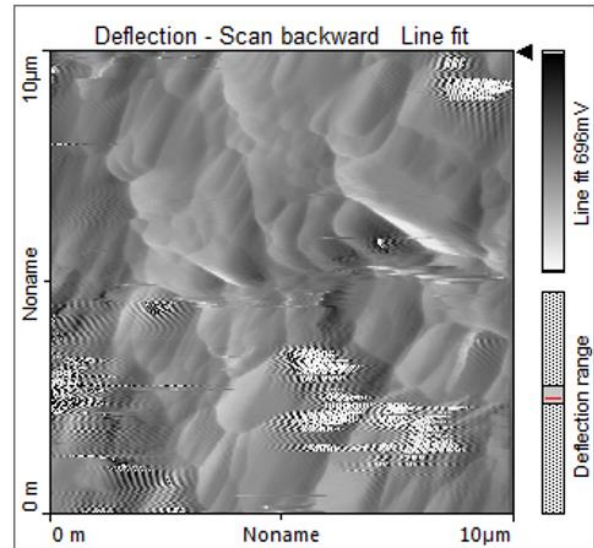
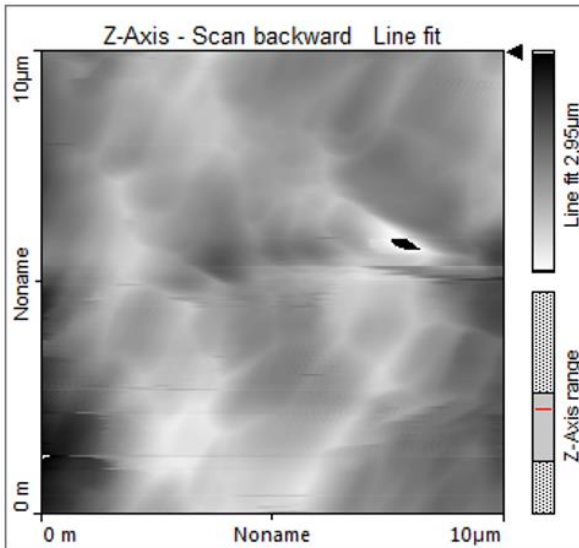
LTT1

Grenoble – MFP-3D Origin



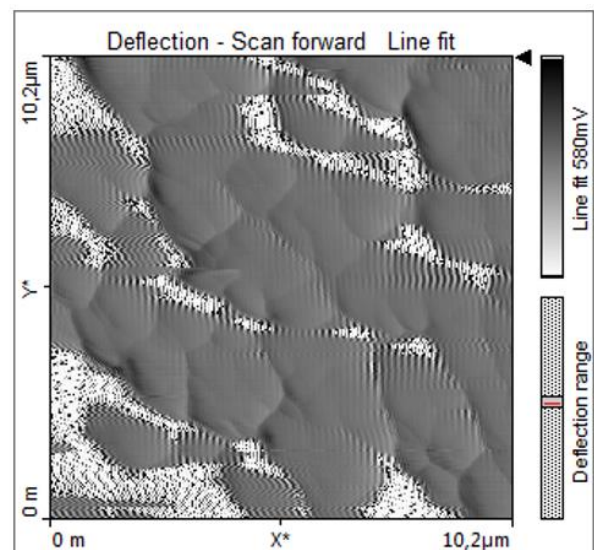
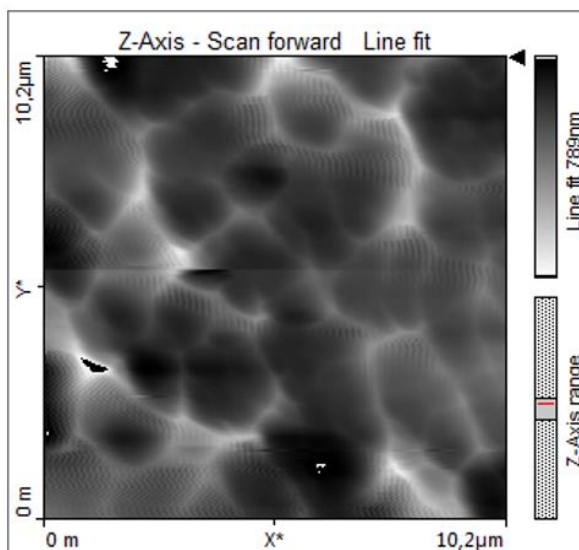
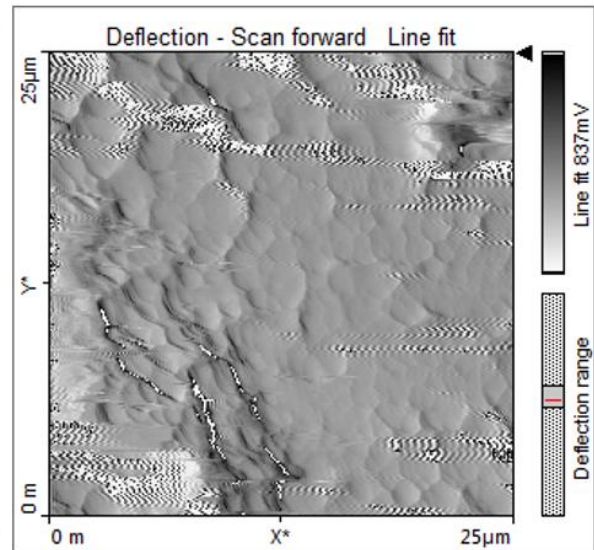
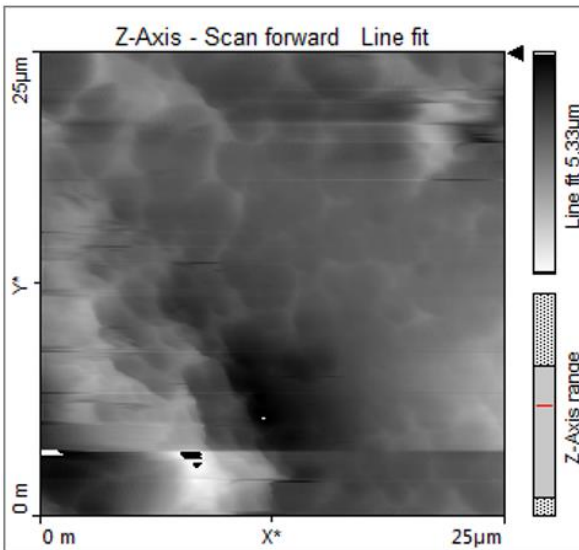
UiS

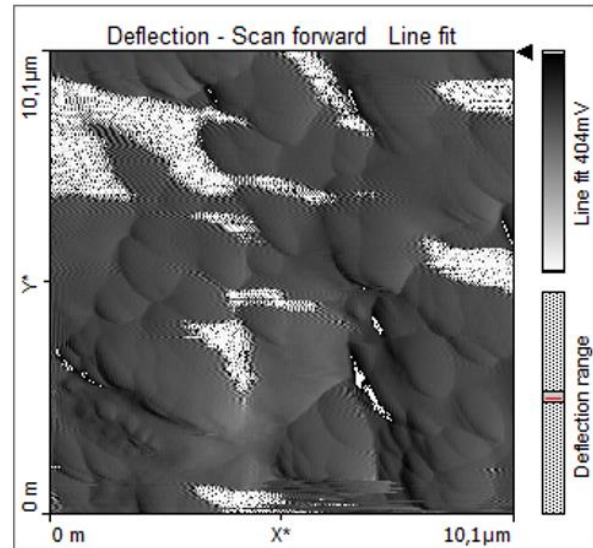
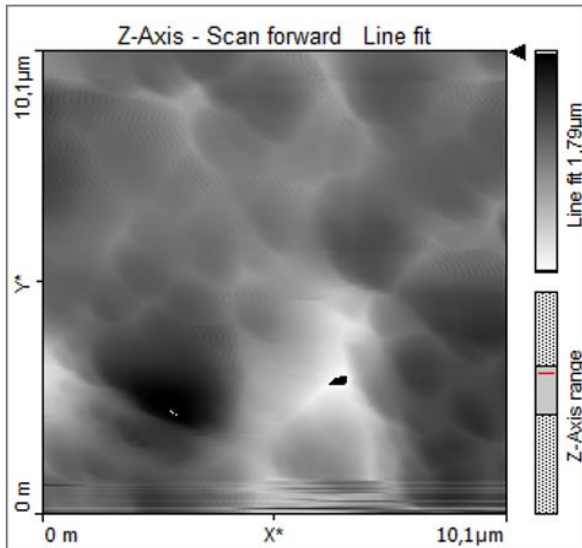




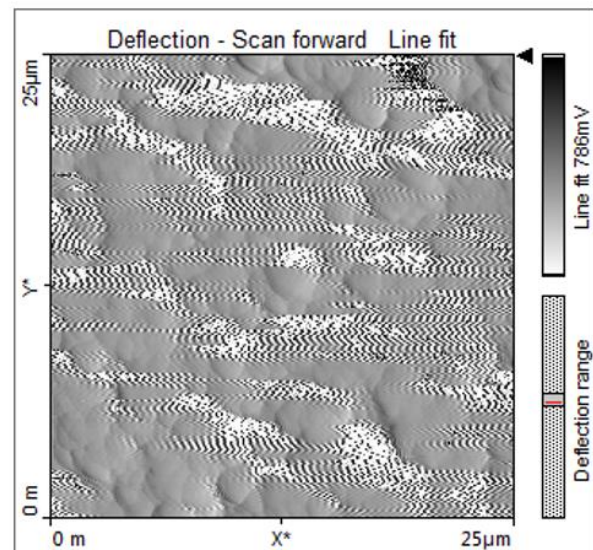
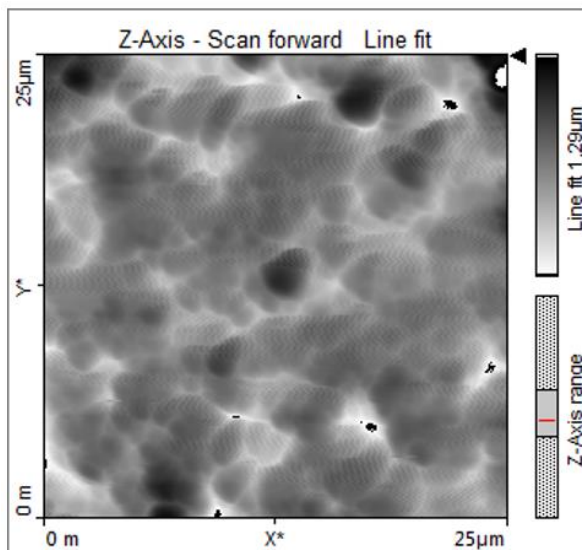
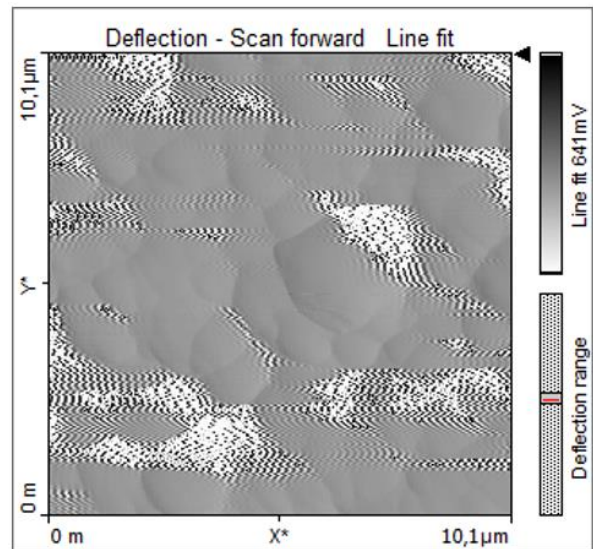
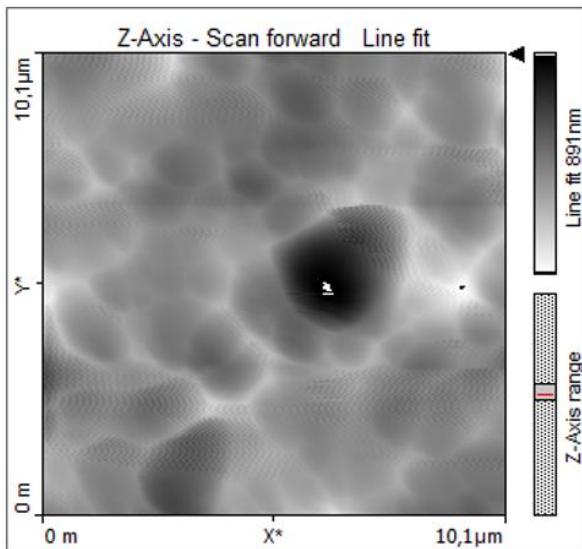
MLTT

Calcite part

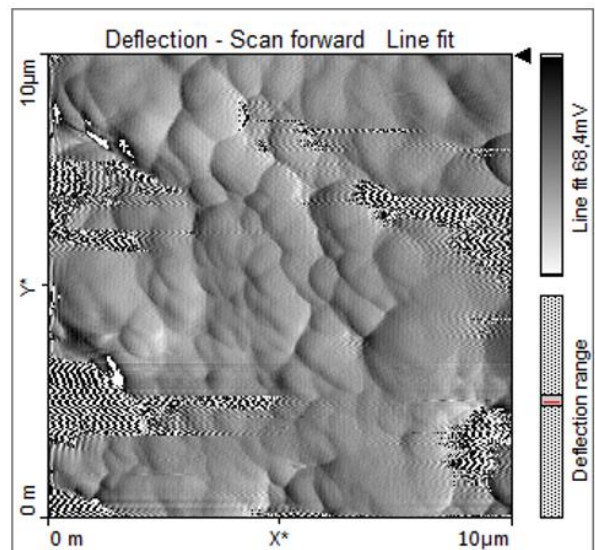
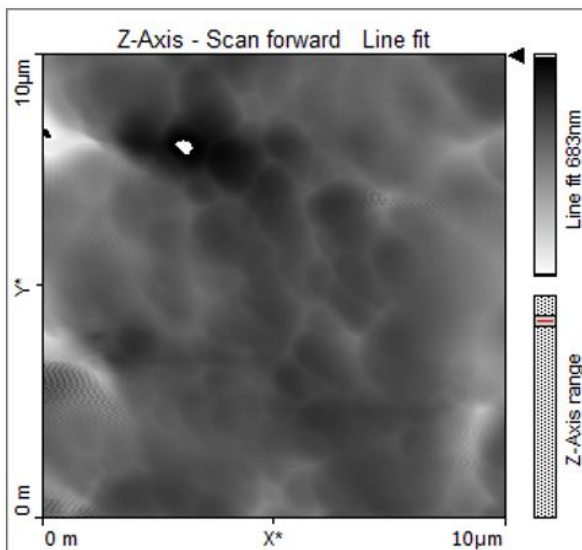
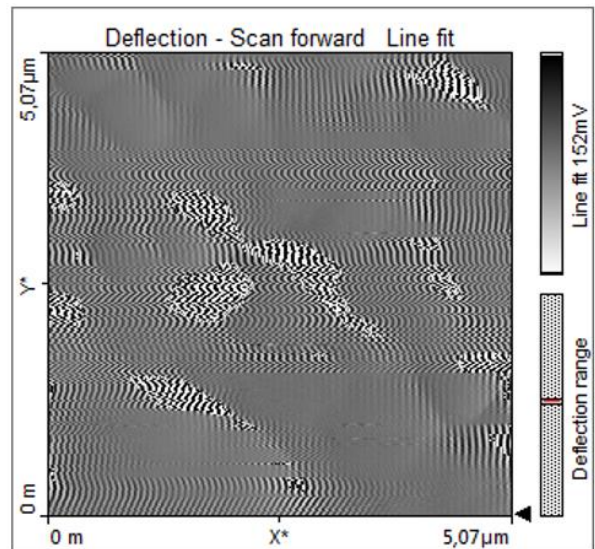
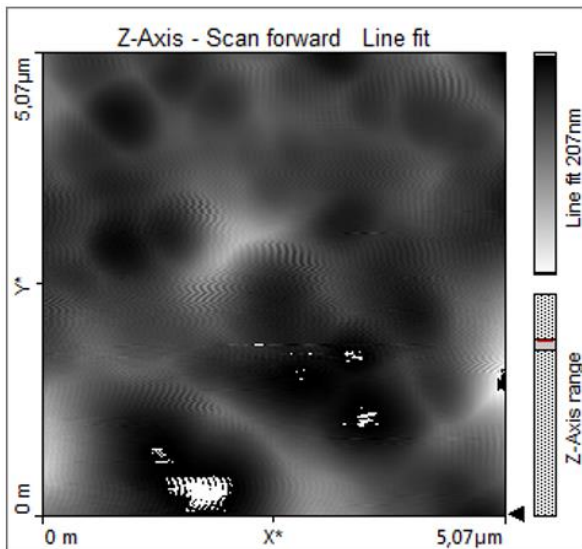
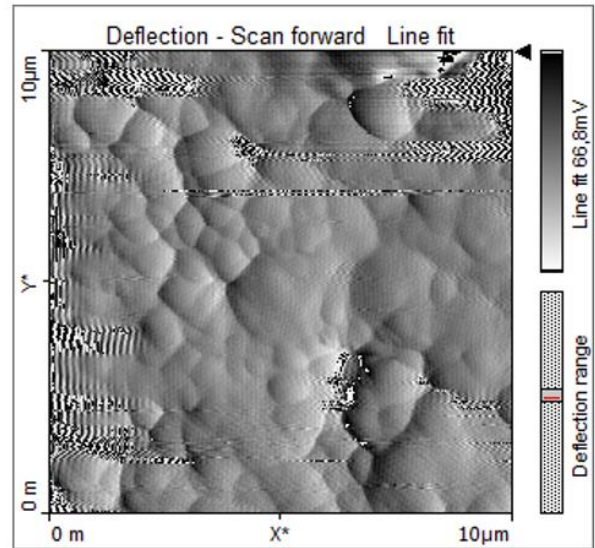
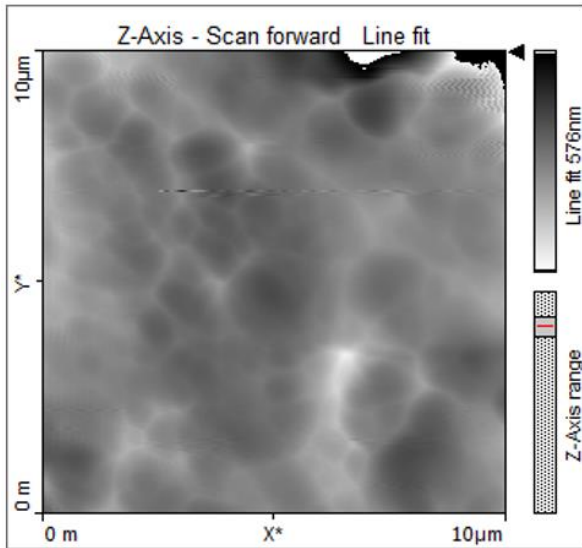




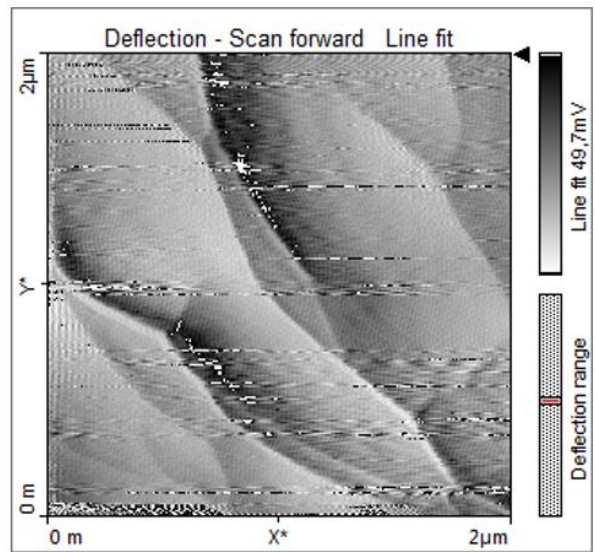
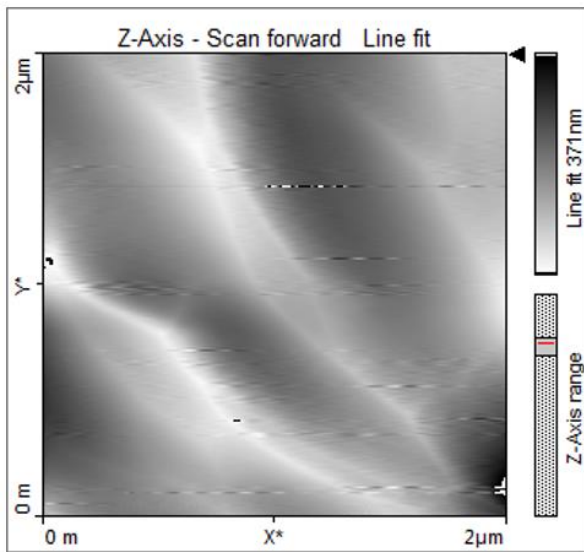
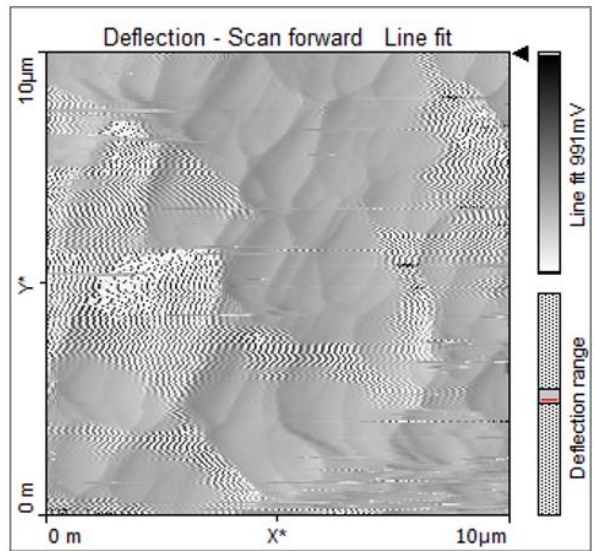
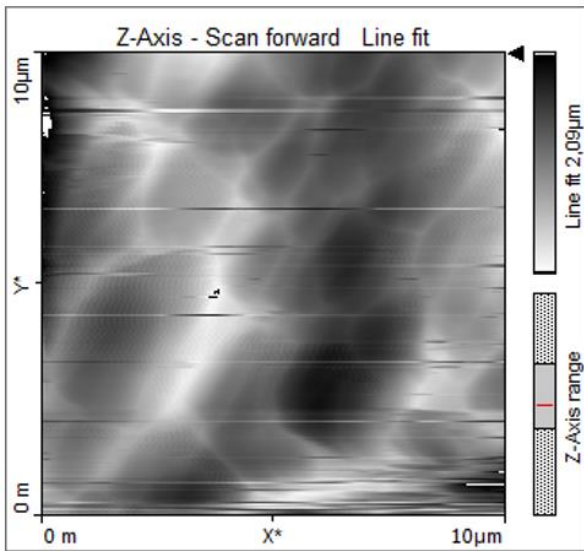
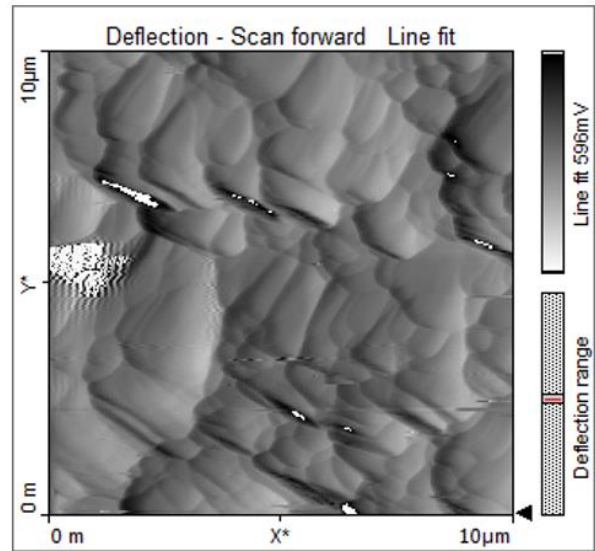
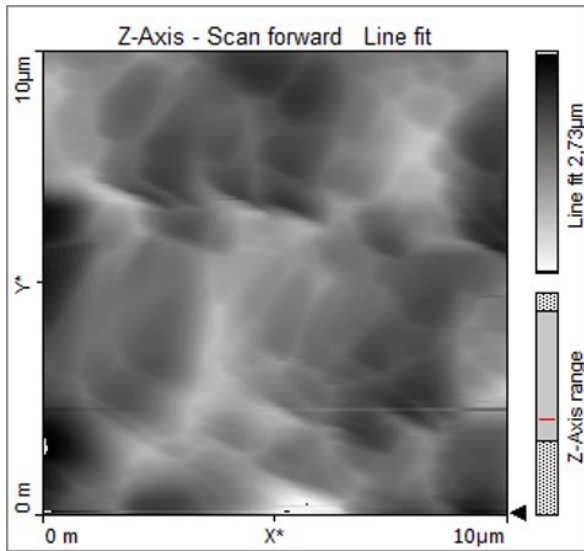
Clay part



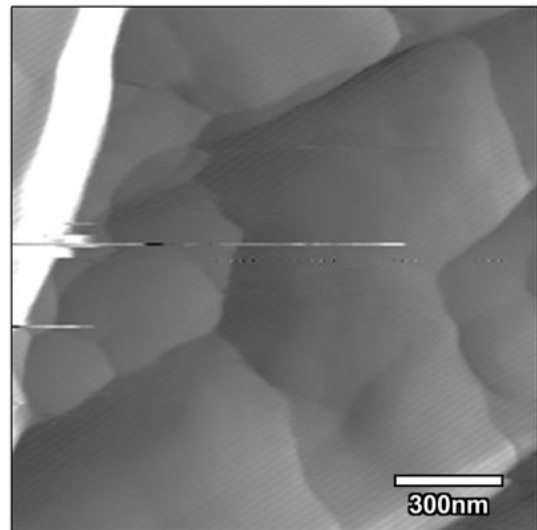
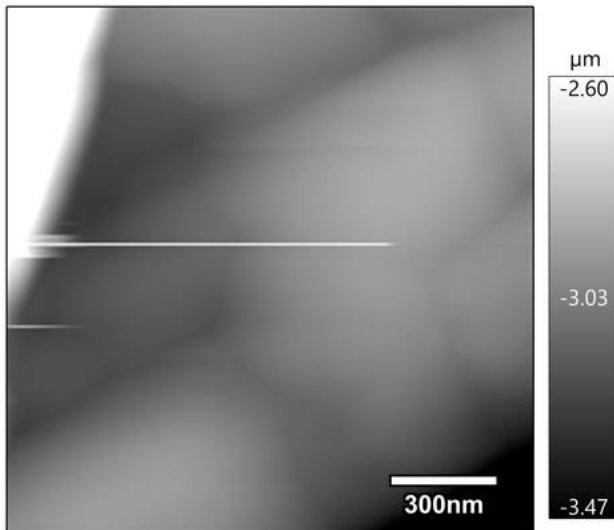
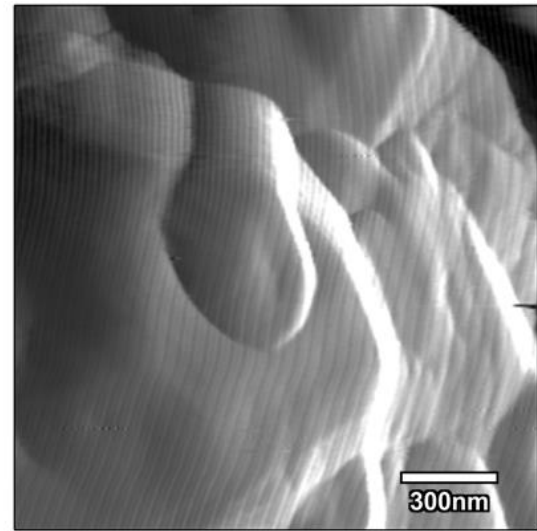
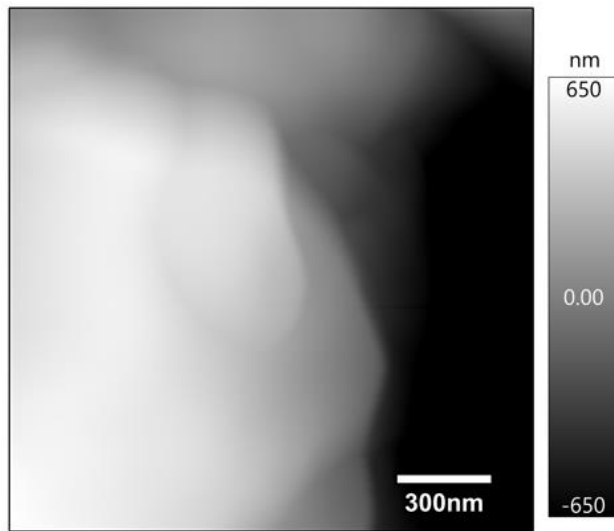
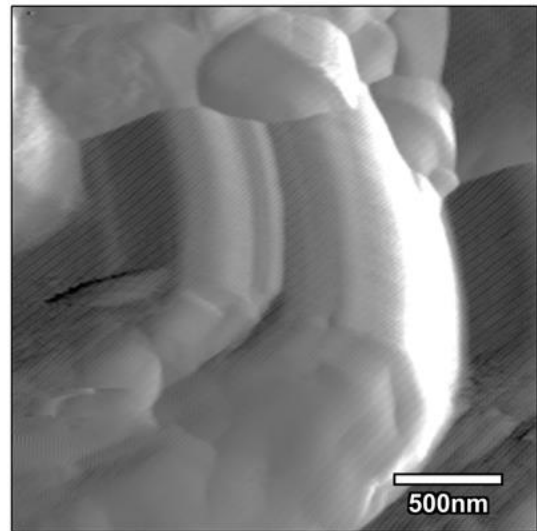
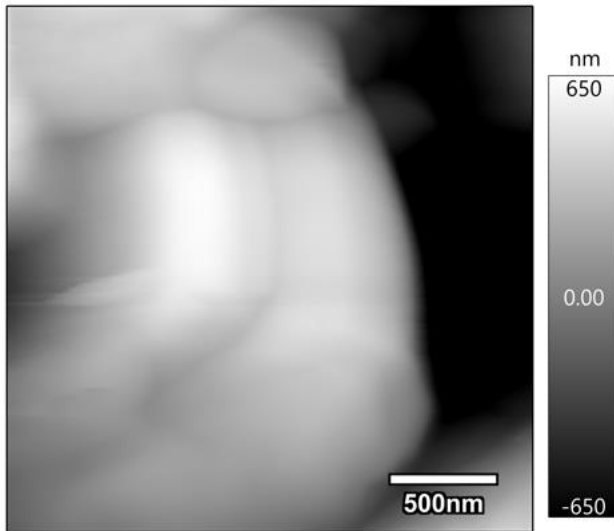
Magnesite part



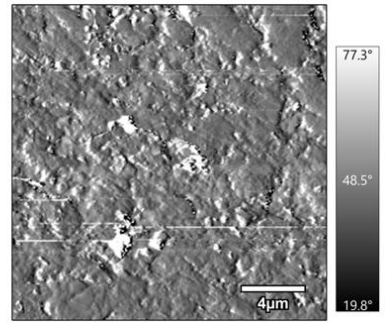
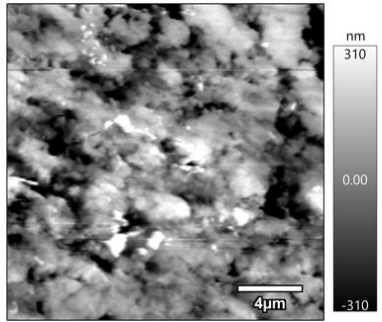
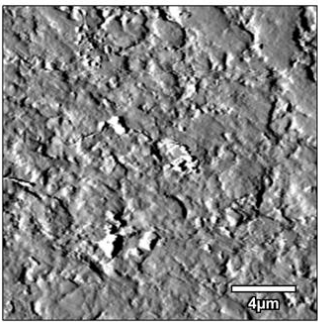
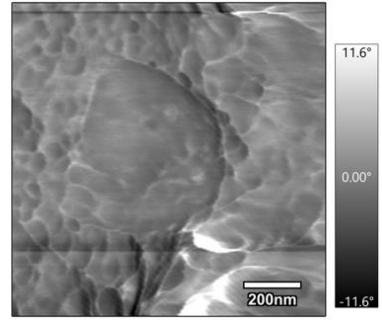
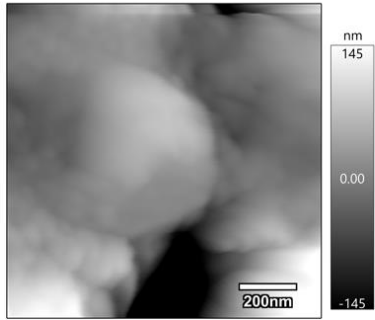
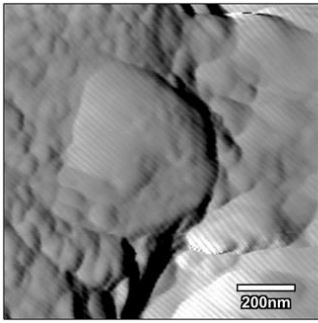
ULTT



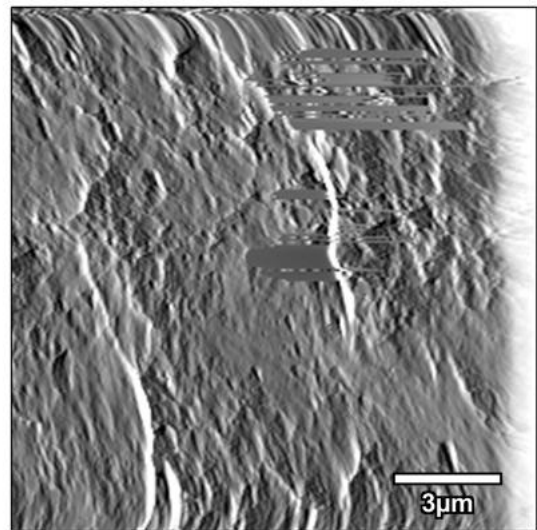
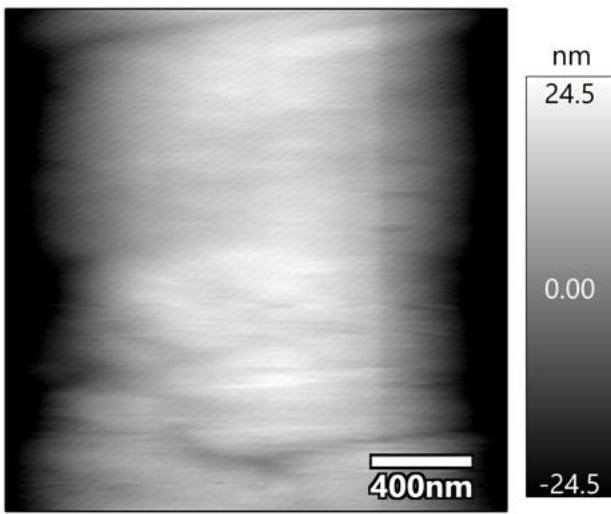
OBSV4_1 - MFP-3D Origin



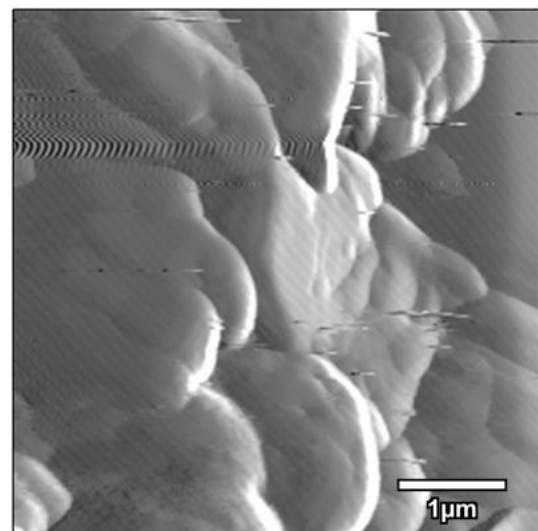
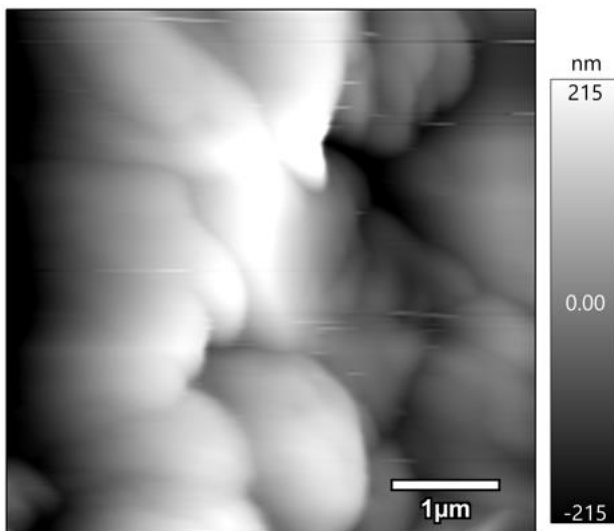
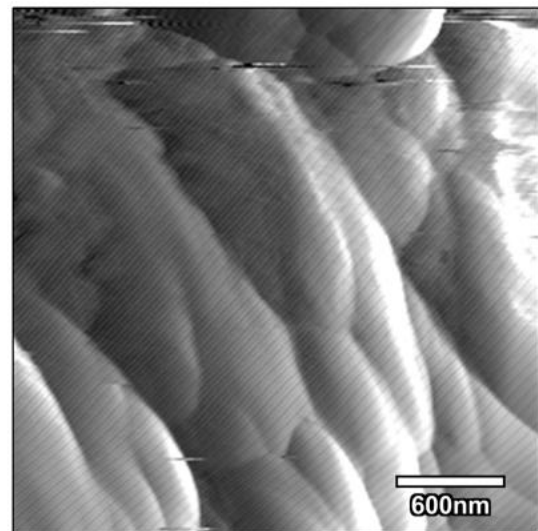
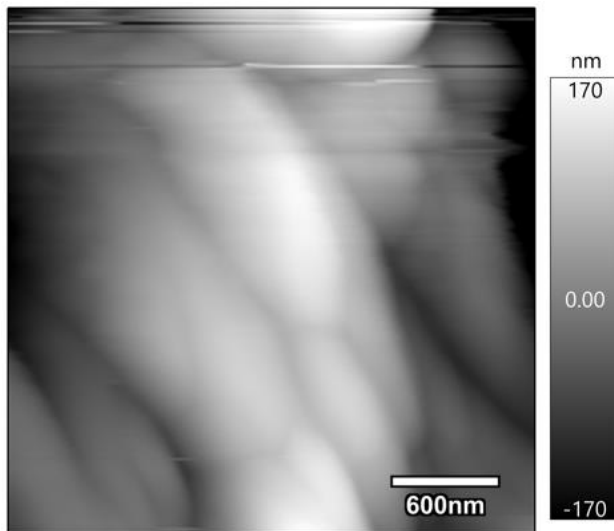
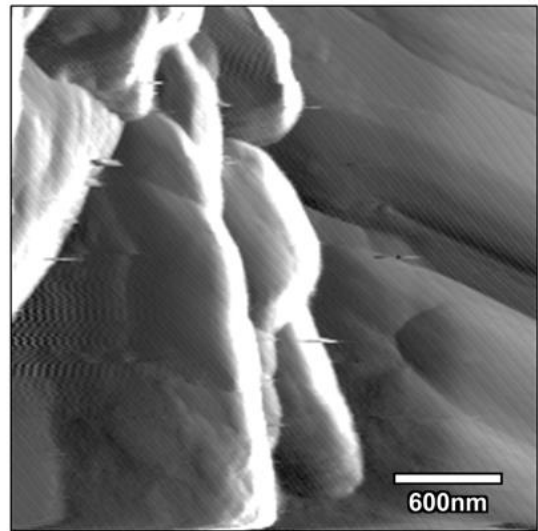
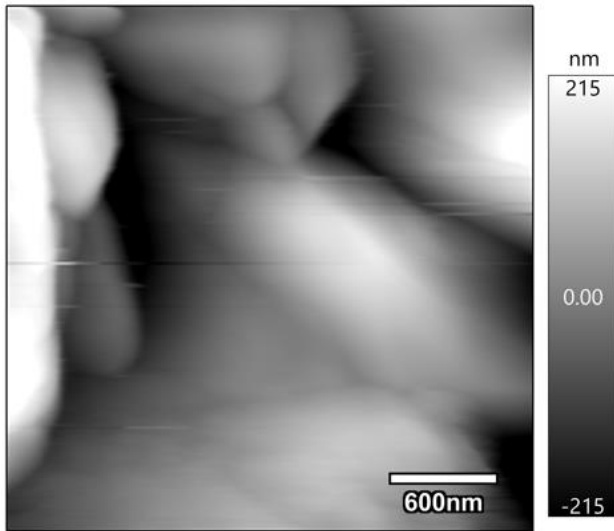
OBSV12_6 - MFP-3D Origin



OBSV12 - MFP-3D Origin

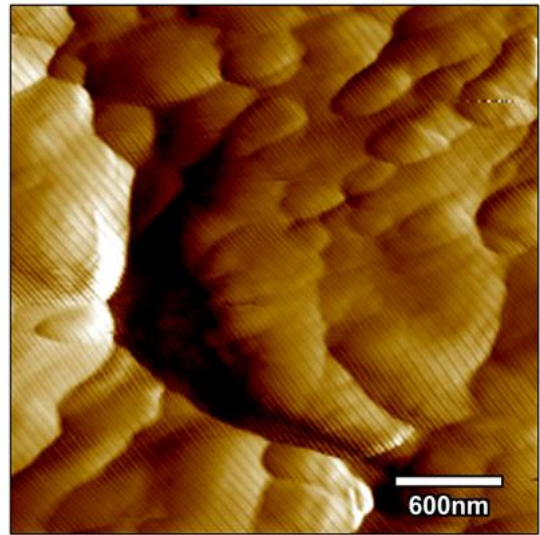
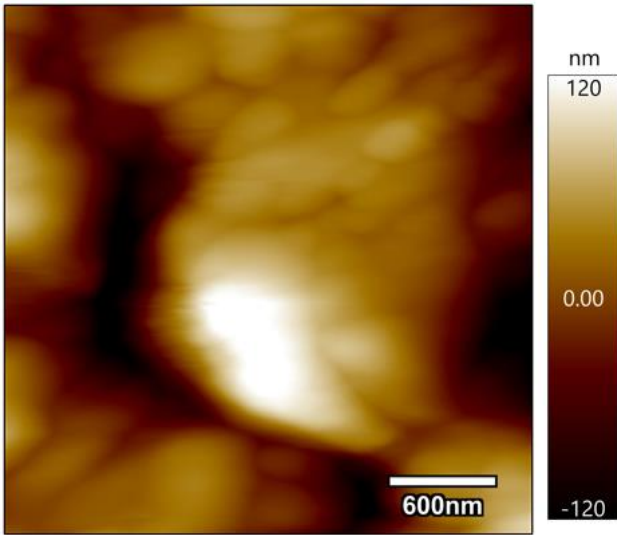
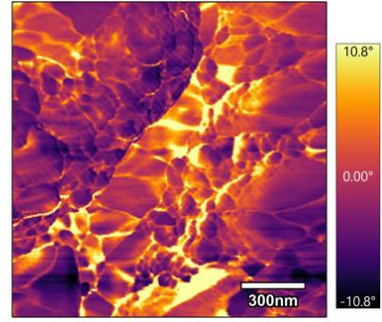
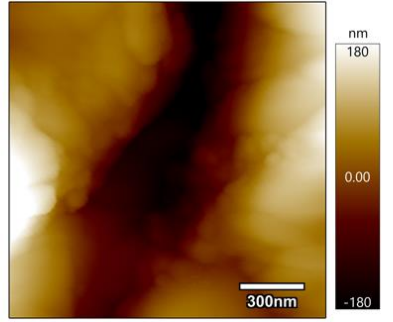
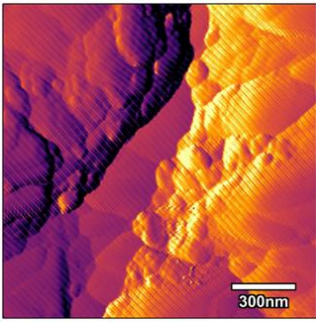


OBSV18 - MFP-3D Origin

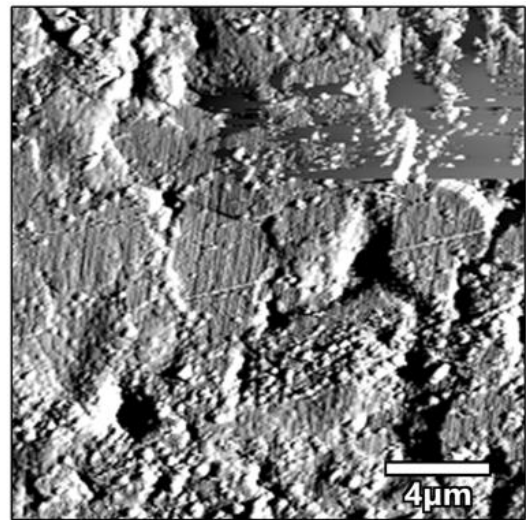
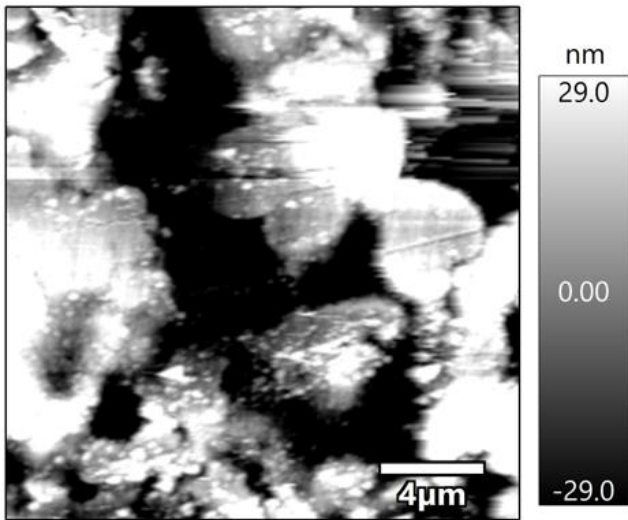


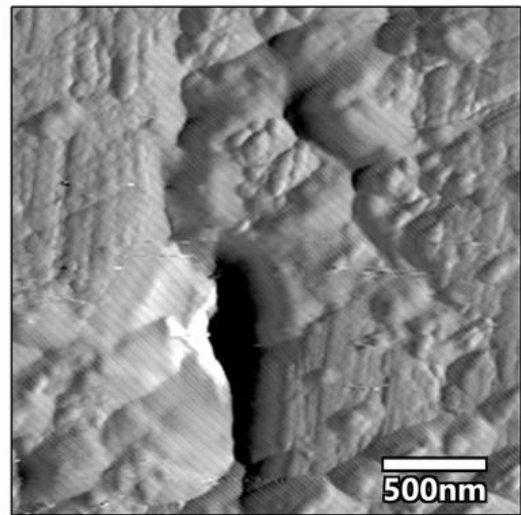
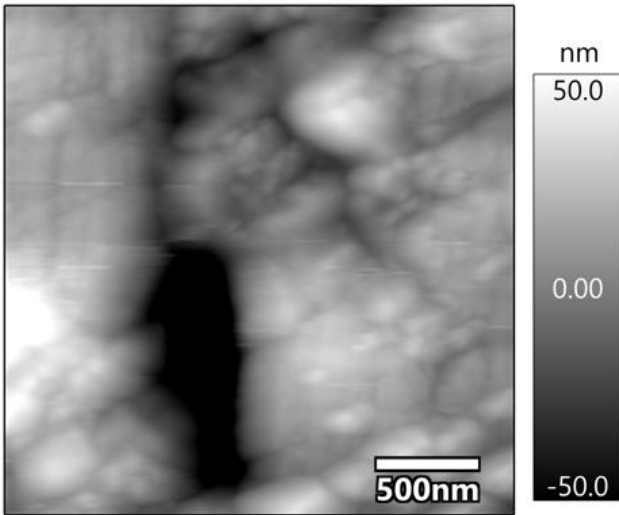
Chalk SK - MFP-3D Origin

Unpolished

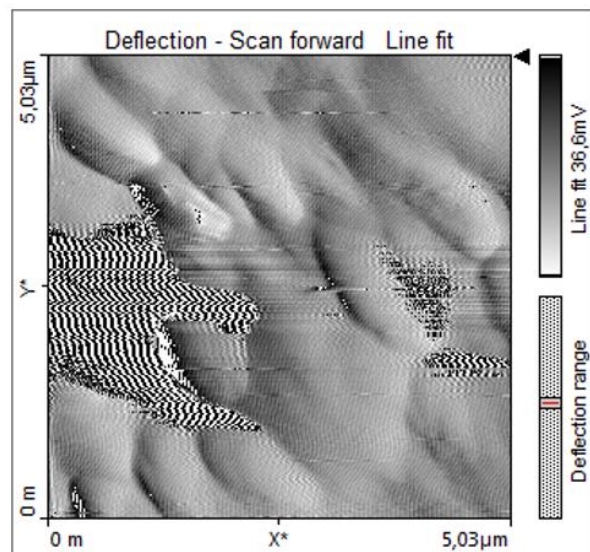
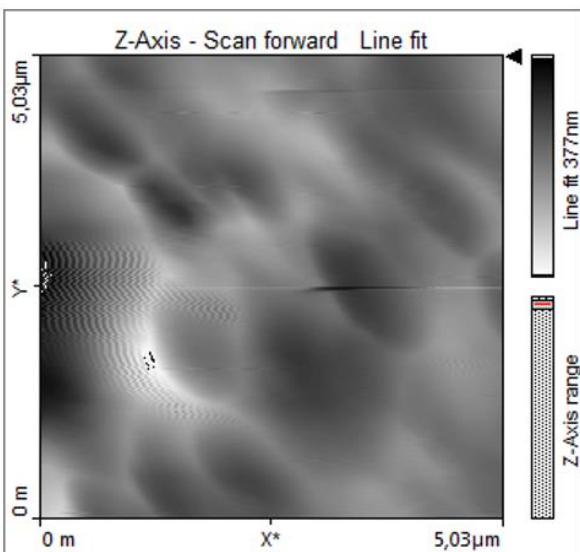
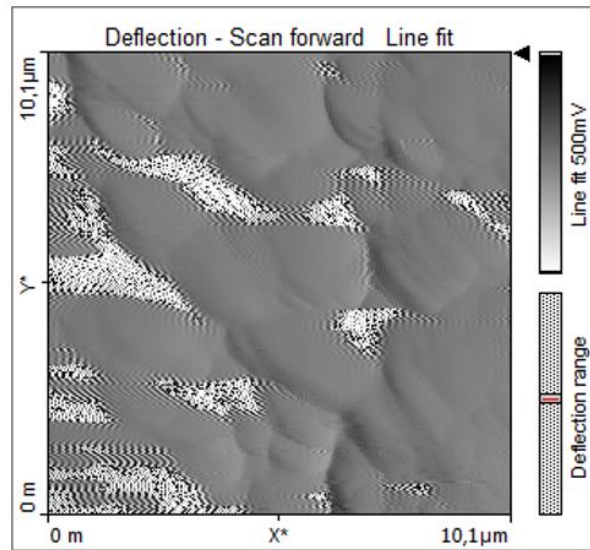
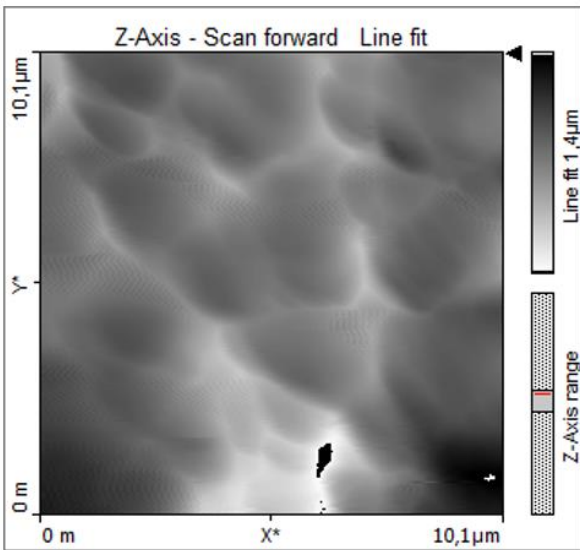


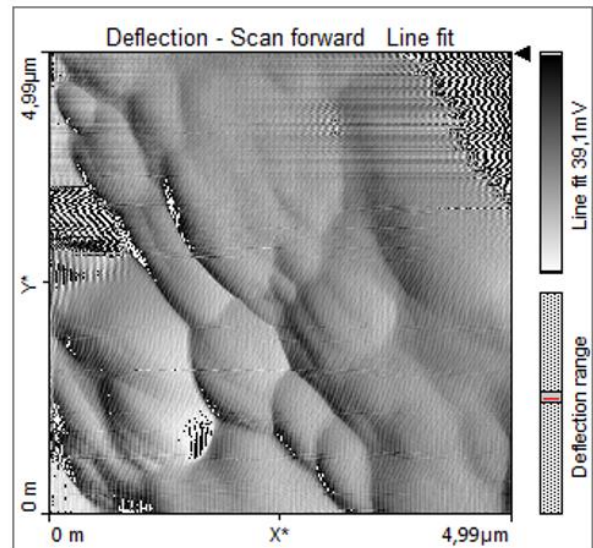
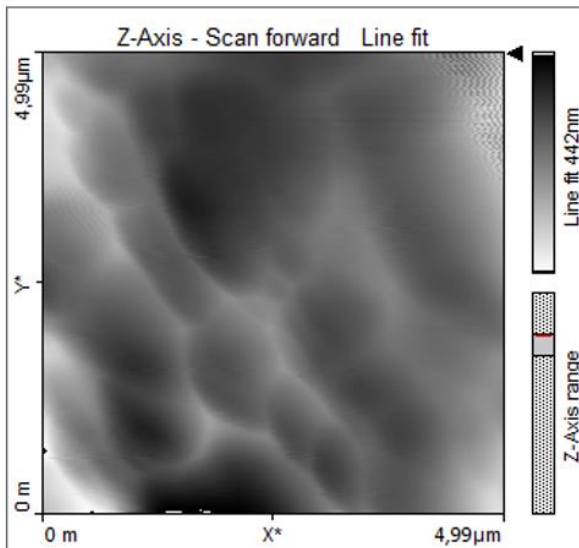
Polished



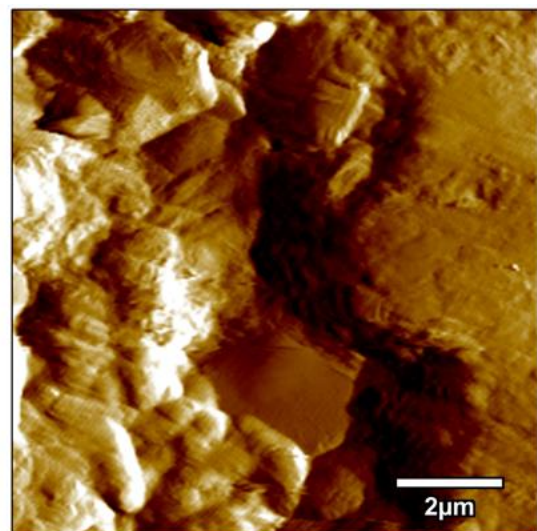
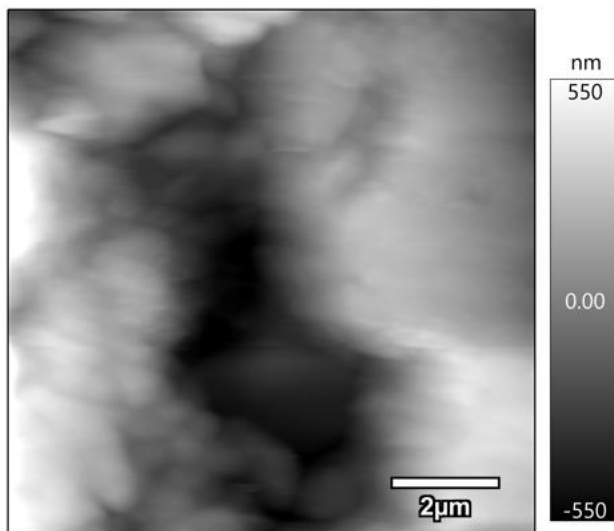


Unflooded Liège





Kaolinite - MFP-3D Origin

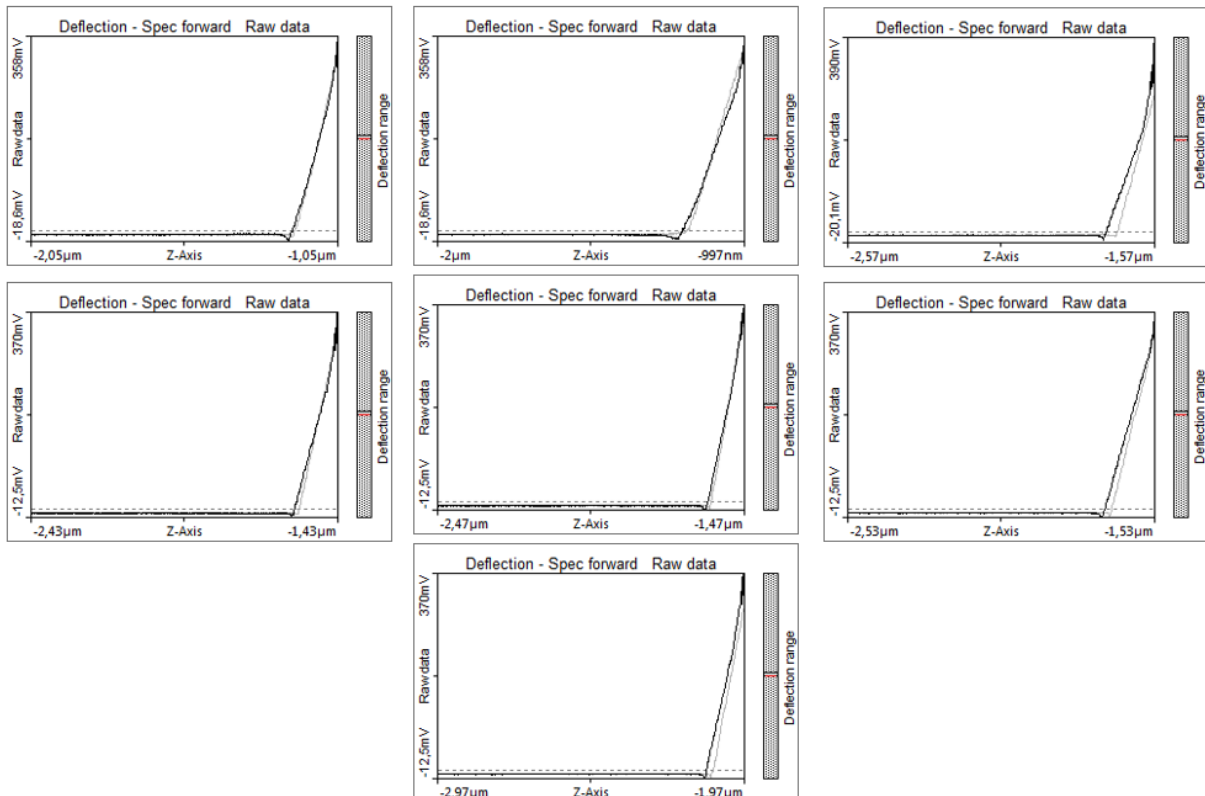
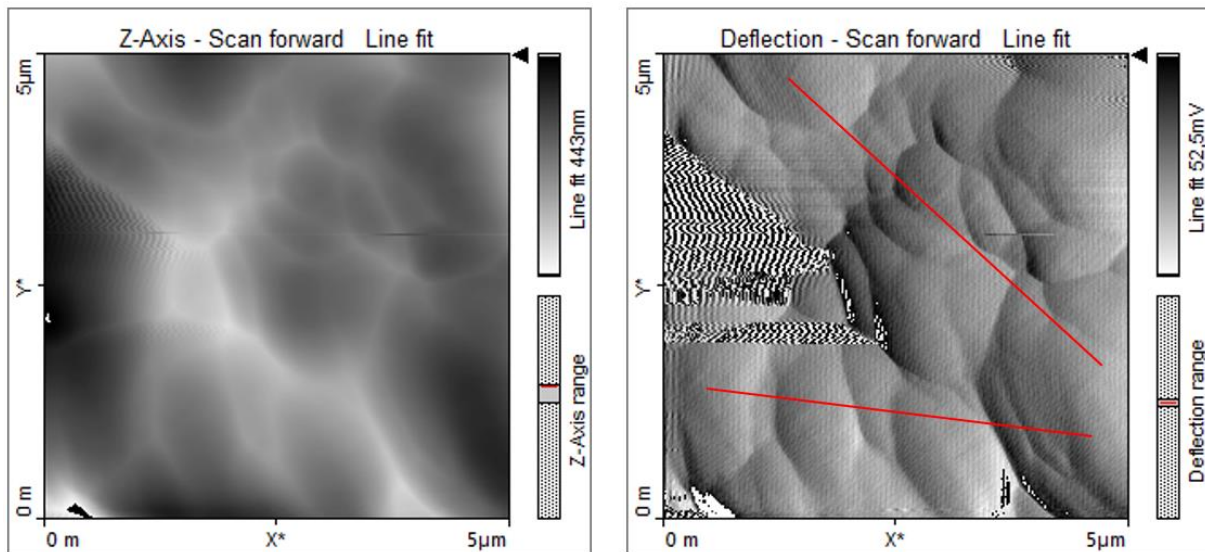


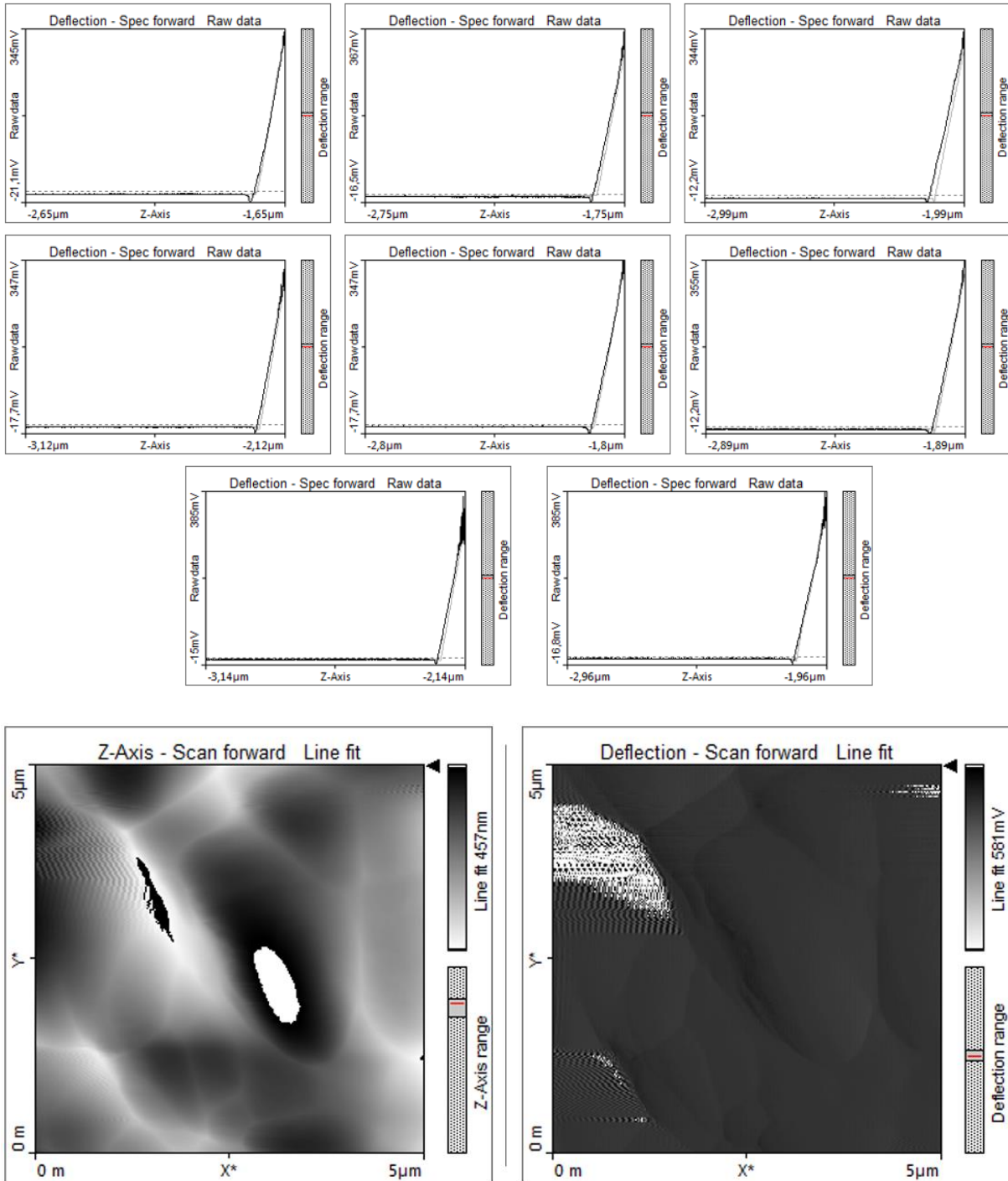
Appendix 2 Force spectroscopy

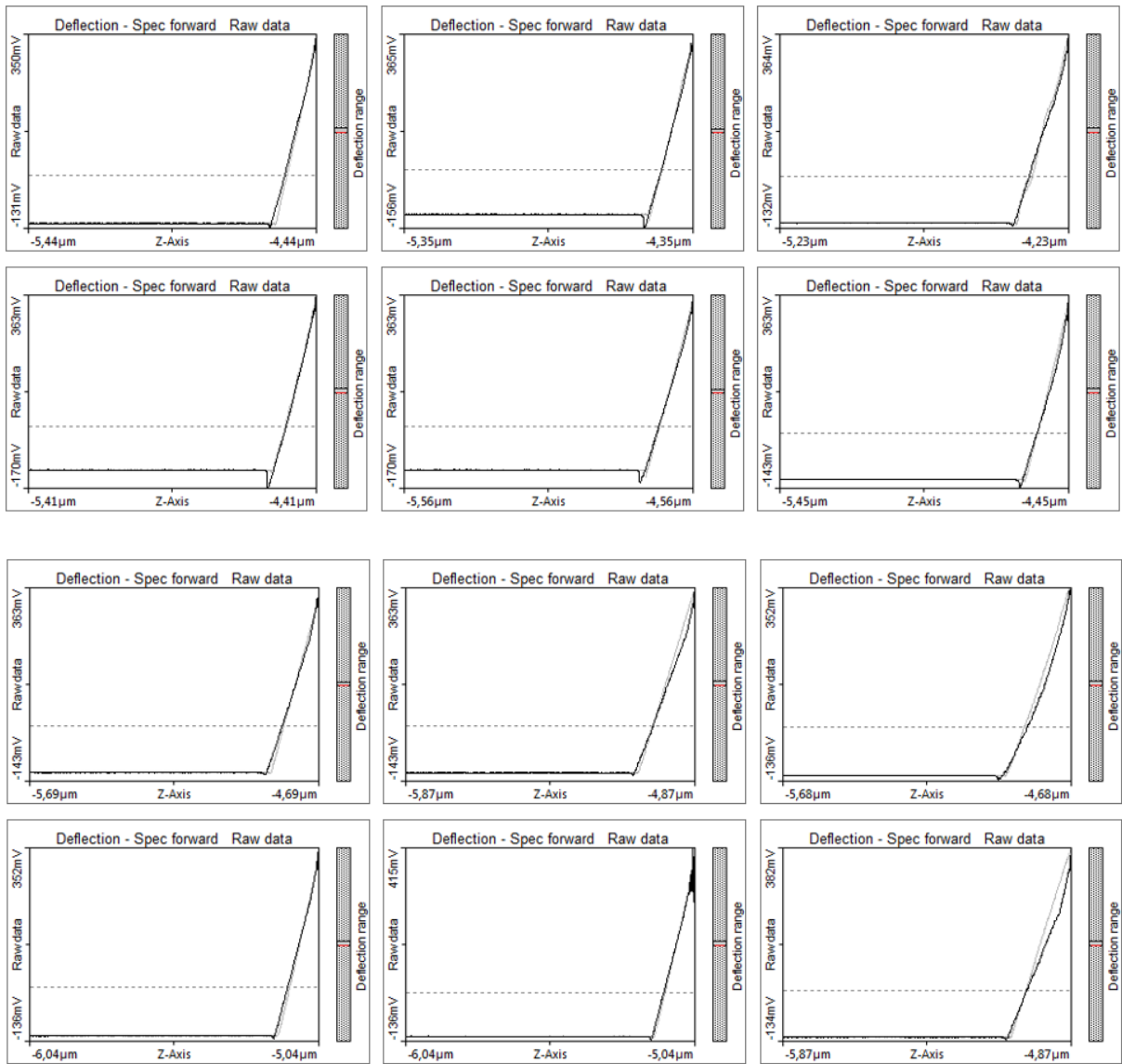
Some areas have 64 curves taken over the whole area, and some selected have been displayed here. Other areas have 8 force curves taken along a line, displayed in the deflection image to the right. The force curves from Grenoble (MFP-3D Origin) are 100 curves measured and some selected to display here.

Standards

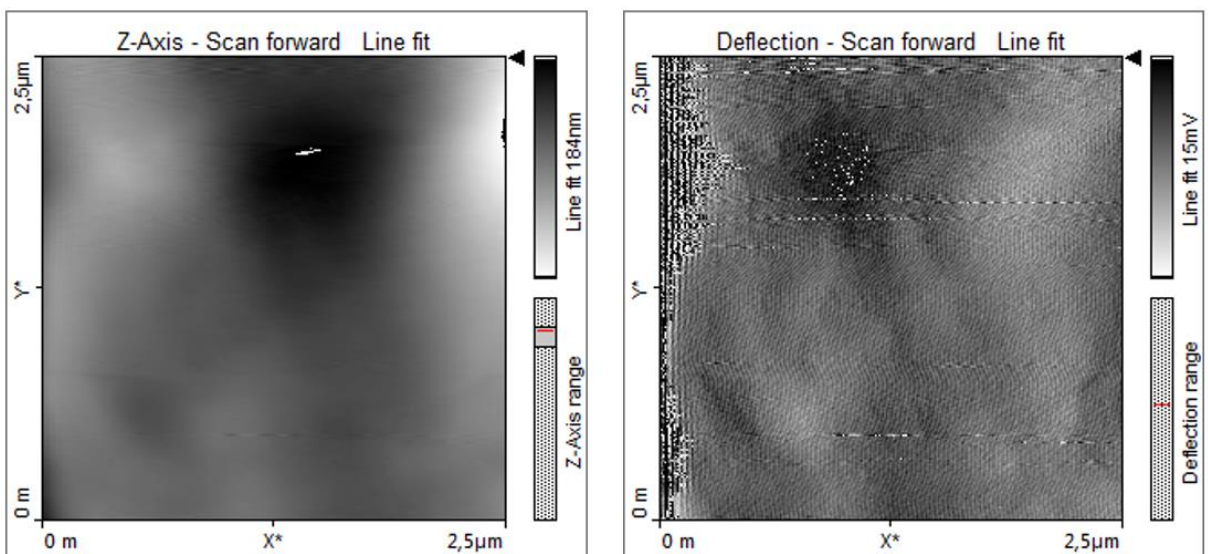
Anorthite

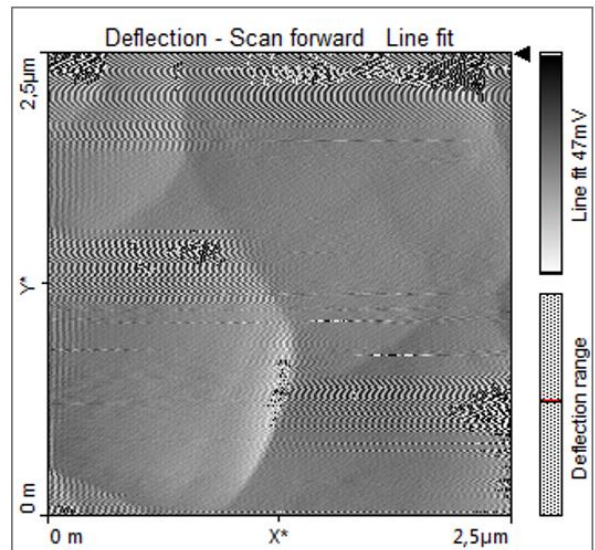
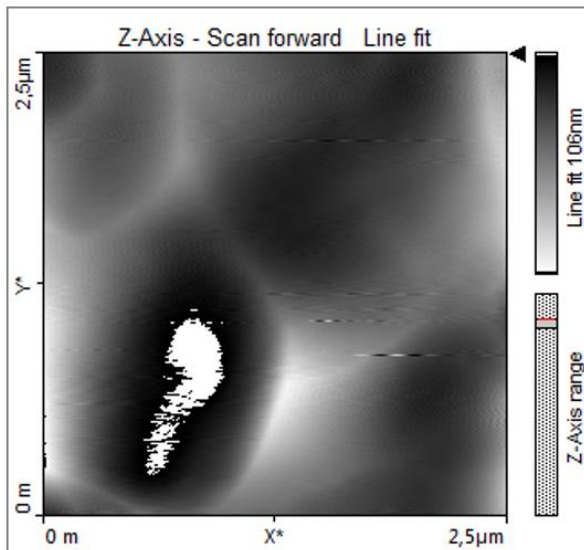
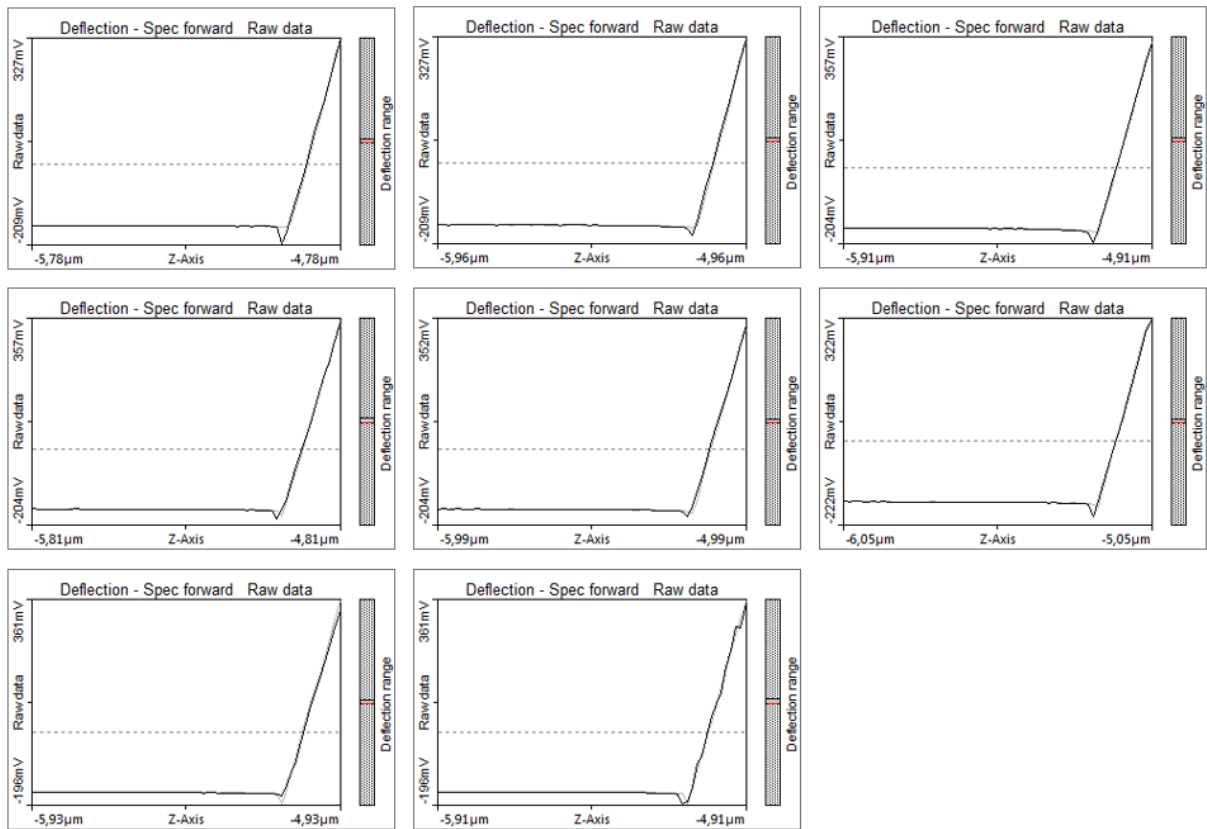


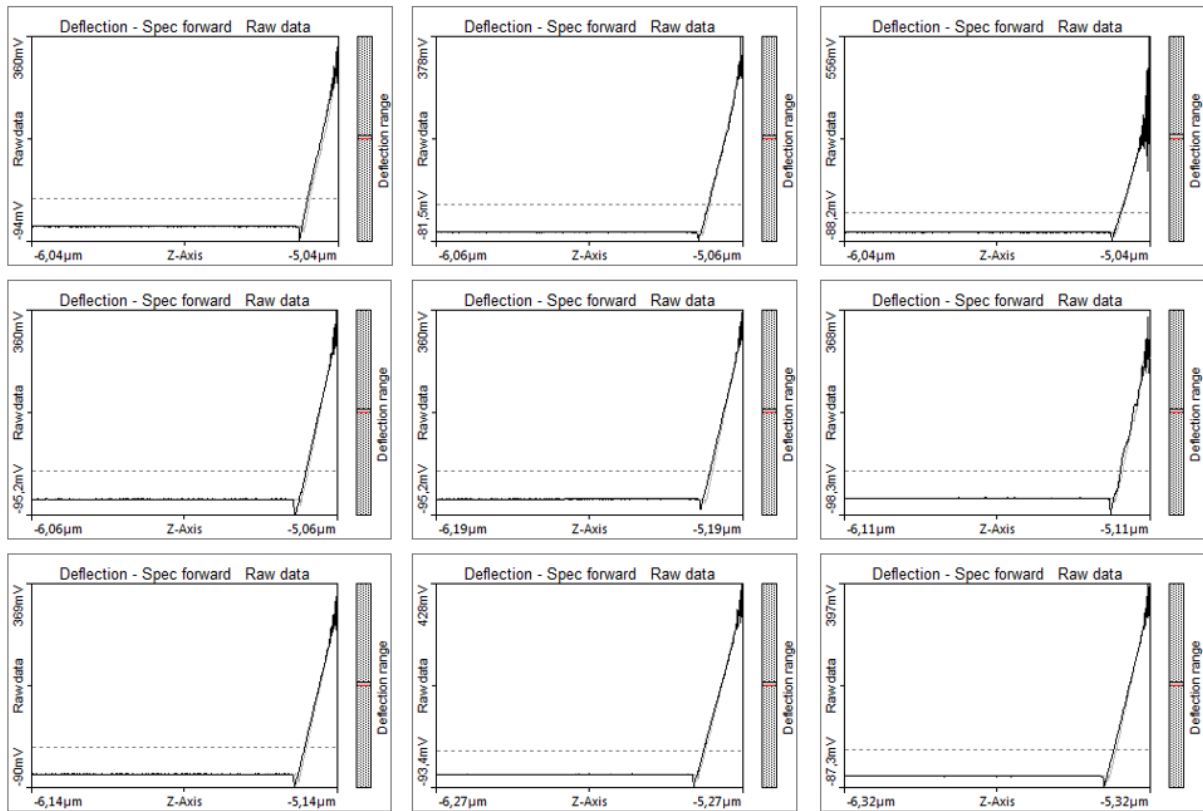




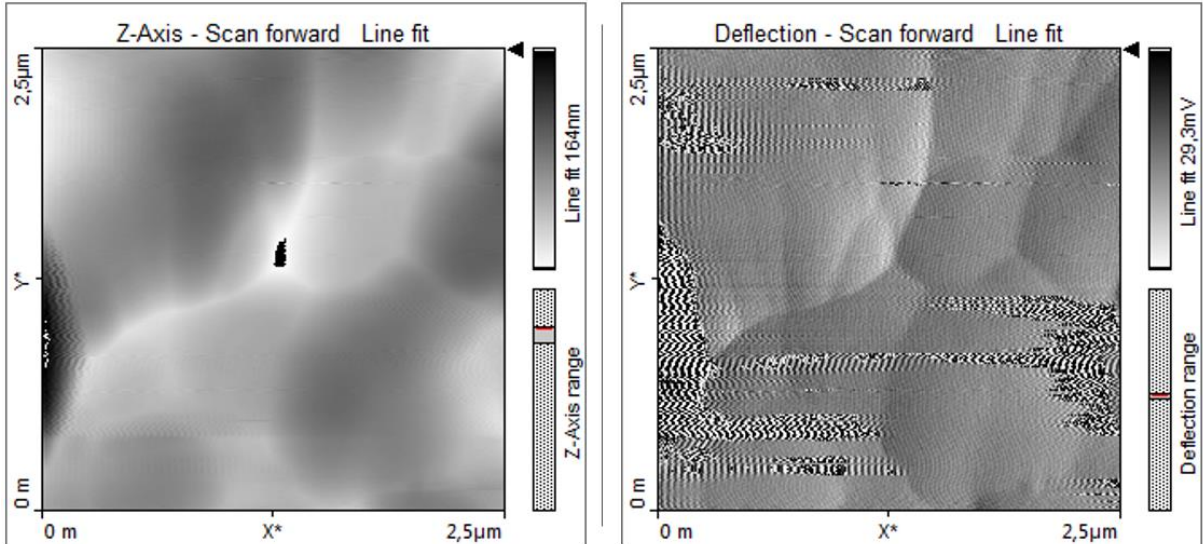
Calcite

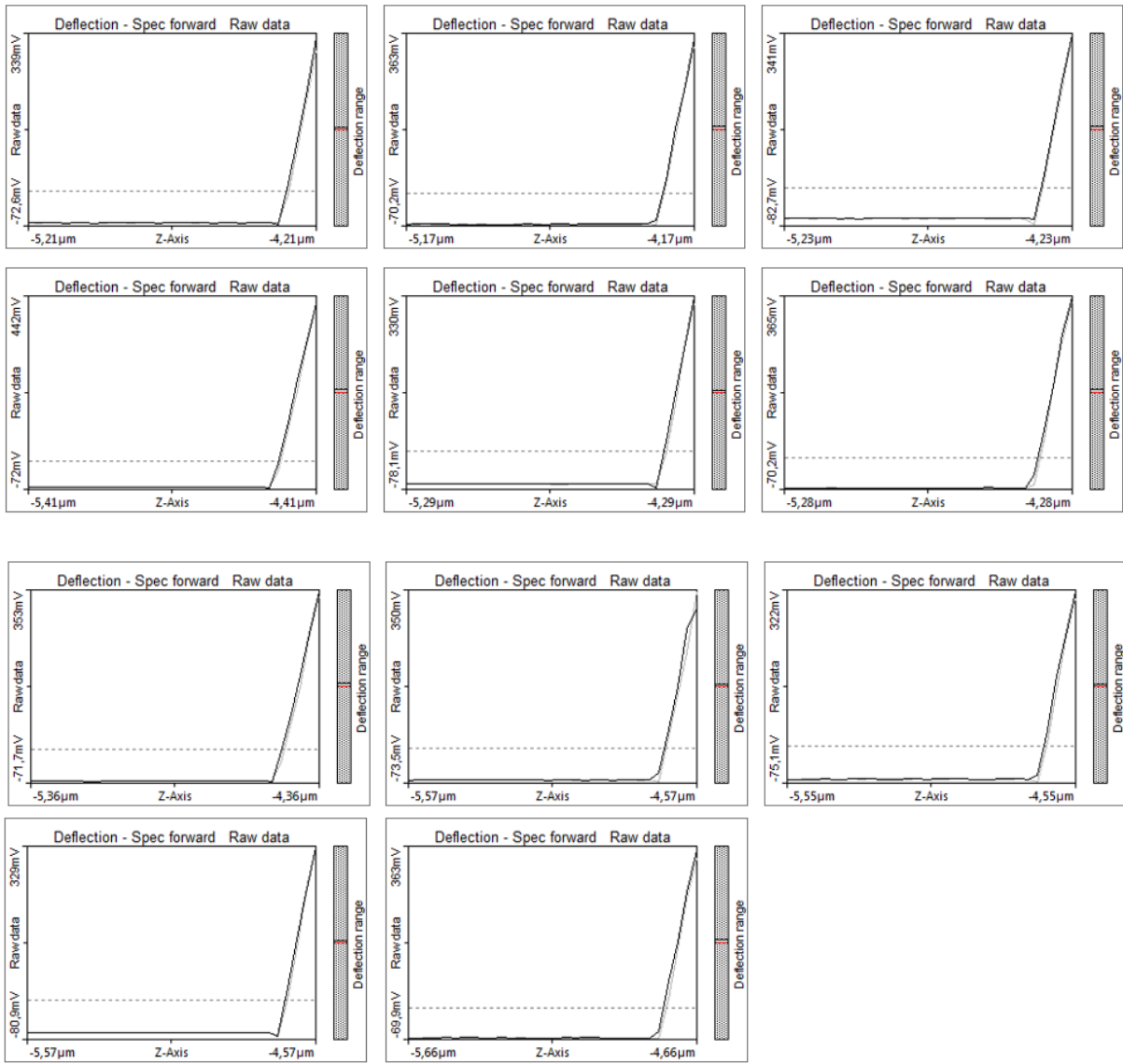




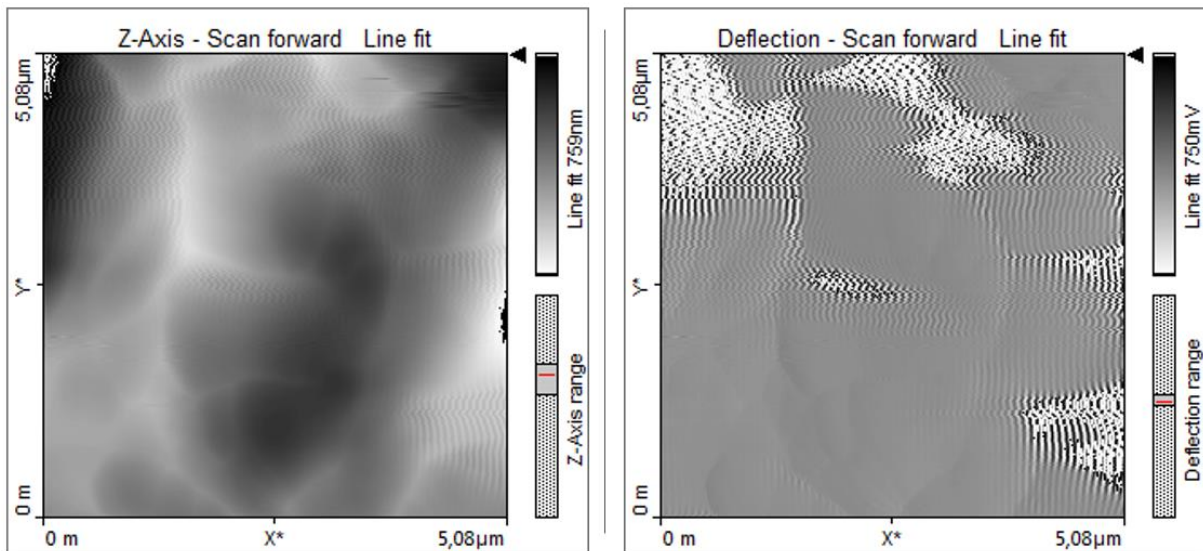


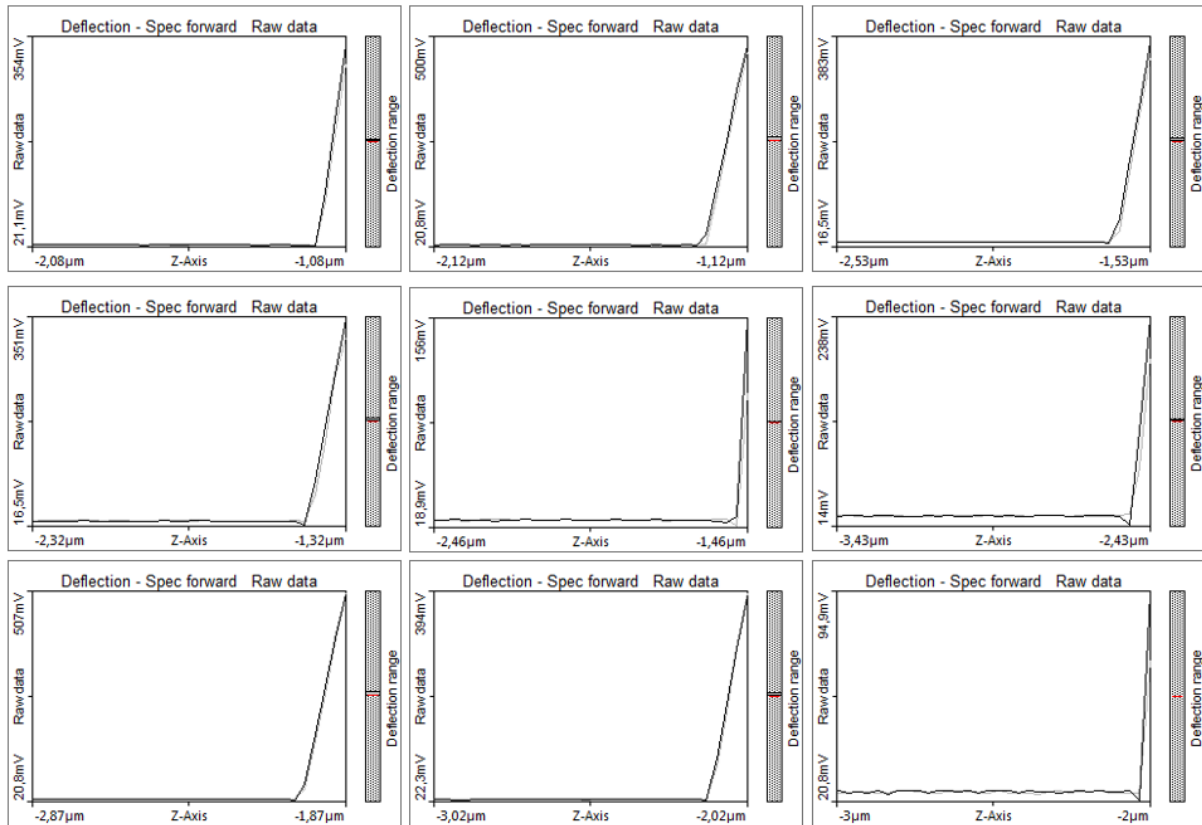
Dolomite



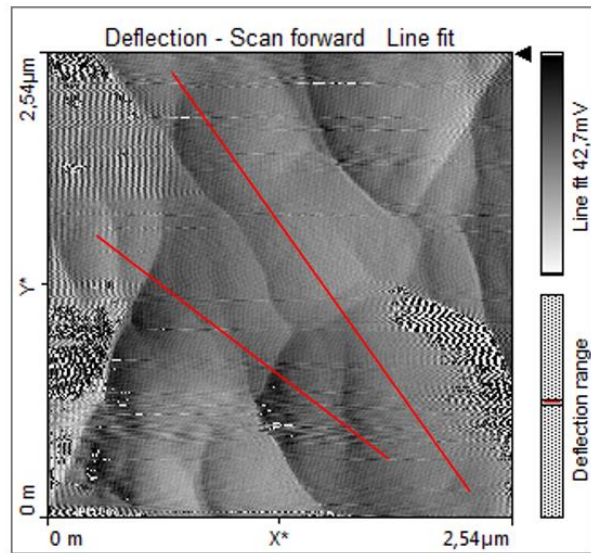
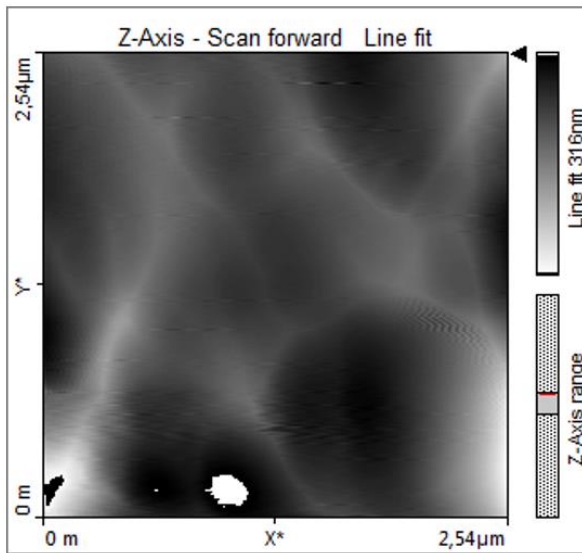


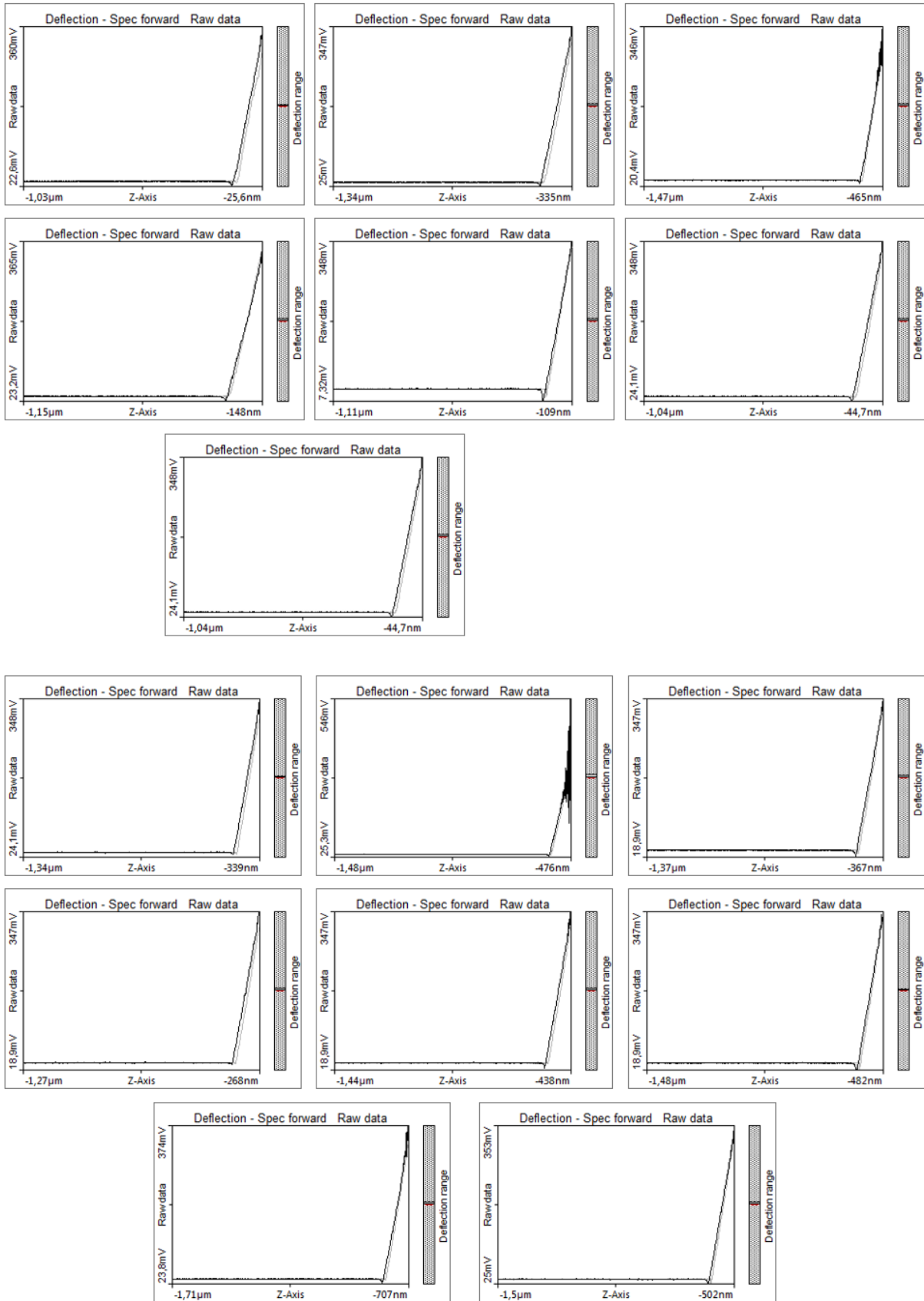
Fluorapatite

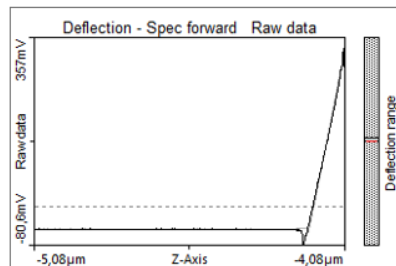
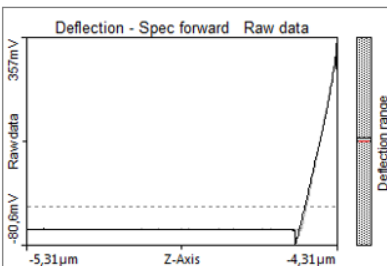
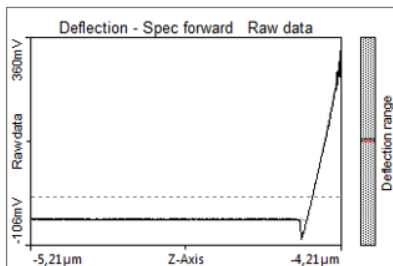
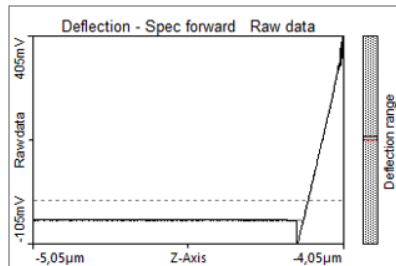
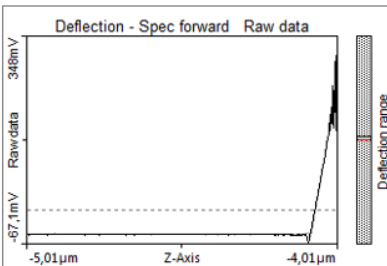
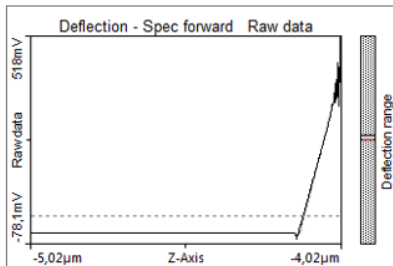
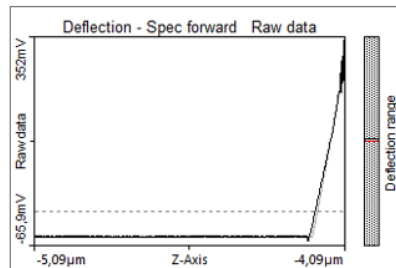
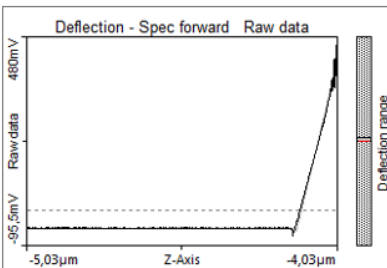
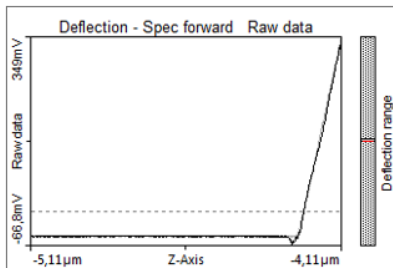
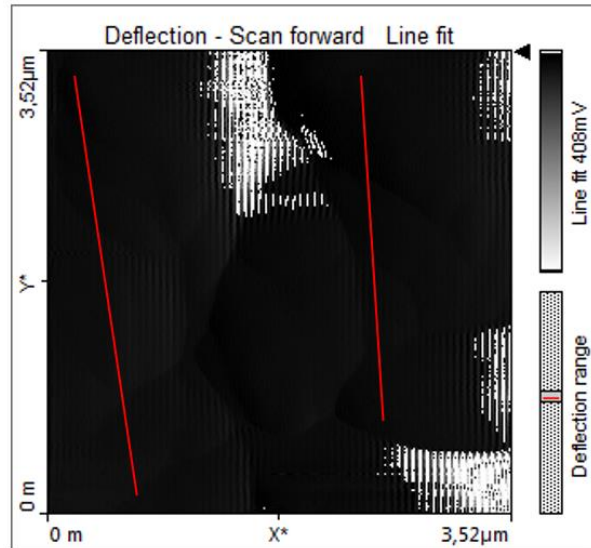
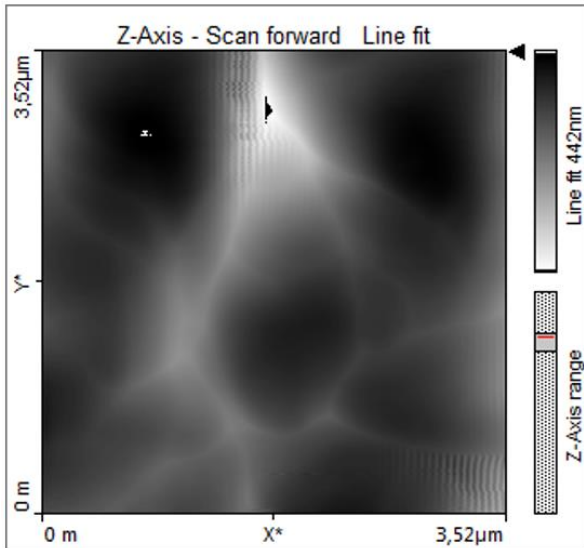


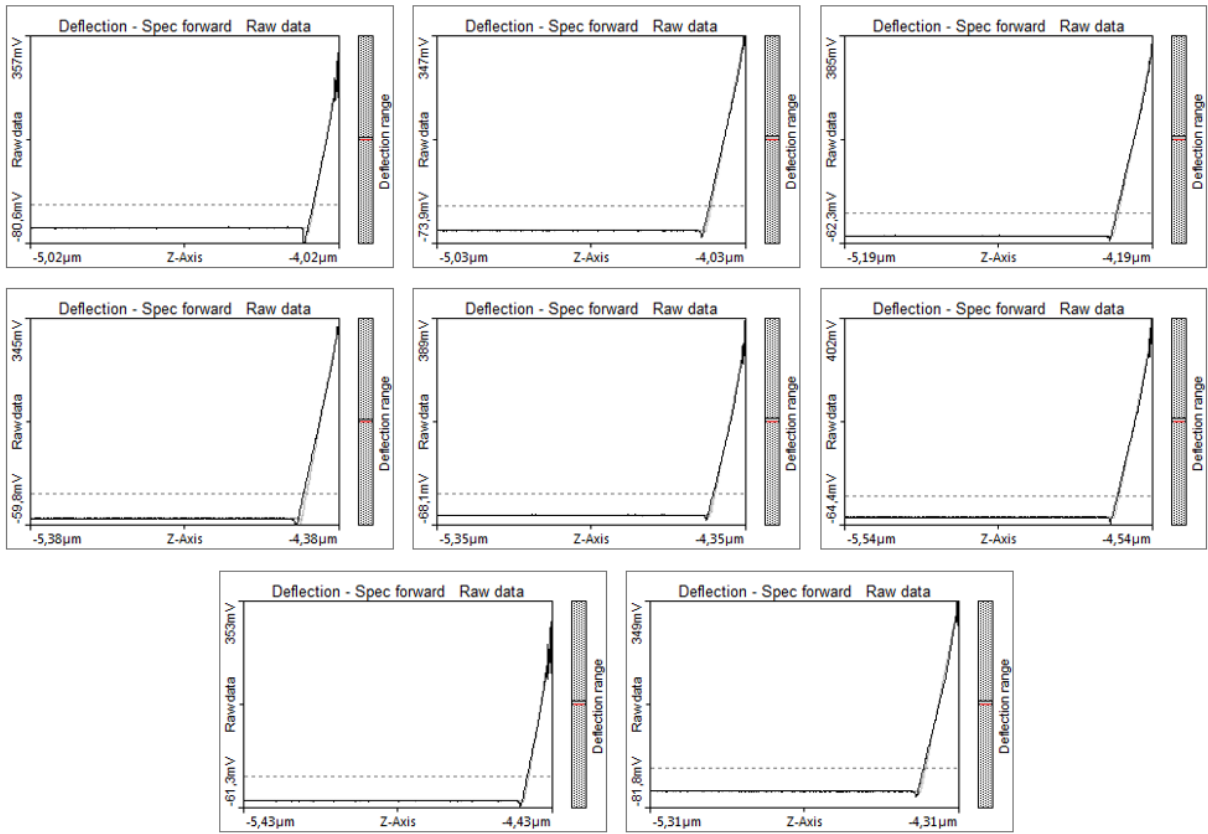


Ilmenite

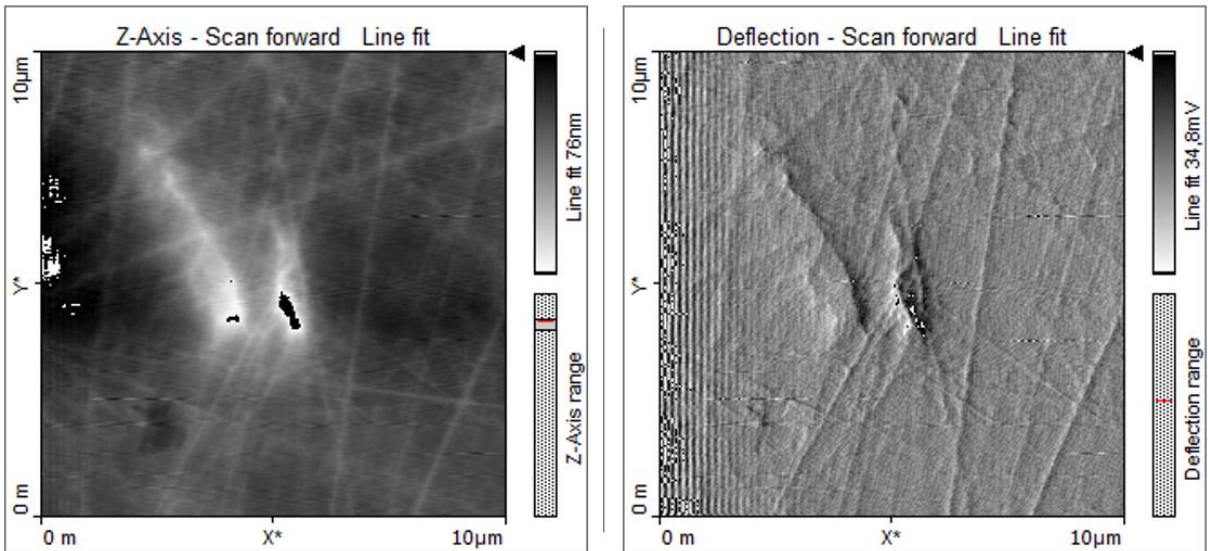


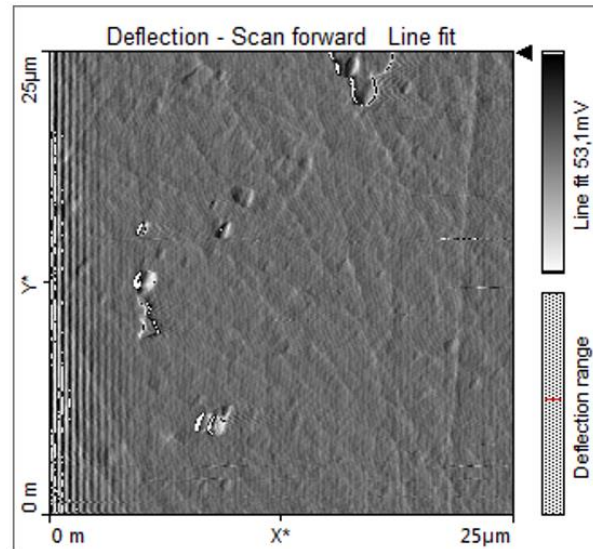
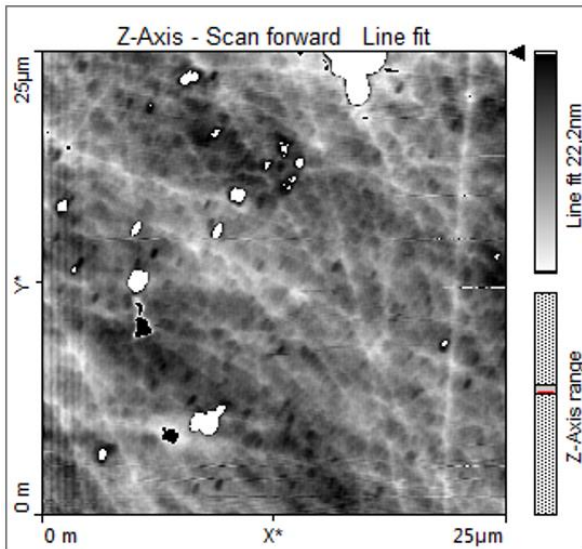
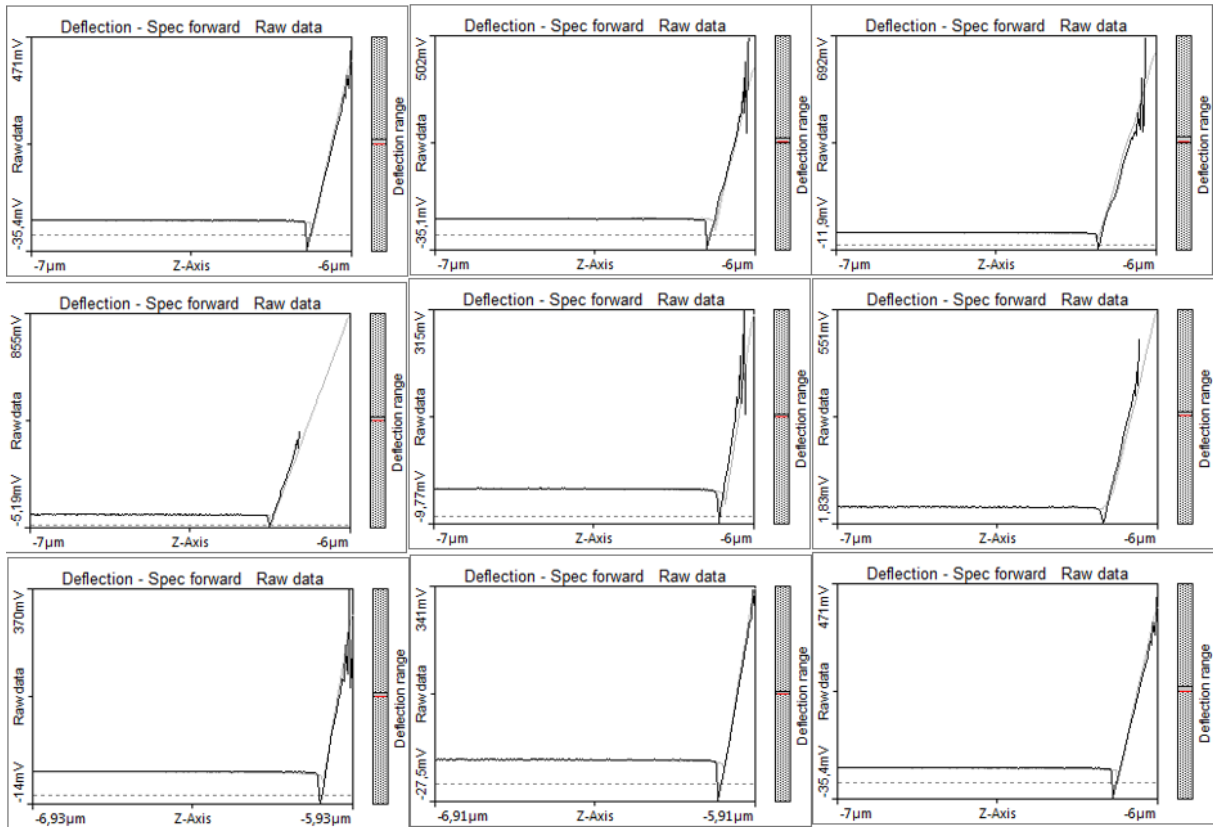


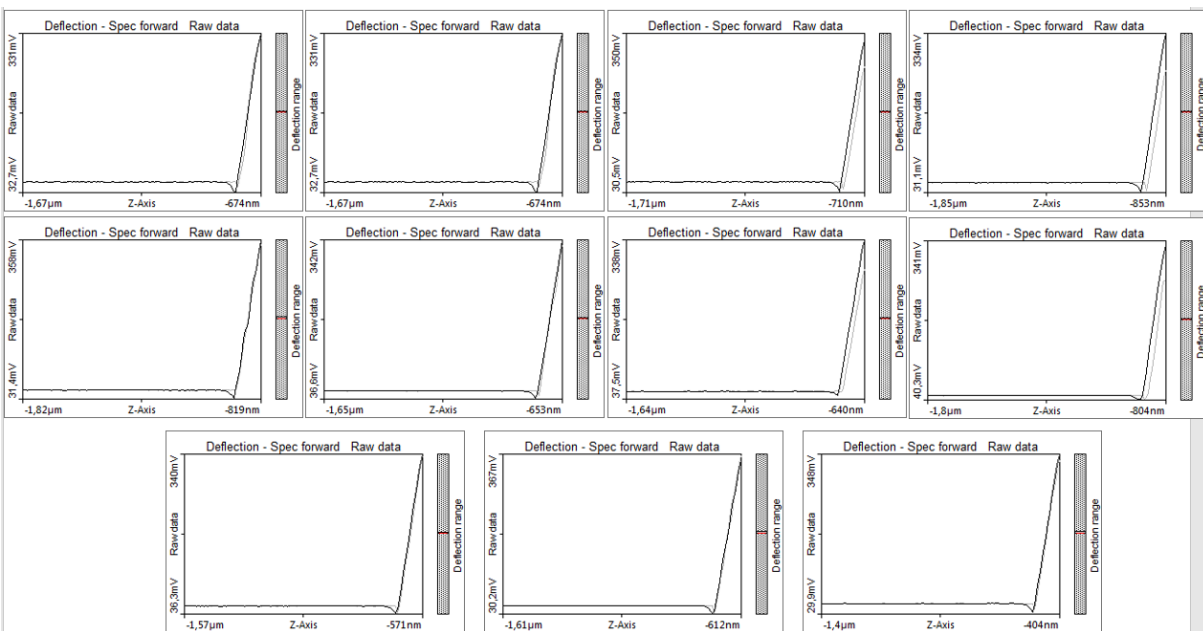
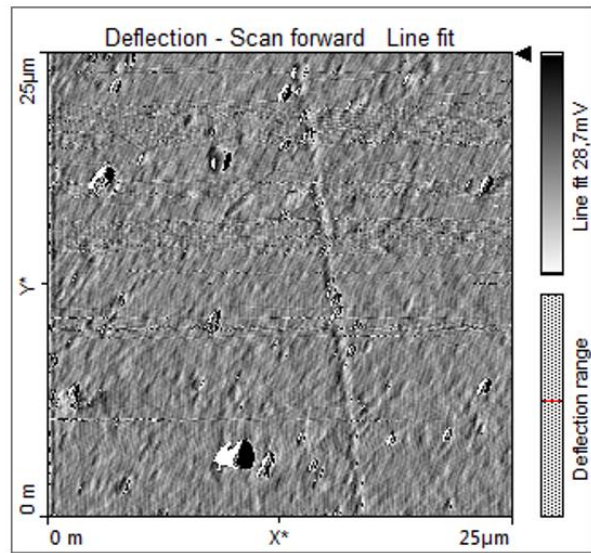
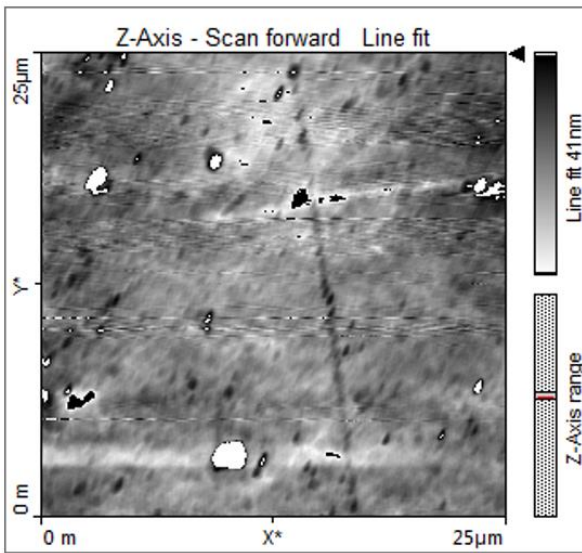
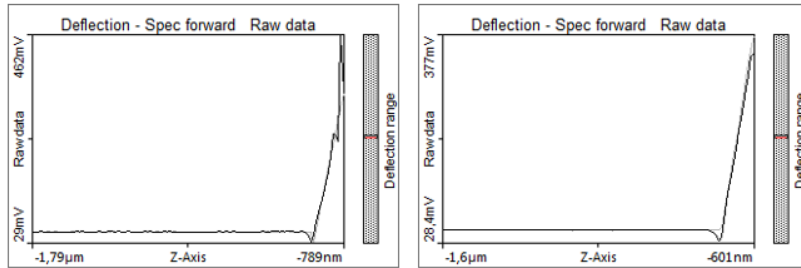
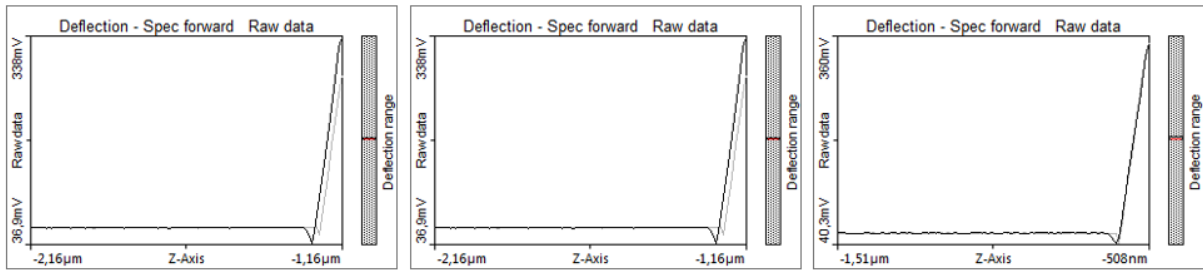


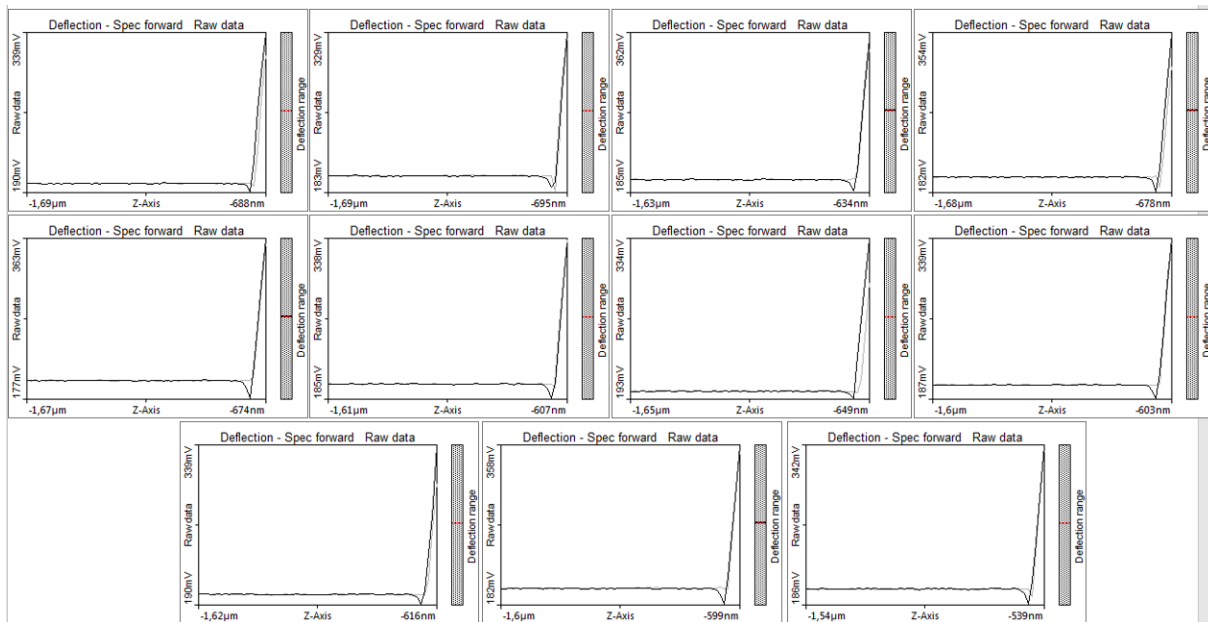
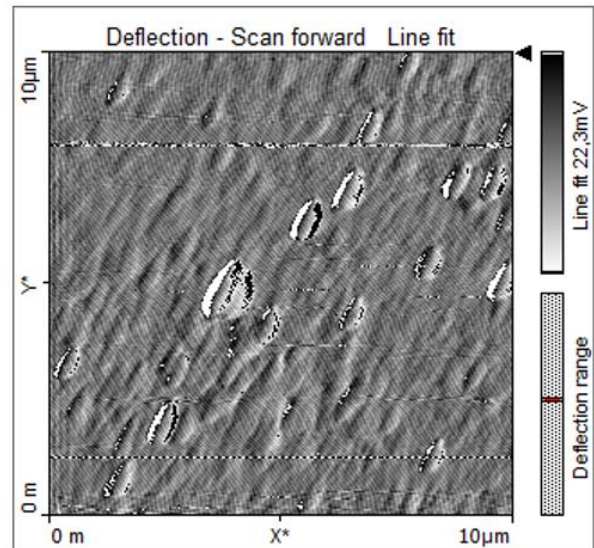
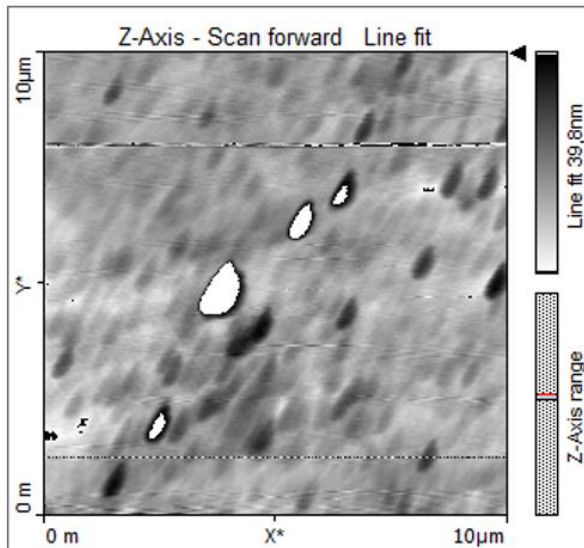


Magnesite

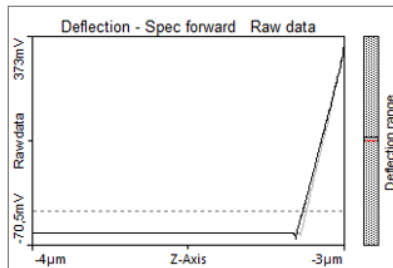
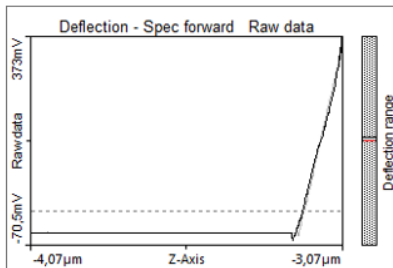
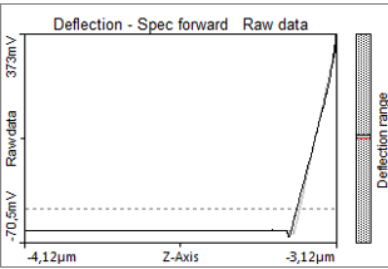
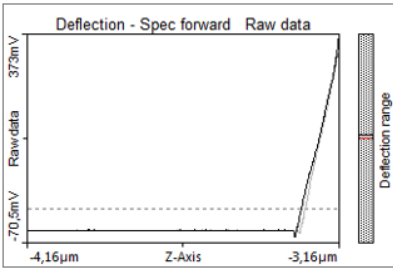
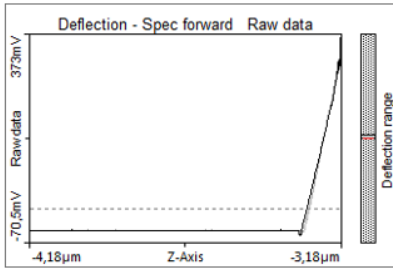
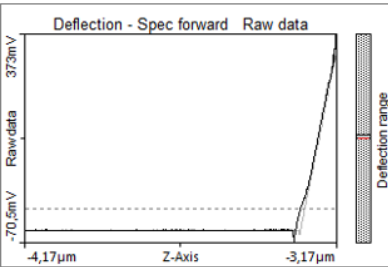
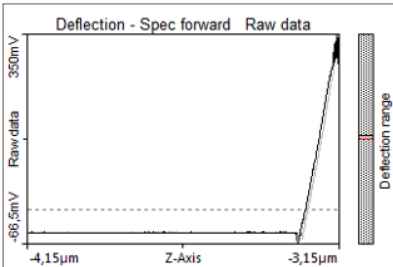
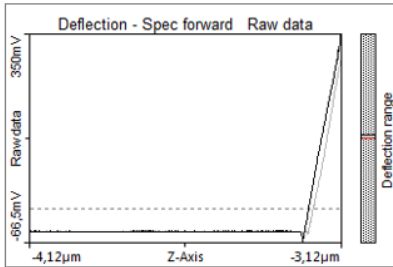
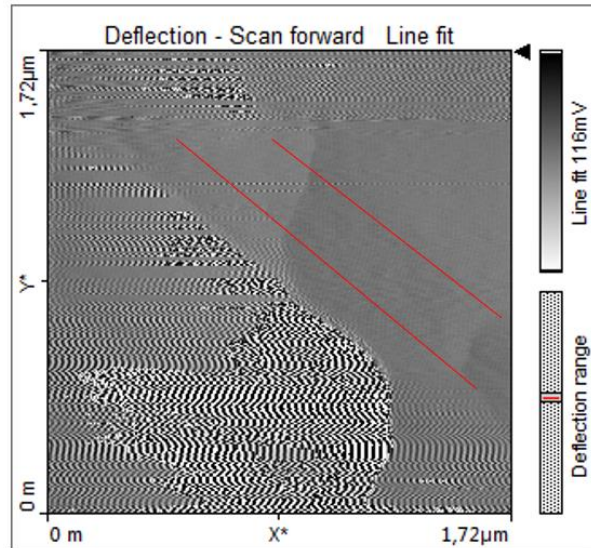
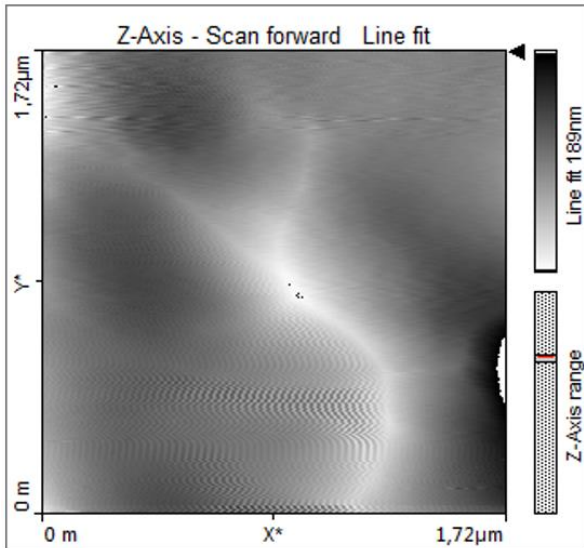


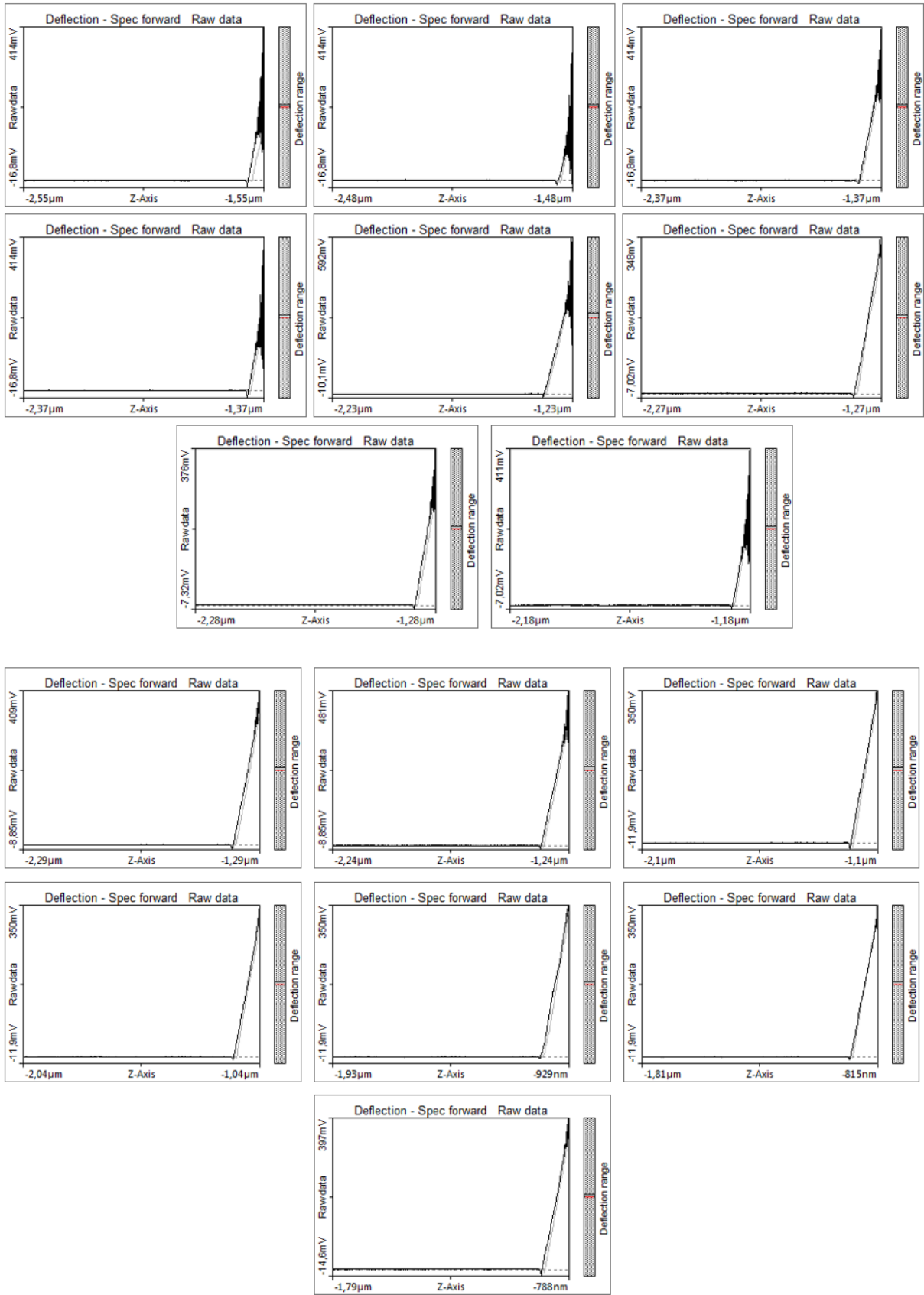


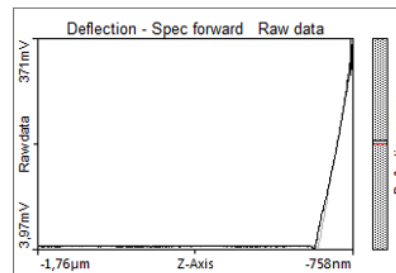
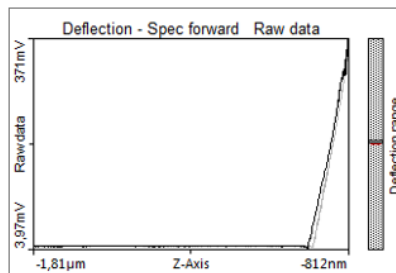
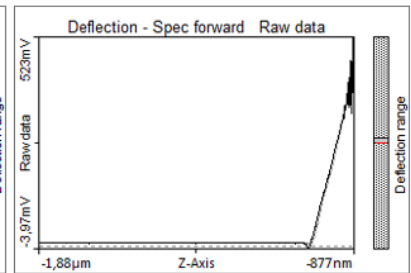
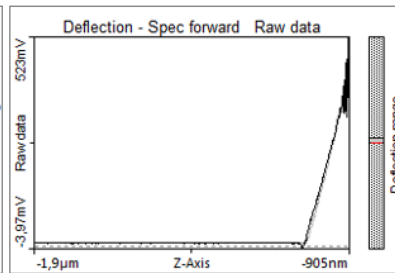
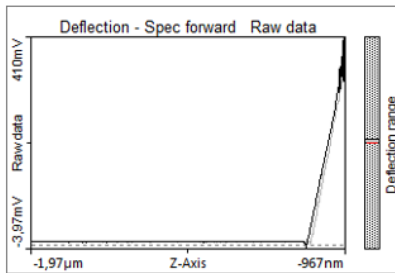
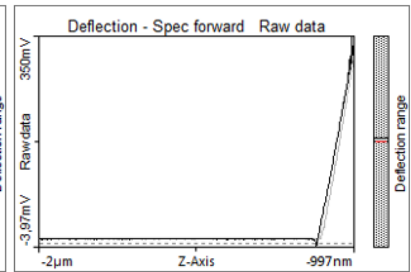
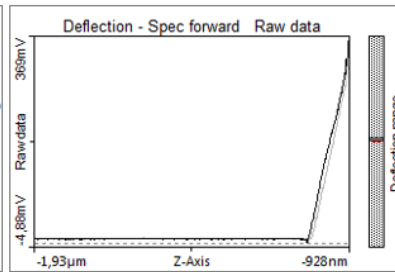
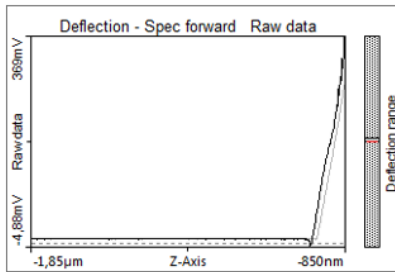
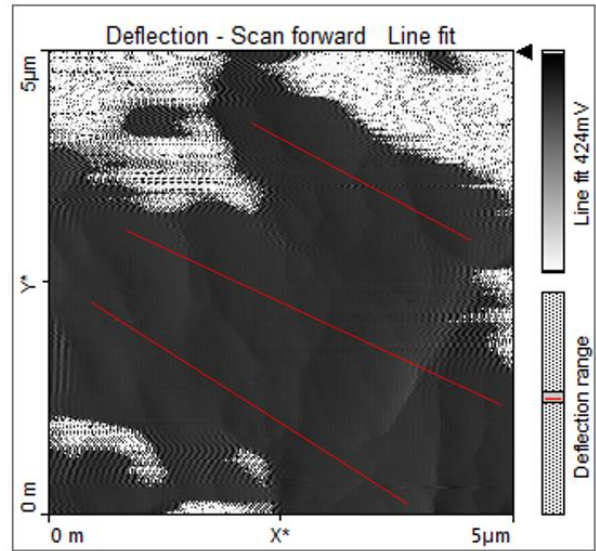
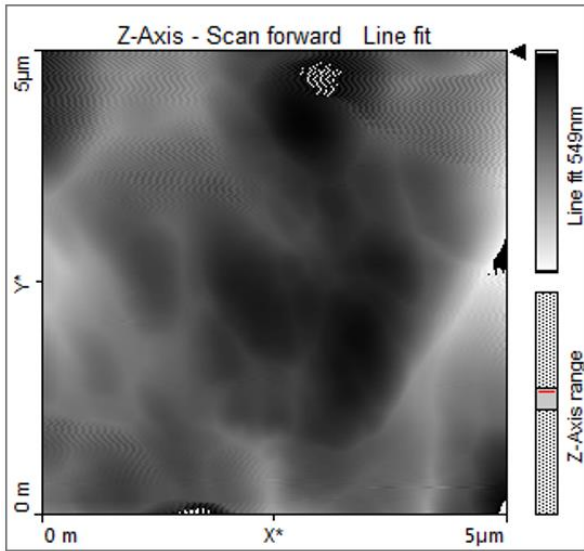


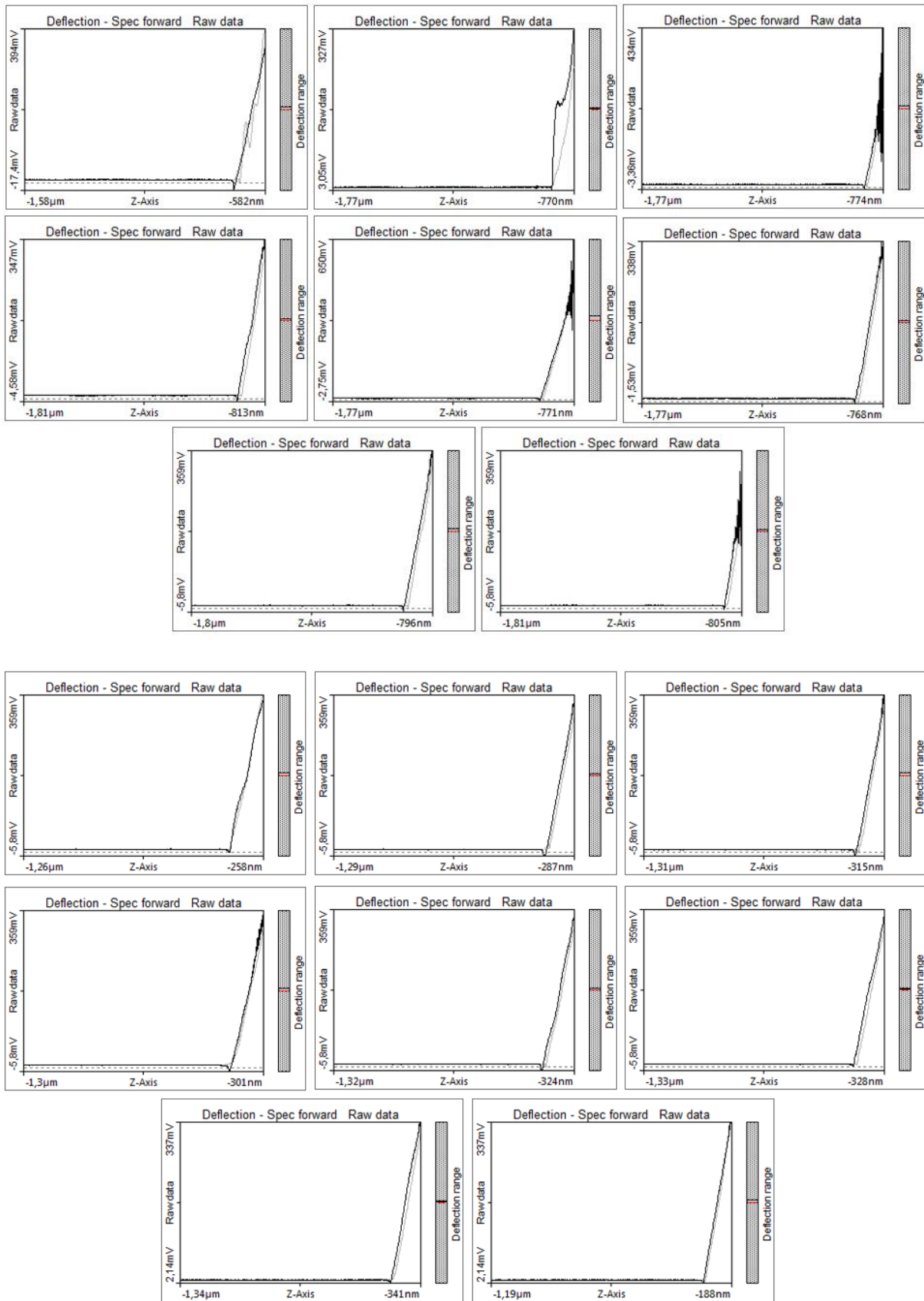


Magnetite

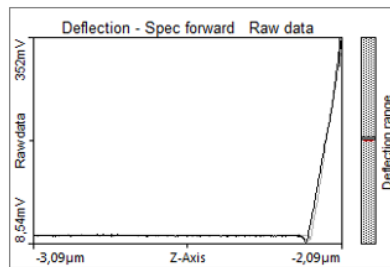
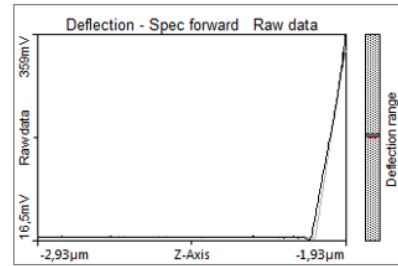
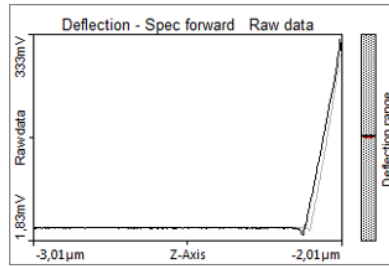
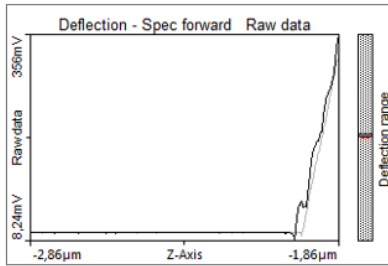
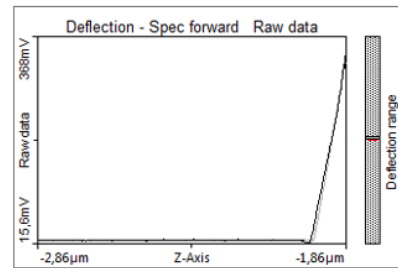
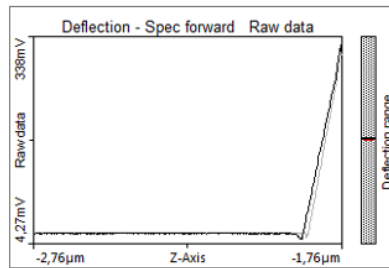
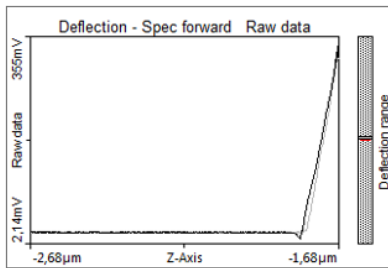
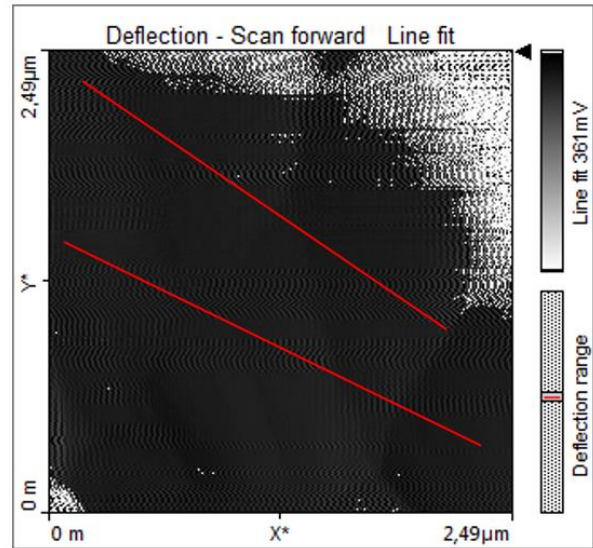
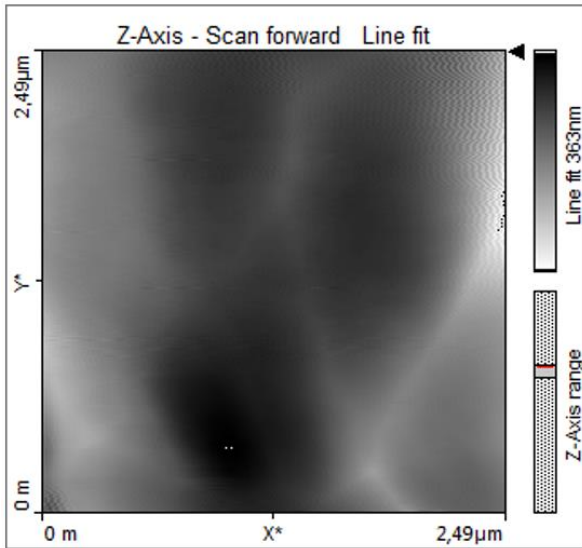


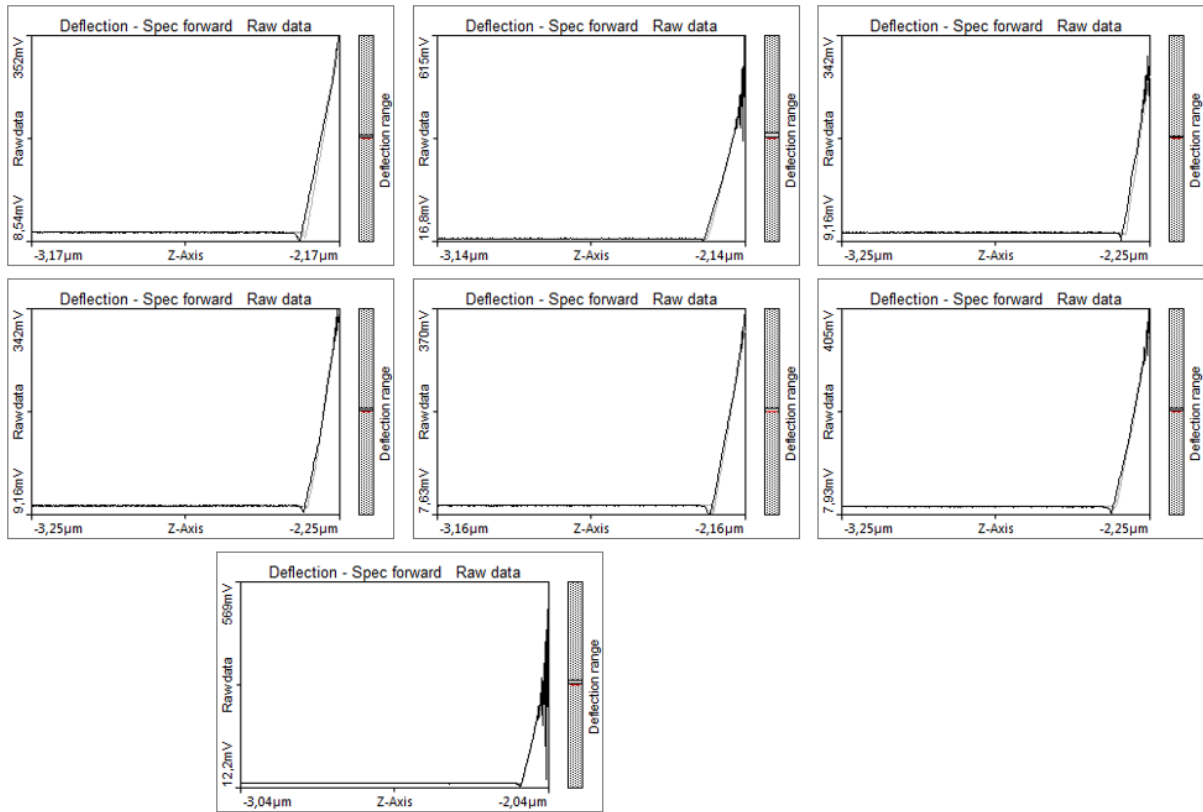




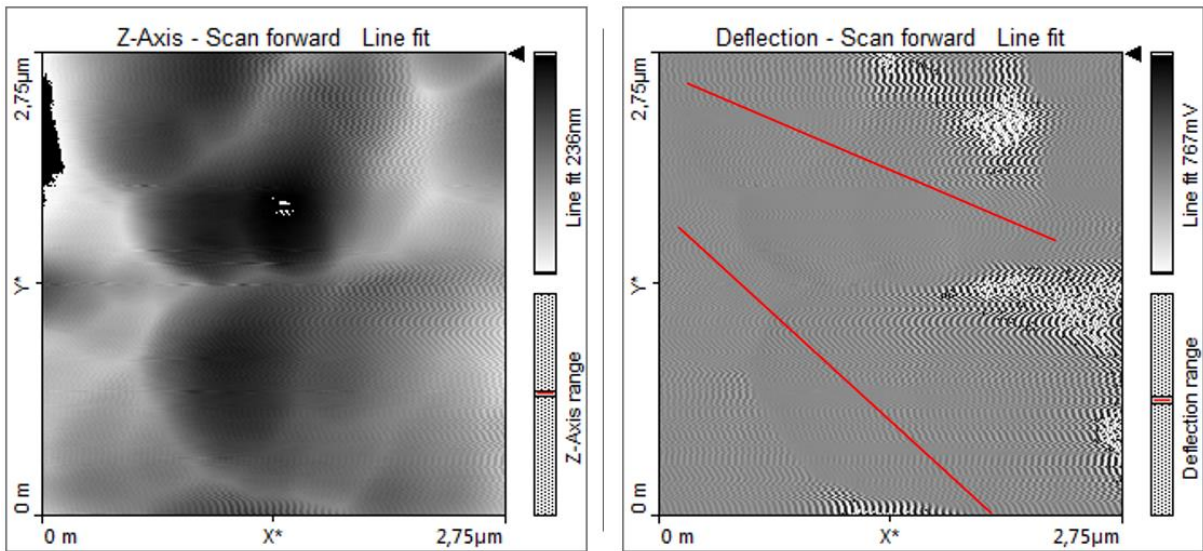


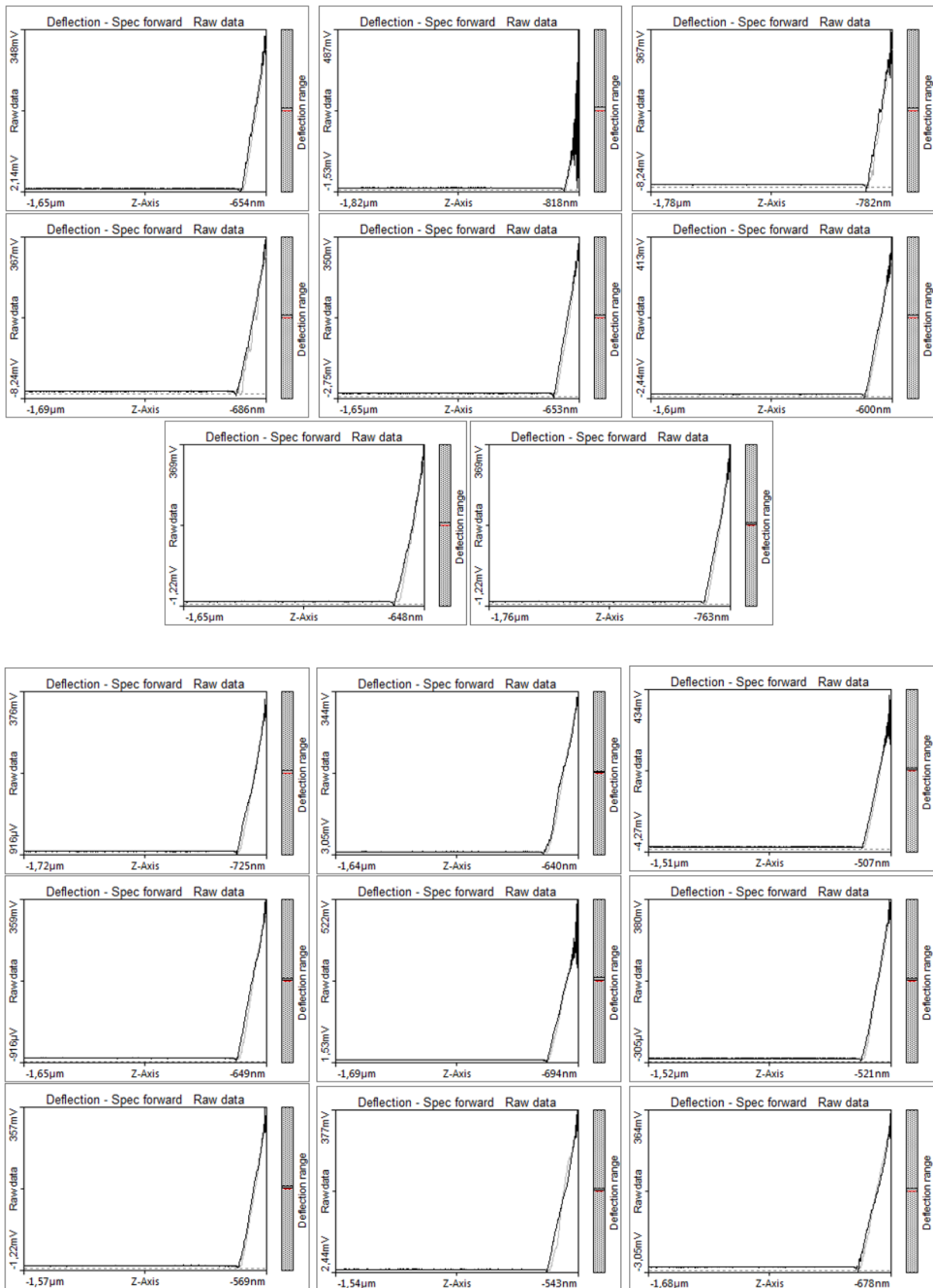
Plagioclase





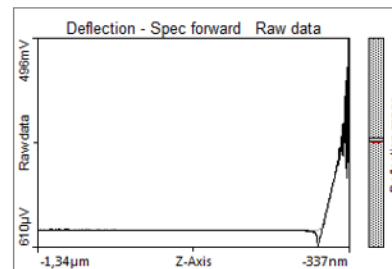
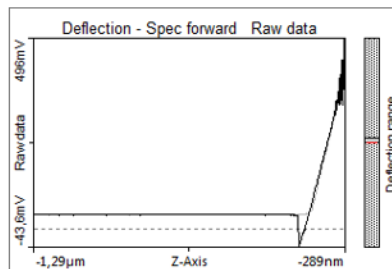
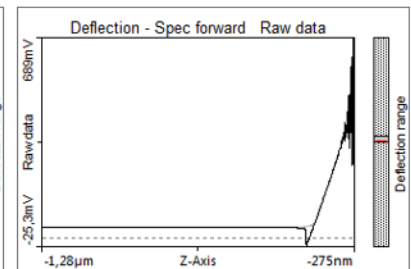
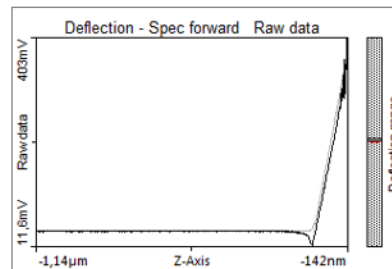
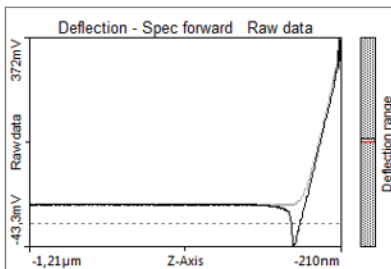
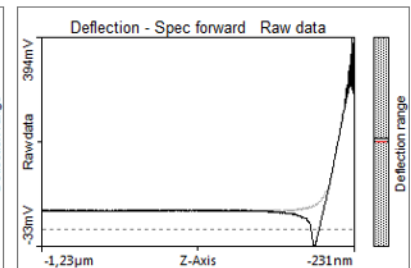
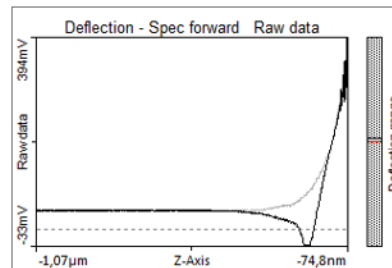
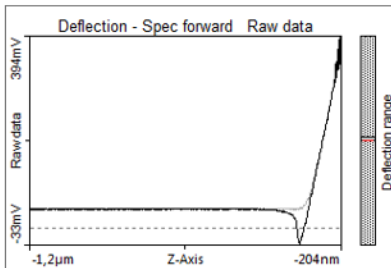
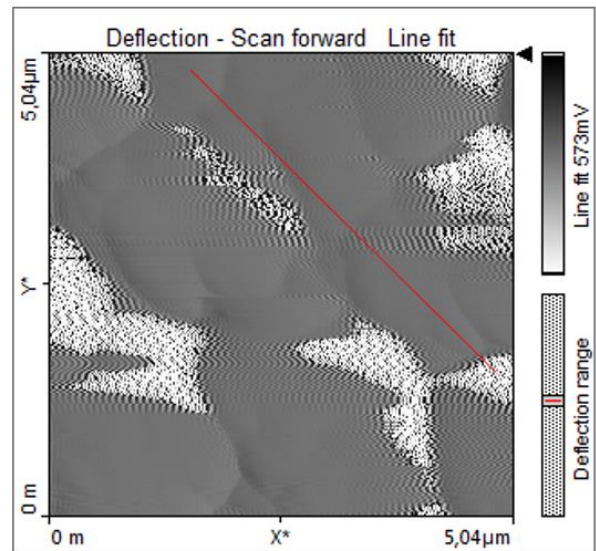
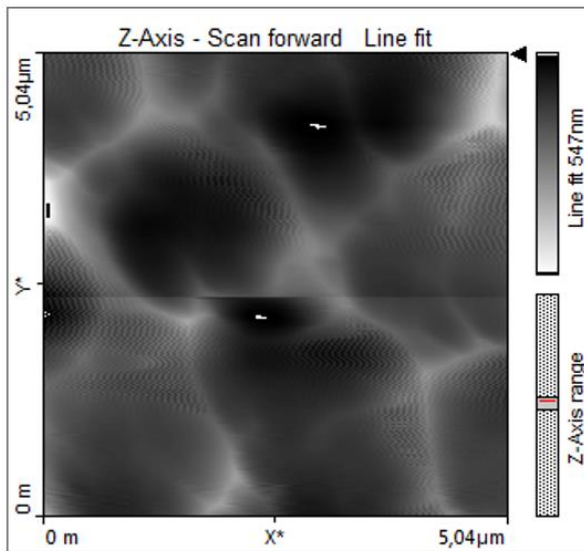
Quartz

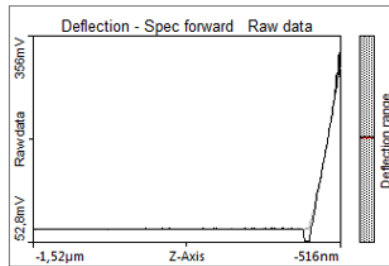
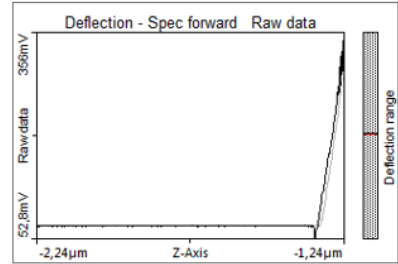
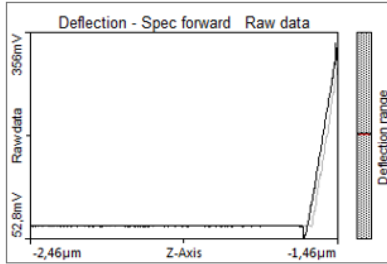
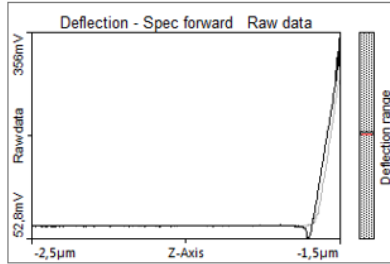
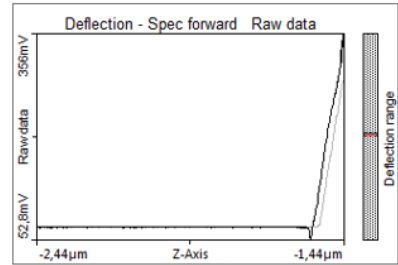
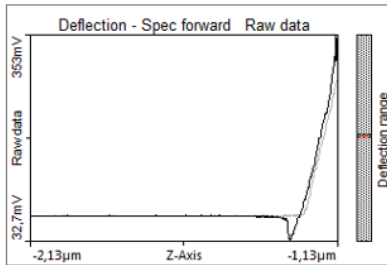
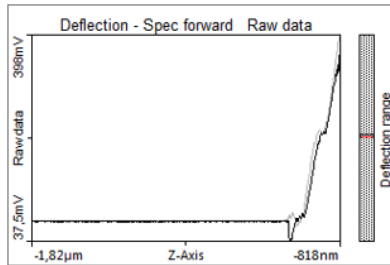
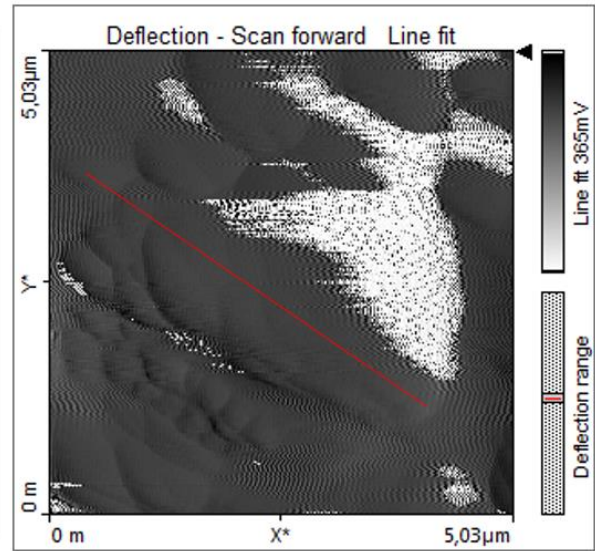
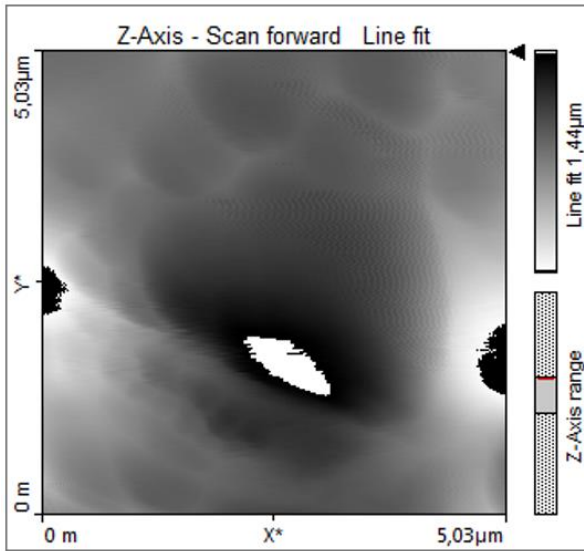




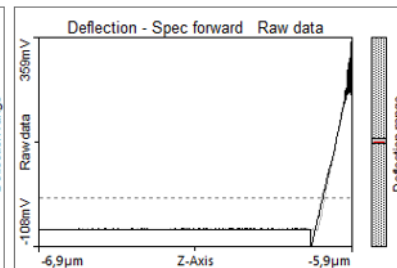
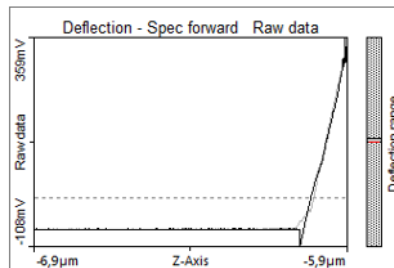
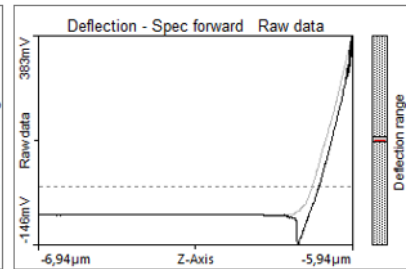
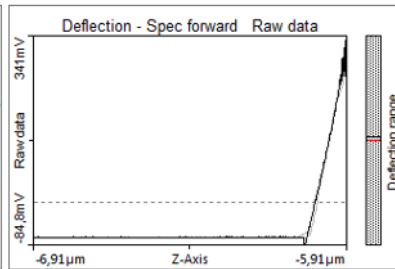
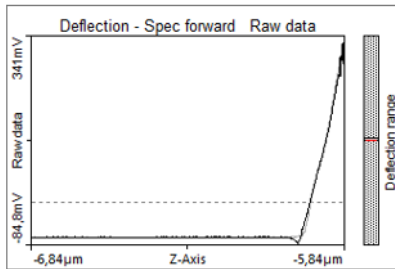
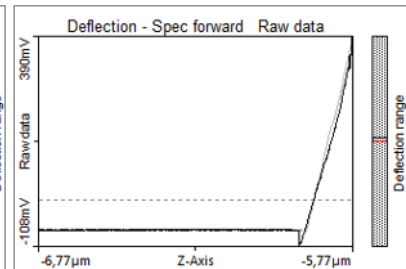
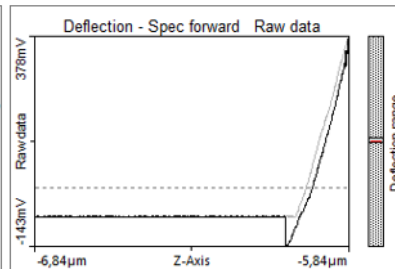
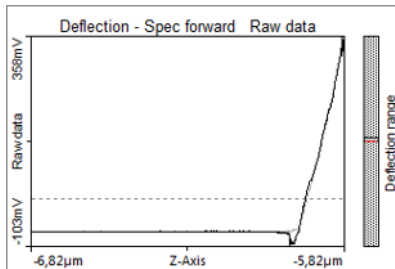
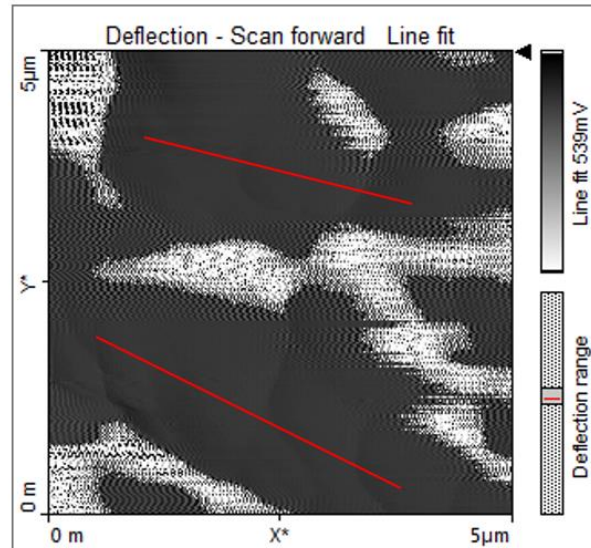
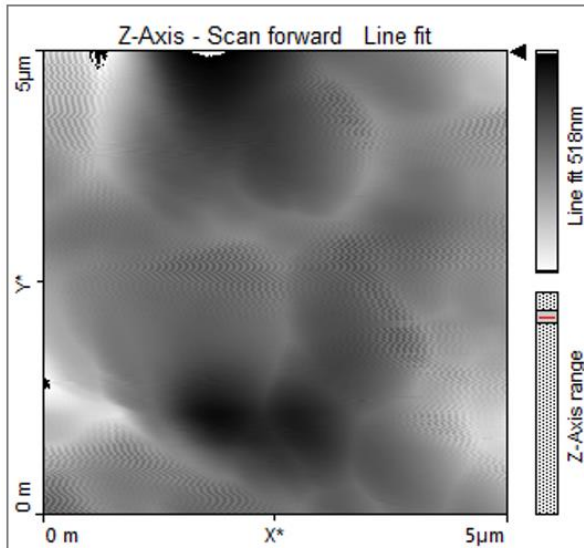
MLTT

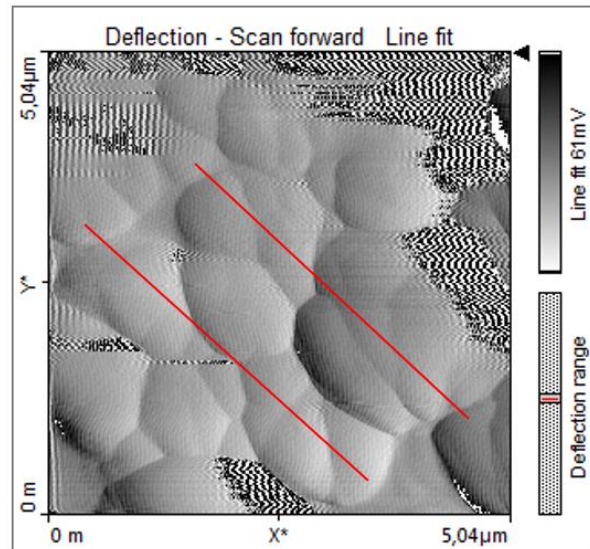
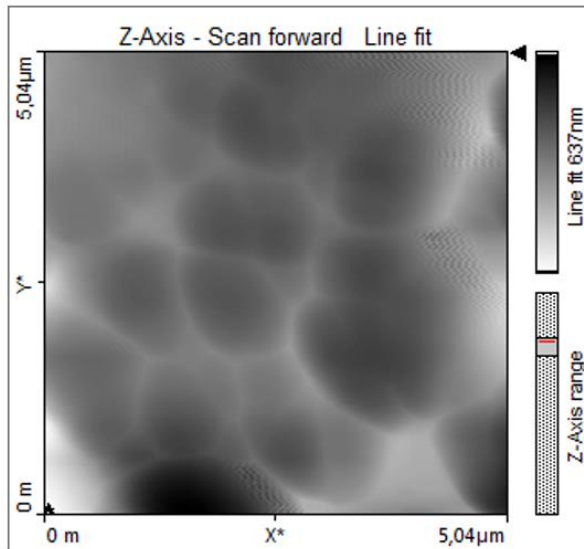
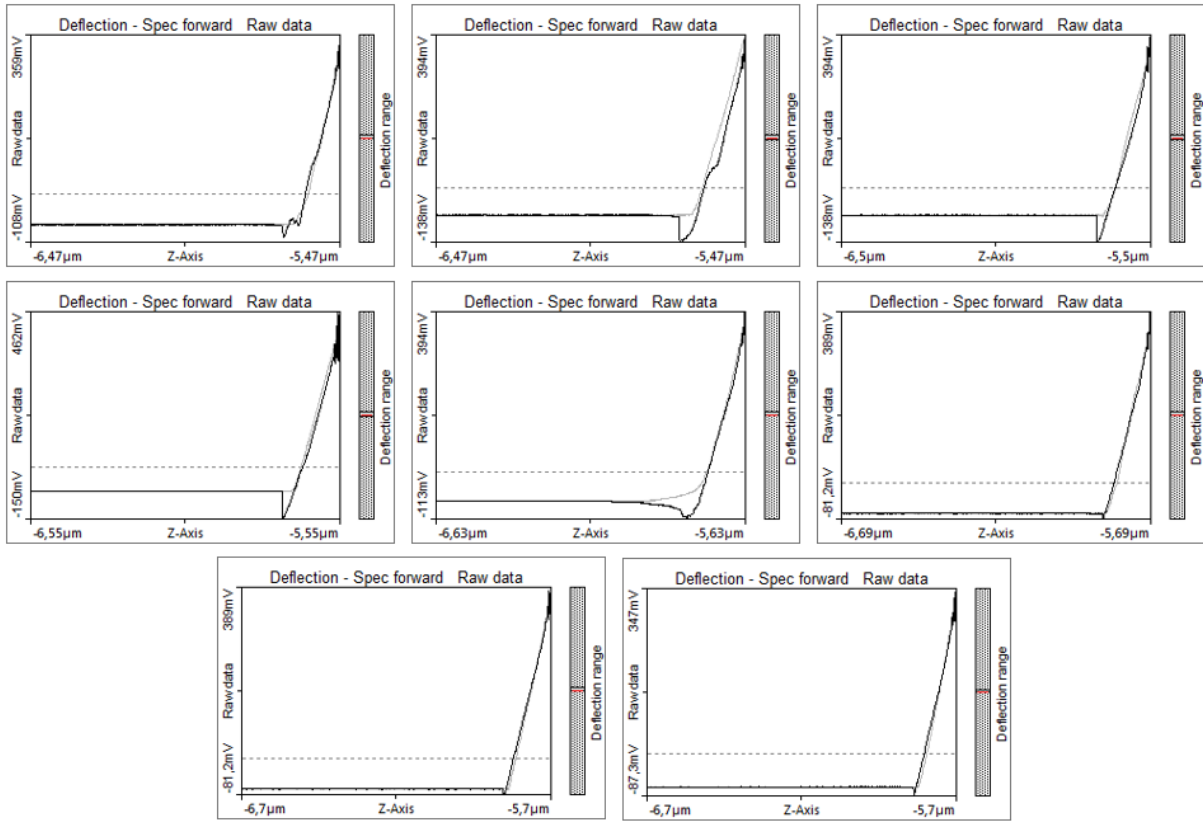
Calcite part

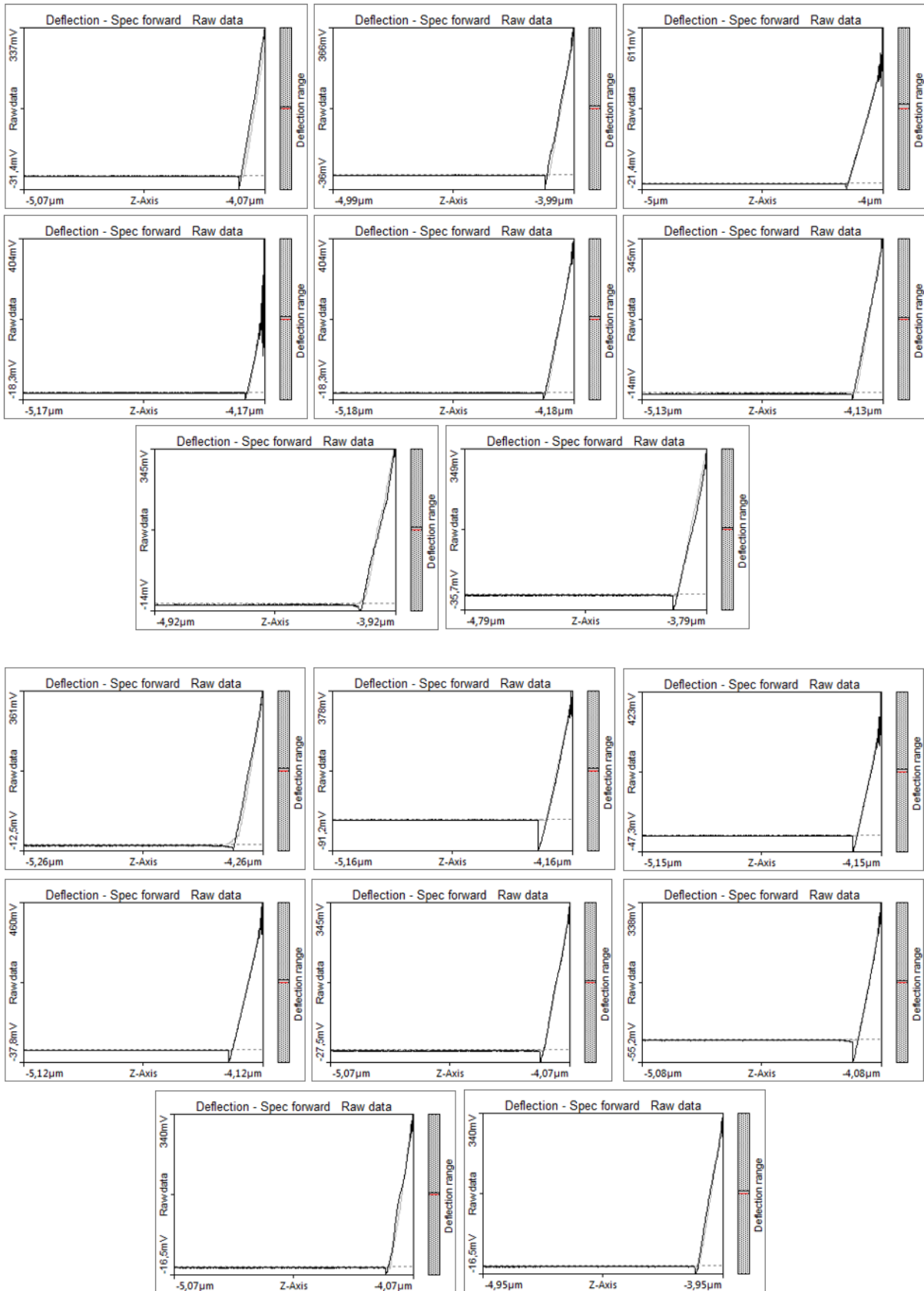




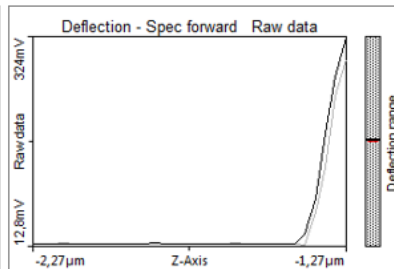
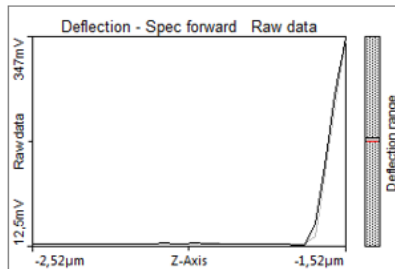
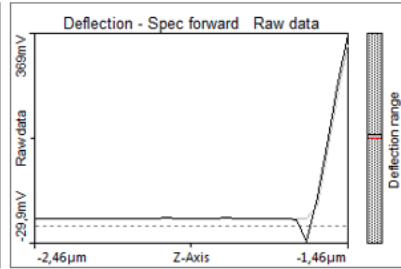
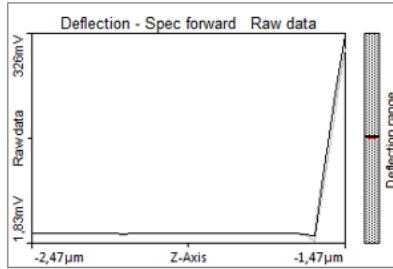
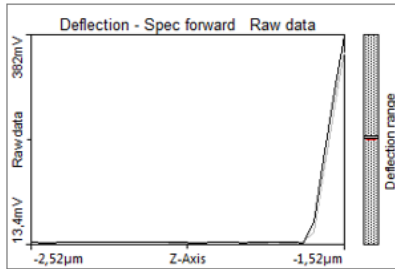
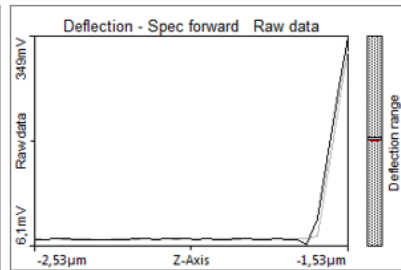
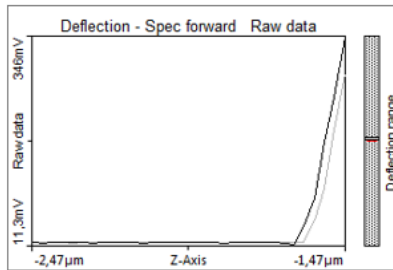
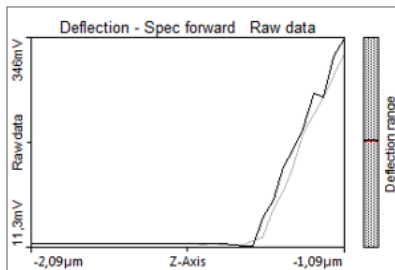
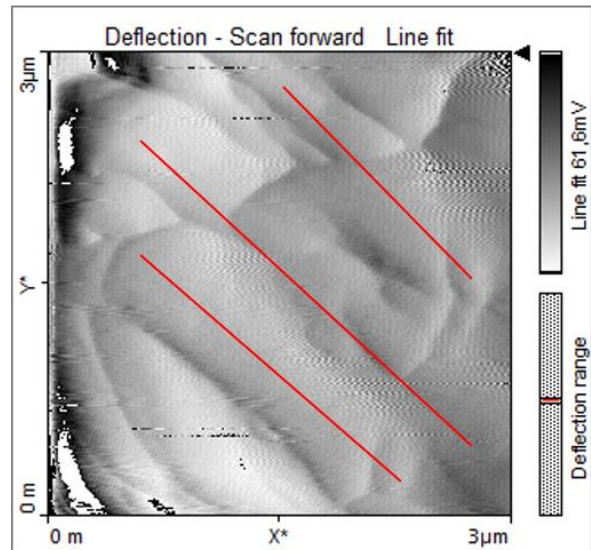
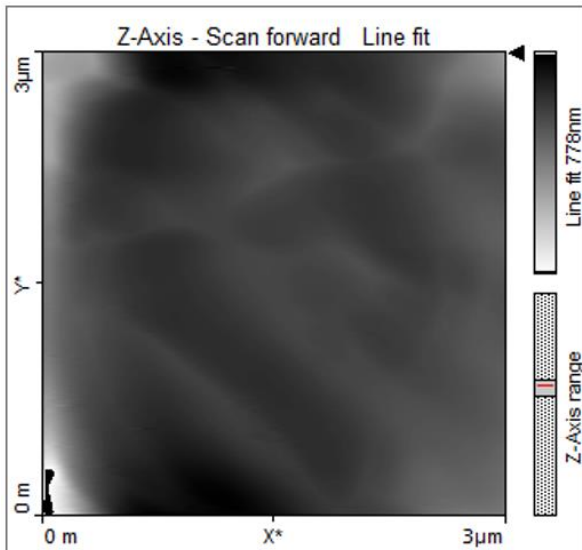
Magnesite part

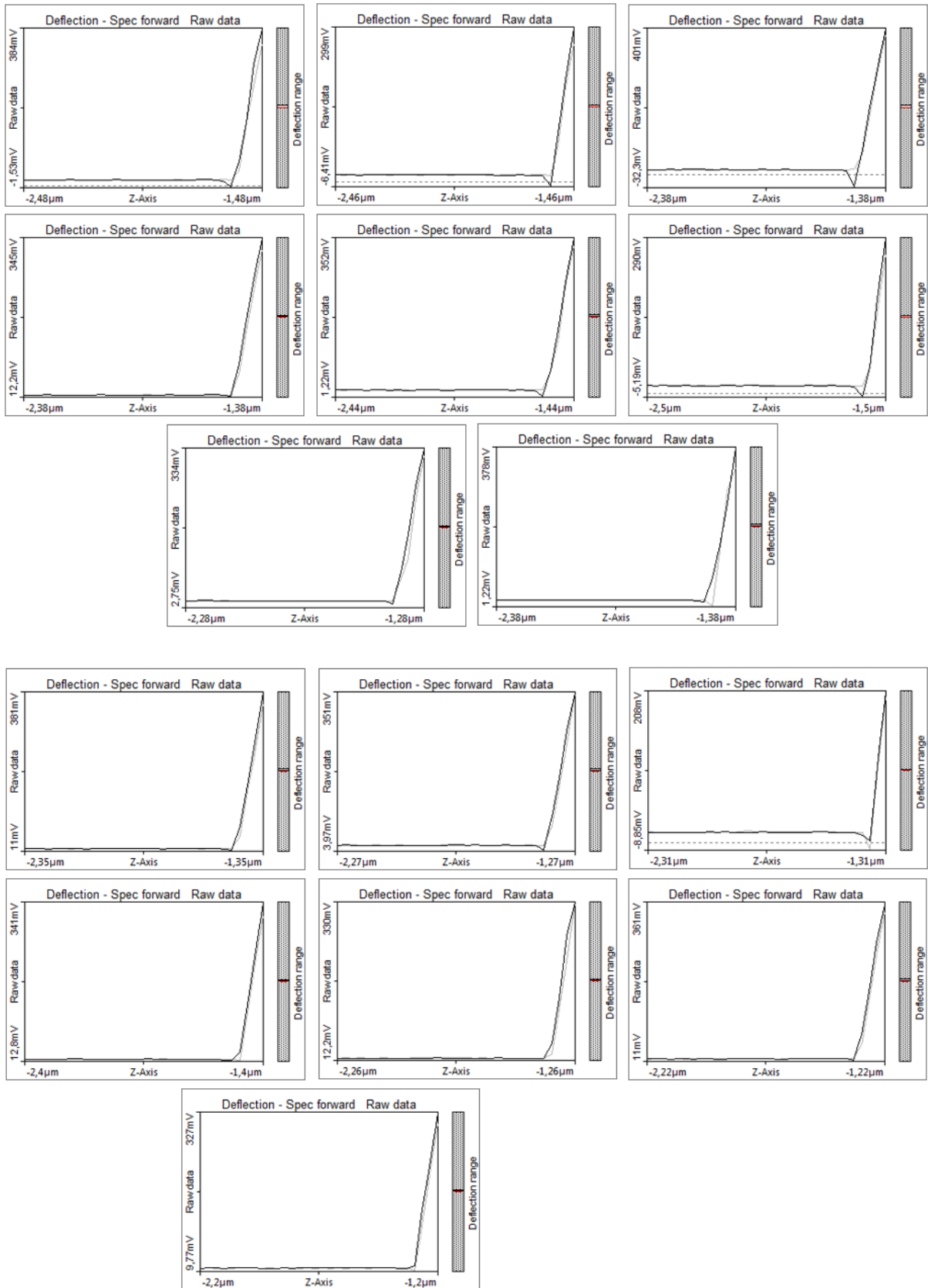


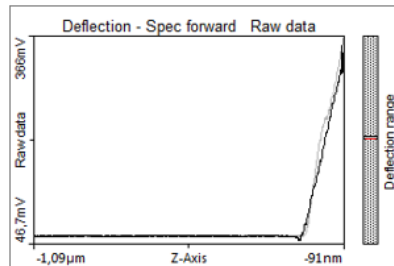
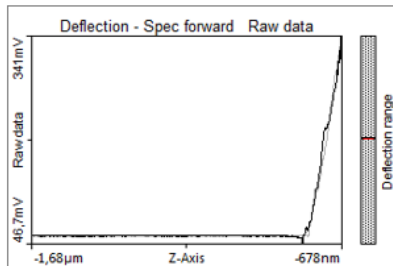
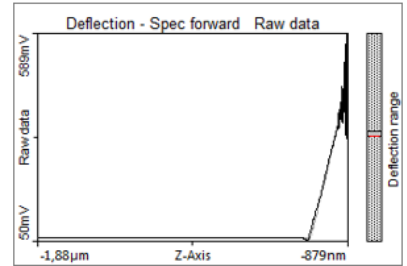
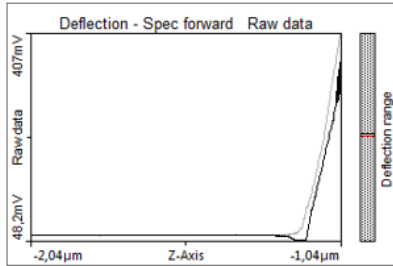
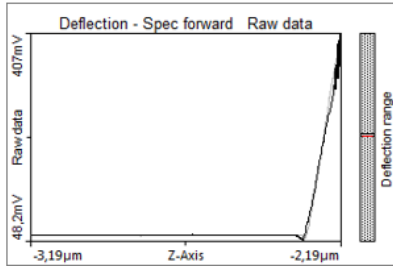
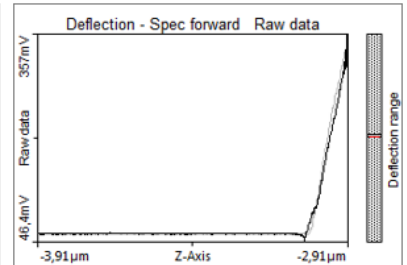
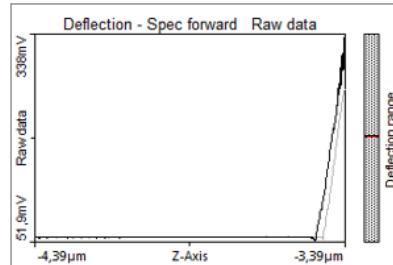
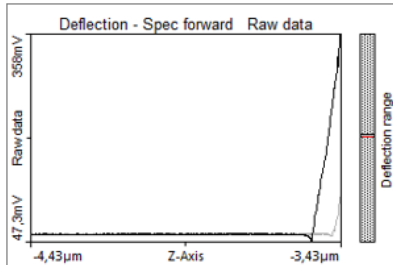
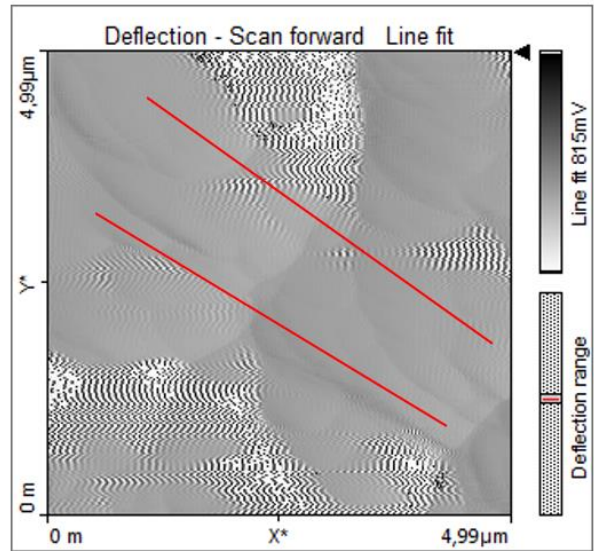
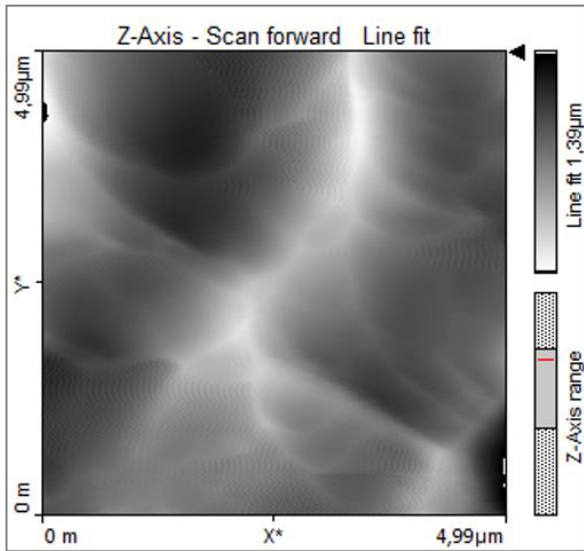


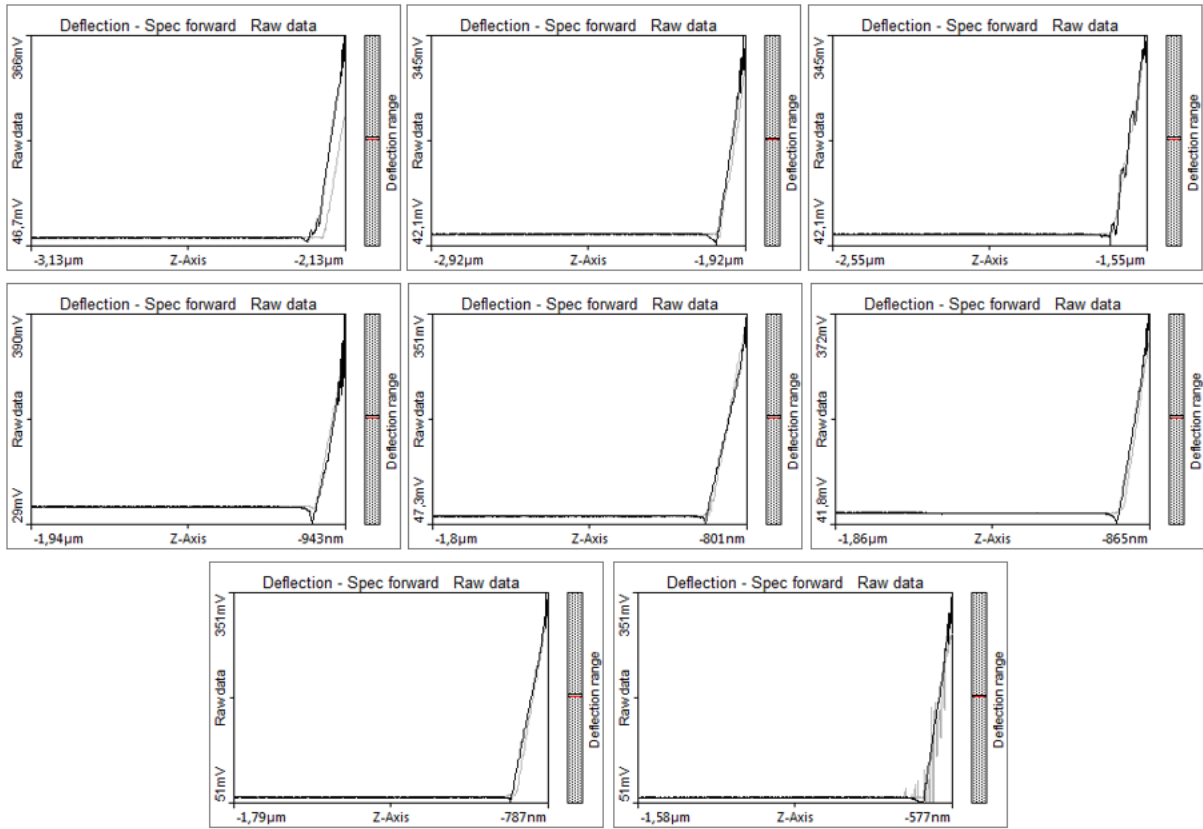


ULTT

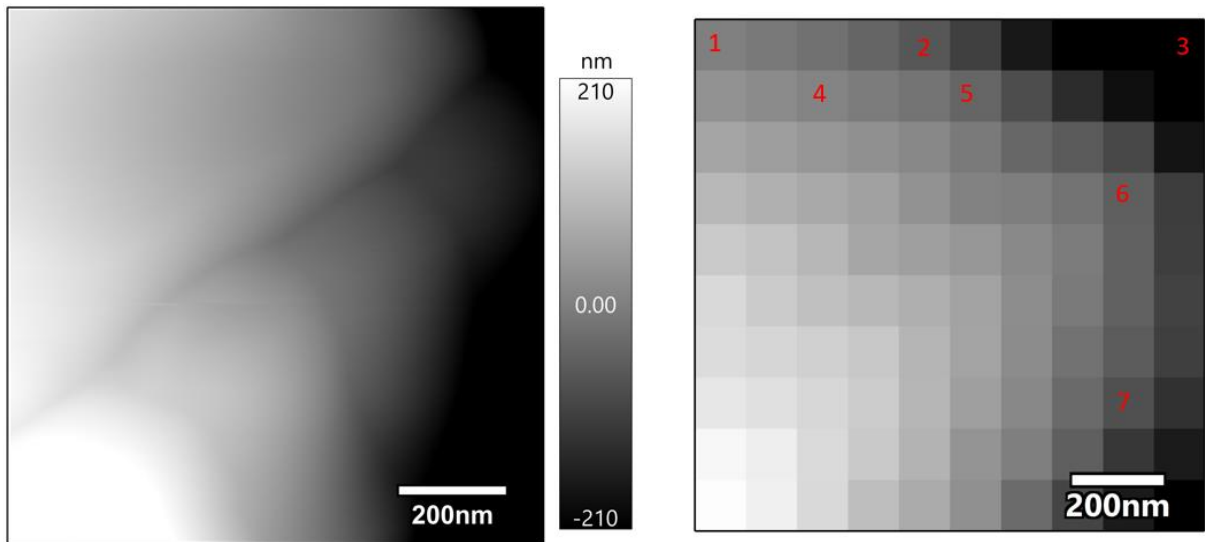


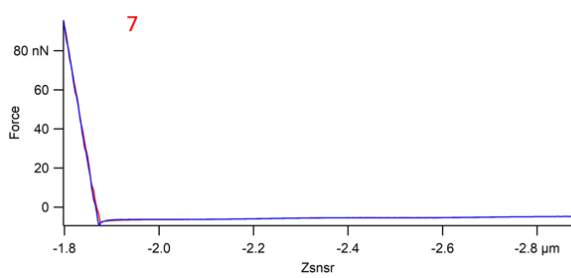
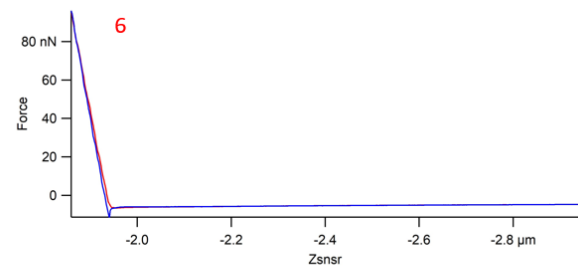
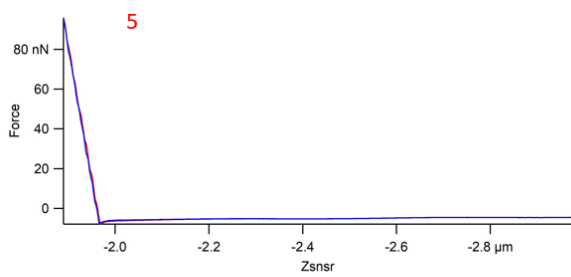
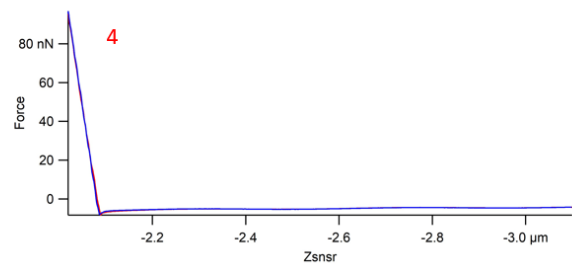
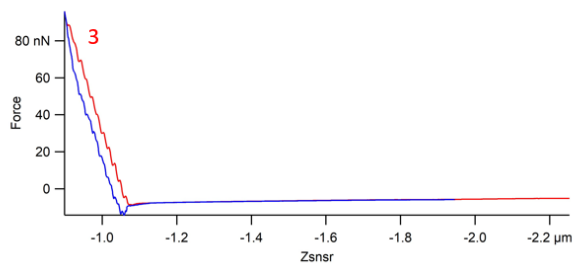
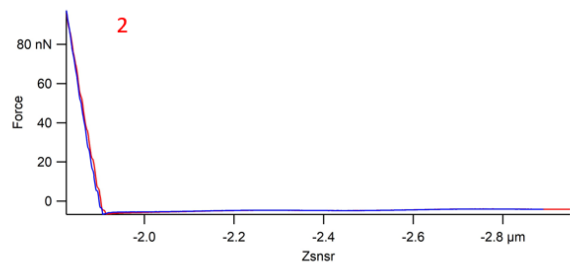
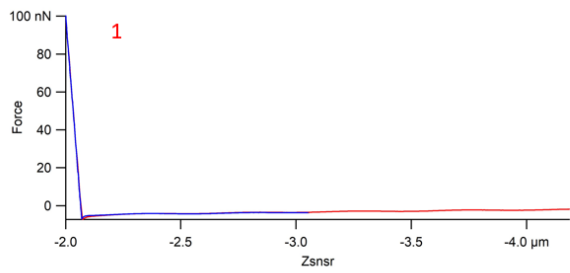
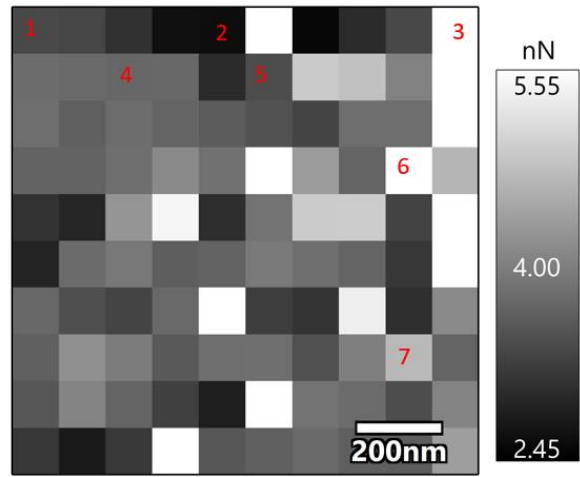
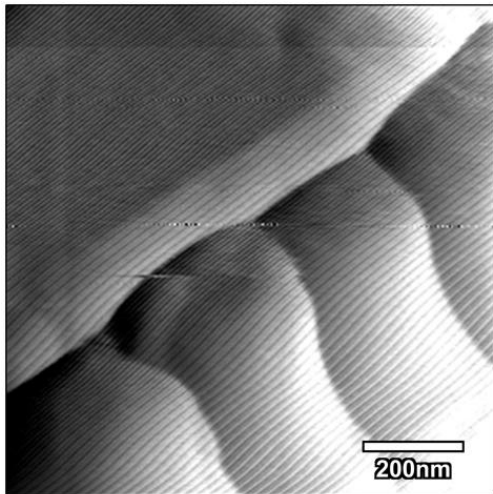




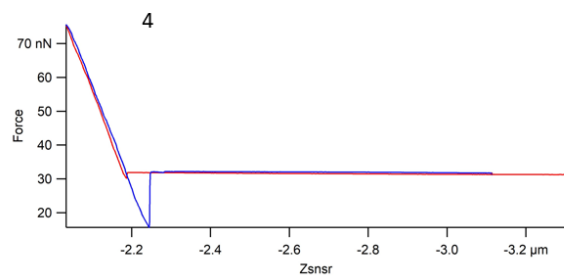
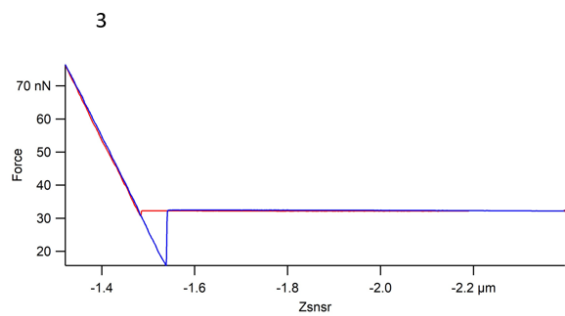
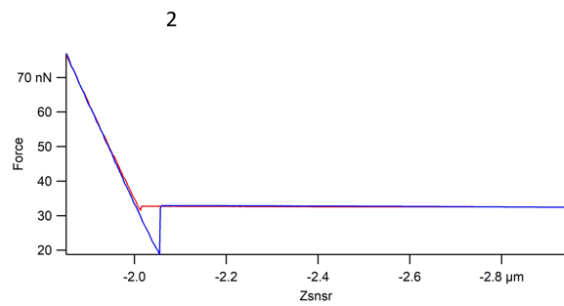
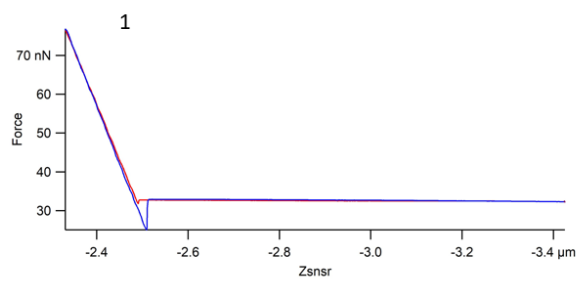
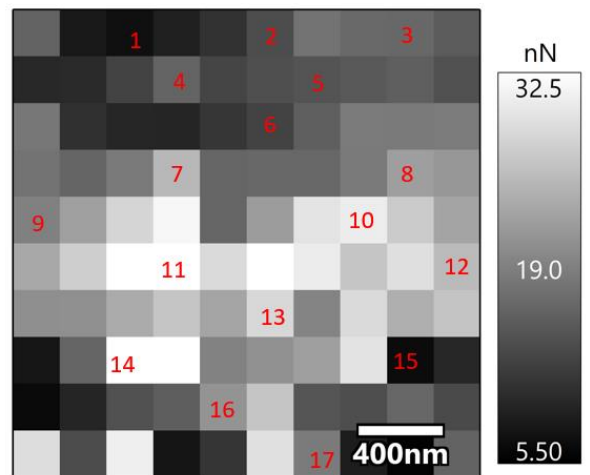
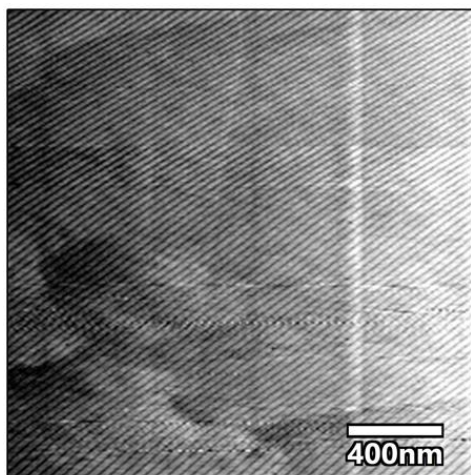
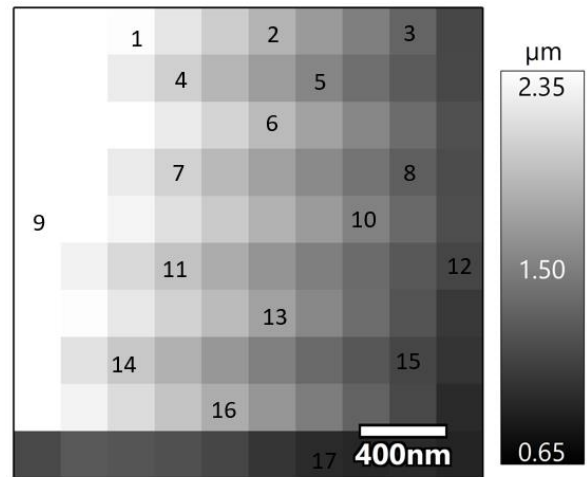
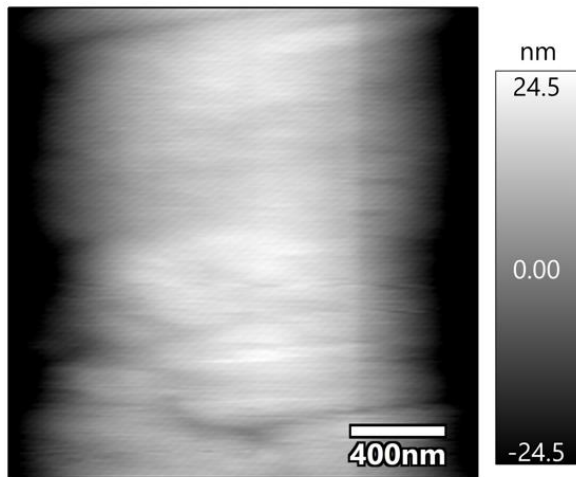


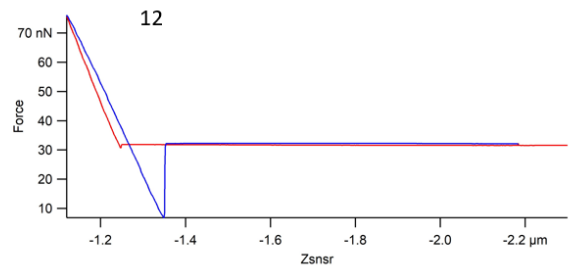
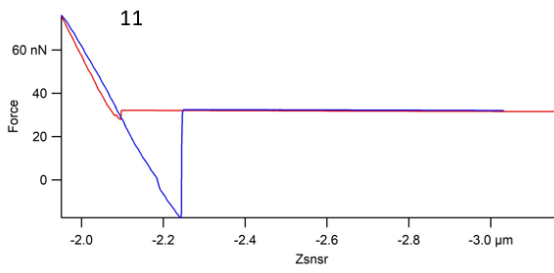
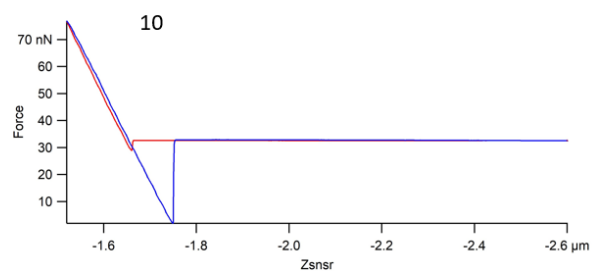
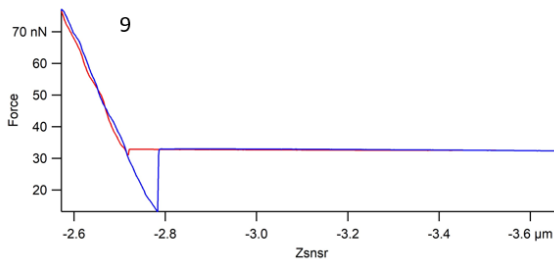
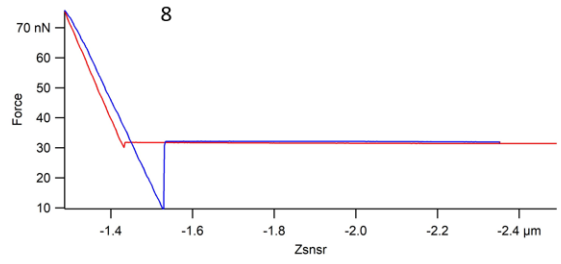
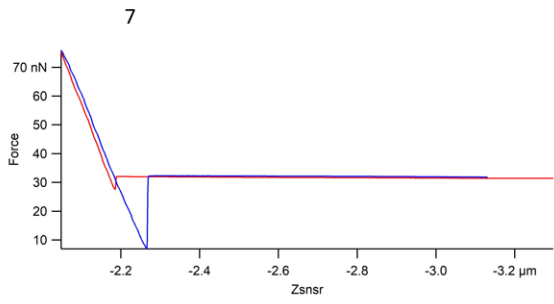
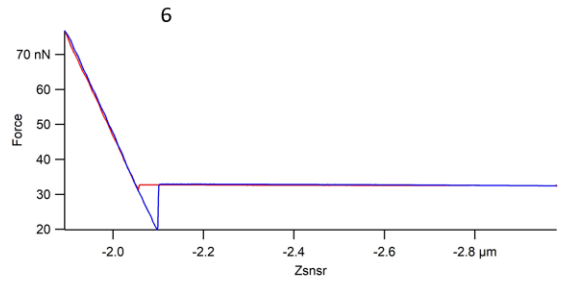
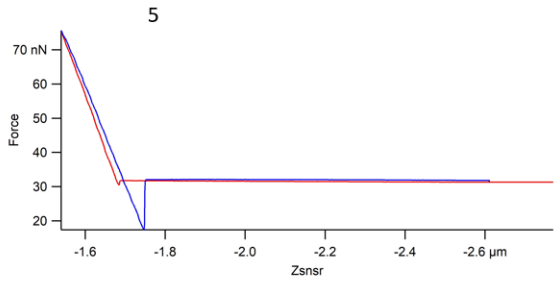
OBSV4_1 - MFP-3D Origin

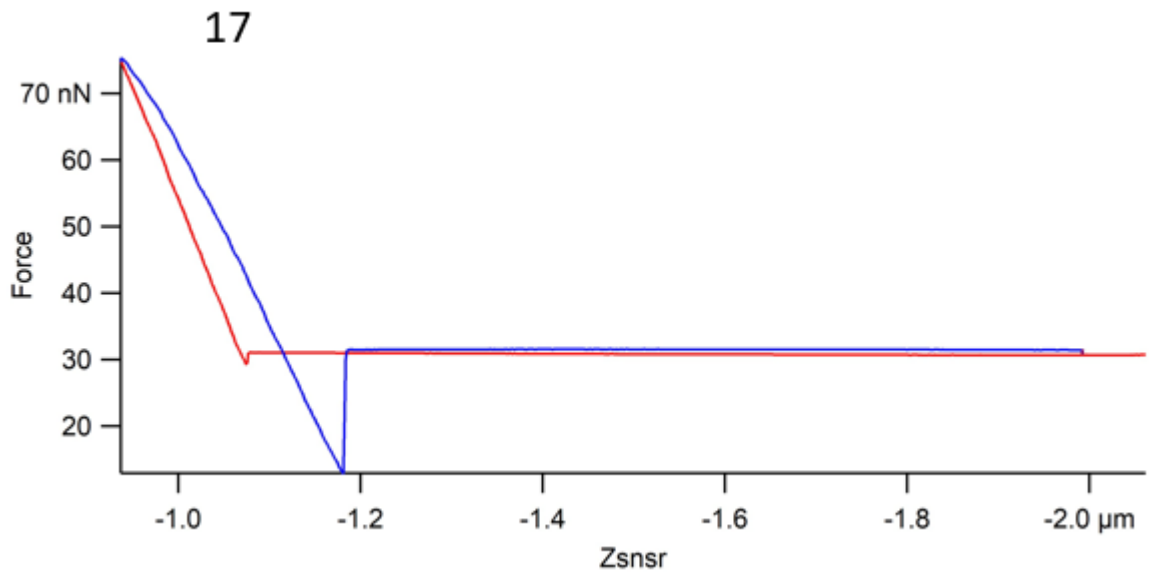
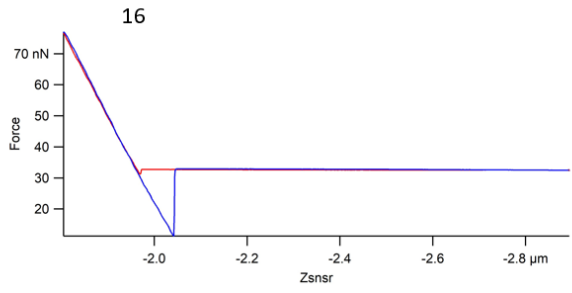
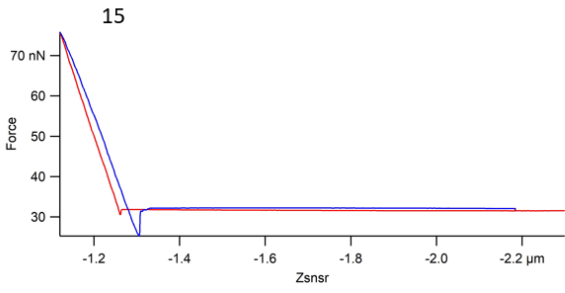
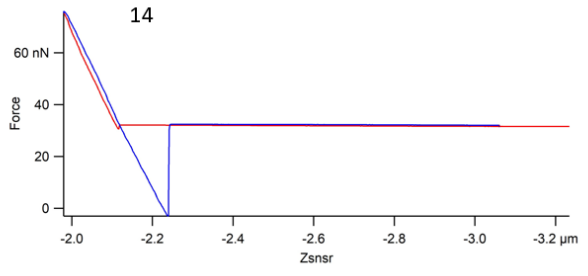
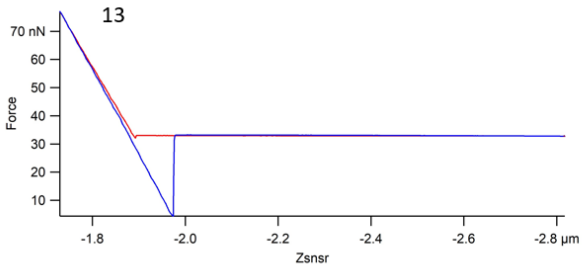


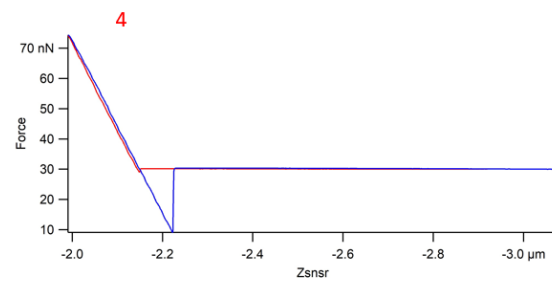
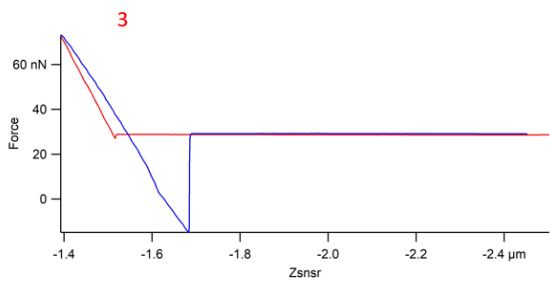
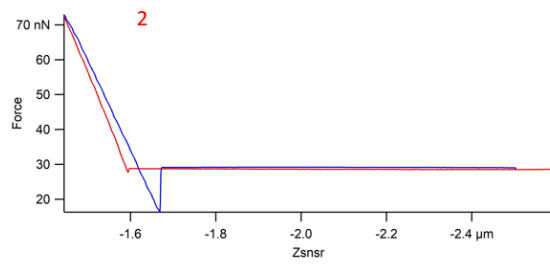
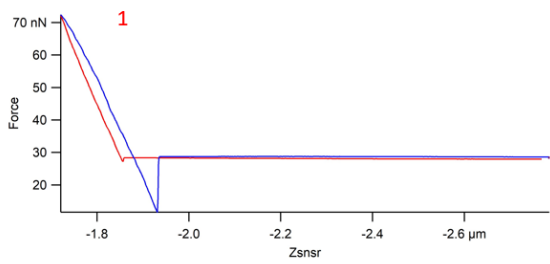
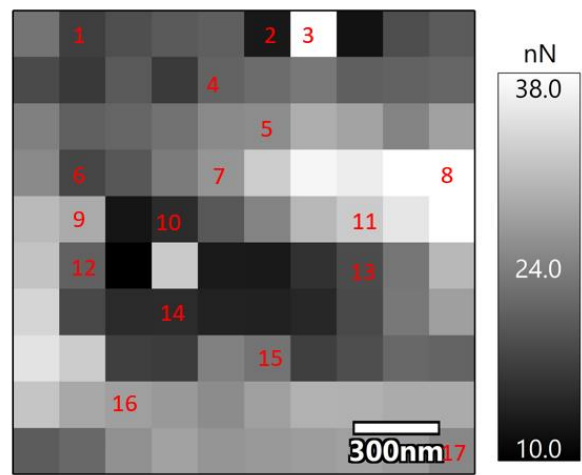
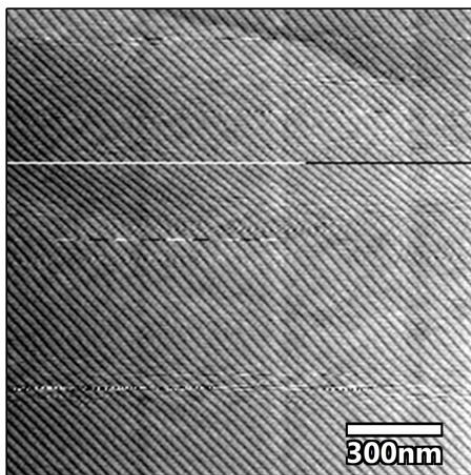
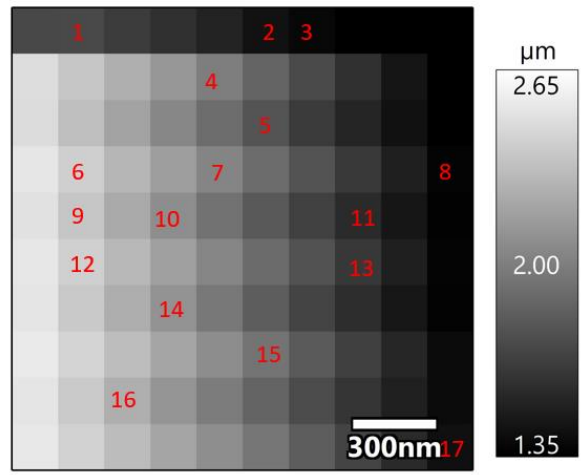
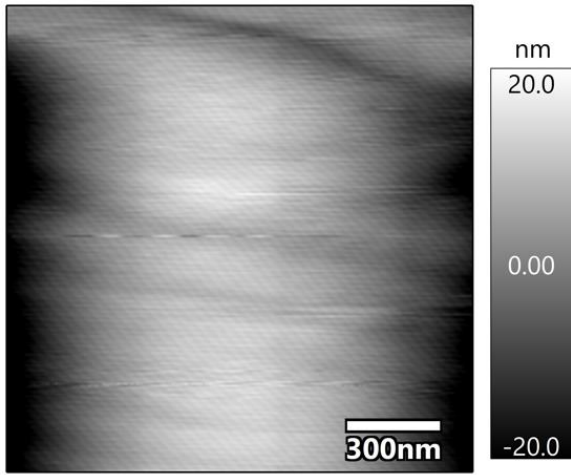


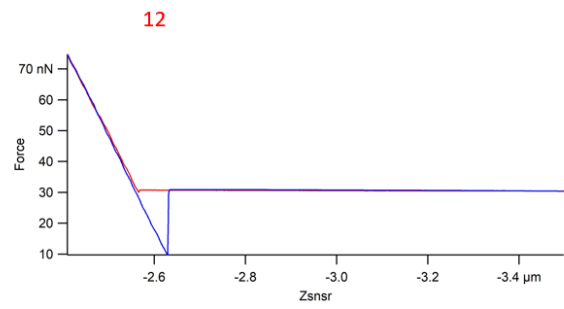
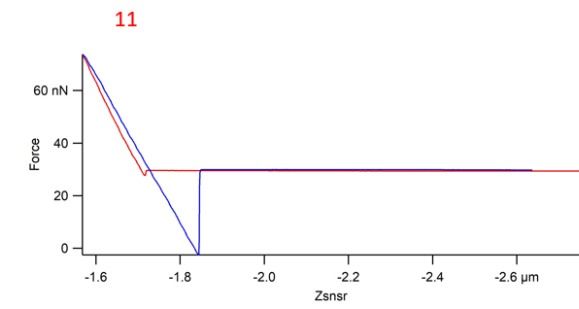
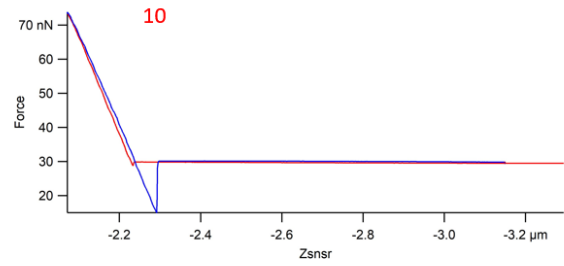
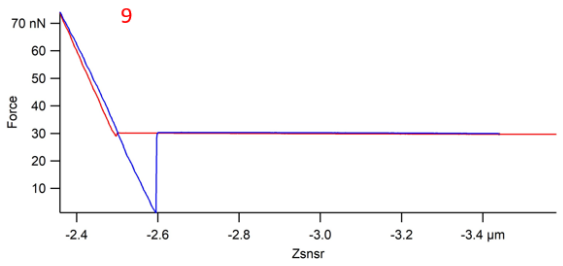
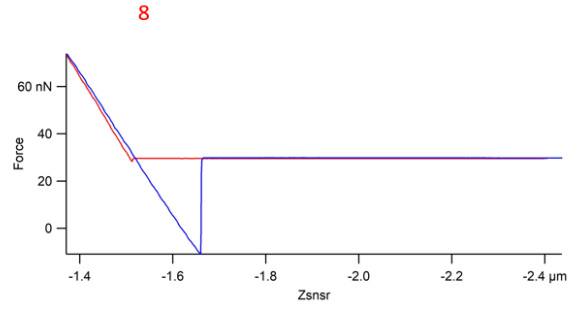
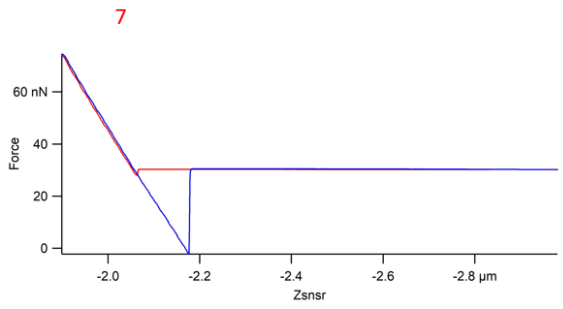
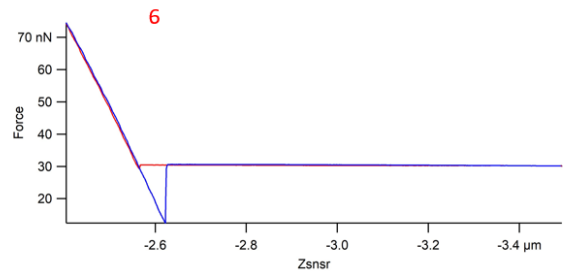
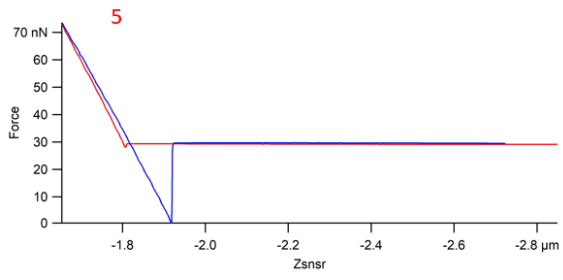
OBSV12 - MFP-3D Origin

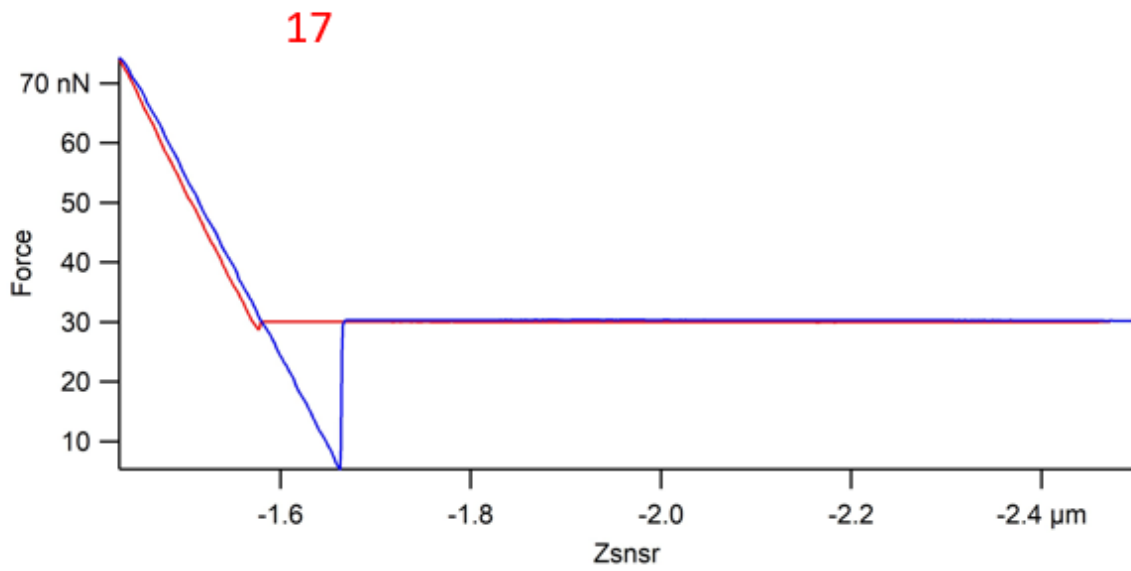
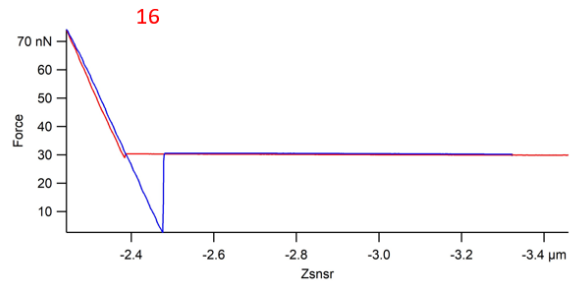
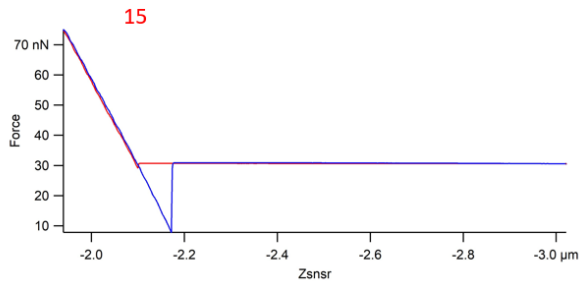
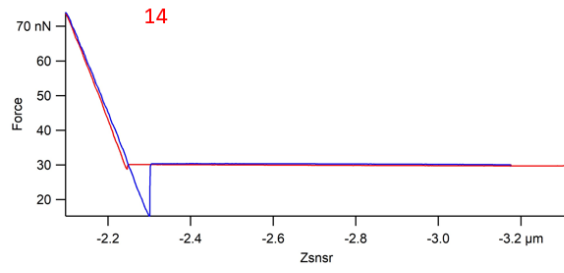
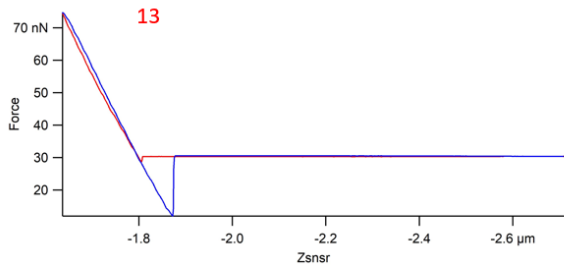






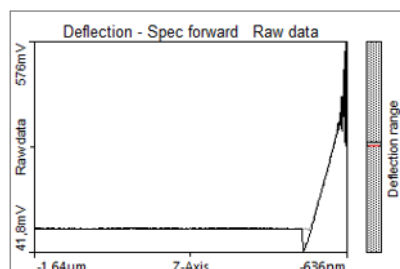
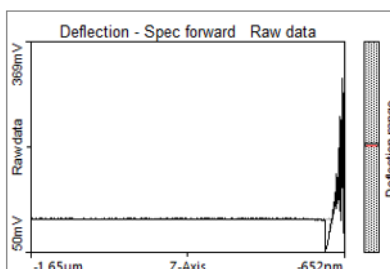
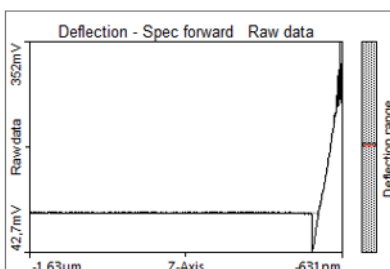
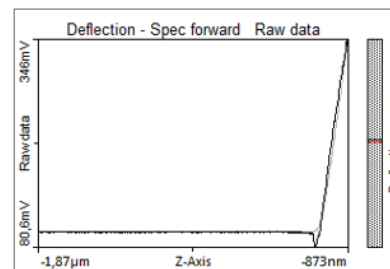
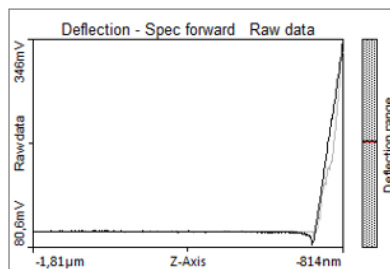
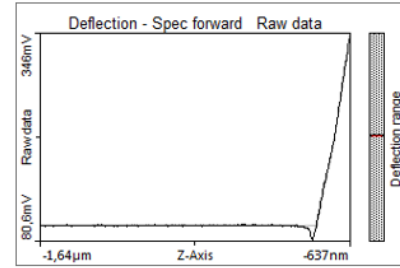
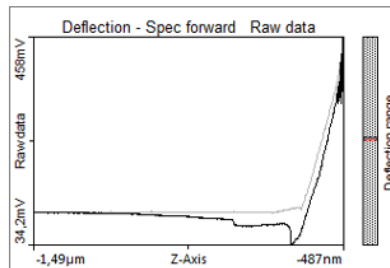
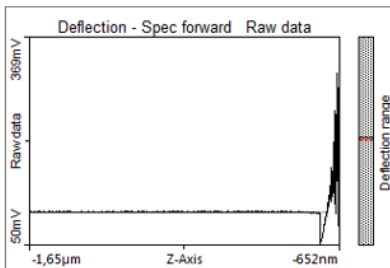
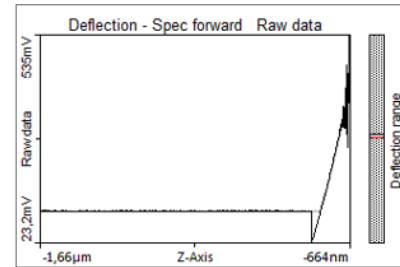
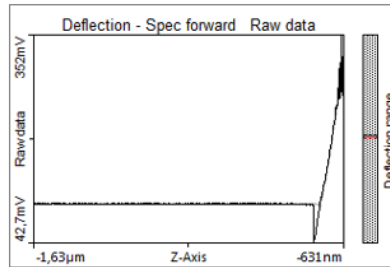
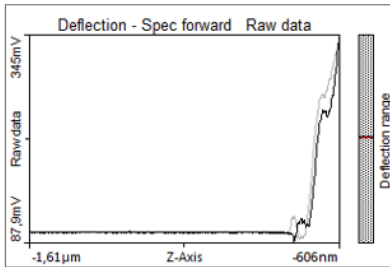
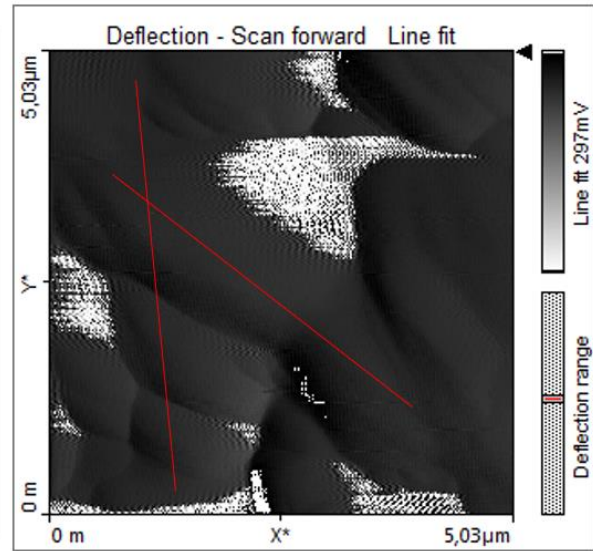
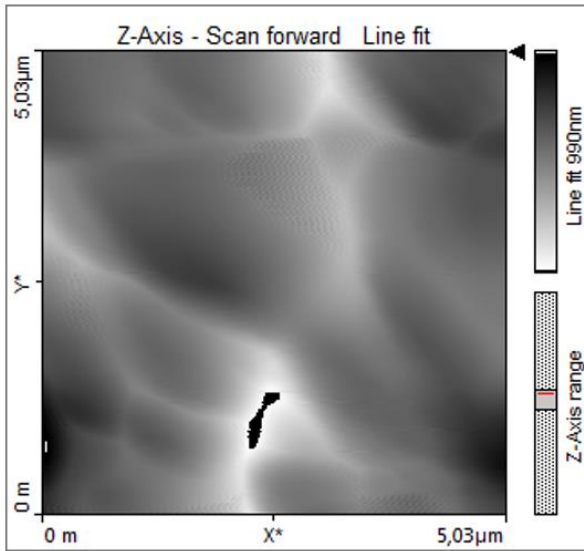


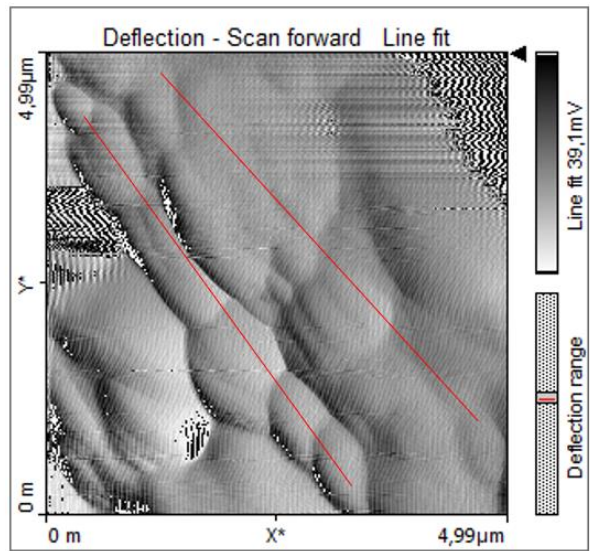
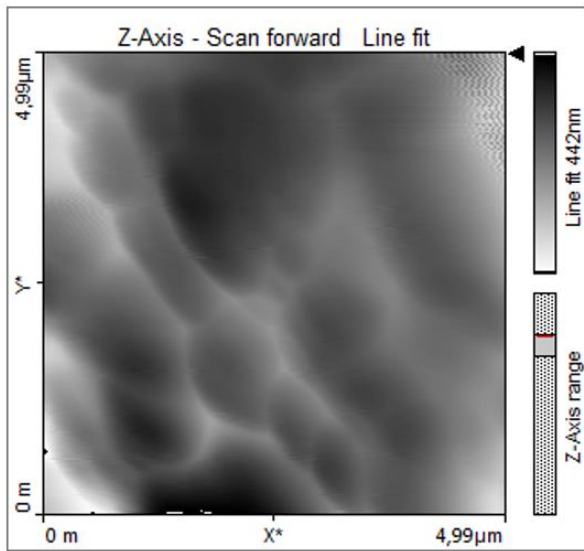
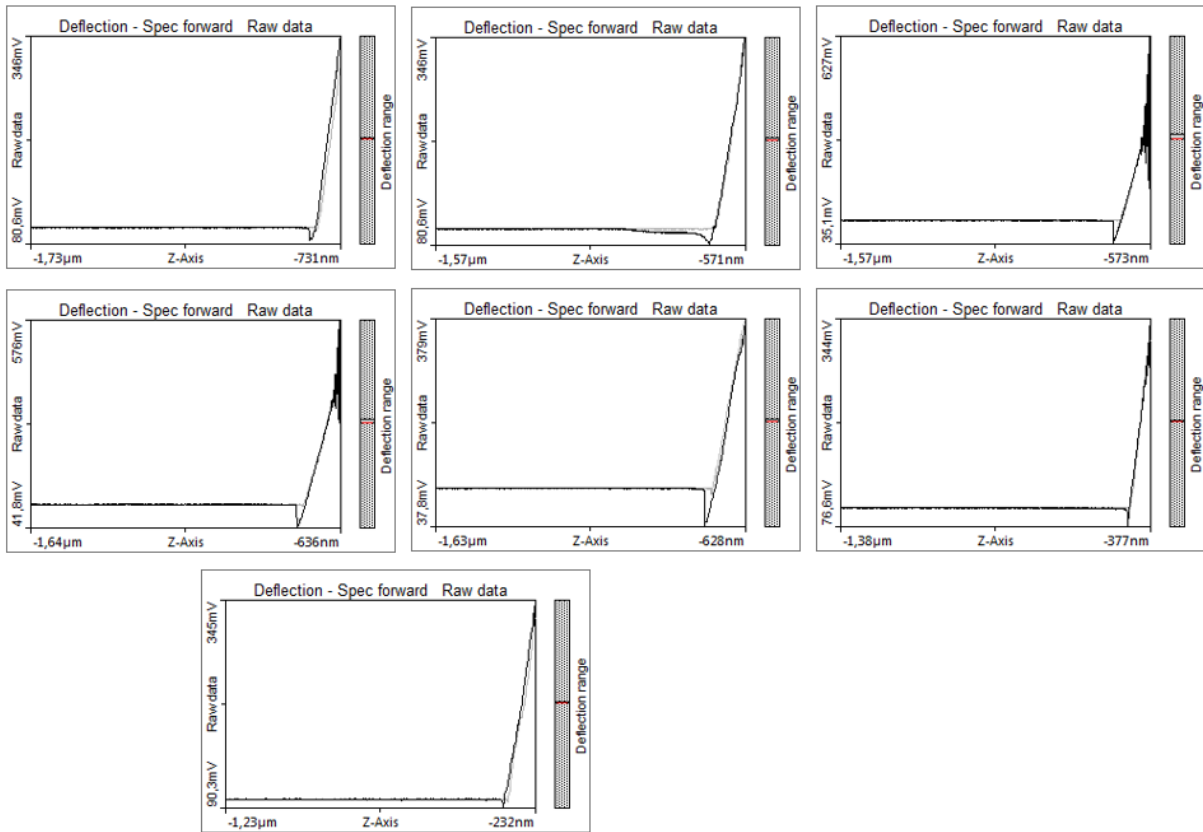


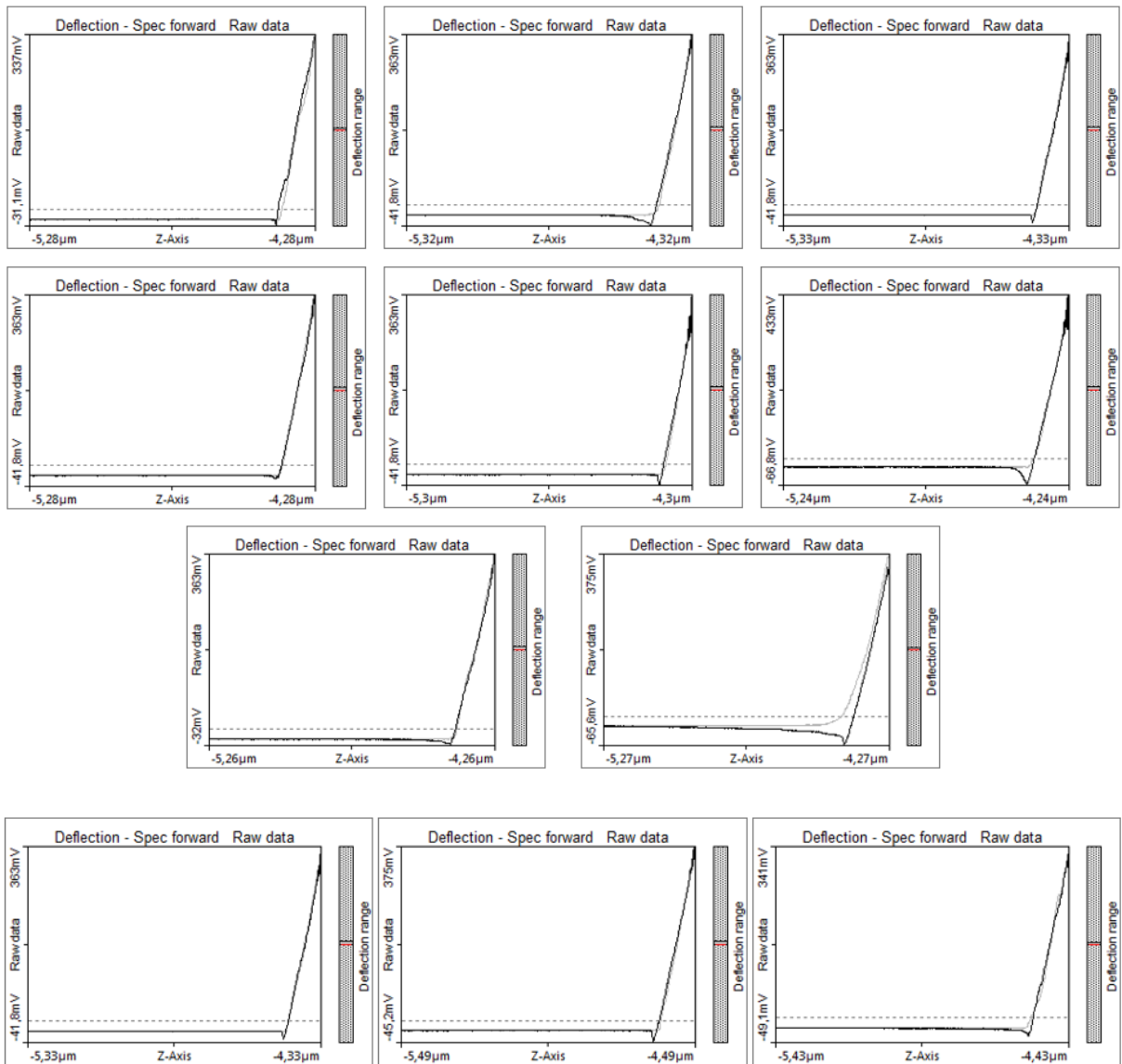


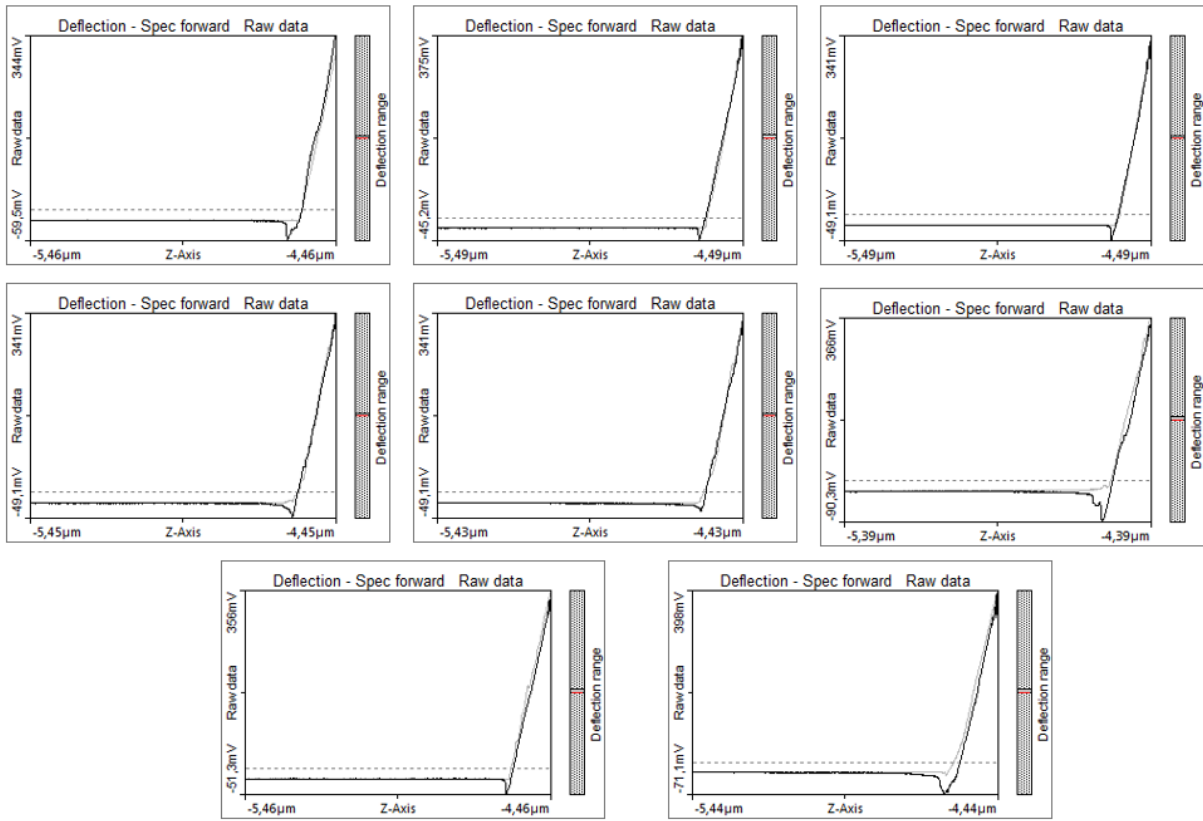
Unflooded Liège

Not coated









Coated

